



**A University of Sussex PhD thesis**

Available online via Sussex Research Online:

<http://sro.sussex.ac.uk/>

This thesis is protected by copyright which belongs to the author.

This thesis cannot be reproduced or quoted extensively from without first obtaining permission in writing from the Author

The content must not be changed in any way or sold commercially in any format or medium without the formal permission of the Author

When referring to this work, full bibliographic details including the author, title, awarding institution and date of the thesis must be given

Please visit Sussex Research Online for more information and further details

**Functional populations in the pyramidal cell layer of hippocampal area CA1**

**By:**

Dorieke Mathilde Grijseels

A thesis submitted in partial fulfilment of the requirements for the degree of Doctor of  
Philosophy

University of Sussex

Submission Date: April 2021

**Statement**

I hereby declare that this thesis has not been and will not be, submitted in whole or in part to another University for the award of any other degree.

Signature:

## Statement of contribution

Chapter 2 of this thesis has been submitted for publication, and has been released on bioRxiv as a preprint (DOI: <https://doi.org/10.1101/2021.02.26.433025>). The candidate contributed significantly to formulation of ideas, performed all experiments and analyses and wrote the manuscript. Dr Kira Shaw performed surgery on 2 of the experimental animals, and contributed to the manuscript. Dr Caswell Barry was involved in formulating the ideas, contributed to the manuscript, and supervising the candidate. Dr Catherine Hall was involved in formulating the ideas, and contributed significantly to the manuscript, and was the main supervisor of the candidate.

For Chapter 3, the candidate contributed significantly to formulation of ideas, performed all hippocampal experiments, executed all analyses and wrote the manuscript. Dr Kira Shaw performed surgery on 2 of the experimental hippocampal animals, and preprocessed the data for all visual cortex recordings. Dr Caswell Barry was involved in formulating the ideas and supervising the candidate. Dr Catherine Hall was involved in formulating the ideas and was the main supervisor of the candidate.

For Chapter 4, the candidate contributed significantly to formulation of ideas, performed all hippocampal experiments, executed all analyses and wrote the manuscript. Dr Kira Shaw performed surgery on 2 of the experimental hippocampal animals, and preprocessed the data for all visual cortex recordings. Dr Katie Boyd performed all visual cortex experiments. Dr Caswell Barry was involved in formulating the ideas and supervising the candidate. Dr Catherine Hall was involved in formulating the ideas and was the main supervisor of the candidate.

## Acknowledgements

This thesis would not have been possible without the help and support of several people.

Thank you Catherine for all your help and guidance, always staying enthusiastic about the work and trying to help me through even when I was being querulous, and of course sharing your cats in trying times. To my (unofficial) second supervisor Caswell, thank you for all your help and guidance with the projects, always being willing to make time for me, and sharing your wisdom on the enigma that is the hippocampus.

I could not have finished this thesis without the lovely Hall lab. Orla, I don't know what I would have done without you. You were always there with helpful advice, trying to make me see the good side of things and helping me work through whatever my latest crisis was. It was an absolute pleasure to do this PhD alongside you, I couldn't have asked for a better friend. Kira, thank you for all your help and advice throughout this process. I will try to honour your motto and pay it forward as much as I can. You are also the best running buddy, and always up for talking things through when I got stuck. Katie, you have taught me more than I ever thought possible. Thank you for always being up for a rant, sharing your extensive wisdom with me, or discussing the latest running shoe controversy. Devin, throughout my PhD I have been continually inspired by your view on life, Barcelona was without a doubt one of the highlights of my PhD. Laura, thank you for all your help with the little creatures, and always being up for cat talk. Silvia, despite this last year having been hard, your drive to power through has inspired and amazed me.

I also owe the world to Katy, thank you for inspiring me in many of my activities outside of the PhD, for being my partner in crime in organising all the LGBTQ+ events over the years, and for always being there to help and advice.

To Sussex Neuroscience, thank you for giving me this opportunity and for all your support throughout the years. Especially Ruth, thank you for everything you have done! Also, thanks to all the SN 4-year students for the community you have created and all your support and advice, especially Rich, thank you for being a fount of wisdom and the best climbing buddy.

Lastly, I want to thank the LGBTQ+ in STEM community who have inspired me and helped me grow these last years. I hope I can one day inspire future scientists the way you have inspired me. This thesis is dedicated to you.

## Abbreviations

|      |  |
|------|--|
| 1D   | One-dimensional                                  |
| CA   | Cornu Ammonis                                    |
| DG   | Dentate gyrus                                    |
| EC   | Entorhinal cortex                                |
| FN   | False negative                                   |
| FP   | False positive                                   |
| GRI  | Goal representation index                        |
| IEC  | Lateral entorhinal cortex                        |
| LIA  | Large irregular activity                         |
| mEC  | Medial entorhinal cortex                         |
| MI   | Mutual information                               |
| OLM  | Oriens lacunosum moleculare                      |
| ORLA | Odd running-active low-frequency aperiodic cells |
| PC   | Place cell                                       |
| PYR  | Pyramidal cells                                  |
| PV   | Parvalbumin expressing interneurons              |
| REM  | Rapid eye movement                               |
| ROI  | Region of interest                               |
| SIA  | Small irregular activity                         |
| SLO  | Stationary low-frequency oscillatory cells       |
| SSE  | Sum of squared errors                            |
| SST  | Somatostatin expressing interneurons             |
| SWR  | Sharp wave-ripples                               |
| TN   | True negative                                    |
| TP   | True positive                                    |
| VR   | Virtual reality                                  |

## Table of Contents

|  |    |
|--|----|
| Acknowledgements.....  | 4  |
| Abbreviations.....   | 6  |
| Abstract.....  | 11 |
| 1 Introduction .....   | 13 |
| 1.1 Spatial representation in the hippocampus.....   | 17 |
| 1.1.1 Place cells.....   | 17 |
| 1.1.2 Beyond egocentric location .....   | 20 |
| 1.1.3 Beyond the hippocampus .....   | 21 |
| 1.2 Network activity in the hippocampus.....   | 22 |
| 1.2.1 Theta oscillations .....   | 22 |
| 1.2.2 Gamma oscillations.....  | 25 |
| 1.2.3 Irregular activity and ripples .....   | 26 |
| 1.3 Virtual reality experiments .....  | 27 |
| 1.3.1 Sensory modalities in virtual environments .....   | 27 |
| 1.3.2 Place cell activity in virtual environments .....  | 30 |
| 1.4 Aims.....  | 32 |
| 2 Choice of method of place cell classification determines the population of cells identified .....  | 36 |
| 2.1 Abstract.....  | 37 |
| 2.2 Author Summary.....  | 38 |
| 2.3 Introduction .....   | 39 |
| 2.4 Results.....   | 42 |
| 2.4.1 Place cell detection by the Combination and Stability methods is sensitive to the properties of place fields and the number of times mice traverse the environment ..... | 42 |
| 2.4.2 Variability and reliability decrease detection of model place cells, particularly by the Combination method.....   | 48 |
| 2.4.3 The Peak method detects the most place cells in real datasets.....   | 51 |
| 2.4.4 Different populations of real CA1 pyramidal cells are identified as place cells by the different methods.....  | 60 |
| 2.4.5 Identified place cell populations differ on key characteristics .....  | 61 |

|        |   |                                     |
|--------|---|-------------------------------------|
| 2.4.6  | Optimisation of the Combination method.....   | 65                                  |
| 2.5    | Discussion.....   | 68                                  |
| 2.5.1  | What is a place cell?.....  | 68                                  |
| 2.6    | Materials and Methods.....  | 69                                  |
| 2.6.1  | Ethics Statement .....  | 74                                  |
| 2.6.2  | Animals.....  | 74                                  |
| 2.6.3  | Hippocampal cranial window surgery.....   | 75                                  |
| 2.6.4  | Two-photon imaging.....   | 76                                  |
| 2.6.5  | Image Analysis.....   | 77                                  |
| 2.6.6  | Model data generation .....   | 78                                  |
| 2.6.7  | Manipulation of place cells .....   | 79                                  |
| 2.6.8  | Performance measures .....  | 81                                  |
| 2.6.9  | Place cell detection methods.....   | 81                                  |
| 2.6.10 | Statistical analysis .....  | <b>Error! Bookmark not defined.</b> |
| 2.6.11 | Data and software availability .....  | 81                                  |
| 2.7    | Acknowledgements.....   | 86                                  |
| 2.8    | Supporting information .....  | 87                                  |
| 3      | The effect of object location novelty and cue abundance on populations in hippocampal area CA1..... | 99                                  |
| 3.1    | Introduction .....  | 99                                  |
| 3.2    | Results.....  | 102                                 |
| 3.2.1  | Mice learn to perform a novel spatial task in virtual reality.....                                  | 102                                 |
| 3.2.2  | Animals do not show behavioural preference for object locations.....                                | 106                                 |
| 3.2.3  | Place cells have increased information about location in novel conditions.....                      | 110                                 |
| 3.2.4  | Object-vector cells place fields follows the location of the cue object .....                       | 114                                 |
| 3.2.5  | Place cells do not remap between conditions with the same novelty condition                         | 119                                 |
| 3.2.6  | Place cells contribute less to decoding of location in novel conditions .....                       | 124                                 |
| 3.2.7  | Hippocampal cells encode the animal's location relative to the cue object ....                      | 129                                 |
| 3.3    | Discussion.....   | 133                                 |
| 3.4    | Materials and methods.....  | 137                                 |
| 3.4.1  | Animals.....  | 137                                 |
| 3.4.2  | Hippocampal cranial window surgery.....   | 137                                 |

|       |   |     |
|-------|---|-----|
| 3.4.3 | Two-photon imaging .....  | 138 |
| 3.4.4 | Behavioural task.....   | 139 |
| 3.4.5 | Image analysis .....  | 141 |
| 3.4.6 | Celltype analysis.....  | 141 |
| 3.4.7 | Overlap analysis .....  | 143 |
| 3.4.8 | Bayesian decoder .....  | 143 |
| 3.5   | Supporting information .....  | 146 |
| 4     | Novel functional cell types with high power in at low frequencies in hippocampal area CA1<br>186              |     |
| 4.1   | Introduction .....  | 186 |
| 4.2   | Results.....  | 188 |
| 4.2.1 | A novel type of hippocampal pyramidal cell is identified using regularity of firing<br>and rest activity..... | 188 |
| 4.2.2 | Novel functional cell type has high power at low frequencies.....   | 191 |
| 4.2.3 | Novel functional cell types are differentially modulated by locomotion .....                                  | 195 |
| 4.2.4 | Periodic and aperiodic components differ depending on cell type and<br>locomotion.....                        | 200 |
| 4.2.5 | Synchrony of functional cell types .....  | 204 |
| 4.2.6 | SLO cells show location encoding during stationary periods, but not locomotion<br>208                         |     |
| 4.2.7 | Visual cortex also contains excitatory cells with SLO characteristics .....                                   | 211 |
| 4.3   | Discussion.....   | 214 |
| 4.3.1 | Potential upstream sites innervating SLO cells.....   | 216 |
| 4.4   | Materials and Methods.....  | 218 |
| 4.4.1 | Animals.....  | 218 |
| 4.4.2 | Hippocampal cranial window surgery.....   | 218 |
| 4.4.3 | Two-photon imaging .....  | 220 |
| 4.4.4 | Image Analysis.....   | 221 |
| 4.4.5 | Frequency analysis .....  | 222 |
| 4.4.6 | Cell type identification .....  | 222 |
| 4.4.7 | Analyses .....  | 224 |
| 4.5   | Supporting information .....  | 226 |
| 5     | Discussion.....   | 232 |

|     |  |     |
|-----|--|-----|
| 5.1 | Aim 1: To understand how the method by which place cells were defined, affected what cells were included in the population.....  | 232 |
| 5.2 | Aim 2: To understand how cue abundance and displacing a cue object, in addition to training on a behavioural task, affects coding of space by hippocampal populations..... | 234 |
| 5.3 | Aim 3: To characterize the activity of two novel types of functional cells in CA1 and their relationship to environmental and behavioural factors .....                    | 237 |
| 5.4 | Final Conclusions.....   | 239 |
| 6   | References .....   | 240 |

UNIVERSITY OF SUSSEX

DORIEKE MATHILDE GRIJSEELS

Submitted for the degree of

Doctor of Philosophy

## Abstract

The hippocampus is an area of the brain that plays a crucial role in spatial navigation. Place cells are hippocampal pyramidal cells which hold a representation of self-location by firing selective in a single location: the place field. Pyramidal cells in CA1, including place cells, respond differently to a variety of external factors, such as cues or rewards in the environment, and internal factors, such a brain state. As such, heterogenous functional populations are present in CA1 both in addition to, as well as within the place cell population. I studied how pyramidal cells in CA1 form different functional populations in response to the manipulation of internal and external factors.

A combination of modelling approaches and mouse experiments was used to investigate this. Models of place cell populations were created to test the performance of place cell detection methods. Mice with a genetically encoded calcium indicator were trained to perform an object location novelty experiment in a virtual reality environment while their hippocampus was imaged using two-photon microscopy.

Our modelled place cells revealed one specific method to be optimal for detecting place cells. Using this method, I found that object location novelty had a stronger effect on place cell coding than cue abundance of an environment. In addition to the place cell populations, I identified two novel functional populations, the Stationary Low-frequency Oscillatory (SLO)

and Odd Running-active Low-frequency Aperiodic (ORLA) cells, within CA1 that are characterized by periodic and aperiodic activity respectively.

These results first contribute to an increased consensus on place cell detection, and by extension place cell identity, used within the field. I also show the impact of both external factors, in the place cell population, and internal factors, in the SLO and ORLA cells, giving us an increased understanding of factors that differentially drive hippocampal activity.

## 1 Introduction

The hippocampal formation is critically involved in spatial memory and navigation. It is located in the temporal lobe and is made up of three parts [1]: the hippocampus proper (usually simply referred to as hippocampus); pre- and parasubiculum; and the entorhinal cortex. The hippocampus consists of three cornu Ammonis (CA) subfields (CA1, CA2 and CA3), dentate gyrus (DG), and subiculum, with each subregion performing distinct functions. The entorhinal cortex is divided into medial (mEC) and lateral (IEC) parts, each with three distinct cell layers (II, III and IV/V) which differently project onto the different hippocampal regions.

All parts within the hippocampal formation are closely connected through various connections, which allow for information to be distributed throughout the formation (Fig 1.1). The main inputs of the hippocampus come from the entorhinal cortex via the perforant pathway. The CA2 and CA3 subfields, as well as DG, mainly receive inputs from layer II, while CA1 and subiculum are innervated by neurons from layer III [2]. Within the hippocampus itself DG projects to CA3 through mossy fibres, and CA3 innervates CA1 through the Schaffer collaterals. CA1 then projects back onto the deep layers (IV/V) of EC as well as the subiculum. The EC receives inputs from the postrhinal and perirhinal cortices, and connects back on to these neocortical areas [3]. The pre- and parasubiculum also have recurrent connections with EC, and additionally connect to DG. As subiculum connects back onto pre- and parasubiculum, this forms a complete loop. Pre- and parasubiculum receive inputs from a variety of subcortical areas, including thalamus and septum. Although this description includes the main connections, it is in some ways a simplification, and many more connections have been found [3]. Together they facilitate the flow and integration of information needed for the memory and navigation function of the hippocampal formation.

The hippocampus shows heterogeneity in both structure and function across its various axes. In mice, the hippocampus curves along the dorso-ventral (longitudinal) axis. Along this axis, its

connectivity to both cortical and subcortical areas varies gradually [4]. For example, reciprocal connections between amygdala and hippocampus are mainly situated in the ventral portion of the hippocampus [5]. As such, lesions to ventral, but not dorsal, hippocampus cause reductions in fear response [6]. Conversely, lesions to dorsal, but not ventral, hippocampus cause impairments in spatial learning and memory, suggesting this function is mainly located in dorsal hippocampus [7].

Despite ventral hippocampus playing a seemingly negligible role in spatial learning and memory, it still contains place cells [8]. However, place cells also show variations across the longitudinal axis: cells in CA3 show an increase in place field size at increasingly ventral locations [9], while CA1 cells have lower spatial resolution at more ventral locations [10]. This reflects the gradient in grid cells characteristics along the dorso-ventral axis in the entorhinal cortex, where grid cells show an increase in spacing towards the ventral side [11].

The hippocampus, and CA1 specifically, also shows variations in cell characteristics and function along the transverse axis [12,13]. CA3 will show more overlap in the cells used to represent distinct environments than CA1 for those same environments. In addition, the distal part of CA1 (i.e. further from CA3) specifically responds to object manipulations [14]. Within CA1, the more proximal area (closer to CA2 and CA3) shows a decrease in place field size compared to the distal area (closer to subiculum) [13]. These functional differences reflect a difference in connectivity: whereas medial entorhinal cortex (mEC) largely connects to proximal CA1, lateral entorhinal cortex (lEC) connects to distal CA1 [12,14]. As such, proximal CA1 receives spatial input from the grid cells, while distal CA1 receives more context-related input.

Lastly, the hippocampus also shows heterogeneity along the radial axis. Along this axis, the pyramidal cell layer CA1 is divided into two layers, though unlike layers in other cortical areas, these are not visually distinct [15]. The deep layer is located closer to the surface in rodents,

and contains more place fields [16] than the superficial layer during navigation. However, this effect is dependent on the type of environment, as cue-poor environments are preferably encoded by superficial place cells, while deep place cells encode cue-rich environments [17]. In addition, deep place cells use a phase code – encode location by their activity relative to theta – while superficial cells use a rate code [17].

The focus of this thesis is the hippocampus, specifically CA1, and how it is involved in facilitating spatial navigation through various functional subpopulations of pyramidal cells. CA1 can be divided into several layers, or strata, from deep to superficial: stratum oriens, stratum pyramidale, stratum radiatum and stratum lacunosum-moleculare. Stratum oriens is where the basal dendrites of the CA1 pyramidal cells are located, as well as the cell bodies of oriens lacunosum moleculare (OLM) and trilaminar interneurons [18,19]. Stratum pyramidale is tightly packed with pyramidal cell bodies, interspersed with the somas of interneurons innervating these pyramidal cells. Stratum radiatum contains the Schaffer collaterals from CA3 to CA1. The most superficial layer in CA1, stratum lacunosum-moleculare, is the main site of EC input [19].

We chose to focus on CA1, and specifically dorsal CA1, for several reasons. CA1 has overlapping representations for environments with similar spatial elements, rather than remapping completely when part of an environment changes [20]. CA1, and specifically dorsal CA1, contains place cells with relatively small place fields [13], and a high spatial resolution [10]. CA1 also rapidly remaps in response to changes in the environment, while other areas of the hippocampus, e.g. CA3, respond more slowly [20,21]. Lastly, dorsal CA1 is located the closest to the brain surface, and thus is most accessible for imaging. Because of these properties the place cells of CA1 are likely to show fast and modular responses to modular

changes in the environment, which would allow for the detection of subsets of cells responding to particular manipulations of the environment.

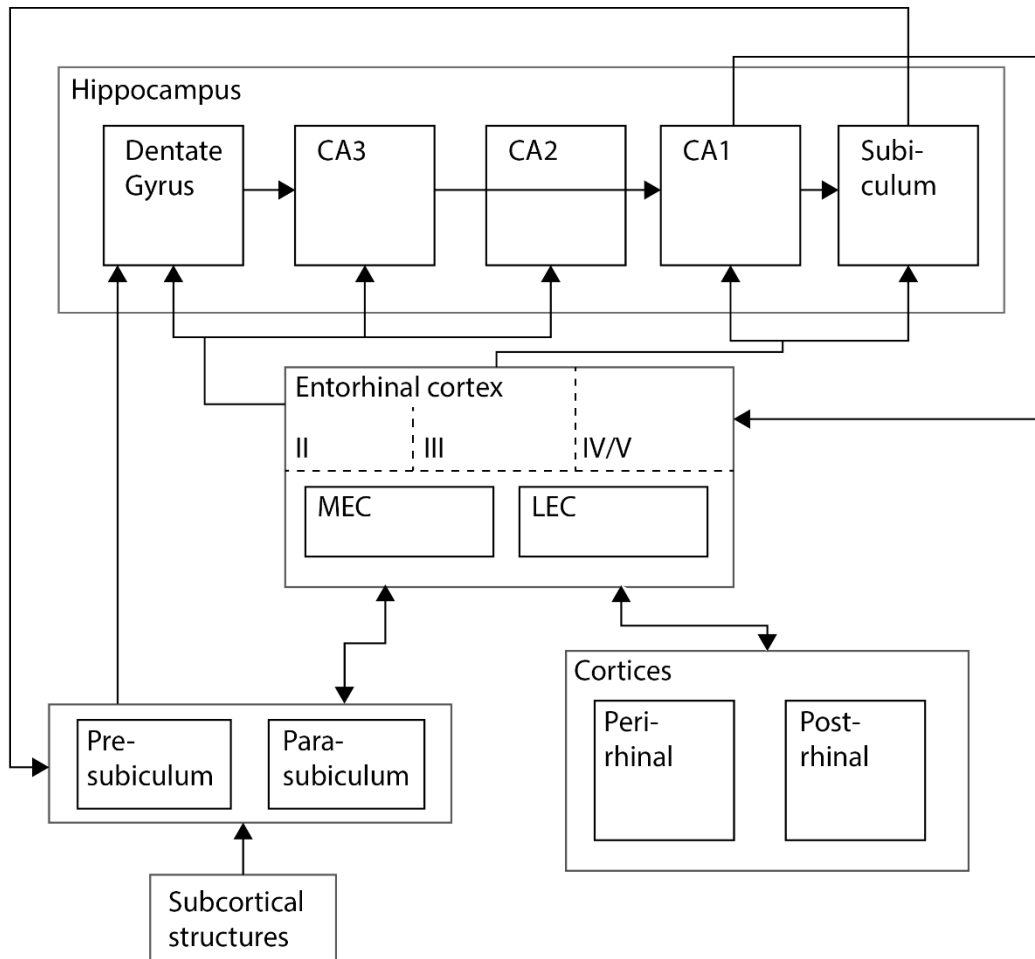


*Fig 1.1. Connectivity of the hippocampal formation. Major pathways connecting the various parts of the hippocampal formation. Arrows indicate the direction of the connections.*

The main excitatory cells in CA1 are the pyramidal cells, which have pyramid-shaped cell bodies and prominent dendritic trees that extend out both apically and basally across the various layers of CA1. These cells receive GABAergic inputs from the axo-axonic and basket interneurons on their axon-initial segment and cell body respectively [18]. The Schaffer collaterals from CA3 innervate the CA1 pyramidal cells both on the apical and basal dendrites, whereas the EC connects on the apical dendritic tuft in stratum lacunosum moleculare. These

various inputs on the different parts of the CA1 pyramidal cell allows it to integrate a range of signals, performing its critical function in memory and navigation [18].

## 1.1 Spatial representation in the hippocampus

The hippocampus has been suggested to hold a spatial map of the environment [22]. The basis of this map are place cells, pyramidal cells that are active selectively in a certain location, called the place field [23]. Together, place fields cover an entire environment, thus forming a spatial map of the environment. Initially it was believed that each unique environment had a single spatial map associated with it. However, more recently it has been shown that the hippocampus can have concurrent maps of the same environment, with cells switching between these maps on separate visits to the same environment [24]. Within a single visit each map is largely stable, and these stable representations can remain for weeks to months. When an animal switches environments, the place fields of individual place cells will change location, a phenomenon called remapping [25].

Although the spatial map was the earliest [26], and is probably still the most prevalent theory of how the hippocampus mediates navigation, other theories have recently gained traction [27,28]. For example, it has been proposed that the hippocampus encodes not just space as a cognitive map, but any structured relationship, but we just so happen to investigate it most in spatial tasks [27,29]. Alternatively, the predictive map theory is based around the idea that rather than place cells reflecting the animal's current position, they reflect a prediction of the upcoming states [28]. As these states are not necessarily spatial, this theory explains how the hippocampus can encode non-spatial paradigms [30].

### 1.1.1 Place cells

Place cells are selectively active at a certain location in an environment, the place field (Fig 1.2). They have distinct place fields in one-dimensional [31], two-dimensional [23], and even

three-dimensional space [32,33]. The speed at which an animal is running affects place cell activity, with higher speeds equating to higher spike rates overall [34]. In 1D environments, their place activity is often directional, meaning they will only fire when traversing the fields in one direction but not the other [31,35,36].



*Fig 1.2. Example place cell. A model place cells firing action potentials (left, red dots) while a mouse is running through an environment (left, black line). Right shows the average ratemap of the firing, with more yellow indicating an increased spike rate.*

When moving between different environments, or when significant changes are made to an existing environment, place cells remap [25,37]. This was first examined by Muller and colleagues [25], who performed a study in which animals were exposed to a grey environment with a white cue card. Upon changing the wall on which the cue card was located, the place cells remapped, by rotating with the cue card. In addition, they changed the environment size and shape, and showed a subset of cells remapped completely when the size was changes, whereas all cells remapped when the shape of the environment was changed. Lastly, introducing a barrier in an existing firing field, caused the field to disappear. A follow-up study showed that replacing a white cue card with a black cue card also elicited remapping [38], but

only after the animals had become familiar with both cards, thus suggesting a role of experience in remapping.

Jeffery and Anderson made the distinction between geometric cues (e.g. shape or size of the environment) that caused cells to change to location of firing, based on earlier modelling work [39], and contextual cues (in their case the colour) which determine whether a cell fires or not. Leutgeb et al. [40] divided the types of remapping into two different distinct forms. Rate remapping involves a minimal change in location of firing for the place cells, but a change in the firing rate, which Leutgeb et al. [40] showed is caused by modular changes to the environment, such as shape or colour. In contrast, global remapping involves place fields moving to new locations, which is caused by moving the environment into a new location, i.e. moving the experimental setup into a new room [40].

However, these rules for rate compared to global remapping do not necessarily persist between experiments with different paradigms. For example, in a two-compartment experiment with identical compartments in different locations, which should induce global remapping according to Leutgeb et al. [40], some cells showed the same maps across the compartments, while others differed between the two [41]. In another multicompartment experiment, where each compartment looked the same but had a different spatial location, only rate remapping was found, but changing the wall colour of one of the compartments caused place cells to change their place field for that environment [42]. Indeed, remapping can be modular, where some environmental changes cause some cells to change their place field location, but not others [43]. So far, this has only been found for contextual changes, particularly the colour and odour of the environment, and not the geometric changes, such as location of the environment. Although a breadth of studies have sought to characterize the changes that could induce remapping, which include shape [40,44,45], size and location [40] of the environment [25]; the visual cues in an environment [25,46]; and the colour of the walls

[40,43,45,47], remapping remains largely unpredictable, and the underlying process causing the remapping is not fully understood. Therefore, one of the key aims of this thesis is to determine how remapping responds to novel manipulations of the environment to build on this work. Specifically, we introduce novel object location as a possible manipulation to induce remapping, which is a relatively small geometric change to the environment, but requires spatial memory, and is highly salient to the animals [48].

Although place cells are often considered as a singular population, their characteristics can vary greatly along the axes of CA1 [49]. Along the radial axis, where deep and superficial layers can be distinguished, place cells respond differently to cue-poor and cue-rich environments [17]. While superficial place cells respond strongly to cue-poor environments and use a rate code to represent these, deep place cells encode cue-rich environments with a phase code. Along the proximodistal axis, place cells have varying spatial specificity, with those more proximal showing smaller place fields and a higher degree of activity phase-locked to the hippocampal theta rhythm, one of the key hippocampal oscillations [13]. These variations along the axes of the hippocampus allow it to encode environments with varying amounts of cues on different scales, which is likely to be vital for animals who will encounter a wide range of environments in the wild.

### 1.1.2 Beyond egocentric location

In addition to place cells, the hippocampus also contains other spatial cells. Landmark-vector cells are active when an animal is in a particular location relative to an external cue. They respond to all or a subset of the same cues (e.g. objects) in an environment [50]. Similarly, reward cells are always active when the animal is in a reward location, and will follow the reward if it is displaced [51]. Although both these types of cells still have a spatial component, as they are active when the animal is in a certain location relative to a cue, they critically differ from place cells in that they follow distinct cues, rather than map the global environment.

A proportion of place cells has been found to respond to another animal's location in both rats and bats [52,53]. Sometimes cells responded to the same location both when the animal itself, or when another animal occupied it, while other cells purely responded to its own or the other's location [52]. These cells are markedly distinct from landmark-vector and reward cells, as they are allocentric rather than egocentric, meaning they respond to the location of an external cue, in this case another animal, regardless of the animal's own location relative to a cue.

In addition to these cells with a spatial component, the hippocampus also contains non-spatial cells [30]. In a task where a mouse was exposed to a tone that gradually rose in frequency, some cells responded specifically to a certain frequency [30]. Although this is a non-spatial task, it could still be explained as a state space, as the relationship between one tone and the next remains the same (i.e. a tone of 10 Hz is always followed by a tone of 11 Hz). This fits in with the idea of the hippocampus encoding sequential information of any kind, spatial or not [27,28].

### 1.1.3 Beyond the hippocampus

Place cells are not unique to CA1 or even the hippocampal formation. Several studies have recently found place cells in the visual cortex [54–56]. These studies cleverly distinguished between visual signals and location, by replicating the same visual scene at multiple locations. Purely visual cells should respond to both visual scenes equally, but the visual cortex also contained cells that only responded in one location, suggesting a location-specific effect. Place cells can be found throughout higher visual areas, but it is not yet clear how spatial information reaches these areas [56].

The medial entorhinal cortex (mEC), which is part of the hippocampal formation and provides inputs to CA1, contains grid cells [11]. These are cells that are active in a hexagonal grid-like pattern throughout an environment. Because of the direct connection between mEC and CA1,

the grid cells are thought to play an important role in modulating place cell firing [57,58].

However, alternative theories pose that grid cells form a scaffolding for path integration, while place cells are for the most part independently modulated by sensory inputs [58,59].

In addition to grid cells, the hippocampal formation also contains a range of other cell types which are relevant for navigation. The subiculum is the main site of head direction cells, which are active when the animal is facing a certain direction, though they are also found in other parts of the hippocampal formation [60,61]. Both subiculum and mEC contain border cells, or boundary-vector cells, which fire selectively near walls and other borders in an environment [62,63]. Both within CA1 and the wider hippocampal formation new cell types are still being discovered, such as the reward cell and object-vector cells [51,64], making it likely more are yet to be found. The exact function each of these spatial cell types play in navigation and how they interact, is yet to be uncovered.

## 1.2 Network activity in the hippocampus

Activity of single cells across the hippocampus, forsooth the entire brain, are modulated by network activity, as measured by the local field potential [65,66]. This network activity is largely characterized by oscillations at varying frequency bands, which largely depend on the behavioural state of the animal. In the rodent hippocampus the predominant oscillatory bands are theta (4-12 Hz), gamma oscillations (30-150 Hz) and ripples (140-200 Hz) [67,68]. Ripples occur only for irregular short periods when network activity without clear oscillatory behaviour in the lower (theta) frequency range, a state called large irregular activity (LIA), prevails [69–71].

### 1.2.1 Theta oscillations

The theta band includes oscillations of 4-12 Hz [72], which are modulated by the behavioural state of the animal. They occur in the hippocampus both during awake movement and REM

(rapid eye movement) sleep, but are largely absent when the animal is immobile [65,73,74].

When the animal is awake, the amplitude of the oscillations is modulated by the running speed of the animal [75,76]. The medial septum [77,78] and entorhinal cortex [72,79] have both been suggested as possible drivers of theta oscillations in the hippocampus. GABAergic cells in the medial septum, specifically parvalbumin-positive (PV) and hyperpolarization-activated cyclic nucleotide-gated (HCN) interneurons, temporally precede theta oscillations in hippocampus, and as such have been suggested as 'pacemakers' [80].

However, theta oscillations can also arise spontaneously in the absence of either of these brain areas [81]. In addition, theta oscillations exhibit a phase shift along the septotemporal axis of the hippocampus, which cannot be explained by a difference in input from entorhinal cortex or medial septum [76]. It is therefore theorized that theta oscillations in the hippocampus actually arise through separate weakly coupled oscillators along this axis, which arise through local subcircuits, where the medial septum may coordinate or entrain the global oscillation [72,76].

The activity of place cells in the hippocampus is modulated by theta oscillations. Place cells fire at a specific phase in the theta cycle depending on the location of the animal relative to that place cell's field, in a process called phase precession (Fig 1.3) [82]. This is the basis of the phase code, where an animal's position can be read out from when the spikes of a cell occur relative to the theta phase. To what degree cells encode place using a phase code compared to a rate code, where the number of spikes encodes the location, depends on the cue abundance of an environment and the location of cell [83]. Sequences of place cells firing during theta sequences may also reflect future or past paths, depending on the environment and animal behaviour [84].

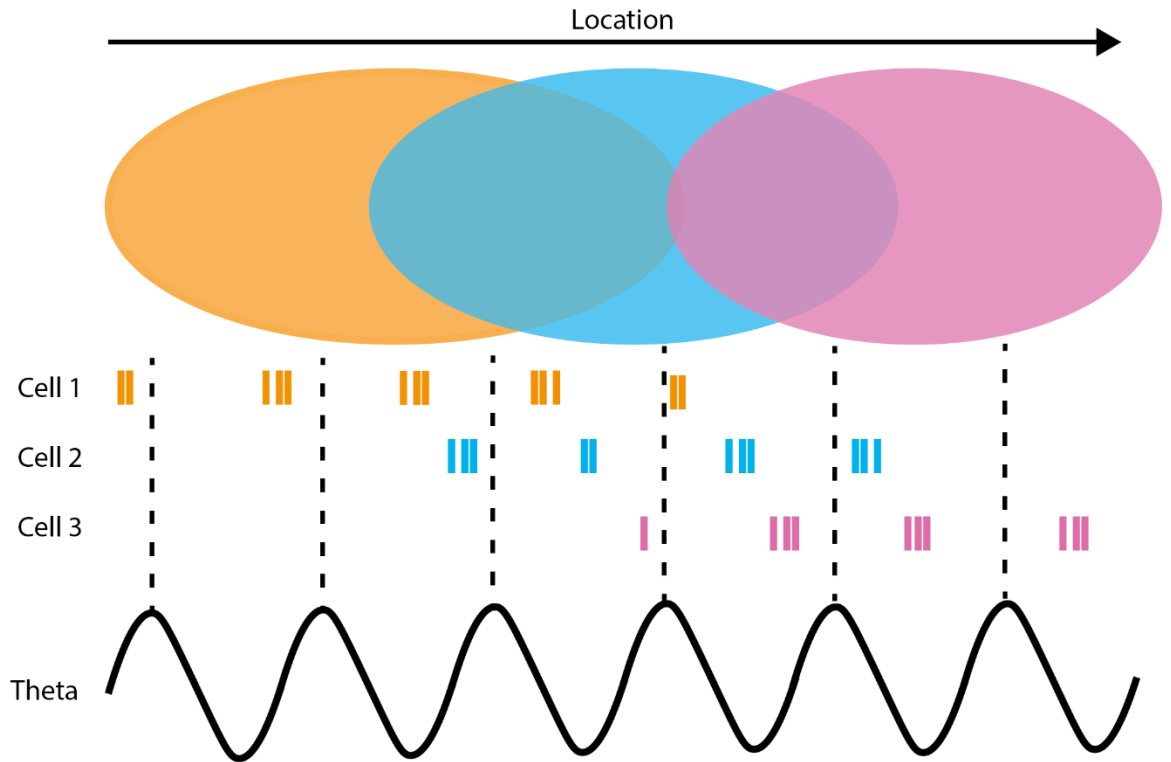


*Fig 1.3. **Phase precession.** Top ovals show the place field of three example cells. As a mouse traverses from left to right, the corresponding cells will fire, showing phase precession relative to the underlying theta oscillations (bottom). Cell 1 will first fire, starting late in the theta cycle. As the mouse progresses through the place field, the action potentials will happen progressively earlier in the cycle. As the place fields overlap, cell 2 will start firing, but later in the cycle, thus causing the cells to fire in a sequence during the cycle.*

In addition to modulating place cell firing, theta oscillations may allow the ability to discretize information, with each cycle corresponding to a single 'package' of information [84,85]. In addition, theta modulation affects learning rates in a spatial task [86]. Theta thus plays an important role not only in spatial encoding through the phase code, but also in separating and organising spatial information and facilitating learning.

Theta oscillations are present continuously during running in rodents, specifically rats and mice, and strongly modulate the place and grid cells. However, this is not the case for other animals, including bats [33], ferrets [87], marmosets [88], and humans [89], raising questions about the role of theta oscillations in hippocampal functioning. In both humans and

marmosets, theta occurs in short bouts, rather than occurring continuously, during movement, which has been suggested to relate to active exploration [88,90]. In ferrets, theta is continuous both during movement and immobility, when theta oscillations cease in rats [87]. In bats, both place cells and grid cells are able to fire without the occurrence of theta [33,91], though they do still show properties of nonoscillatory phase coding and synchrony [92]. Together, these cross-species findings suggest continuous theta oscillations during movement are not required for the proper function of the hippocampus, at in least in species other than rodents.

### 1.2.2 Gamma oscillations

Gamma oscillations have a frequency of about 25-140 Hz, though definitions vary [93,94]. They were originally divided into slow (25-55 Hz) and fast (60-140 Hz) bands [95], though later studies suggested three bands: slow (30-80 Hz), mid (60-120 Hz) and fast (>100 Hz) [96]. In CA1 gamma oscillations can appear independently of theta oscillations, but the gamma power is overall higher during theta-associated behaviours [97–99]. Like theta, gamma oscillations arise from multiple sources [99]. CA3 largely drives slow gamma oscillations in CA1, while medial entorhinal cortex drives fast gamma oscillations [95]. Local interneurons have additionally been shown to play a role in modulating the oscillations [99–101].

Only a proportion of excitatory pyramidal cells in CA1 are phase-locked to gamma oscillations and they are only phase-locked to the gamma phase in the local network [99]. This phase-locking increases for place cells when they respond to an attended stimulus while distractors are present [102], suggesting a role of gamma oscillations in attention. Single cells can be phase-locked to more than one gamma band at a time [103]. As each gamma band has a distinct source [96], this suggests gamma oscillations may play a role in integration of multiple signals. In addition, the separate bands differentially modulate place cells, with place cells encoding current location during fast gamma, and encoding future locations during slow gamma [104].

Although gamma has been suggested to be important for attention processes, integration of information and communication between brain areas [97,105], much is still unknown about how it functions in the hippocampus and how it affects spatial representation. It is likely theta and gamma oscillations are working in concert to facilitate hippocampal functions [103], and their interaction may depend on the location in the hippocampus, the behavioural state of the animal, or even cell class [106], making it harder to pinpoint the exact mechanisms.

### 1.2.3 Irregular activity and ripples

In the absence of theta oscillations, the network activity is marked by irregular activity [74]. During periods of large irregular activity (LIA), which primarily occur during immobility and slow wave sleep, irregular occurrences of sharp wave-ripples (SWRs) take place [107,108]. These events are combinations of sharp waves, which are propagated from CA3 through the Schaffer collaterals, and high frequency (140-200Hz) ripples [68,107,108].

During these SWRs place cells reactivate in replay events, encoding the path previously taken by the animal [109]. These replay events are crucial for spatial learning and memory [110,111], which likely happens through consolidation of experienced spatial events [112]. Another replay-like event, termed 'preplay', has also been identified, where the cell activity reflects a future rather than a previously experienced path [113]. They are hypothesized to be involved in planning of future actions [114,115].

Periods of LIA are occasionally interrupted by small irregular activity (SIA), when SWRs are absent, both while an animal is awake and asleep [71]. During this time the majority of CA1 cells become silent, while a small portion increases its activity [71,116]. These cells are location-dependent, suggesting they may provide some form of spatial code [71]. Additionally, this state has been linked to increased arousal during sleep, as it can be induced by presenting auditory stimuli during sleep [117]. It has therefore been suggested as an intermediate state of arousal between awake and sleep [117,118].

### 1.3 Virtual reality experiments

Although historically many navigation experiments were performed in real-world environments, in recent years virtual reality (VR) has become an increasingly important technique to study navigation in rodents [31,35,119,120], insects [121–123], fish [124], and humans [125,126]. VR provides a unique paradigm for studying navigation, as it allows animals to perform navigational behaviours while they are restrained to a single location. This makes it easier to perform optical and electrophysiological recordings, such as two-photon imaging [35] or patch-clamp recordings [31], in these animals. Although VR is often implemented as a closed-loop system [127], meaning the animal's movements control its surroundings, one can also perform open-loop experiments, where the surroundings and the movements are unrelated (e.g. [124,128]). This may provide unique insights into how animals use sensory feedback to plan future movements [128,129].

#### 1.3.1 Sensory modalities in virtual environments

Many VR systems are mainly vision-based [127], meaning the animal only gets visual input, often projected onto a screen, but lack of other types of sensory input, such as somatosensory or olfactory. These other sensory modalities, in addition to vision, may be able to drive or improve navigation, and their omission in visual virtual reality can thus impact the representation of these environments. However, the extent to which they impact navigation differs from one sensory modality to the next.

Overall, auditory cues are weak drivers of navigational behaviour, though some inconsistencies exist between species of rodents. Mice are able to perform a version of the Morris water maze task using only auditory cues [130], while rats are unable to perform the Morris water maze task using auditory cues alone [131]. However, the addition of auditory cues to a visual cue results in increased performance in rats, suggesting they can use auditory cues to supplement other sensory cues, particularly visual cues, when they are available.

In natural environments, mice use active whisking to perceive objects around them [132].

Whisking, unlike other sensory modalities, requires the mouse to be next to an object or wall, meaning it can only guide navigation in limited circumstances. Nevertheless, this behaviour likely provides important information about location, as mice are able to use it to discern object location with a high accuracy [133]. In VR environments the mice are often not able to whisk the cues that they see, as they are presented as visual only stimuli, but the effect of this absence of input from the whiskers on the spatial representation in the hippocampus has not been thoroughly tested.

Lastly, both rats and mice can use olfactory cues for navigation [43,134–137]. Mice are able to follow odour plumes around an environment, and use odour gradients to navigate to a location [136]. Olfactory cues also contribute to the stability of place cell firing [137]. The contribution of olfactory cues to navigation has also been studied in a virtual setting, where mice were exposed to odours depending on their location in a virtual environment [138]. In this setting mice could be trained to navigate based on odour, but only after being trained with a combination of visual and olfactory cues. It is thus unclear if olfactory cues alone can drive navigation in a virtual setting, but they certainly contribute to the overall encoding of the environment.

As animals use various sensory modalities, a range of virtual reality setups have been developed to engage these. An auditory VR was developed where mice were able to use auditory cues to determine reward location [139]. However, this task did not necessarily require spatial representation, so the effect of auditory stimuli in VR, or the lack thereof, is still unclear. To study the effects of whisking, another VR system used movable walls to simulate the mice running near, and touch, walls [140]. However, this study only focused on the behaviour of the animals, so the effect of this on hippocampal activity is not clear.

Although animals use various sensory modalities for navigation, and virtual reality setups engaging a range of modalities have been developed, visual-only setups are still the most popular [127]. This is likely because, despite missing out on other sensory modalities, visual virtual reality environments have several advantages [141]. First, researchers can precisely control what (visual) sensory input the animals receive at any given time. Second, they allow for the study of the effect of differences in visual input on spatial representation in the brain, separately from the effects of other modalities. Lastly, the visual environment can easily and quickly be manipulated (unlike e.g. odour), allowing for experiments that would be impossible to perform in real-world conditions.

Mice are able to do a range of tasks in visual VR, and it seems that the key to successful navigation in virtual reality environments is the combination of sensory input and idiothetic cues, such as proprioception. Although idiothetic cues are limited in most setups, especially when animals are head-fixed and cannot get any vestibular input, running alone has a considerable effect on place cell firing [129]. This is also illustrated in a study where mice were unable to run, but were still presented passively with a virtual environment. This discrepancy caused firing in the majority of place cells to alter, with individual cells having reduced firing rates and carrying less information about location. Thus, having a closed-loop system where the mouse is able to run and control the environment is likely to promote place cell stability. Indeed, mice and rats, among other animals, are able to successfully perform navigation in visual only environments, even in the absence of other sensory inputs [31,120,123]. This is likely because both rats and mice rely heavily on visual cues, despite other sensory cues being available. Place cells in rats are strongly affected by visual input [142–144], and when presented with conflicting cues across modalities, they will preferably follow visual cues [145]. In mice, lack of visual cue input disrupts grid cell firing [146], while adding visual cues increases

place cell accuracy [147]. Overall, visual cues seem to be sufficient to drive navigation, making visual virtual environments a powerful tool to probe the neuronal basis of navigation.

### 1.3.2 Place cell activity in virtual environments

Despite animals being able to perform navigational tasks in virtual reality environments, their representation of these is not identical to that of real-world environments. This has been attributed to the lack of vestibular input as well as other sensory elements that might be uncontrolled for in real-world environments [148]. Differences in behaviour, such as running speed or place preferences, may also play a role in the altered representation [148,149]. There is also a wide range of paradigms between VR experiments. Some experiments use a 1D virtual track, where the animal can only run back and forth [31,35,148], while others use a 2D paradigm, where an animal can run in any direction [119,149]. Rats are usually suspended in jackets, allowing for limited movement of their head, while mice are often head-fixed so cannot move their head at all [127]. Although, some systems allow for the mice to physically rotate their head while still being head-fixed [149,150].

These different paradigms will differentially affect place cell activity. On identical 1D virtual and real-world tracks, where a rat is only exposed to distal visual cues, the number of cells active on the track is significantly lower in VR compared to a real-world environment [148]. Although place cells in both conditions hold spatial information, the information content per cell is also lower in VR. In addition, place cells are less stable, with lower firing rates and wider place fields in the VR environment. Together these changes suggest a decrease in spatial representation of the environment in VR settings.

On a 1D track where rats were running back and forth, and were passively rotated at the end of the track in the VR environment, most cells were unidirectional in both VR and real-world. However, the cells that were bidirectional in VR, but not real-world, encoded distance from the start or end of the environment, rather than position along the track, meaning their firing

location in the two directions was at a different location relative to the environment [148]. Though other studies in mice do not report similar findings [35,147], these often do not specifically distinguish between distance and place coding. Therefore, their place cells may indeed include distance-encoding cells, especially as VR recordings in the dark has shown that they exist in mice [151].

In a 2D environment, place cells in rats also showed reduced spatial information, stability and mean firing rate in VR compared to a real-world environment, more so than in the 1D condition [119]. Depending on the task, cells again encoded distance more strongly than location in a 2D VR world, and this distance encoding was increased compared to location encoding when the animals had more stereotyped running paths, such as running from one goal to another. This suggests the distance encoding observed in the 1D task might be caused by a combination of the VR environment and the stereotyped running animals are forced to do by being in a 1D corridor. In another variation of a 2D virtual environment where mice's heads were fixed at a specific bearing, mice were able to freely rotate their head meaning they were able to use vestibular input [149]. Here, similar results were found: the place fields were bigger and place cells contained less spatial information. However, place cells did not have reduced firing rates. In addition, cells also showed increased directionality compared to a real-world environment. Overall, this shows that although head rotation affects place cell firing, the lack of head rotation is not the driving factor for the differences in space encoding between VR and real-world.

Theta oscillations were also altered in VR compared to real-world environments. Using VR causes changes in theta amplitude [119], theta frequency [148,149], reduction of phase precession [119], and reduced or abolished modulation by the animal's running speed [148,149]. As these studies compared directly between VR and real-world, they controlled for any effect of location of the cells [83,152], or differences between animals. The difference in

theta oscillations is thus likely to arise from the difference in sensory input, as well as possibly a difference in behaviour of the animals between the two paradigms.

Although many papers find spatially selective cells in VR environments [31,35,119,147–149], it is clear that their activity is altered compared to real-world environments. This is in part due to a lack of vestibular input, though not entirely, as shown by the persistence of some of the difference in a paradigm where the animal does get vestibular inputs [149]. Other causes may be a lack of unpredicted or unmeasured sensory inputs, such as animals leaving olfactory cues while running through an environment [135]. Overall, these differences should be considered when designing and interpreting VR experiments.

#### 1.4 Aims

Although place cells have been extensively researched, the advance of VR systems has opened up the possibility for new questions to be addressed. It allows for the easy manipulation of environments and precise control of sensory stimuli. Therefore, it is possible to present animals with a range of modular environmental changes and record their place cells responses. VR is often combined with two-photon imaging of cells, which allows for a large number of cells to be simultaneously recorded in a single axial plane. However, this means that traditional measures for place cell identification, using spiking rates for example, cannot be applied. VR itself also creates altered place cell firing. This leads to the question of how place cells should be defined in VR experiments. Lastly, much navigational research has focused on place cells alone, while non-place cells have not received similar attention. It is therefore still unclear how place and non-place cells work in concert to facilitate spatial navigation.

To address some of these questions, this thesis aims to elucidate the effect of environmental manipulations and behavioural correlates on hippocampal populations during a novel behavioural task in a virtual reality environment. Specifically, a population-wide approach was

taken, where not just place cells, but the entire hippocampal population was considered. The research was guided by three aims:

1. To determine the best method for defining place cells, and in doing so, understand how the method by which place cells are defined, affects what cells are included in the population.
2. To understand how cue abundance and displacing a cue object, in addition to training on a behavioural task, affects coding of space by hippocampal populations.
3. To characterize the activity of two novel types of functional cells in CA1 and their relationship to environmental and behavioural factors.

The focus of Chapter 2 is the classification of place cells in two-photon data in a one-dimensional virtual environment. As discussed, place cell responses vary depending on the behavioural and experimental factors, and using virtual reality will also affect their activity. In addition, when VR is combined with two-photon recordings, traditional place cell classification methods cannot be used, but no clear consensus has arisen to identify place cells in virtual reality paradigms. In this chapter, three methods for place cell classification on two-photon data recorded in one-dimensional virtual reality environments are tested for their ability to classify model place cells with varying characteristics. Not only does this elucidate the effects of the various methods on the populations included as place cells, but it also provides a framework for future methods to be tested, thus creating a better understanding, and hopefully a consensus, of what is considered a place cell across various studies.

The optimal method for place cells classification is then used in Chapter 3, which studies the effect of object location novelty and cue abundance during a novel behavioural task in virtual reality. Object location novelty is often used as a benchmark for hippocampal function [153], and objects and their locations have neural correlates in the hippocampus and wider hippocampal formation [46,50,64]. However, previous studies have been performed in freely

moving animals, allowing the animals to perform certain behaviours around the objects, such as sniffing, whisking or rearing. We used a VR task where an object was displaced randomly, and we trained mice to recognize this displacement. This uniquely shows the effect of visually seeing an object in a novel location, without the confounding effect of the behaviours around the object. In addition, we manipulated the cue abundance of the environment and studied whether the two manipulations showed modular effects on the hippocampal populations. We found that place cells particularly, and the wider hippocampal population in general, are strongly modulated by object location novelty, but not cue abundance, resulting in an increased encoding of animal location when an object in the environment was displaced. This effect was present even in untrained animals, suggesting it was not an effect of the task, though the encoding does change with training. Overall, the results give an increased understanding of the representation of object location novelty in the hippocampus, and increased understanding of how modular changes to an environment affect hippocampal populations.

In Chapter 4 the wider hippocampal population is examined, with a focus on activity at rest, which leads to the discovery of two novel functional cell types. SLO (stationary low-frequency oscillatory) cells are a small population of cells that are active at 2-5 second regular intervals while the mouse is immobile during a behavioural task. They are highly synchronous and show location specificity, suggesting possibly a role in retaining spatial information during rest. We also identify a running-active population of cells with a high power in a low (0.2-0.5 Hz) frequency band, which show aperiodic activity (ORLA cells: odd running-active low-frequency aperiodic cells). Overall, this research examines the activity of cells during an understudied behavioural state, and importantly linking individual cell activity to overall network behaviour. This shows the importance of hippocampal cells not just during active navigation, but also when an animal is at rest.



## 2 Choice of method of place cell classification determines the population of cells identified

Grijseels, D.M.<sup>1\*</sup>, Shaw, K.<sup>1</sup>, Barry, C.<sup>2</sup>, Hall, C.N.<sup>1\*</sup>

<sup>1</sup> School of Psychology and Sussex Neuroscience, University of Sussex, Brighton, United Kingdom

<sup>2</sup> Research Department of Cell and Developmental Biology, University College London, London, United Kingdom

\* Corresponding authors

Email: [catherine.hall@sussex.ac.uk](mailto:catherine.hall@sussex.ac.uk).

Email: [D.Grijseels@sussex.ac.uk](mailto:D.Grijseels@sussex.ac.uk)

## 2.1 Abstract

Place cells, spatially responsive hippocampal cells, provide the neural substrate supporting navigation and spatial memory. Historically most studies of these neurons have used electrophysiological recordings from implanted electrodes but optical methods, measuring intracellular calcium, are becoming increasingly common. Several methods have been proposed as a means to identify place cells based on their calcium activity but there is no common standard and it is unclear how reliable different approaches are. Here we tested four methods that have previously been applied to two-photon hippocampal imaging or electrophysiological data, using both model datasets and real imaging data. These methods use different parameters to identify place cells, including the peak activity in the place field, compared to other locations (the Peak method); the stability of cells' activity over repeated traversals of an environment (Stability method); a combination of these parameters with the size of the place field (Combination method); and the spatial information held by the cells (Information method). The methods performed differently from each other on both model and real data. In real datasets, vastly different numbers of place cells were identified using the four methods, with little overlap between the populations identified as place cells. Therefore, choice of place cell detection method dramatically affects the number and properties of identified cells. Ultimately, we recommend the Peak method be used in future studies to identify place cell populations, as this method is robust to moderate variations in place field within a session, and makes no inherent assumptions about the spatial information in place fields, unless there is an explicit theoretical reason for detecting cells with more narrowly defined properties.

## 2.2 Author Summary

Place cells are hippocampal cells that have spatially constrained receptive fields, the place field. These cells have been widely studied in the context of navigation, more recently using virtual reality environments in combination with optical methods of recording neuronal activity. However, there is a lack of consensus regarding how to identify place cells in these data. In this study we tested the sensitivity and specificity of four methods of identifying place cells. By comparing these methods and quantifying the populations of place cells they identify, we aimed to increase our understanding of exactly the populations that are currently being studied under the name “place cells”. Although the appropriate method may depend on the experimental design, we generally recommend a single method going forward, which will increase consensus within the field about what should be included in a place cell population, and allow us to better compare results between studies.

## 2.3 Introduction

Place cells are a subset of hippocampal pyramidal cells that fire selectively when the subject is in a certain location [23], and provide a sparse population code for self-location. Studies revealing their properties, including location-specific firing [23], directional selectivity [34] and context-dependence [43] have been vital for our understanding of how the hippocampus codes space. [154]. Place cells are characterised by their place field, which is a spatially stable location where the cell preferentially fires. Depending on the size of the environment, place cells can have one or multiple place fields [155]. The place fields may change location between different environments, a phenomenon called remapping. Place cells are also relevant to understanding clinical conditions such as Alzheimer's disease, as in mouse models of Alzheimer's disease they show impaired firing [156] linked to memory deficits.

Since their discovery, place cells have been extensively studied in real world environments – both open field and constrained - using electrophysiological recordings while animals either explore freely or perform directed spatial tasks. In these studies, cells are generally included in analyses based on a variety of properties, including their peak firing rate, waveform, sparseness of the place field or spatial selectivity (e.g. [32,43,157,158]). Further analyses sometimes requires the place fields of these cells to have additional properties, such as a maximum number of place fields allowed, or a stable place field over time (see e.g. [32,157,159]).

However, methodological advances now also allow place cells to be studied in vivo using calcium imaging [35,160,161], enabling large populations ( $n > 100$ ) of cells to be recorded for multiple sessions. This method requires the brain to be stationary during recording, which necessitates the use of a Virtual Reality (VR) environment. Often a visual VR is used during imaging, consisting of one or multiple screens displaying an environment that the mouse can control by running on a ball or wheel. With a ball, the mouse is able to move in two

dimensions (e.g. [162]), whereas with a wheel, mice can only move backwards and forwards. These types of VR limit the animal's ability to look around, and provide sparse sensory feedback; for example, whisking does not provide information about the environment. Place cells also respond differently in VR environments compared to the real world, showing broader place fields and increased directionality [149].

Several studies using one-dimensional environments (i.e. corridors) have revealed that hippocampal pyramidal cells represent other features in addition to location, such as reward [51] and travelled distance [151]. It is unclear to what extent these features are coded by separate populations of cells in the hippocampus or cells that, under other circumstances such as a dedicated navigation task, might be recruited as place cells. To resolve this, it is important to be able to accurately define place cells within such one-dimensional environments, but currently different studies use widely varying methods making comparisons between studies problematic.

Varying definitions of place cells have been chosen to account for the constraints imposed by the imaging methodology. Unlike electrophysiological recordings, imaging detects changes in intracellular calcium levels rather than direct readouts of action or synaptic potentials. The non-linear relationship between calcium transients and spike rates makes it hard to accurately estimate spike rates from two-photon data [163], so adopting exactly the same methods as used in electrophysiological recordings is not possible. In addition, the exact waveform of the spikes, another characteristic used to classify place cells (e.g. [32]), is unknown. Instead, studies have tended to use adaptations of some, but not all, of the imaging equivalents of peak firing rate, sparseness of off-location firing, and place field stability to define a cell as a place cell: Dombeck et al. [35] categorised a cell as a place cell based on a combination of properties of that cell's apparent place fields, including the size, peak calcium fluorescence and the ratio of the firing within and outside the field. This method, or variations of it, have subsequently

been adopted in several studies (e.g. [21,164,165]). Fournier et al. [166] proposed a statistical method that uses the peak activity in the rate map of a cell and compares it to the peak activity in shuffled versions of the cell. An alternative approach [167] detects place cells from the stability of their activity as a function of location, a method based on those used in electrophysiology experiments [43]. Lastly, Ziv et al. [168] defined place cells based on the mutual information between the cells and the location of the animal, a method which is also used widely [24,169,170]. However, it is unclear what biases these different methods exhibit and to what extent their classification criteria are equivalent – in short, do they identify the same neurons as place cells?

In this paper we aim to address the lack of consensus on how to identify place cells in two-photon data in a one-dimensional VR environment. We compare the performance of two established methods for the identification of place cells in two-photon data (the methods used by Dombeck et al. [35] and Ziv et al. [168]), another method that is often used to characterize place cells in electrophysiological studies (e.g. [32,43], described by O’Leary et al. [167]) as well as one method developed for use on electrophysiology data which has been adapted for use in imaging – described by Fournier et al. [166]. We applied them to a range of synthetic model cell populations to explore whether cells identified as place cells by each of these methods possess similar characteristics. We conclude that in a range of mock datasets the method developed by Fournier et al., which we call the Peak method, is best suited to identify place cells, having a high sensitivity and specificity, and lacks assumptions about spatial information held by the place cells. As a result, we recommend this method for the identification of place cells in two-photon imaging data. Our data also show that choice of identification method is important, as the methods classify different, largely non-overlapping populations of cells as place cells.

## 2.4 Results

### 2.4.1 Place cell detection by the Combination and Stability methods is sensitive to the properties of place fields and the number of times mice traverse the environment

We evaluated the performance and suitability of four different approaches for detecting place cells (S Fig 2.1):

- 1) The Peak method, which classifies cells as place cells based on the average rate of firing (approximated by fluorescence change in two-photon data) in one location being higher than in the rest of the environment [55];
- 2) The Stability method, which identifies place cells as those with stable firing patterns across locations over time [167];
- 3) The Combination method, which requires place cells to fire more across a contiguous stretch of the environment than at baseline and to fire in this location on at least 20% of traversals [35].
- 4) The Information method, which classifies cells based on the increased amount of spatial information the cells hold about the animal's location [168].

We selected the four methods for varying reasons. The Peak method was originally applied to electrophysiological data, and its simplicity allows for the application to fluorescence data with minimal adaptations. Similarly, the Stability method was based on methods used for characterising place cells in electrophysiological recordings (e.g. [3]), while the Information method, or variations thereof, have previously been used to detect place cells in both electrophysiological [170] and fluorescence data [24]. This makes these three methods promising candidates for application across the two recording paradigms. In contrast, the

Combination method was designed specifically for fluorescence data, and has been widely employed in the field (e.g. [35,165,169]).

To characterise the four different approaches for detecting place cells we applied them to synthetic datasets consisting of 20 true place cells and 80 random cells, matching the prevalence of place cells found using patch-clamp recordings [31]. Mouse location for each dataset was generated using experimentally acquired locomotion time courses from mice running through a linear virtual reality environment (S Fig 2.2, 8 datasets: 4 mice, 2 sessions per mouse). The dataset contained a total of 184 traversals of the environment, with mice running 23 traversals per session on average. Model fluorescence maps were generated by applying the synthetic cell profiles to 50 randomly selected traversals (Fig 2.1A and B). Periods where the mouse was not running – defined as having a velocity below 2 cm/s – were removed (Fig 2.1C and D).

Fluorescence maps of the place cells were modelled using a Gaussian to simulate changes in fluorescence as a function of location, where the mean determined the place field centre and sigma the field width. We used a default width of 50 cm, based on widths previously reported in a virtual environments [31,35]. Synthetic data was linearly scaled to match the peak values observed in our own two-photon CA1 data (Fig 2.1E). We distributed place field centres evenly across the 200 cm long track, then convolved the place field with the position of the mouse to determine the fluorescence map of each cell over time (Fig 2.1E, bottom 20 cells, Fig 2.1F). We also included 80 control cells (Fig 2.1E, top 80 cells, Fig 2.1G) without place-dependence. Poisson noise, which in the default model had an average fluorescence of 0.18% of the default peak height, was then added to the traces of all cells. Lastly, the four different place cell classification methods were applied to these fluorescence maps.

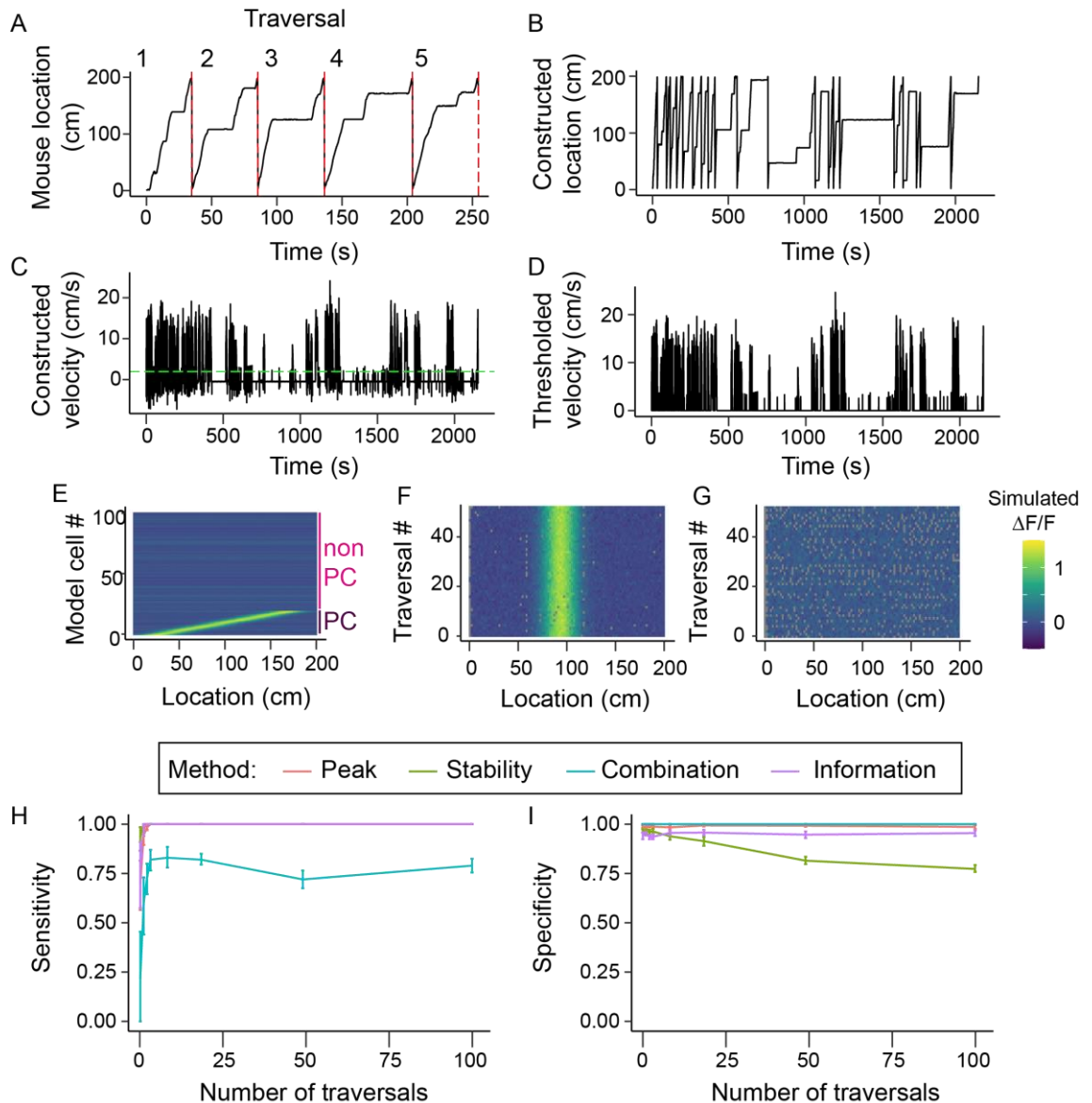


**Fig 2.1 Model locomotion profile generation and effect on methods.** (A) Section of a locomotion profile collected in a 200cm long virtual environment. This was cut into individual traversals of the environment (numbered, separated by red dashed lines) (B) locomotion profile generated from 20 randomly selected traversals. (C) Velocity profile of the locomotion profile shown in B. The green dashed line indicates the threshold for detecting running (2 cm/s) (D) Trace in C after thresholding. Time points with below threshold velocity were excluded from further analysis. (E) Fluorescence maps of 20 model place cells (cells 1-20) and 80 non-place cells (cells 81-100). (F) Activity over location of a single model place cell over 50 traversals. (G) Activity over location of a single non-place cell over 50 traversals. Grey points in F and G are missing data caused by the mouse across this location between acquisition of two frames. (H) The sensitivity of each method as a function of the number of traversals included in the locomotion trace. (I) The specificity of each method as a function of number of traversals. Lines in (H) and (I) show means over 10 randomly generated data sets. Error bars represent 95% confidence intervals.

We could therefore vary the parameters that determine the fluorescence map (Gaussian peak, width and location, number of traversals of the environment), each with a different effect on the properties of the model cells (S Fig 2.3), to determine how much the properties of the place field affect their detection by the different methods. To assess place cell classification performance, we first calculated how many place and non-place cells were correctly identified by each method (true positives and true negatives), versus the number of false positive and false negative identifications. From these values, we then calculated the sensitivity (the proportion of place cells that were correctly detected), and the specificity (the proportion of cells identified as place cells that actually were place cells) of each method (Methods, equations (1) and (2)). A perfect detection method would therefore have a selectivity of 1 and a specificity of 1.

*Number of traversals.* First, we determined the impact of the number of times the mouse ran through the environment on place cell detection by varying the number of traversals used to generate the model datasets from 2 to 100 (Fig 2.1H and I). We generated 10 model datasets for each number of traversals.

The Peak, Stability and Information methods had a high sensitivity regardless of the number of traversals included in the dataset (Fig 2.1H). Both the Peak and Information methods also displayed a stable specificity across the range of traversals, with a mean of 0.99 and 0.95 respectively, reflecting their requirement that a true place cell's activity is in the top 1% and 5% (respectively) of shuffled data (Fig 2.1I). However, the Stability method saw a decreasing specificity with an increase in traversals, with a specificity of 0.76 at 100 traversals, i.e. more non-place cells were classified as place cells as the number of traversals increased. This is likely because with an increase in traversals, the Poisson noise of the non-place cells will increasingly average out over the traversals, thus resulting in an increased correlation between the fluorescence maps of the first and second halves of the session for the non-place cells. This

increases the number of false positives, and thus results in a decrease in specificity. The Combination method increased in sensitivity as the number of traversals increased from 2 to 20, above which it stabilised with a sensitivity of 0.79. The specificity of this method remained 1 regardless of the number of traversals included.

Thus our simulations predict that the Combination method would fail to detect at least 27% of hippocampal place cells, while up to 23% of the place cells identified by the Stability method would be false positives, and accuracy for both methods is affected by the number of times mice run through the environment.

*Place field properties.* We next tested the effect of manipulating the width of the model place fields and their peak “fluorescence” on the ability of the four methods to detect the place cells (Fig 2.2C-F). First, we varied the width of the place field between 20 and 200 cm, equivalent to 10 to 100% of the total environment length, while keeping the peak value at a  $\Delta F/F$  of 1.3 (see S Fig 2.4 for example place cells). For the Peak, Stability and Information methods, varying place cell width did not materially affect sensitivity. However, the sensitivity of the Combination method was generally lower than the other methods, only approaching their sensitivity for place fields between 80 and 120 cm, and failing to detect any place field narrower than 40 cm or broader than 160 cm. Specificity of place cell detection was high for the Peak, Combination and Information methods and unaffected by the place field width, whereas it was generally lower when using the Stability method (Fig 2.2D). It increased linearly with place field width for this method, presumably because the correlation between the fluorescence maps of the non-place cells and place cells decreases as the width increases.

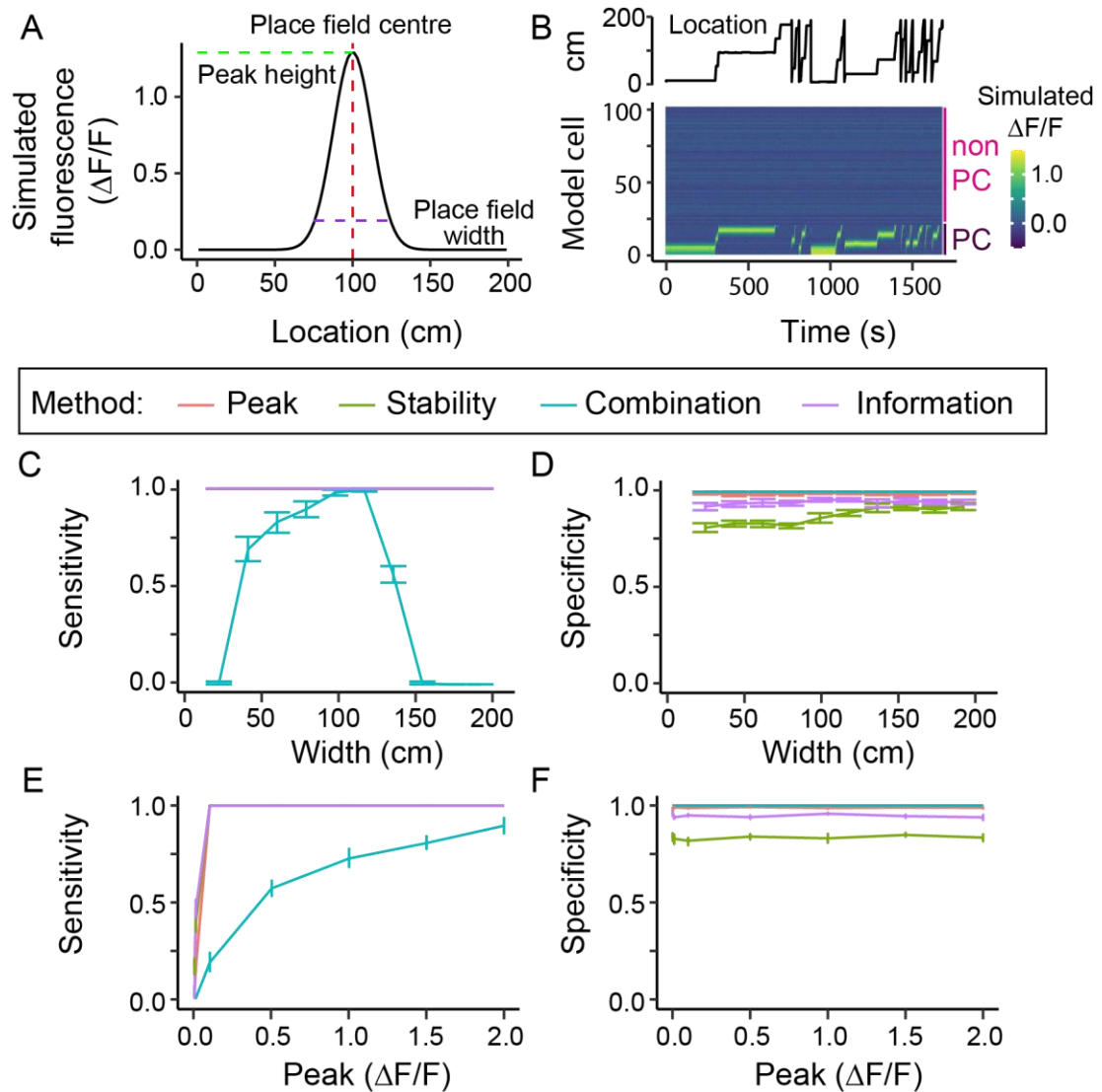


**Fig 2.2 Place cell model and its effect on place cell detection.** (A) Gaussian model of the fluorescence of a place field depending on the location (x-axis). The model takes the following parameters: the centre of the place field (red dashed line), the place field width (purple dashed line) and the peak of the Gaussian (green dashed line). (B) example fluorescence profile over time of a model data set containing 20 place cells (cells 1-20) and 80 non-place cells (cells 21-100), generated using the location trace shown. (C, E) Specificity and (D, F) sensitivity of the different methods as a function of the place field width (C, D) or peak (E, F). Note in D all methods except the Combination method had a sensitivity of 1 across all widths, and the lines overlap. In E there is similar overlap for peak values above 0.1. Data are means of 10 simulations. Error bars represent 95% confidence intervals.

We then varied the peak of the place field between a  $\Delta F/F$  of 0.0001 and 2 (equivalent to 0.008% to 155% of the average fluorescence map peak measured in our two-photon data), keeping the place field width at 50 cm. Sensitivity was only affected using the Peak, Stability

and Information methods at extremely low, and therefore unrealistic, peak values ( $< 0.1$ , or fewer than 8% of peaks in our real data; Fig 2.2E). The sensitivity for the Combination method was generally lower and increased with place cell peak size. The specificity was not affected by changes in peak values for any of the methods (Fig 2.2F).

Next, we varied the number of place fields for each place cell, up to 4 place fields per cell (S Fig 2.5). The Peak, Stability and Information methods were able to identify the model place cells, regardless of the number of place fields, with a high sensitivity, while the Combination method showed a dramatic drop in sensitivity above 2 place fields. Specificity was relatively unaffected in all methods by increasing the number of place fields, though was maximal using the Stability method when cells had 4 place fields.

Finally, we varied both the place field width and peak values at the same time (S Fig 2.6). The results reflect those when varying each parameter individually, illustrating the high general sensitivity of the Peak, Stability and Information methods and the much narrower performance of the Combination method, which has high sensitivity at only a narrow range of widths and with high peak fluorescence values. Conversely specificity is high overall for the Peak, Combination, and Information methods, but for the Stability method is lower across the range of parameters tested and lowest for narrow place fields.

In summary, the Combination method detected fewer model place cells and was the most affected by realistic variations in place field properties, while the Stability method classified more non-place cells as place cells and this tendency increased with narrower place fields. Both the Peak and Information methods were sensitive and specific over the whole range of place field properties tested, though the Peak method slightly outperformed the Information method, having a higher specificity.

#### 2.4.2 Variability and reliability decrease detection of model place cells, particularly by the Combination method

Because, physiologically, cells do not fire with identical profiles to repeated presentations of a stimulus [171], we simulated how the inherent variability of place cells affected their detection by the different methods. We manipulated the reliability of place cell responses by varying the percentage of traversals in which they fired (Fig 2.3A) and the location of the place field centre, by shifting the position of the activation peak with respect to the average firing field a percentage of the place field width (Fig 2.3B). The exact traversals that cells fired in were uniformly randomized, while the exact deviation of the place field centre was randomized using a Gaussian probability curve, and was repeated 10 times for each parameter.

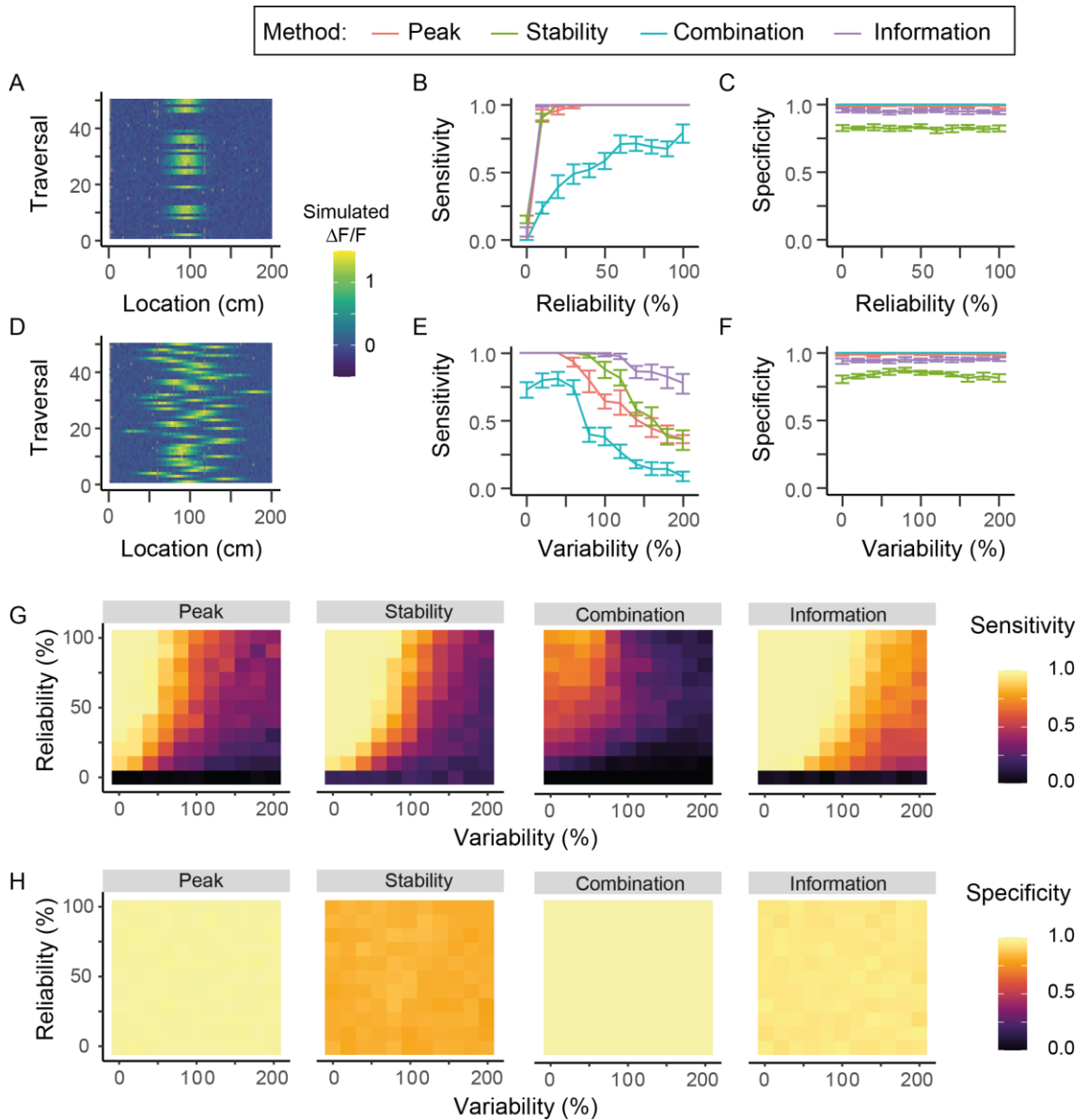


**Fig 2.3 Place cell identification in variable and unreliable place cells.** (A) Fluorescence map for a place cell with a reliability of 40% (B) Sensitivity of methods as a function of the reliability of a place cell. (C) Specificity of methods as a function of reliability. (D) Fluorescence map for a place cell with 60% variability. (E) Sensitivity of methods as a function of the variability of a cell's place field across different traversals. (F) Specificity of methods as a function of variability. (G) Surface plots of the sensitivity of each method as a function of both reliability and variability. (H) Surface plots of the specificity of each method as a function of both reliability and variability. Grey points in A and D indicate the mouse did not record at that location in that particular traversal, due to the limited frame rate of our recordings. Data shown are the means of 10 randomly created datasets, with the error bars representing 95% confidence intervals.

The Peak, Stability and Information methods increased their sensitivity as cells became more reliable, reaching a maximum when cells fired in over 30% of traversals. The Combination method also increased in sensitivity with increased reliability, but at a slower rate, reaching a lower maximum sensitivity only when cells fired in 100% of traversals (Fig 2.3C). Varying reliability did not affect the specificity of any of the methods (Fig 2.3D). The effect of reliability on the Peak and Information methods comes not from any explicit comparison of cells across traversals, but because unreliability decreases the size of the place field peak in the average fluorescence map, due to the existence of traversals in which the cell is inactive.

Increased variability of the location of the place field centre caused a reduction of sensitivity above 50% variability for the Peak and Combination methods, above 80% variability for the Stability method, and above 120% for the Information method (Fig 2.3E). Specificity of all methods was again unaffected by changes in variability (Fig 2.3F).

When changing both the variability and reliability, results were again similar to varying each individually, with maximal sensitivity for all methods occurring when cells had high reliability and low variability (Fig 2.3G), and stability being similar across all conditions (Fig 2.3H).

Overall, the Information method had the highest sensitivity, especially across highly variable model cells. However, its specificity was lower across the board than the Peak method, for which the sensitivity was lower at a high variability. This difference is likely due to the respective percentile thresholds (99<sup>th</sup> for the Peak method and 95<sup>th</sup> for the Information). The response pattern of the Peak method is arguably preferable in this instance, as highly variable cells which are active in different locations from traversal to traversal do not fit within what is understood to be a place cell. Conversely, the Combination method's sensitivity was decreased by even small decreases in reliability, while the Stability method was more robust than the Peak method to high variability, but less so compared to the Information method, and had low overall specificity.

### 2.4.3 Place cell parameters affect methods differently in variable populations

Although the modulation of the various place cell parameters (peak, width, reliability and variability) illustrate the effect of the singular parameters on the performance of the methods, having the same parameter setting for each place cell is unlikely to reflect real place cell populations. Moreover, we only combined 2 subsets of parameters (peak and width, reliability and variability), but not all four. Therefore, to mimic a more realistic model population, we performed a further simulation, where we randomly selected a place field peak, width, variability and reliability for each individual cell of the population (Fig 2.4A). As a result, each of the 100 cells in the population had a different combination of these parameters. In this simulation, we did not include control cells, as we expected enough modelled cells to behave unlike place cells (i.e. those with a low reliability, high variability, low peak and/or high width, Fig 2.4B). We repeated this simulation 20 times, each time determining the percentage of cells classified as place cells by each of the methods.

We found a significant difference in the number of place cells identified by each of the methods (Fig 2.4C,  $p=1.14 \times 10^{-14}$ , repeated measures ANOVA), with the Information method detecting the highest number (65.6 +/- 5.7% (mean +/- std)), followed by the Peak method (40.2 +/- 5.3%) and the Stability method (27.8 +/- 3.4%), while the Combination method only classified 10.2 +/- 3.4% of cells as place cells. Interestingly, despite the Stability method having a high sensitivity and low specificity in the previous simulations, this method classified a lower number of cells as place cells compared to the Peak and Information methods, which previously had a higher specificity. This is likely because the increased variability of the population will cause an increase in the intercell correlation compared to the simulations where the place fields were all strictly in different positions and equidistant from each other. This will therefore cause an increase in the correlation threshold required for cells to be

included as place cells, and thus an increase in specificity and decrease in sensitivity, resulting in a lower number of cells included as place cells overall. At the same time, on average the place cells will be less correlated than in our previous simulations, where cells always were highly consistent in all but the manipulated variable, and thus fewer are presumably sufficiently correlated to be classified as place cells (e.g. many will have higher variability and lower reliability so activity will vary from traversal to traversal).

We were interested to see if the same model place cells were identified by the different methods, or if different methods identified independent populations. To this end, we determined the overlap between each of the methods (Fig 2.4D), and compared this to the overlap expected by chance. All combinations of methods had a higher overlap than expected by chance (Fig 4D,  $p=4.4 \times 10^{-15}$ ,  $p=2.2 \times 10^{-10}$ ,  $p=2.2 \times 10^{-16}$ ,  $p=5.8 \times 10^{-10}$ ,  $p=4.4 \times 10^{-15}$ ,  $p=2.1 \times 10^{-10}$  for the Peak-Stability, Peak-Combination, Peak-Information, Stability-Combination, Stability-Information and Combination-Information comparisons respectively, paired t-tests with Holm-Bonferroni correction for multiple comparisons), indicating that an overlapping population of cells were identified as place cells by the different methods.

Lastly, we examined how the various place field parameters affected the percentage of cells identified by the methods. For each population, we determined the percentage of cells with a particular value for each parameter (e.g. all cells with a width of 100 cm, regardless of the values for the other parameters) that were identified as place cells. This illustrates again the difference in the percentage of cells identified by each method (Fig 2.4E-H), but shows that the effect of the parameters is largely the same across the methods (e.g. increasing place field width decreases the number of place cells identified by each method). In addition, the way each parameter affected the percentage of place cells showed a similar trend to the effect of these parameters on the sensitivity in the previous model (Figs 2.2 and 2.3), though the

maximum percentage of place cells detected is lower in each case than the suggested by the sensitivity. This is presumably due to the increased sources of variation in the place cell activity in this simulation: a cell with optimal reliability is likely to be sub-optimal in the other parameters. The notable exception to this is the Combination method, which previously only identified cells as place cells when their field width was within a window between 20 and 120 cm (Fig 2.2C). In this latest simulation, however, no such defined window exists and, like the other methods, the number of cells decreases gradually as place field width decreases. This is likely because a place cell with a small place field but a high variability can still be classified as a place cell by the Combination method, as increased variability will cause the place field in the average fluorescence map to seem wider, as illustrated in S Fig 2.3M, so that it falls within the window for detection.

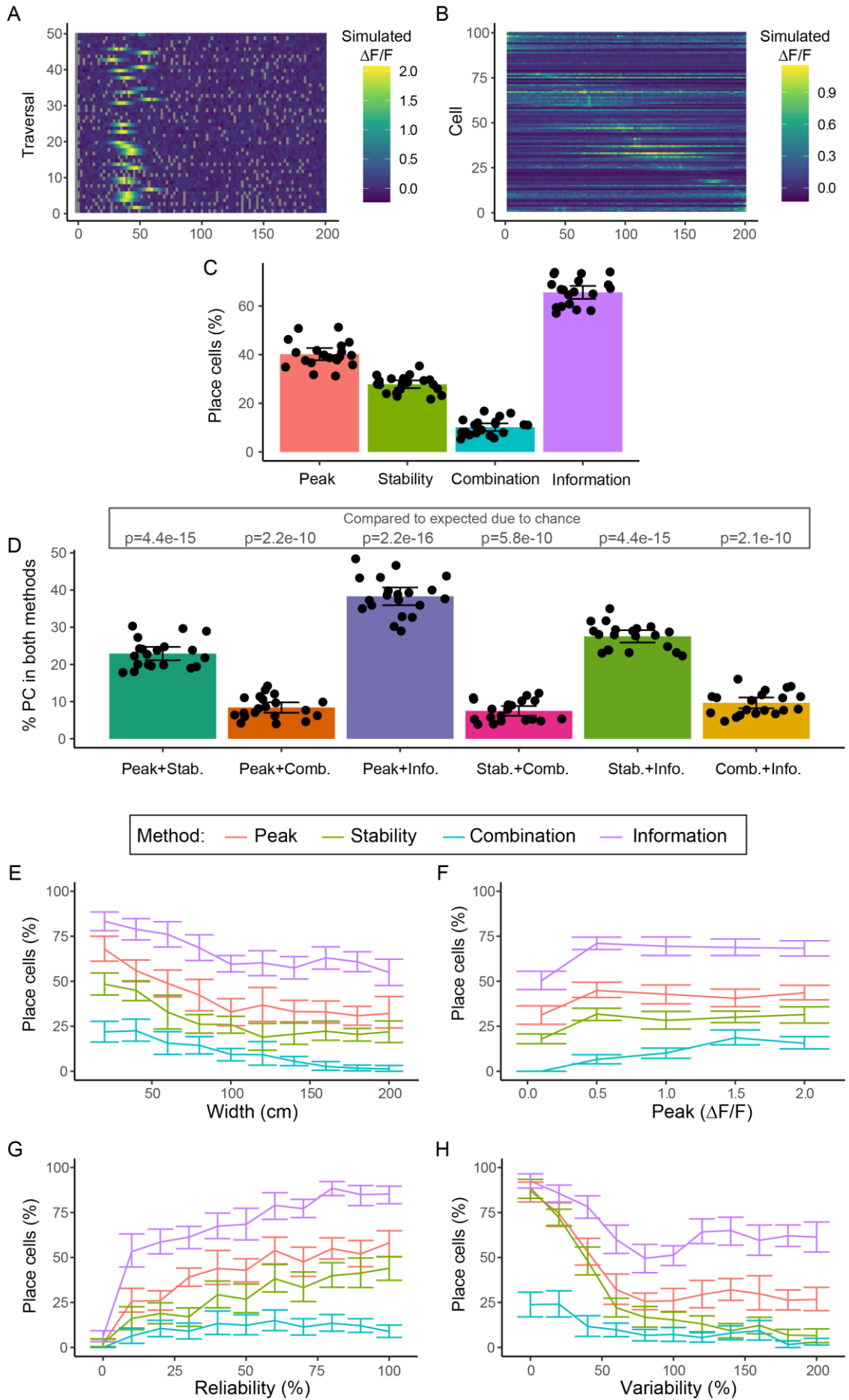


*Fig 2.4 Place cell identification in modelled populations. (A) Example place cell with a width of 20 cm, a peak fluorescence of 2, a reliability of 50% and a variability of 40%. (B) Fluorescence maps over location of example population ordered by the location of the highest fluorescence peak in the fluorescence map. (C) Percentage of modelled cells identified as place cells by the methods. (D) Comparison of percentage of modelled cells identified as place cells by two methods. P-values from comparison between observed and expected overlap, using paired t-tests with Holm-Bonferroni correction for multiple comparisons. The percentage of cells classified as place cells by the four methods depending on its (E) width, (F) peak, (G) reliability and (H) variability. For C and D, each data point is a repeat, bars show means, with error bars showing 95% confidence intervals.*

#### 2.4.4 The Information method detects the most place cells in real datasets

The performance of the different methods of place cell detection on model data predicts that, on real datasets, the Peak method will have the highest sensitivity and specificity, with the Combination method being less sensitive and the Stability method often being less specific. This would suggest that in a real dataset, the Combination method would identify fewer place cells than the other two methods, while the Stability method, because it has a higher false positive rate on model data, might (inaccurately) detect more cells than the Peak method.

To test this, we collected neuronal calcium data from the stratum pyramidale of dorsal CA1 in 4 mice (8 imaging sessions in total) traversing through a 1D virtual reality corridor of 200 cm (Fig 2.5A). We applied each of the four methods to these data to identify which cells could be categorised as place cells (Fig 2.5B). There was a highly significant difference in the percentage of cells classed as place cells by the different methods ( $p = 1.35 \times 10^{-9}$ , linear mixed-effects model with method as a fixed-effect and mouse ID, with session number nested, as a random effect), with the Information method detecting the highest number (47.0 +/- 12.2% (mean +/- std)), followed by the Peak method (34.5 +/- 11.1%) and the Stability method (16.5 +/- 8.8%), while the Combination method only classified 3.9 +/- 1.9% of cells as place cells. The properties of these cells can be seen in an example recording showing the fluorescence maps of all cells, ordered by location (Fig 2.5C). In addition, the populations of cells identified by each of the

methods are shown Fig 2.5D-G). Although no ground-truth exists for what should be included as a place cell, most identified cells seem to have place fields, suggesting classifications are largely appropriate.

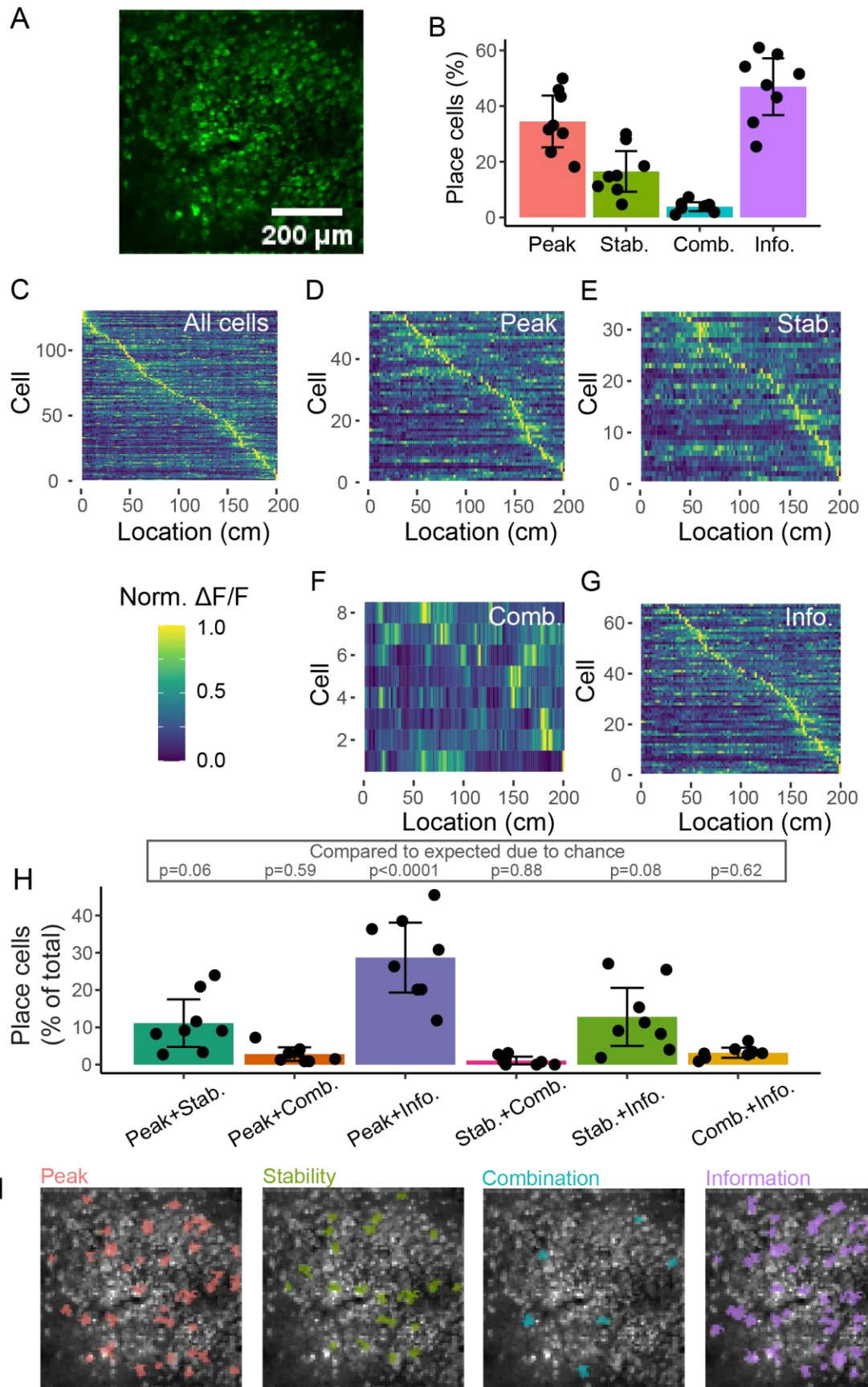


*Fig 2.5 Place cell identification in real datasets. (A) Two-photon recording of GCaMP6f in pyramidal cells. Image is a standard deviation Z projection of a single recording. (B) Percentage of ROIs identified as place cells by the methods. (C) Fluorescence maps over location of all ROIs in an example recording. Cells in this recording identified as place cells by (D) Peak, (E) Stability, (F) Combination and (G) Information methods. (H) Comparison of percentage of ROIs identified as place cells by two methods. P-values from comparison between observed and expected overlap, using paired t-tests with Holm-Bonferroni correction for multiple comparisons. (I) Two photon image from A showing ROIs identified as place cells by the four methods. For B and H, each data point is a recording, bars show means, with error bars showing 95% confidence intervals.*

#### 2.4.5 Differences between detection in modelled and real data

Based on the results from our modelled datasets, we expected the Stability method to classify more cells in a real dataset as place cells than the Peak or Information methods, but in fact it identified significantly fewer ( $p=0.0012$  and  $p<0.0001$  respectively, Tukey post-hoc comparison). We probed the reasons for this difference both by modulating the properties of the modelled cells and inspecting examples of real cells identified differently by the different methods. Because the Stability method compares the activity of each cell to that of other cells in the population, while the Peak and Information methods compare each cell to a shifted version of themselves, the properties of non-place cells could preferentially affect the performance of the Stability method. We therefore modulated the number and firing properties of the modelled non-place cells to see if this reduced the number of cells identified by the Stability method. Increasing the percentage of place cells and adding random calcium peaks to the non-place cells resulted in an increase in specificity (S Fig 2.7A-F), likely because it decreased the correlation of the fluorescence maps of the first and second halves of the sessions for the non-place cells. In addition, we tested the effect of having a population with fully overlapping place fields, which again caused an increase in specificity (S Fig 2.7G-I). Lastly, adding in random calcium peaks to the place cells in addition to the non-place cells caused a similar increase in specificity for the Stability as adding them only to non-place cells (S Fig 2.7J-

L). Although these factors decrease the overall number of place cells detected by the Stability method, due to the reduction of false positives, this could not wholly account for the observed decrease in cells detected in real data compared to the other methods.

Visual inspection of the firing properties of cells identified by the Peak and Information methods, but not by the Stability method, however, showed that the difference in detection is caused largely by cells that have different place fields at different times in the session (S Fig 2.8), in addition to cases where cells either gain or lose a place field during the session. The Stability method fails to identify these cells, because their mean activity over location for the first half of the session is different from the second. This type of structured variation in the place field location was not captured by our simulations of place field activity, because reliability and variability were varied randomly, which did not affect the ability of the Stability method to detect place cells. Minor changes to the Stability method or experimental design should prevent this effect, for example by comparing odd to even traversals, or by adding a familiarisation period for the animals at the start of each session which could ensure place fields are more stable when the experiment begins. In addition, a paradigm where the animals repeatedly enter the environment, as is the case in our experiment because traversals are separated by a tunnel, may induce switching between concurrent spatial maps [24], thus decreasing the overall stability of the cells. However, it is an open question whether some of the cells identified by the Peak and Information methods should really be classified as place cells, for example those with unstable place fields over the session.

2.4.6 Different populations of real CA1 pyramidal cells are identified as place cells by the different methods

To understand whether the different methods simply identify more or fewer of the same population of cells as place cells, we determined the percentage of all ROIs that were identified by two methods. Only 1.1% of cells were classed as place cells by all four methods. 11.1 +/- 7.6% of ROIs were identified as place cells by both the Peak and Stability methods (Fig 2.5H), while only 2.8 +/- 2.2% of ROIs were identified as place cells by the Peak and Combination methods. The Peak method showed a large overlap with the Information method, with 28.7 +/- 11.2% of cells identified as place cells in both methods. Only 1.1 +/- 1.2% of cells were classed as place cells in both the Stability and Combination methods, while 12.8 +/- 9.3% of cells were identified as place cells in both the Stability and Information methods. The information and Combination methods identified 3.2 +/- 1.6% as place cells. These overlaps were significantly different between pairs of methods, when corrected for expected overlap given the different percentages of cells identified by each method ( $p=0.0014$ , linear mixed-effects model with method as a fixed-effect, expected overlap as a covariate and mouse ID, with session number nested, as random effects). This significant difference is due to a higher overlap between the Peak and Information methods compared to the other combinations of methods ( $p=0.075$ ,  $p=0.01$ ,  $p=0.003$ ,  $p=0.002$ ,  $p=0.004$  compared to Peak-Stability, Peak-Combination, Stability-Combination, Stability-Information and Combination-Information respectively, Tukey post-hoc comparison). Indeed, we only observed a significant different overlap from the expected overlap by chance for the Peak-Information comparison ( $p<0.0001$ , Tukey post-hoc comparison), but not for any of the other comparisons ( $p=0.059$ ,  $p=0.59$ ,  $p=0.88$ ,  $p=0.084$  and  $p=0.62$  for the Peak-Stability, Peak-Combination, Stability-Combination, Stability-Information and Combination-Information comparisons respectively). This suggests that the Peak and Information methods identify an overlapping population of cells, but this population is independent of the cells identified by the other two methods. These results are notably different from our findings in the simulated populations (Fig 2.4), where all methods identified an overlapping population of cells. This suggests that additional

variation is present in the real data that we did not capture in our datasets, but that influences place cell identification by the different methods. Such variation could include out of field firing or structured variations in the place field over a session, as demonstrated in S Fig 2.8.

#### 2.4.7 Identified place cell populations differ on key characteristics

To better understand the nature of the different populations of cells identified by each method, we characterised their properties, comparing basic physical features, and functional characteristics. Place cells and non-place cells identified by the different methods were of similar sizes (Fig 2.6A; a smaller size could indicate a noisier image and a higher chance that the automated cell detection by Suite2P had made a mistake as identifying it as a cell). Place cells and non-place cells identified by all methods were also similarly active, as assessed by both mean and maximum spiking rate (Fig 2.6B and C, calculated from the fluorescence profile [172]).

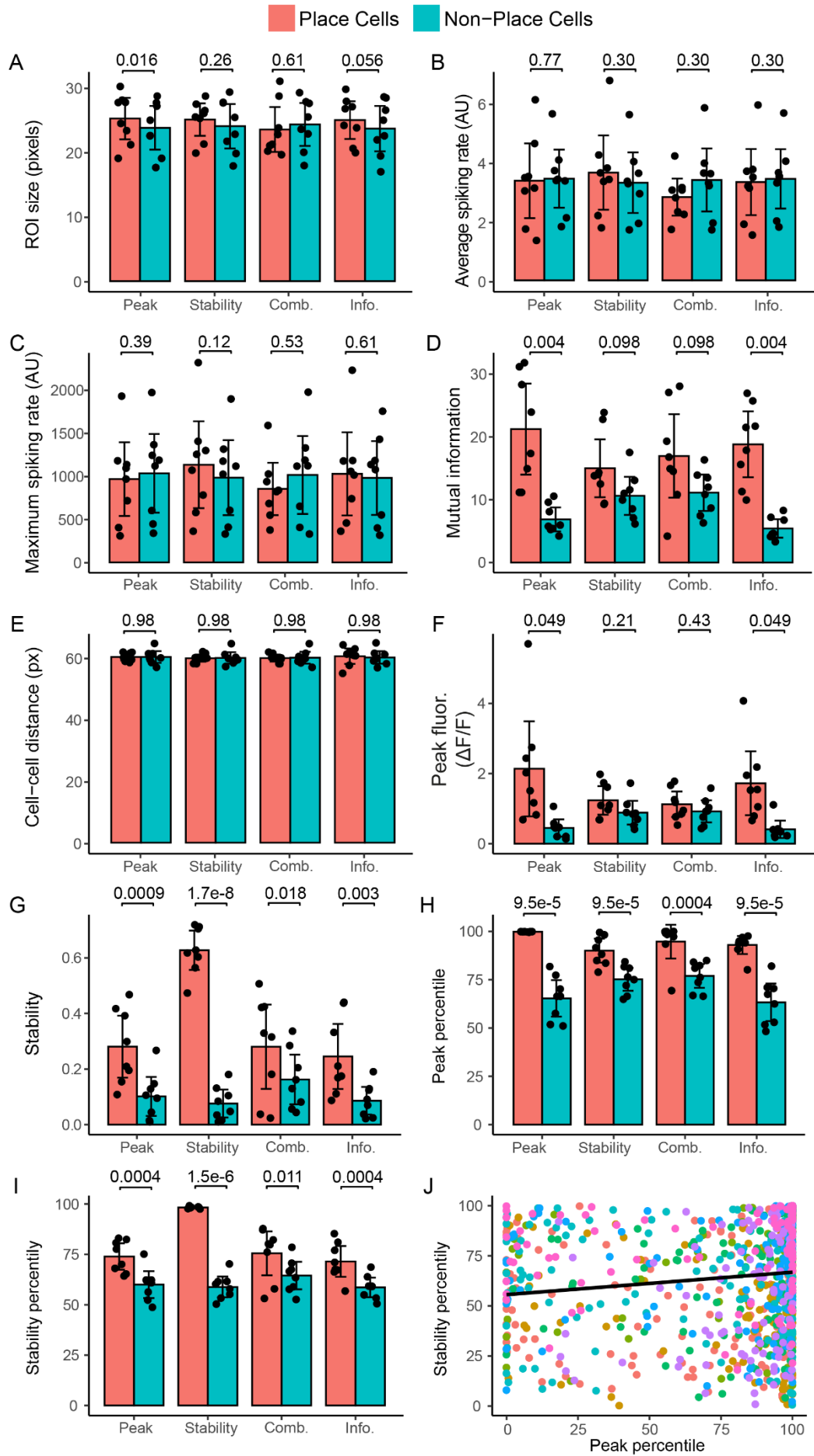


*Fig 2.6 Characteristics of place cell populations. (A) The ROI size, as a percentage of the size of the largest ROI in that recording, of the place cell and non-place cell population in the three methods. (B) Mean spiking rate of place cells and non-place cells. (C) Maximum spiking rate of place cells and non-place cells. (D) Mutual information between cell activity and location for each classification by the three methods. (E) Mean distance between the centroids of the place cells (pink), and the distance from place cells to non-place cells (blue). (F) Peak intensity in the fluorescence maps, the main characteristic used in the Peak method. (G) Intrasection stability, measured using the Pearson correlation coefficient, between the fluorescence map of the 1st half and the fluorescence map of the 2nd half for place cell and non-place cell, the main characteristic used in the Stability method. Percentile of (H) peak intensity and (I) intrasection stability compared to shuffled controls. (J) Correlation between percentile of peak intensity and intrasection stability for all cells. In J, each colour indicates a single dataset. For the other figures, bars are the means of 8 datasets, black dots are values for each individual dataset and error bars represent the 95% confidence interval. P-values for A-I are from multiple paired t-tests with Bonferroni-Holm correction.*

To investigate the information about location carried in place or non-place cells identified by the different methods, we calculated the mutual information between the cell's activity and the animal's location, providing an approximation of the spatial information carried in each cell's calcium signals [173–175]. More spatial information was carried in place cells identified by the Peak and Information method compared to non-place cells, but there was no difference in mutual information held by the place cell and non-place cell populations for the Stability or Combination methods (Fig 2.6D). This is likely because cells containing spatial information that the Peak and Information methods would call place cells are classified as non-place cells using the Stability or Combination method. However, even the cells classified as non-place cells in the Peak and Information method contain some level of spatial information. Indeed, a previous study found that cells may convey information about location without being defined as a place cell [176]. For example, a cell whose activity ramps up gradually as the mouse progresses through the environment does not have a clear place field and will not be included as such in these methods but does communicate substantial spatial information.

Place cells exhibit no particular spatial organisation [35], and any such organisation compared to non-place cells might indicate an unwanted selection by one of the methods, e.g. based on

illumination levels in one part of the field of view. Therefore, we determined the physical location of the detected place cells within the field of view of the recording. We expect the place cells and non-place cells to be randomly distributed within the field of view, as previously reported [35]. We determined the location of the centroid of each cell, labelled them as either place cell or non-place cell according to the different methods and then determined the distance from each place cell to all other place cells, and each place cell to all other non-place cells (Fig 2.6E). Place cells were no more similar in location to other place cells than to non-place cells for any of the methods, suggesting that place cell detection is not being influenced by position within the field of view.

#### 2.4.8 Dependence of place cell detection on model parameters

The lack of overlap between cells identified by the different methods suggests that they identify fundamentally different populations of cells as being place cells, i.e. there is not a single population of cells that fits all the different definitions of place cells used by the different methods. To explicitly test for this, we calculated the extent to which the parameters which underlie classification for the Peak and Stability (peak intensity and correlation in firing across the session, respectively) were represented in the groups of place cells that were selected by each other method (The Combination method uses several parameters so could not be analysed in this way, and the parameter for the Information method was already compared by testing the mutual information). The Peak and Information methods had significantly higher peak intensity in the place cell group compared to the non-place cells (Fig 2.6F), while there was no difference between the place and non-place cells for the Stability and Combination methods.

Place cells identified by all methods had an increased correlation in activity across the session in place cells compared to non-place cells – i.e. they were more stable (Fig 2.6G). Thus, the Peak, Combination and Information methods also selects for stable cells – likely because stable

place cells are consistently active in the same location across traversals, yielding on average a robust peak, which in turn leads to increased spatial information.

Though both the peak intensity and stability are parameters used as a measure to identify place cells in their respective methods, the Peak method compares the values of each individual cell to the peaks of shuffled versions of that same cell, while the Stability method compares the correlation to randomly selected other cells, rather than comparing the values to an absolute threshold. This means that place cells are not necessarily the cells with the highest absolute peaks or highest correlation, but rather the highest value relative to their own shuffled controls. Therefore, we calculated the percentile these values fell in, relative to the shuffled controls, for each cell. Place cells identified by all methods had an increased percentile score for both the stability and the peak parameters (Fig 2.6H and I).

To understand why the methods select place cell populations with similar peak intensity and stability, we determined to what extent the parameters used to define place cells were independent from each other. We correlated the percentiles for the peak intensity and intra-session correlation for each cell across all datasets (Fig 2.6J). There was a small but significant correlation between the percentiles for peak fluorescence and intra-session correlation (Pearson correlation coefficient,  $R=0.13$ ,  $p=3.7 \times 10^{-5}$ ). Although this suggests the two measures are not completely independent – cells with high peak values have a tendency to have more highly-correlated firing patterns within a session – we did not see this reflected in the overlap between the methods (Fig 2.4H, S Fig 2.7H). This may be because the correlation coefficient between peak intensity and intra-session correlation is too low to have an impact. In addition, it may be the case that the more correlated cells are not the same as those that reach the threshold for inclusion as a place cell in one or both methods, so are not reflected in the place cell overlap.

#### 2.4.9 Optimisation of the Combination method

The Combination method identified many fewer cells in our data than in previously published [35,165] or the other two methods applied here. We wondered if this could be due to the number of thresholds the Combination method applies, ([35,165] code to implement the Combination method shared by the authors), requiring putative place cells to fall within specific parameter ranges. These were presumably optimised for the published datasets and may make the method less transferable to other datasets. To test this, we investigated how varying these parameters and thresholds affected place cell detection in our model and experimental datasets (S Fig 2.9; Methods). Sensitivity for detecting model place cells could be improved by increasing the threshold for place field fluorescence compared to baseline (S Fig 2.9B) or reducing the threshold in-field/out-field fluorescence ratio to 2 (S Fig 2.9E), but neither modification caused a substantial increase in the number of cells classed as place cells in experimental data (3.9%; S Fig 2.9G). Instead, the critical feature of the Combination method is the bootstrapping method, which splits the fluorescence data into chunks and shuffles them. Cells are only classed as place cells if fewer than 5% of that cell's shuffles also fit the classification criteria. If we replaced the bootstrapping methods from the Combination method with that of the Peak method, which instead offsets fluorescence traces relative to time, causing more disruption to the association between fluorescence and location, we identified 14.8% of ROIs in our experimental data as place cells (S Fig 2.9G), which is within the published range using the Combination method [35], though below the numbers identified by the Peak or Information methods in our data (Fig 2.5B). Some of these newly identified cells now overlapped with those identified by other methods, 9.3% of all ROIs now overlapping with cells identified by the Peak method, 5.6% overlapping with those identified with the Stability method (S Fig 2.9H), and 11.7% with the Information method. Therefore, when using the new bootstrapping method, around 75% of PCs identified by the Combination method were also identified by the Peak method. However, the levels of overlap between the

Combination method and the other methods were still as expected given the frequency of detection by each method ( $p=0.17$ ,  $p=0.30$ ,  $p=0.10$  for the Peak-Combination, Stability-Combination and Combination-Information comparisons respectively, Tukey post-hoc comparison following a linear mixed-effects model with method as a fixed-effect and mouse ID, with session number nested, as a random effect). This means that the cells identified by each method are still likely to be from independent populations (i.e. if a cell is classified as a place cell by one method that does not increase its chance of being classified as a place cell by another method).

## 2.5 Discussion

We compared four different methods for detecting place cells in two-photon calcium imaging data from mice running through a one-dimensional environment, comparing sensitivity and specificity of the different methods to model cell data, and whether they identified the same real populations of cells as place cells. The methods performed very differently at detecting model place cells and were differentially sensitive to changing parameters (e.g. number of traversals of the environment, place cell width, consistency of firing). This suggested that variability in firing properties across real hippocampal CA1 pyramidal cells would lead to different cells being classified as place cells by the different methods. This proved to be the case: there was very little overlap in real CA1 place cell populations classified by the different methods, except for the Peak and Information methods, which largely overlapped, because the key features used by the different methods to classify place cells proved only weakly correlated. When research groups use these different methods to detect place cells, they therefore identify and study largely independent populations of cells. Researchers should therefore explicitly consider the properties they are selecting for when choosing a place cell detection method, as this decision will determine which cells they do and do not select. In the future, use of a single method across different groups would better allow comparison of

results across the field. The increased selectivity and specificity of both the Peak and Information method when using model data, leads us to conclude that these methods will usually be the best for detecting place cells in calcium imaging data. However, compared to the Information method, the Peak method does not inherently make assumptions regarding the spatial information held by potential place (or non-place) cells, and this neutrality to the information contained within the activity better reflects the capacity of cells without a clear location peak to contain spatial information [176]. Finally, the Peak method has previously been successfully employed to detect place cells in electrophysiological recordings [24], making it widely applicable beyond two-photon recordings. Therefore, we believe the Peak method will usually be the preferred method for place cell classification. Nevertheless, some curation of detected cells may still be desirable, as some cells identified by the Peak method showed unstable firing patterns that may be considered too dissimilar to the firing properties of a traditional place cell.

### 2.5.1 What is a place cell?

Because our results reveal that the choice of detection method will determine the population of cells identified as place cells by a given experiment, it is important to consider what the “desirable” properties of a place cell are, and whether the different classification methods detect these properties. O’Keefe’s first description of place cells defined them as “those for which the rat’s position on the maze was a necessary condition for maximal unit firing.” [23]. Of the four methods we assess here, the Peak method comes perhaps closest to this original definition, requiring cells to have high and consistent firing in one location compared to others, by statistically comparing whether the peak response consistently occurs at the same location. The Combination method achieves something similar by requiring firing to be above a certain threshold for a defined range of place field sizes, while the Stability method only requires the firing pattern to be stable over location and time without the explicit requirement for the peak

to be highest in one location. The Information method uses the spatial information, which does capture the definition, but also makes the assumption that place cells always have an increased amount of spatial information, which is not necessarily the case [176]. For example, cells' activity could ramp over space, thus containing spatial information without having a clear peak in activity in a given location.

The reason for the divergence of place cell definitions from the initial more constrained description is the increased emergence of variability in "place cell" properties. We now know that the size, shape, number and stability of place fields are not constant but can be affected by the environment and where in CA1 they are recorded: Place fields are wider, and more numerous, in larger environments, more stable in the presence of cues and smaller and less spatially selective in dorsal vs. medial CA1 [10,25,177–179]. Clearly methods that discriminate place from non-place cells according to a rigid interpretation of the "classic" definition will miss cells with these more variable properties. Indeed, we found that the Combination method has a lower sensitivity to detect cells with a place field outside a narrow range (100-120 cm), and failed to detect place cells as variability of place field position increased or reliability of firing reduced. Thus, we predict that experimental manipulations that alter the size of the environment and number of cues provided would reduce the number of place cells identified using the Combination method, but not using the Peak method.

Similar changes in place cell properties can occur due to the method of acquiring neural data, impacting on which might be the most appropriate method to choose to detect these cells.

Many experiments that record the activity of large populations of cells, either using calcium imaging, as here, or multi-channel electrode arrays are conducted in head-restrained mice, while the animals are running on a 1D linear track [35,54,127,147]. These conditions likely cause place cells in our experiments to have broader place fields than in real world

environments [119,149], and to be more directionally-sensitive, due to the 1D nature of our linear track [35,180]. The place cell detection method used for such imaging data therefore needs to recognise these less sharply tuned activity patterns. Both the Peak and Information methods found larger numbers of place cells in the experimental data, and selected cells which were both relatively stable and spatially selective. This increased number selected as place cells in our head-restrained imaging data occurred perhaps because of their broader spatial selectivity compared to classic tetrode recordings, suggesting that similar studies using head-fixed mice and linear tracks would also miss spatially-selective cells if a more conservative method were employed.

Less controllable variations in experiments between labs, for example the amount the mice run in an experiment, will also differentially affect the number of cells classed as place cells by the different methods. Our simulations suggested that all four methods would be more sensitive at detecting place cells as mice made more traversals of the environment, but the Combination method would miss cells with even relatively high numbers of traversals (missing over 50% of cells when 10 traversals were made). Furthermore, the Stability method increasingly falsely characterised non-place cells as place cells as the number of traversals increased, because non-place cells had higher intracell correlations as the number of traversals increased. Thus, only the Peak and Information methods could correctly identify place cells with low or high numbers of traversals. Choice of place cell categorisation method will therefore clearly affect the number of cells identified in experiments where animals run to different degrees. Crucially, however, the confounding of place cell identification with running behaviour in 2 of the 3 methods could lead to inaccurate conclusions about how experimental manipulations affect place coding. If, for example, mice of a certain genotype run less, generating fewer traversals, they could appear to have fewer place cells using the Combination

method, or more place cells if using the Stability method, without the number of “true” place cells having changed.

In this study, we only investigated the effect of varying the number of traversals on place cell detection, but other characteristics of the locomotion may also have an effect, for example running speed or the amount of starting and stopping. As these effects may interact with the environment or task, (for example, mice slowing down before a reward delivery), we suggest testing the performance of a chosen method of place cell detection on a model dataset with the expected locomotion characteristics before using it to detect place cells experimentally. We provide source code ([https://github.com/DoriMG/place\\_cell\\_methods](https://github.com/DoriMG/place_cell_methods)) to facilitate this process, into which experiment-specific patterns of locomotion can be loaded and used to predict place cell detection using the four methods described here.

Lastly, in our simulations we modelled each cell independently. By modelling our cells this way, we are potentially missing out on network dynamics within the population, where cells fire dependently of each other, or are synchronously affected by a third factor, such as global theta oscillations. However, because each cell is individually evaluated in the Peak, Combination and Information methods, these methods will not be affected by such dynamics, and as such adding network dynamics to our models would not affect these results. In the case of the Stability method, the cells are compared to shuffles across the population, and both the sensitivity and the specificity of this method will very likely be affected by network dynamics. An increased correlation across the population will cause an increase in the shuffled correlation, thus a higher threshold for intracell correlation for cells to be classified as a place cell. If the increase in threshold is large enough, the sensitivity of the Stability method will therefore decrease, classifying fewer place cells, while increasing the specificity, meaning fewer non-place cells will be falsely marked as place cells. Indeed, we saw a similar effect on

specificity for the Stability method when all place fields in the population were in the same location, causing an increased correlation across the population (S7 Fig I).

In addition to correlations of activity across the population of pyramidal cells, network dynamics may also cause the activity of a cell in a given traversal to depend on its own prior activity (e.g. if a cell fires in traversal  $n$ , it might be more likely to fire in traversal  $n+1$ ). Such an intracell dependence will affect the Peak, Combination and Information methods in the same way as they are affected by altering the reliability (i.e. how much activity varies across location across all traversals), as these methods classify place cells based on the average fluorescence map across all traversals, and do not take individual traversals into account. However, the Stability method may be affected if such dependency between traversals causes a cell to lose or gain a place field, or if the place field shifts position between the first and second half of the session, as demonstrated in S8 Fig. Therefore, if one expects strong network dynamics to be present in a population of place cells, we recommend using caution when employing the Stability method.

In conclusion, because place cells have a more variable activity pattern than was originally thought, particularly across the large populations and range of experimental paradigms permitted by calcium imaging, classification methods should be sufficiently able to identify cells that vary in terms of the size, and reliability and variability of their place field location. However, the different methods we tested select largely different populations of cells which differ in key characteristics, highlighting that choice of place cell classification method is critical for the conclusions a study will draw as to the nature of place cells. We provide model place cell code to help researchers test their how their chosen methods or experimental manipulations might affect detection and the properties of place cells in their data. However, we suggest that consensus in the field for an identification method would help inter-study comparability. Overall, we found that the Peak method demonstrated the optimal high

selectivity and specificity for selecting model place cells that was robust to moderate changes in place field properties but decreased appropriately as the reliability and variability for the place field decreased. It detected many place cells in a real dataset and these cells carried more mutual information about location than non-place cells, but without the concerns of false positives of the Information method. The Peak method has previously been successfully applied to electrophysiological recordings [55], and we therefore would predict that the properties of place cells in imaging data detected using the Peak method will most accurately reflect the properties of place cells detected in a similar manner in electrophysiological studies. Because of its simplicity and lack of assumptions about the spatial information held by place and non-place cells, for most experimental designs we would therefore recommend use of the Peak method for classifying place cells in calcium imaging data, but advise that whichever method is chosen, experimenters consider the likely impact of that method choice on the cells identified.

## 2.6 Materials and Methods

### 2.6.1 Ethics Statement

Experiments were approved by the UK Home Office, in accordance with the 1986 Animal (Scientific Procedures) Act as well as the University of Sussex Animal Welfare Ethical Review Board.

### 2.6.2 Animals

Experiments used four C57/BL6 mice (2 female, 2 male) expressing the genetically-encoded calcium indicator GCaMP6f under the control of a Thy-1 promoter (C57BL/6J-Tg(Thy1-GCaMP6f)GP5.5Dkim/J). The mice were housed in a 12h reverse dark/light cycle environment at a temperature of 22°C and were given ad libitum access to food and water.

### 2.6.3 Hippocampal cranial window surgery

Surgery was performed when mice were a minimum age of eight weeks. Before surgery, mice received subcutaneous injections of dexamethasone (60  $\mu$ L, 2mg/mL), saline (400  $\mu$ L) and buprenorphine (40  $\mu$ L, 0.3mg/mL diluted 1:10 in saline) to reduce inflammation, for hydration, and pain relief respectively. Mice were maintained at 0.8-2.0% isoflurane anaesthesia for the duration of the surgery. Body temperature was maintained at 37 °C using a homeothermic blanket (PhysioSuite, Kent Scientific Corporation). A craniotomy was inserted above dorsal CA1 as previously described [31]. Briefly, the skin above the skull was removed and the skull was scored to increase the surface area for binding dental cement. A custom-made stainless steel headplate was then fixed to the skull with black dental cement (Unifast Powder mixed with black ink (1:15 w/w) and Unifast Liquid). A 3 mm diameter craniotomy was then performed 2mm posterior to bregma and 1.5 mm lateral to the sagittal suture. Following the removal of the skull flap and the dura, brain tissue overlying the hippocampus was aspirated (New Askir 30, CA-MI Srl) until vertical striations of the corpus callosum were visible. We then inserted a custom 3D printed cannula (2.4 mm ID, 3 mm OD, 1.5 mm height) made of a biocompatible Dental SG resin (FormLabs) so that the glass coverslip at the bottom of the cannula lay directly on top of the brain tissue. The top of the cannula had a rim (0.2mm height, 3 mm OD) resting on top of the skull, which was attached using tissue adhesive (3M VetBond) and then covered with more dental cement. A rubber ring was then attached on top of the headplate for subsequent use as a well for the water needed for the water-immersion microscope objective. The mice were given an injection of meloxicam (125  $\mu$ L, 5 mg/ml) as an analgesic near the end of the surgery and then received meloxicam (200  $\mu$ L, 1.5 mg/mL) for 4 days following the surgery via oral admission. Their health was monitored and they were weighed daily.

#### 2.6.4 Two-photon imaging

*Habituation.* A week or more after surgery, the mouse was habituated to the imaging rig by head-fixing it for an increasing amount of time each day for at least a week before it was imaged. During the habituation it was also presented with the virtual reality environment several times to make it familiar with this setup.

*Imaging rig (S Fig 2.2).* The mice were head-fixed above a polystyrene cylinder, on which they could run. The cylinder was fitted with a rotary encoder (Kübler, 4096 pulses per revolution). Two screens in front of the mice were used to display a custom virtual reality (VR) environment designed using ViRMEn [150].

*Stimulus presentation.* The virtual reality environment presented to the mice was a wide corridor, 200 cm long and 80 cm wide, with patterned walls (30 cm high) and floor (see S Fig 2.2). Three sets of objects (spatial cues) were present outside the walls: blue square pillars with white stripes, light blue cones with white and gray diagonal stripes and grey cylinders with green dots. The objects were placed at 65 cm, 140 cm and 200 cm from the start of the corridor. All objects were 100 cm high and visible from the start of the arena. Both before and after the wide corridor was a dark grey tunnel with a diameter of 30 cm, 50 cm long before the corridor and 45 cm long after the corridor) which served to allow smooth transitions between multiple presentations of the environment. The mice were not required to perform a task while in the virtual environment.

*Data acquisition.* The stratum pyramidale of dorsal CA1 was imaged using a two-photon microscope (Scientifica) with a water-immersion objective (CFI75 LWD 16X W, Nikon; 0.80 numerical aperture, 3 mm working distance). GCaMP6f was excited using a Chameleon Vision II Ti:Sapphire laser (Coherent) at a wavelength of 940nm with a gallium arsenide phosphide photomultiplier tube. We used the ScanImage software (Vidrio Technologies, MATLAB) to control the microscope and collect data. The stratum pyramidale was identified from the

presence of densely packed cell bodies. Image acquisition used a wide field-of-view (547 x 547  $\mu\text{m}$ ) at a low resolution to optimise the acquisition rate (128x128 pixels, 7.51Hz, pixel size 4.27  $\mu\text{m}$ ). Sessions lasted between 44 and 45 minutes.

### 2.6.5 Image Analysis

*Preprocessing.* Preprocessing was conducted using Suite2P software [172]. Firstly, images were registered using the default settings, then regions of interest (ROIs) corresponding to pyramidal cell bodies were identified based on their morphology (having a diameter of approximately 2 pixels/8.5  $\mu\text{m}$ ) and a tau, the decay time for the calcium indicator, of 0.8. We trained a classifier by manually curating the detected ROIs based on the mean image of the original recording, the shape and the activity pattern of the ROI. On average 58 +/- 4% of ROIs were excluded per imaging session. We obtained the calcium signal corrected for neuropil activity for each ROI from the Suite2P output.

For each ROI, fluorescence time courses were normalised to baseline fluorescence by dividing the whole trace by the average intensity in that ROI during the first 100 frames of the recording. For calculations of fluorescence maps, any frames where the mouse was stationary were excluded (defined as the speed being below 10 % of the maximum speed).

An extra pre-processing step was used in Dombeck et al. [35] and associated papers, described in full in [160], so we at first used this step as well when replicating this method (hereafter referred to as the Combination method). After ROI extraction and normalisation the whole time series was divided by the baseline, which was defined as the 8<sup>th</sup> percentile of values in each ~15 second interval. Significant transients were then identified as calcium events that started when fluorescence deviated more than 2 standard deviations from the baseline and ended when the fluorescence returned to less than 0.5 standard deviations from the baseline. Fluorescence outside of the significant events was set to 0. However, we noticed that this preprocessing step led to place cell activity appearing negative, and thus these cells being

rejected, if their activity was shorter than 15s and occurred in the presence of a negative baseline. For our data, this led to all cells being rejected at this stage. We therefore did not use this preprocessing method in our analyses.

Subsequently, to test whether the lack of preprocessing explained the low number of cells identified using this method, we amended the preprocessing method to correct for slow drifts in the baseline while preventing division by a negative baseline, by subtracting rather than dividing by the baseline. This caused a small but significant increase in the sensitivity of the Combination method compared to non-preprocessed traces (S Fig 2.9A).

#### 2.6.6 Model data generation

We generated model place cells to test the performance of the place cell detection methods. Time series of calcium responses of model cells were generated using real locomotion traces of mice running through a linear virtual environment. 8 datasets containing 184 traversals were split into separate traversals and model locomotion traces were generated by randomly selecting the required number of traversals (each traversal could be selected more than once). Model place cell properties (described below) were convolved with these locomotion traces to generate a fluorescence map for each cell, with the same “frame rate” as used in the real imaging sessions used to acquire locomotion (7.51 Hz).

For each dataset, we included 20 model place cells – in which fluorescence was modulated by spatial location – and 80 non-place cells – whose fluorescence was independent of location. This ratio was chosen to mimic the percentage of place cells typically reported in experiments using a one-dimensional track and two-photon microscopy [35]. The inclusion of non-place cells was crucial as some of the place cell detection methods use comparisons with other cells in their definition, and thus rely on the population containing non-place cells as well as place cells.

For the model place cells each place field was modelled as a 1D Gaussian field centred at a randomly selected location (Fig 2.2A). The sigma of the Gaussian was set to 12.5 cm, such that 95% of values – 4 times sigma – fall within the place field width of 50 cm, the average place field width reported by Dombeck et al. [35]. The peak of the Gaussian (1.3) was determined using the top 10% of each cell's fluorescence in its fluorescence map from 992 cells from 8 datasets.

The noise in all cells was modelled using a Poisson distribution (generated using the MATLAB `poissrnd` function), with lambda estimated from the raw traces of 992 cells from 8 datasets. The median lambda of the 10% of cells that had the best Poisson fit (235.1, as estimated from the sum of squared errors; SSE) was used as the lambda for our model noise. Raw noise was generated using this parameter, then  $\Delta F/F$  of this noise was calculated to obtain the normalised noise used in the model cells. The average  $\Delta F/F$  of the noise, as tested on 10000 traces each with a length of 1000, was  $0.0024 \pm 0.0467$ , which is 0.18% of the peak value.

Non-place cell traces usually consisted of only noise (Fig 2.2B, top 80 cells), generated as above, while the noise was added to the generated place field for the place cells (Fig 2.2B, bottom 20 cells). For S Fig 2.7, we also considered the impact of non-spatial firing of non-place cells. In our real data, there were on average 0.0062 peaks per frame, i.e. a calcium peaks occurred about every 160 frames. We therefore randomly added a range of peaks to non-place cell traces, from 0- 0.02 peaks per frame.

#### 2.6.7 Manipulation of place cells

We manipulated the place cell properties in order to model the imperfect nature of real place cells. We varied the place field width, peak, reliability, spatial variability and the number of place fields per place cell. We performed further simulations where we varied the percentage of place cells, the occurrence of random calcium peaks and the coverage of the environment by the place fields.

*Place field width.* The place field width was varied by varying the sigma of the Gaussian field for each place cell.

*Place field peak.* The place field peak was varied by scaling the Gaussian model using a single scalar. This way, the shape of the Gaussian remained, while the overall peak could be increased or decreased.

*Number of place fields.* We varied the number of place fields between 1 and 4, spaced to cover the whole environment but with no overlap. The upper limit of 4 place fields was therefore set by the size of the place field (50 cm) and the environment length (2 m).

*Reliability.* We defined the reliability of a place cell as the probability it will have a place field in a given traversal. The probability  $P_{\text{field}}$  was between 0 and 1, where  $P_{\text{field}} = 0$  meant the place cells did not have a place field in any traversal, and  $P_{\text{field}} = 1$  meant the place cells had place fields in every traversal. At a probability between the 0 and 1 the place cells had place fields in a randomly selected proportion of traversals equal to  $P_{\text{field}}$  times the total number of traversals.

*Spatial variability.* We defined the variability of a place cell as the average deviation of the place field per traversal from the centre of the average place field. We modelled this by defining a Gaussian centered around the centre of the average place field, with a flatter Gaussian (i.e. higher sigma) equating to a higher variability. For each traversal we drew a value from this Gaussian distribution to be the centre of the place field for that traversal.

*Percentage of place cells.* The percentage of cells that were designated as place cells out of 100 total cells was varied.

*Occurrence of random calcium peaks.* We varied the occurrence of random calcium peaks in the control cells alone (S7 Fig D-F) or all cells (S7 Fig J-L). The occurrence in a measure of peaks per frame was measured, and this number was used as the probability for any given frame to

contain a calcium peak, to create an occurrence map. This occurrence map was then convoluted with the calcium shape extracted from our real data, to create a realistic calcium peak.

*Place field coverage.* In the default simulations the place fields of the place cells were at equidistant locations covering the entire environment. We performed an additional simulation where the place fields of all place cells were in the same location, thus not covering the entire environment.

### 2.6.8 Performance measures

To calculate the performance of the place cell detection methods, we calculated the sensitivity and specificity of each method using the number of true positives (TP), true negatives (TN), false positives (FP) and false negatives (FN). The sensitivity is a measure of how well the method is able to find all the true place cells in the dataset, while the specificity is a measure of how specific the method is for identifying just true place cells without false positives.

$$\text{Sensitivity} = \frac{TP}{TP+FN} \quad (1)$$

$$\text{Specificity} = \frac{TN}{TN+FP} \quad (2)$$

### 2.6.9 Place cell detection methods

We tested four methods for place cell detection (S Fig 2.1) all of which have all been used in previous studies to identify place cells.

*Peak method.* This method of place cell detection was described for electrophysiology data from mice running through a 1D virtual corridor [166]. We adapted the original method for use with fluorescence data as follows: We first calculated the fluorescence maps (the average fluorescence in each location bin) for each cell from which we determined the peak fluorescence for each cell. The neuronal fluorescence data was then randomly shuffled 500

times relative to the location data by shifting the fluorescence data in time randomly by at least 5 seconds. Because the running speed of the mouse is not constant, this alters the fluorescence at each location and therefore the “peakiness” of the fluorescence map. Each cell’s fluorescence map and peak fluorescence was then determined for each shuffle. Any cell with a true peak fluorescence in the top 1% of all shuffles was deemed a place cell. Thus, the peak method detects cells with high fluorescence in a place field compared to the baseline.

*Stability method.* The stability method was developed by O’Leary [167] and is based on classic methods of detecting place cells in real-world two-dimensional (2D) environments which require place cells to have a consistent place field over multiple traversals (e.g. [43]). First, a separate fluorescence map was calculated for each cell for each of the two halves of a recording session and the linear correlation between these two fluorescence maps was calculated. These correlation coefficients were then compared to control values obtained by comparing the fluorescence map of the first half of a session for that cell with the fluorescence maps of the second half of other randomly selected cells in the dataset (100 repeats per cell with redraws). The within-cell correlation of the cell was compared to all the shuffles for that cells, and if the correlation was above the 95<sup>th</sup> percentile of the shuffles, it was deemed a place cell.

*Combination method.* The Combination method [35,164,165] uses a combination of the level of fluorescence above baseline, with stability of firing over different traversals. It uses pre-processed fluorescence traces of cells that have been thresholded so they only include significant transients, followed by a number of thresholding steps to find “true” place fields. This method has been modified over the three publications cited above, the most recent of which was used here. First, the fluorescence map was calculated from the preprocessed traces for each cell and possible place fields were determined by thresholding the fluorescence map with a cut-off value of 0.25 times the difference between the peak fluorescence value and the

baseline. Possible place fields were defined as having above-threshold fluorescence in contiguous locations for at least 20 cm and less than 120 cm. Each field was also required to have one bin with a value of at least 10% of the mean fluorescence of that cell over the session. The mean fluorescence in each place field was then divided by the mean fluorescence outside of the place field, and cells were only deemed place cells if the in-field/out-field ratio was higher than or equal to 4. Lastly, the cells were required to have a significant transient, as defined in the pre-processing thresholding step, in at least 20% of the traversals of the environment. All traces were shuffled 1000 times with respect to location and classified using the above methods. Only cells that were classified as place cells in fewer than 5% of the shuffles were considered to be true place cells. Thus, the Combination method requires place cells to significantly increase fluorescence from baseline over a contiguous place field, with some stability of responding over time.

*Information method.* This method of place cell detection has been used in freely moving mice running either through a square or circular environment [168], or a corridor [24]. The original method relied on the detection of calcium events, but to reduce the effect of such preprocessing we adapted the method to be applied directly to the relative fluorescence. As using the fluorescence directly has been shown to accurately reflect the spatial information [175], we do not expect this to negatively impact the method's ability to detect place cells. We first calculated the fluorescence maps (the average fluorescence in each location bin) for each cell from which we determined the spatial information using equation 3, where  $N$  is the number of bins,  $f_i$  is the fluorescence in bin  $i$  of the fluorescence map, and  $f$  is the average fluorescence across the map. For the spatial information we assumed a uniform occupancy (i.e. that the mouse spent the same amount of time in each location bin). The neuronal fluorescence data was then randomly shuffled 500 times relative to the location data by shifting the fluorescence data in time randomly by at least 5 seconds, the same procedure we employed for the Peak method. Each cell's fluorescence map and spatial information was then

determined for each shuffle. Any cell with spatial information in the top 5% of all shuffles was deemed a place cell. Thus, the peak method detects cells with high level of spatial information in a place field compared to the baseline.

$$SI = \sum_{i=1}^N f_i \log_2 \frac{f_i}{f} \quad (3)$$

#### 2.6.10 Model cell properties

The way in which varying the different characteristics of model place cells affects their properties was illustrated (S3 Fig). By comparing real cell properties (e.g. of FWHM) to the modelled variables (e.g. width), experimenters can predict the impact of their choice of place cell classification method on detection of their real world cells.

*Full width at half maximum.* We used the full width at half maximum (FWHM) as representation of the place field width. We calculated the maximum value within the fluorescence map, and then determined the width of the place field at half this value. Notably, this value will be lower than the width defined in the model, because the FWHM is a conservative representation of the width.

*Stability.* The stability was again defined as the correlation coefficient between the fluorescence maps of the first and the second half of the session, as used in the Stability method.

*Mutual information.* Mutual information between the fluorescence traces and the location of the animal was calculated using equation 3, as described above.

*Out/in ratio.* The out/in ratio was the mean fluorescence outside of the place field divided by the fluorescence within the place field, and is a measure of the signal to noise ratio of the place field. A lower number represents a higher signal to noise ratio.

### 2.6.11 Place cell properties

The place cells were characterized using several of the Suite2P outputs (ROI size, average and maximum spiking rate) [172], in addition to characteristics that were calculated using custom analyses:

*Mutual information.* Mutual information between the fluorescence traces and the location of the animal was calculated using equation 3, as described above.

*Cell-cell distance.* The cell-cell distance was calculated as the mean distance in pixels between the centre of the ROIs for all cells of one type (i.e. place cell or non-place cell) within the field of view.

*Peak intensity.* The peak intensity was the size of the largest peak (in  $\Delta F/F$ ) in the fluorescence cell, as used in the Peak method.

*Stability.* The stability as defined as the correlation coefficient between the fluorescence maps of the first and the second half of the session, as used in the Stability method.

*Peak percentile.* The peak percentile was the percentile score of the peak intensity compared to the peak intensity of the shuffles, as used in the Peak method.

*Stability percentile.* The peak percentile was the percentile score of the stability compared to the stability of the shuffles, as used in the Stability method.

### 2.6.12 Statistical analysis

All statistical tests were conducted in R [181]. Where appropriate, a Shapiro–Wilk test was used to test the data for normality. If the data was determined not to deviate from a normal distribution ( $p > 0.05$ ), we performed the appropriate parametric test, otherwise a non-parametric test was applied. The tests performed for each comparison are detailed in the text. Linear mixed models were performed in R using the lme4 package (version 1.1-23). All other statistical tests were performed in R using the rstatix package (version 0.6.0).

### 2.6.13 Data and software availability

The MATLAB used to automatically generate model datasets is available on GitHub ([https://github.com/DoriMG/place\\_cell\\_methods](https://github.com/DoriMG/place_cell_methods)). This repository also contains the locomotion dataset we used to generate the model data. We further provide an explanation of how to use the code to generate novel model datasets with varying parameters. Experimental data used for each relevant figure is available via FigShare (10.6084/m9.figshare.13560548).

## 2.7 Acknowledgements

With thanks to Alice O'Leary and Daniel Dombeck for sharing their code. We would like to thank O. Hall-Bird and M. Hall-Bird for their insights and useful suggestions on this project.

## 2.8 Supporting information

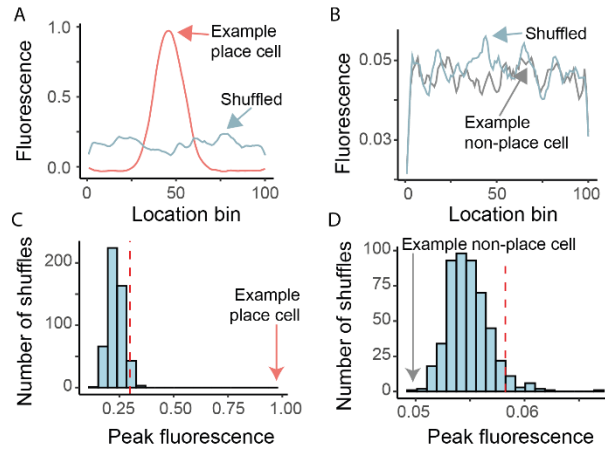
### A: Peak Method

1. Calculate rate maps across locations for each cell and determine peak (place cell (A): pink arrow, non-place cell (B): grey arrow)

2. Shuffle data a random number of frames (>5 s) in the time domain

3. Recalculate the rate maps across location and determine peak (blue-grey arrows) (A-B)

4. Repeat shuffle 500 times, cell is place cell when original peak (C-D, arrows) is higher than 95th percentile of peaks (red dashed line).



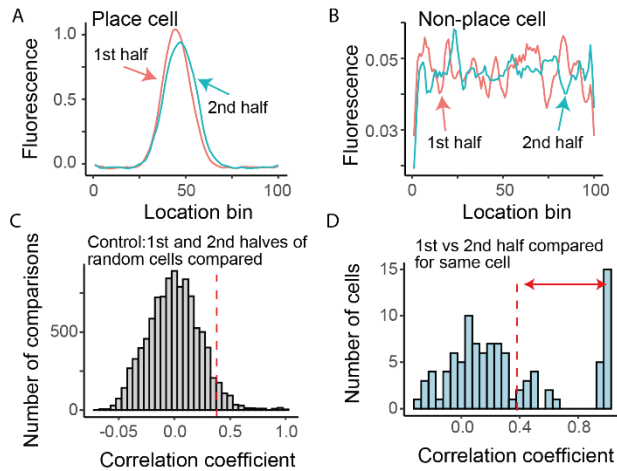
### B: Stability Method

1. Calculate fluorescence maps for 1st and 2nd halves of trials (A-B)

2. Calculate correlation between the fluorescence maps for the two halves

3. Control: Calculate correlation between first half of one cell, and second half of randomly selected cell

4. Cell is place cell when within-cell correlation is higher than 95th percentile of correlation coefficients of control (red dashed line, C). Blue-grey bars to right of dashed line are place cells (range shown by red arrow, D).



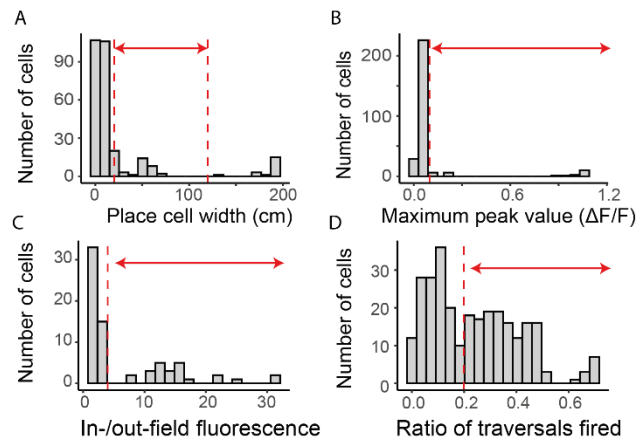
### C: Combination method

1. Calculate fluorescence maps and threshold using 25% of overall peak minus baseline

2. Calculate field width (A), peak in-field/mean value (B) and in-field/out-field activity (C)

3. Determine percentage of traversals where cell has a significant event in the place field (D)

4. Include cell when it is within the set ranges (dashed red lines) for each of these measures (range shown with red arrow)



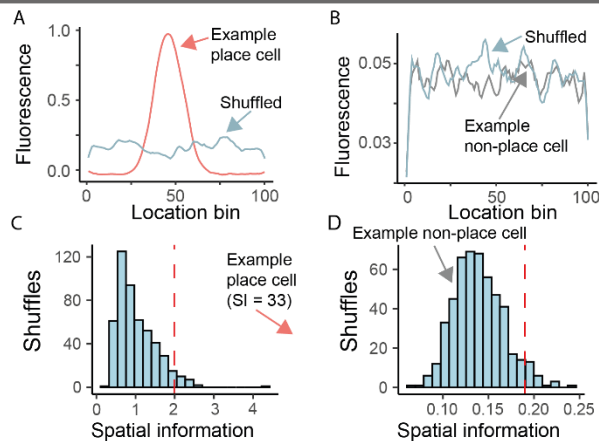
### D: Information method

1. Calculate rate maps across locations for each cell (A-B) and calculate the spatial information

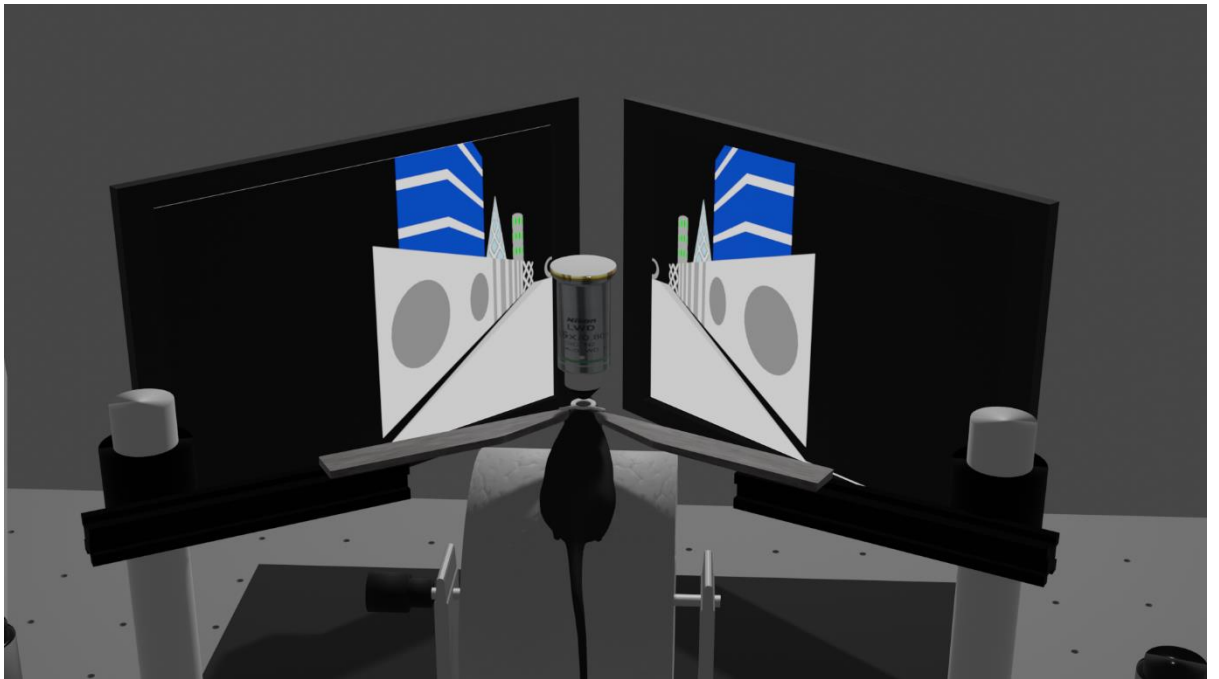
2. Shuffle data a random number of frames (>5 s) in the time domain

3. Recalculate the rate maps across location and determine peak (blue-grey arrows) (A-B)

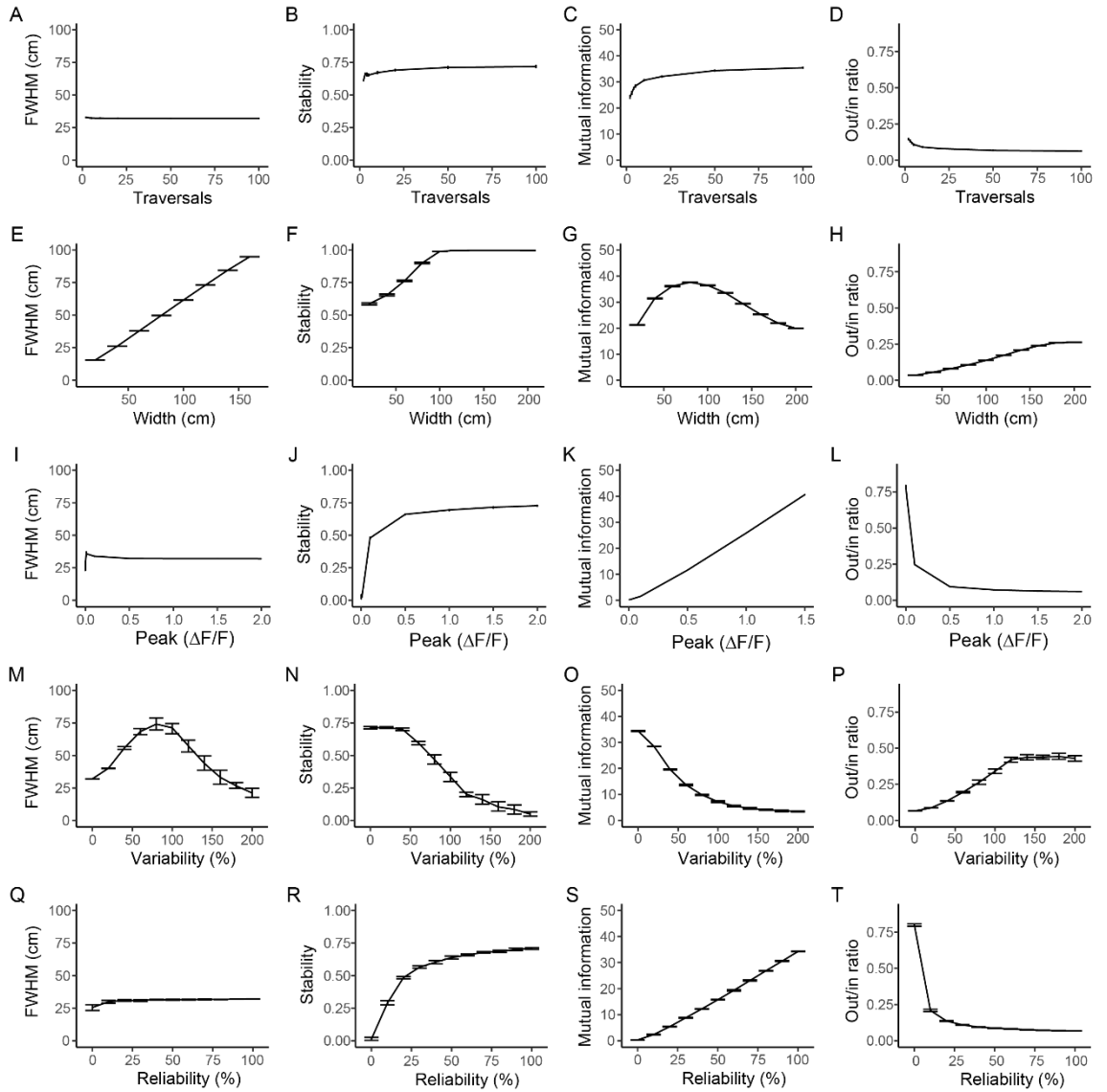
4. Repeat shuffle 500 times cell is place cell when original SI (C-D, arrows, SI is off the graph for the place cell example) is higher than 95th percentile of peaks



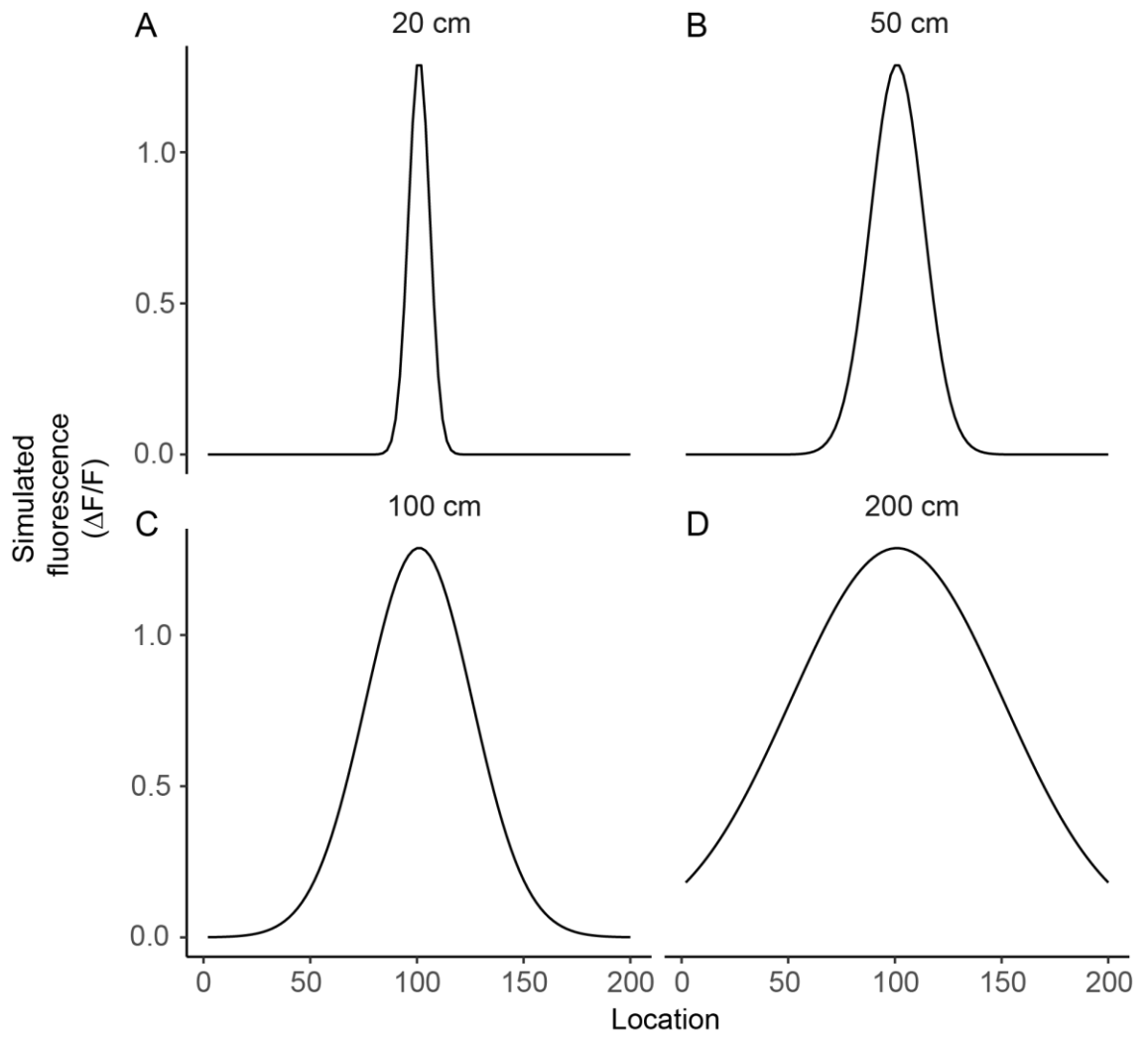
*S Fig 2.1 Graphical summary of tested methods. A graphical representation of how the (A) Peak, (B) Stability, (C) Combination and (D) Information methods define a place cell based on its fluorescence map.*



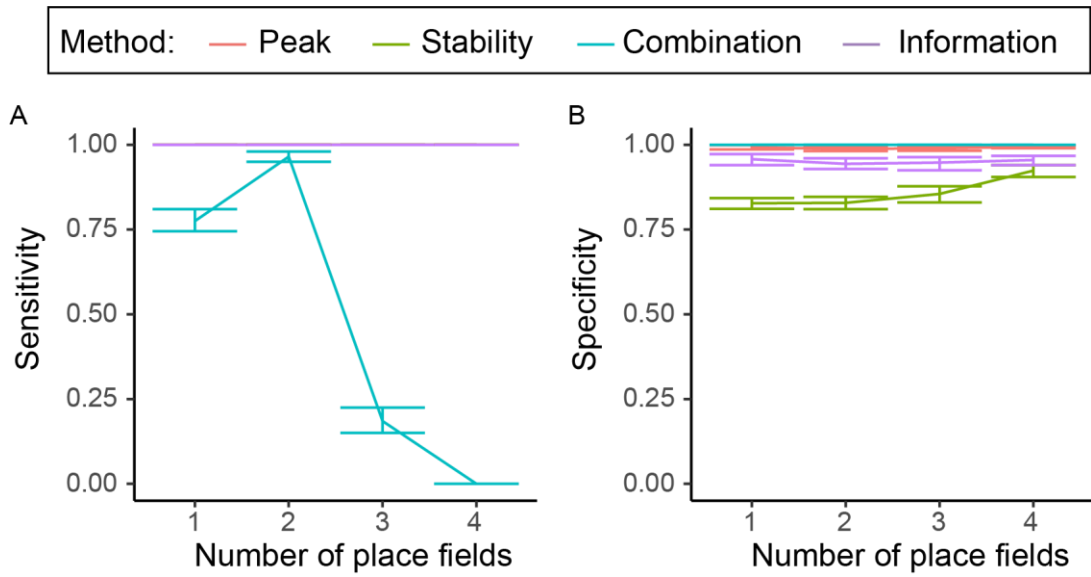
*S Fig 2.2 Experimental setup. The two-photon experimental setup as seen from behind the mouse. The mouse is head-fixed and standing on a wheel that it can use to control the environment projected onto the screens in front of it.*



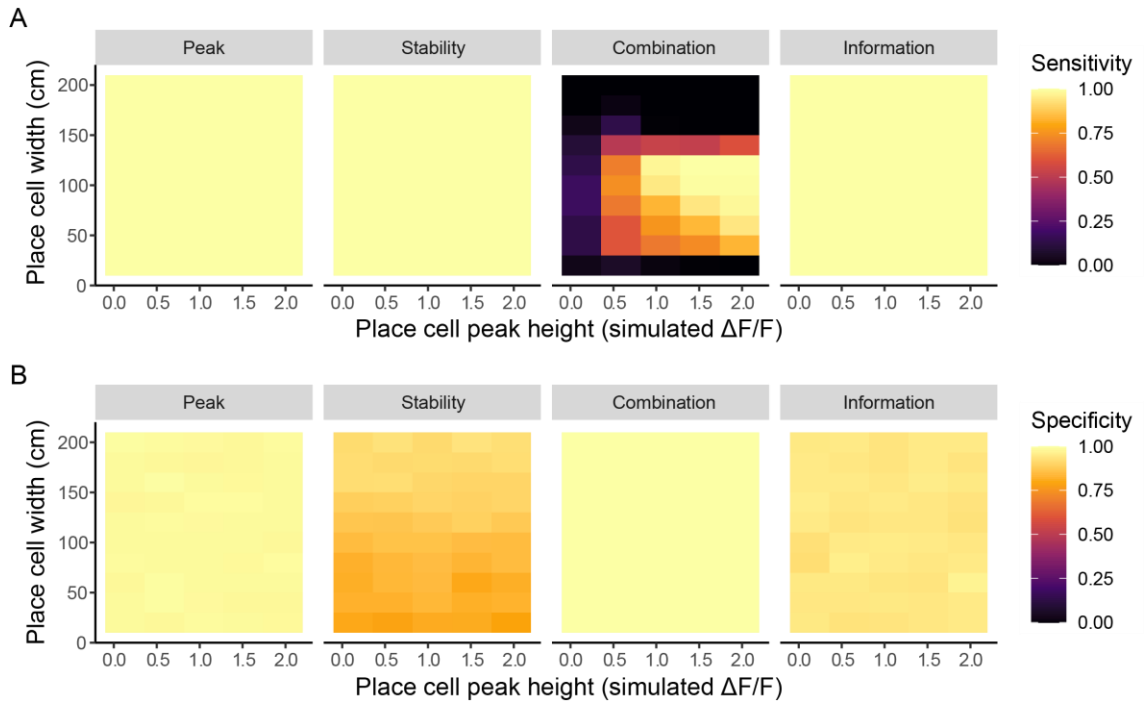
*S* Fig 2.3 **Properties of model place cells.** Full width half maximum, stability, mutual information and out/in fluorescence ratio of modelled place cells with varying number of traversals (A-D), width (E-H), peak fluorescence (I-L), variability (M-P) and reliability (Q-T).



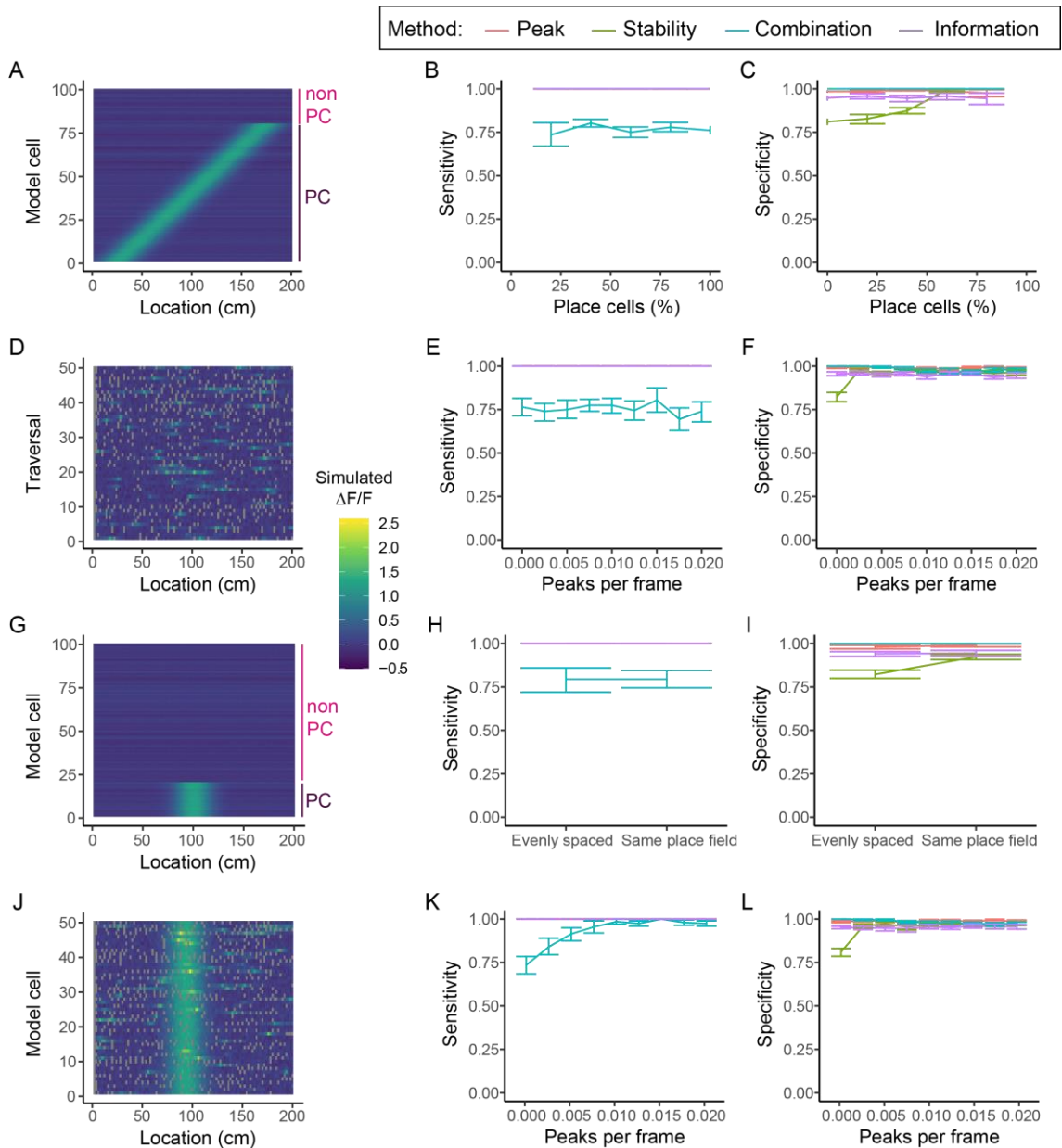
*S* Fig 2.4 **Model place cells of varying widths.** Fluorescence maps of model place cells with a width of (A) 20 cm, (B) 50 cm, (C) 100 cm and (D) 200 cm.



*S Fig 2.5 The effect of the number of place fields on detection. (A) Sensitivity and (B) specificity of methods as a function of the number of place fields. Data shown are the means of 10 trials with randomly created data using the set parameters, error bars show 95% confidence interval. Sensitivity of all methods except for Combination method are 1 in A, resulting in overlapping lines.*

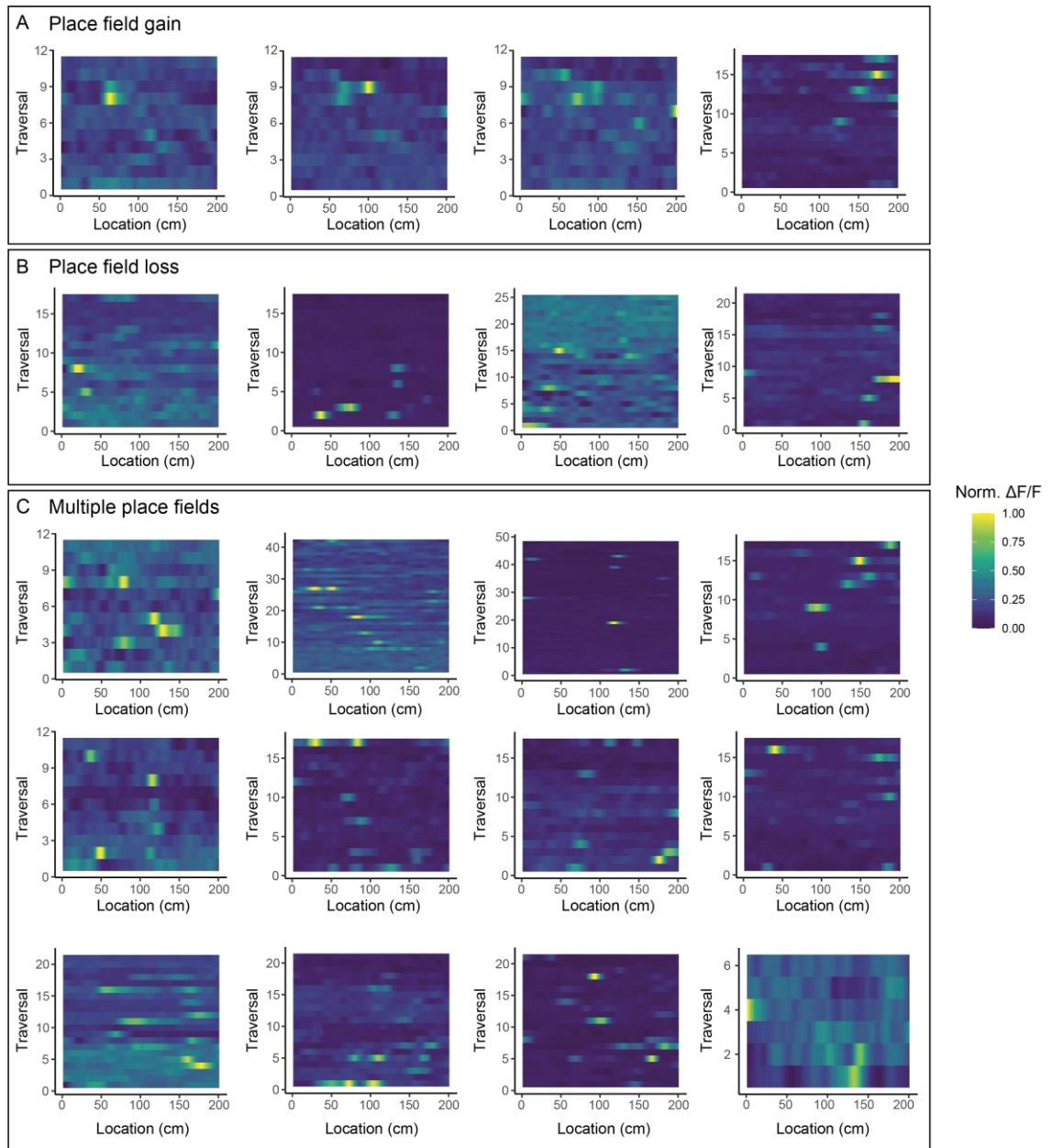


*S Fig 2.6 The combined effect place field width and peak. Sensitivity (A) and specificity (B) of the Peak, Stability, Combination, and Information methods (as labelled) as a function of the peak of the place field and the width of the place field (up to 200 cm, the full environment length). Data shown are the means of 10 trials with randomly created data using the set parameters.*

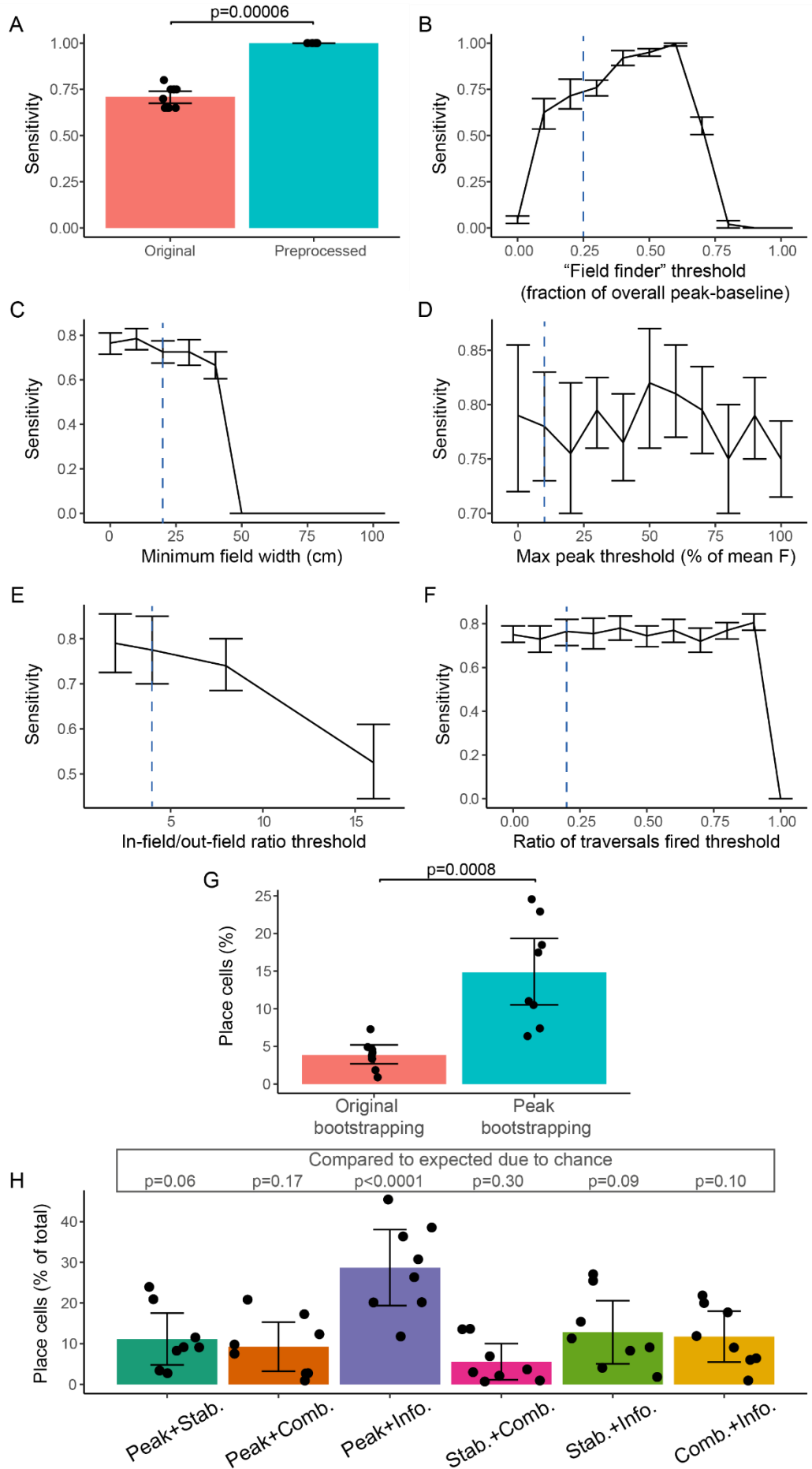


*S Fig 2.7 The effect of number of place cells and firing probability of non-place and place cells. (A) Example cell population with 80% modelled place cells. Sensitivity (B) and specificity (C) of the Peak, Stability, Combination, and Information methods as a function of the percentage of modelled place cells in the population. Altering the number of non-place cells increased specificity of the Stability method (i.e. fewer non-place cells, and therefore fewer total cells, were identified) when the number of place cells was increased beyond what is likely to be physiological (20-30%, [29]). (D) Example activity of a non-place cell with 0.01 random calcium peaks per frame. Sensitivity (E) and specificity (F) of the Peak, Stability, Combination, and Information methods as a function of the activity (peaks per frame) of the non-place cells. In the originally modelled datasets, the non-place cells all contained random background levels of Poisson noise with no firing, whereas the non-place cells in real data most likely do fire, though in a location-independent manner. We therefore introduced calcium peaks in the non-place cells with shapes and*

numbers of peaks modelled on our real data. There was no effect on sensitivity of increasing the activity of non-place cells, but the specificity of the Stability method increased with increasing non-place cell activity. (G) Example cells population with all place fields in the same location. Sensitivity (H) and specificity (I) of the Peak, Stability, Combination, and Information methods depending on the location of the place fields, showing an increase in specificity for the Stability method when all place cells have the same place field. This is likely due to an overall increase in correlations in the shuffled controls, as place cells will now correlate more highly with other place cells. This increase in average correlation for the shuffles, and thus an increase in threshold for being included as a place cell, increases the specificity. (J) Example activity of a non-place cell with 0.01 random calcium peaks per frame. Sensitivity (K) and specificity (L) of the Peak, Stability, Combination, and Information methods as a function of the activity (peaks per frame) of the all cells. Adding random calcium peaks to the place cells, in addition to the non-place cells, affects the specificity of the Stability method similarly to adding these peaks only to the non-place cells. This manipulation also causes an increase in sensitivity for the Combination method. These results can therefore not fully explain why the Stability method found fewer cells in our real data set. Data shown are the means of 10 trials with randomly created data. Error bars show 95% confidence intervals. Sensitivity of methods except for Combination method are 1 across the various manipulations in B, E, H and K, resulting in overlapping lines.



*S Fig 2.8 Examples of cells identified by the Peak and Information method, but not the Stability method. Smoothed fluorescence maps of example cells that either (A) gain or (B) lose a place field, or (C) that have different place fields at different times in the session. The colour represents the normalized fluorescence.*



*S Fig 2.9 The effect of altering Combination method thresholds on identification of place cells in model and real data. (A) The sensitivity of the Combination method on detecting place cells in model data is increased when preprocessing is introduced, The sensitivity of the Combination method as a function of (B) in-field threshold (the minimum peak within a place field allowed as a fraction of the difference between the overall fluorescence peak in the data and the baseline), (C) minimum field width, (D) maximum fluorescence peak in the field, (E) in/out-field ratio, (F) ratio of traversals the cell fired in. (G) The percentage of ROIs in real data identified as place fields using Combination or Peak bootstrapping methods. (H) The percentage of ROIs identified as place cells by different methods, using the Peak bootstrapping method within the Combination method. Blue dashed lines indicate parameters used in published data and earlier analyses here. P-value in A is from an unpaired two-sample Wilcoxon test, p-value in B from a paired t-test.*

### 3 The effect of object location novelty and cue abundance on populations in hippocampal area CA1

#### 3.1 Introduction

The hippocampus plays a crucial role in navigation [22,26] and spatial memory [182]. It contains spatially tuned cells, such as place cells [22], in addition to cells tuned to particular task-related or environmental features, such as reward or object location [50,51,183]. The activity patterns of these populations of cells in the hippocampus are affected by a wide range of factors, including local and global cues [46,184], environmental context [43], and internal state of the animal [185,186].

Behaviourally, animals respond strongly to novel objects in an environment, as well as familiar objects that have been displaced from their normal location [48,153,187,188]. When a novel object is introduced into an environment, animals tend to spend more time exploring this object [153,187,188]. Similarly, when a familiar object is moved to a novel location, this also causes increased exploratory behaviour [48,187,188]. The hippocampus is especially important for the latter behaviour, as it involves spatial memory, and lesions to the hippocampus cause a reduction in these exploratory behaviours [187].

Individual cells in the hippocampus also respond strongly to objects in and around the environment [50,147,189]. Some place cells alter their activity in response to local cues, such as local objects, and global cues, including distal landmarks [46]. When these cues are displaced, their firing may follow the local or global cues, or change independently of the displacements [46,184,190]. The addition of local cues to an environment can also cause overrepresentation of the object locations in the place fields [147]. How individual cells respond to local object changes depends on the location of its field with cells closer to the change object being more likely to remap [189]. In addition, the hippocampus contains

specialized object-vector cells, also called landmark-vector cells, which always fire at a certain distance and direction relative to objects in an environment [50,64].

Reward locations provide a particular salient cue that affects place cell firing. Many studies report an overrepresentation of place fields at reward locations [51,111,191,192], while others don't see such overrepresentation, but do see out of field activation at the reward location in place cells [193]. This overrepresentation is affected by both visual cues at the reward and the amount of training or experience a mouse has [111,194]. It includes, at least partially, the presence of a separate population of cells with firing fields linked to a reward location [51].

Lastly, changes in the contextual cues in an environment, such as the colour of an environment, or the task-related context, lead to changes in place cell activity [43,137,195,196]. Individual cells may respond more to particular contexts and not to others, such as single cells always responding to an environment with white walls, regardless of the odour [195]. The environmental context can also control how single cells respond to cues, for examples cells responded differently to the same visual cue depending on the shape of the environment [197].

Although many studies have interrogated how single factors, such as environmental components or internal state, affect hippocampal populations separately, it is still unclear how multiple factors interact to create a single environmental representation. It has been suggested that place cells integrate heterogenous input of the different environmental changes [43]. Here, we aim to combine several factors in a novel object location recognition task, to look at how an interaction of factors influences the firing of pyramidal cells in CA1. We exposed our animals to environments that varied in cue abundance and cue object location, and trained them to recognize the displacement of the cue object in order to receive reward. The cue object location variation is equivalent to an object location memory task, which is used to measure hippocampal-dependent memory function in mouse models [48]. As such, we

would expect this manipulation to strongly drive hippocampal cells. The cue abundance manipulations involved adding patterns to the floors and walls, and adding distal objects. The patterned walls and floors are similar to context cues used in previous studies, where the floor and wall colours was changed [43], which could drive place cell remapping. In addition, distal objects or landmarks have also previously been shown to drive remapping in a subset of place cells [46,143]. We would therefore expect the changes applied in the cue abundant condition to strongly drive place cell remapping.

Previous studies have often focused on the effect of one manipulation (e.g. [147]), or multiple manipulations of one kind (e.g. two types of objects [46] or two types of context cues [43]). Here, we use two distinct manipulations, that both separate have been shown to strongly drive place cell remapping, to investigate how the hippocampal population responds to either manipulation separately, and both manipulations at the same time. Our aim is to study how various manipulations of the environment are encoded in the hippocampus to create a single representation of the environment. In particular, we are interested to see whether the two manipulations affect different subsets of place cells, which are then combined to represent the full environment, as previously proposed for the integration of contextual cues [43].

We imaged CA1 pyramidal cells of these mice at several time points while they were learning to perform this task, allowing us to look at the effect of cue abundance, object location novelty and level of training on the activity of hippocampal cell populations. We expected a modular effect of our two factors, with some cells remapping when cue abundance changed, others when object location novelty changed, and some responding only to unique combinations of cue abundance and object location novelty.

As our task uniquely dissociated cue object location from reward location, we could distinguish between responses to the cues and reward responses. In addition, in the novel object location condition, the cue object was displaced to a random location, thus allowing us to distinguish

between place cells and cells responding specifically to the cue object location. We expected to see an increase of place cell response around both the cue and control objects, and the recruitment of object-vector cells in the novel object location condition.

Surprisingly, we did not find a modular effect of the two environmental factors. Instead, cue abundance did not affect hippocampal cell population activity. However, displacing the cue object decreased the number of place cells and increased location encoding. In addition, a change in object location novelty caused place cells to remap, which was not the case for changes in cue abundance. This suggests that the hippocampal cells respond strongly to the displacement of an object, even when the animals cannot explore the objects by whisking or sniffing, and that the displacement of an object leads to place cell remapping. Lastly, non-place cells contribute more to the encoding of location in environments with a displaced object compared to the object in the familiar condition, highlighting the role of the wider hippocampal population in location encoding.

## 3.2 Results

### 3.2.1 Mice learn to perform a novel spatial task in virtual reality

To study the effects of environmental factors on hippocampal representation, we first trained our mice to perform a behavioural task in a virtual reality environment. The mice traversed in the same direction repeatedly through a 200 cm long virtual corridor while they were head-fixed (Fig 3.1A,D). Between each traversal of the corridor, the mice ran through a 95 cm dark pipe, during which we rendered the next environment. Using the pipe made the rendering of the new environment undetectable to the animal. We manipulated two characteristics of the environment: the cue abundance and the spatial location of a cue object. The cue abundance of the environment was either sparse (Fig 3.1B), with grey walls and a grey floor and no distal objects, or abundant (Fig 3.1C), with patterned walls and floors and two distal objects. In 33%

of the traversals (novel condition), the blue ball (Fig 3.1B,C) was displaced along the length of the corridor, compared to its regular position (familiar condition).

For the task, the mice had to lick for a reward in the reward zone at the end of the corridor (Fig 3.1D, 180-200 cm), which was marked by a lighter area on the floor, when they had recognized that the object was in an unfamiliar location (novel condition). We trained the animals in three steps (S Fig 3.1A). First, we trained them to lick in the reward zone by presenting a reward every time they entered the reward zone in the rewarded traversals (step 1). Once they licked at least 40% of the trials, we stopped presenting the reward on every rewarded traversal and only delivered it if the mouse started licking (step 2). Once the mouse learned to lick in the reward zone prior to receiving the reward in 40% of the trials, we started introducing punishment, a full screen white flicker, when the mouse licked in the non-rewarded traversals, to train it to distinguish between the novel and familiar conditions. We deemed a mouse fully trained when it showed an absolute difference of 30% in traversals licked between the novel (rewarded) and familiar (unrewarded) condition.

We trained a total of 12 mice, 9 of which (75%) completed step 3 of training (Fig 3.1E). We imaged seven of these mice throughout their learning process. On average, it took these mice 27 days (range: 16 to 37 days) to reach step 3, with training sessions occurring 2-3 times a week. Although the performance varied from day to day (S Fig 3.1B), we saw an overall increase in rewards obtained as the training progressed (Fig 3.1F).

We first studied the effect of the environmental manipulations (i.e. cue abundance and object novelty) on the behavioural performance of the mice. We looked separately at the performance in the familiar condition, where the correct choice was abstaining from licking, and the novel condition, where the correct choice was licking, as the measure of correct trials is different between the two, which may be biased by the mouse's predilection for licking. We did not see an effect of cue abundance in either of the conditions, and only an interaction

effect between cue abundance and training in the familiar, but not the novel condition (Fig 3.1G, Table 1, linear mixed model). We did see a strong effect of training in both conditions (Table 1, familiar:  $p=0.0001$ , novel:  $p=1.6\times 10^{-6}$ ). Interestingly, in the familiar condition there was a decrease in performance with training, whereas in the novel condition there was an increase. This is likely because mice learned to lick for reward as they were trained, so the untrained mice had a tendency to abstain from licking overall, resulting in a high performance in the unrewarded trials. As they went through training, they were encouraged to lick, increasing both licking in unrewarded trials (thus reducing performance) and rewarded trials (increasing performance).

Lastly, we looked at the effect of the amount of displacement on the performance of the task in the novel environments. We expected to see an increased performance if the object was more displaced, as the displacement would be more obvious for the mouse. We divided traversals into those with a displacement less than 60 cm (roughly the average displacement across all trials), and more than 60 cm. Surprisingly, the amount of displacement did not affect the performance of the task (S Fig 3.1C, Table 2, linear mixed model), nor did cue abundance or an interaction between the two. The performance across all conditions did increase after training. The lack of effect of displacement suggests that mice can recognize that the object was displaced even when it was only moved a short distance from its familiar position.

We present here a new behavioural task in virtual reality with a novel object location recognition element that is designed to engage the hippocampus. These results show that the mice are able to perform this task, even when they only get visual input about their surroundings, compared to the multisensory input in the real world. Overall, the mice show an increase in performance after training, and cue abundance did not affect their behaviour, meaning any potential hippocampal difference between the sparse and abundant condition is not mediated by performance.

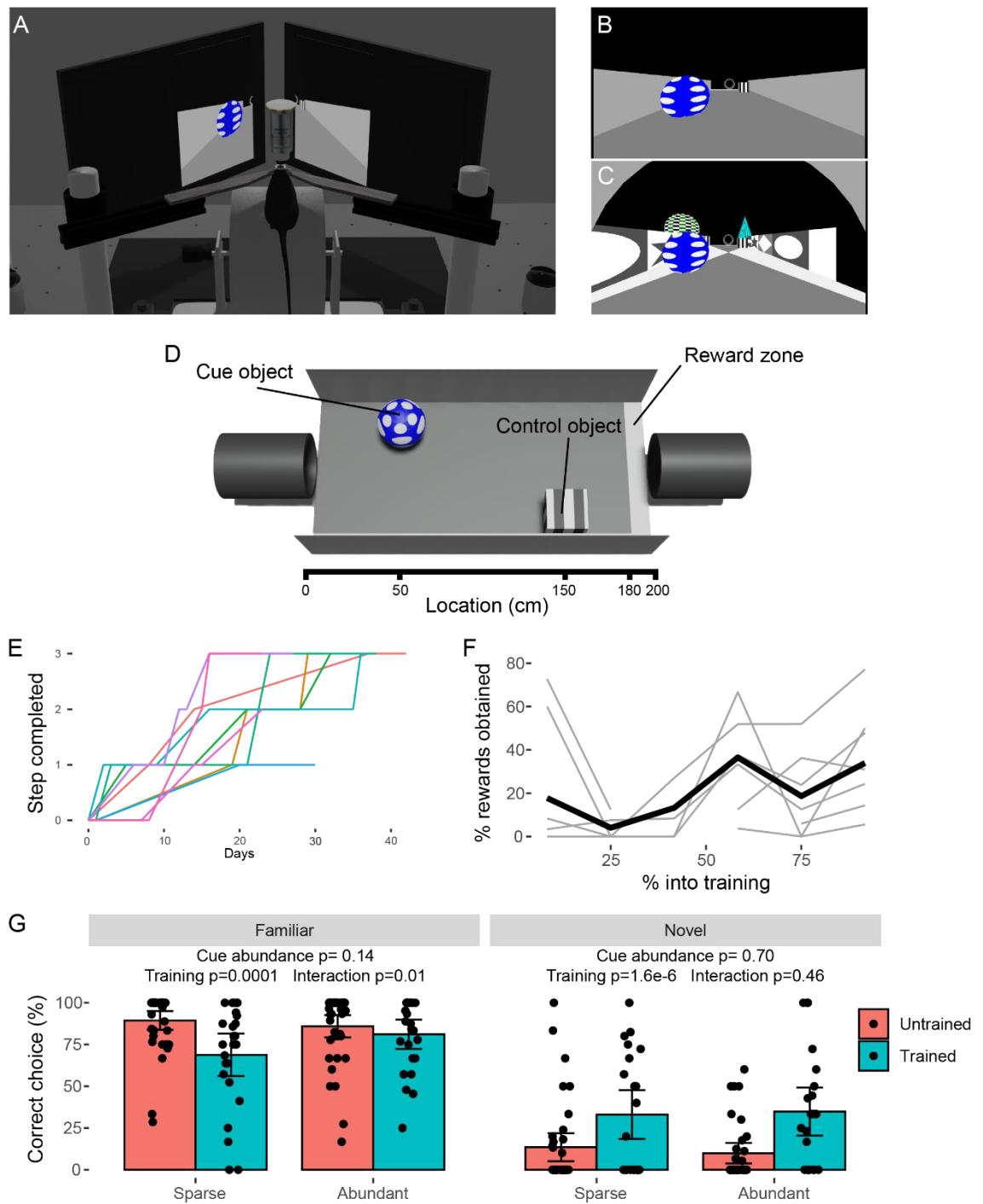


**Fig 3.1 Behavioural setup and task performance.** (A) A 3D representation of the two-photon experimental setup. The headfixed mouse is seen standing on a wheel with the objective over its head, while the virtual reality is displayed on the screens in front of it. (B-C) Example mouse view at the start of the (B) sparse and (C) abundance conditions. (D) Top view of the sparse environment showing the location of the cue object, control object and the reward zone. (E) Number of days it took for each mouse to reach each of the three training steps. (F) Percentage of rewards gained as a function of the amount of training received. Grey lines are separate mice, black line indicates the average. (G) Percentage of correct choices made before and after training in the four different conditions. In G,

*each data point is a session, bars show means, with error bars showing 95% confidence intervals. See Table 1 for N numbers for comparisons and all statistical analysis.*

### 3.2.2 Animals do not show behavioural preference for object locations

In real-world environments behavioural tasks, such as a novel object recognition or object location memory tasks, animals spend an increased amount of time around novel or displaced object compared to control objects [187,188]. Although our animals could freely run and stop whenever they wanted, they could only ever move in one direction along the corridor. As such, they were unable to explore objects as they would in a real-world task, by whisking or sniffing around the object. We wanted to test if they nevertheless still maintained a behavioural preference for slowing down or stopping around the object locations, and we expected our animals to slow down in particular around the cue object when it was displaced.

Both cue abundance or an interaction effect between cue abundance and object location novelty, did not affect the speed of the animal (Fig 3.2A, Table 3). However, the animals ran faster in the environments with the displaced object, than when the object was in the familiar location (Fig 3.2A, Table 3,  $p=0.010$ ). In addition, trained mice ran faster than untrained mice ( $p=0.011$ ). Thus, the cue abundance of the environment did not cause the animals to change their running behaviour, but both object location novelty and training did. The increase in speed suggests that, contrary to what we expected, the animals spend less time exploring the cue object when it was displaced.

To further study this, we looked at the average speed at the different locations within the environment (Fig 3.2B). We expected the mice slow down around the cue object compared to the control object location, and in the reward zone in the rewarded (novel) condition. We quantified the speed of the animals in areas of interest by averaging over the location bins around the control object (130 to 170 cm), around the familiar location of the cue object (30-70 cm) and the reward zone (170 to 200 cm). As expected, trained mice still ran faster than

untrained mice across conditions (S Fig 3.2A, Table 4,  $p < 2 \times 10^{-16}$ , linear mixed model), and mice were faster when the cue object was in a novel location ( $p = 1.8 \times 10^{-7}$ ), but the cue abundance did not affect the animal's velocity ( $p = 0.86$ ). As the location bin also affected the animal's velocity ( $p = 0.004$ ), we compared the speed in the location bins for each of the novelty conditions. In the familiar condition, but not the novel condition, the mouse slowed down in the reward zone compared to around the control object ( $p = 0.04$ , post-hoc Tukey test, Table 4) and the cue object ( $p = 0.03$ ). As we saw no difference in speed between the cue and control object locations in either familiar or novel conditions ( $p = 0.99$  and  $p = 0.44$ ), the mice do not seem to change their behaviour at the cue object.

The lack of difference between the cue object and the control object in the novel condition might be due to the cue object moving in the novel condition. Therefore, we also analysed the speed of the mouse relative to the cue object (Fig 3.2C). We again quantified velocity in three location bins, this time using different areas of interest: before the object (-100 to -30 cm), around the object (-30 to 30 cm) and after the object (30 to 100 cm). Again, trained mice ran faster than untrained mice across conditions (S Fig 3.2B, Table 4,  $p < 2 \times 10^{-16}$ , mixed linear model) and mice were faster when the cue object was in a novel location ( $p = 0.0004$ ), but cue abundance had no effect on velocity ( $p = 0.99$ ). Although the location bin did not affect velocity across the conditions ( $p = 0.39$ ), there was a significant interaction effect between location bin and object location novelty ( $p = 0.0002$ ). Therefore, we compared the location bins for each of the novelty conditions. In the familiar condition, the mice were significantly slower before compared to around or after the object ( $p = 0.025$ ,  $p = 0.003$ , post-hoc Tukey test) and after ( $p = 0.003$ ) the object. Conversely, in the novel condition the mice ran faster before compared to after the object ( $p = 0.023$ ). In both conditions, we do not see a clear decrease in speed around the object, suggesting the mice did not slow down around the cue object, regardless of whether it was in the familiar or a novel location.

In summary, we consistently saw an effect of novelty on the speed of the mice across all tests, with the mice running faster in the novel conditions. However, our results suggest that the animals also did not slow down around the displaced cue object. This is unexpected, as we would expect the novel object location to elicit exploratory behaviour resulting in decreased running. A possible explanation is that the mice know they are in a rewarded trial, and are therefore more motivated to reach the reward zone at the end, resulting in an increased velocity. Overall, these results show that although the mice learn our behavioural task, they do not show the characteristic behavioural patterns seen in similar real-world tasks.

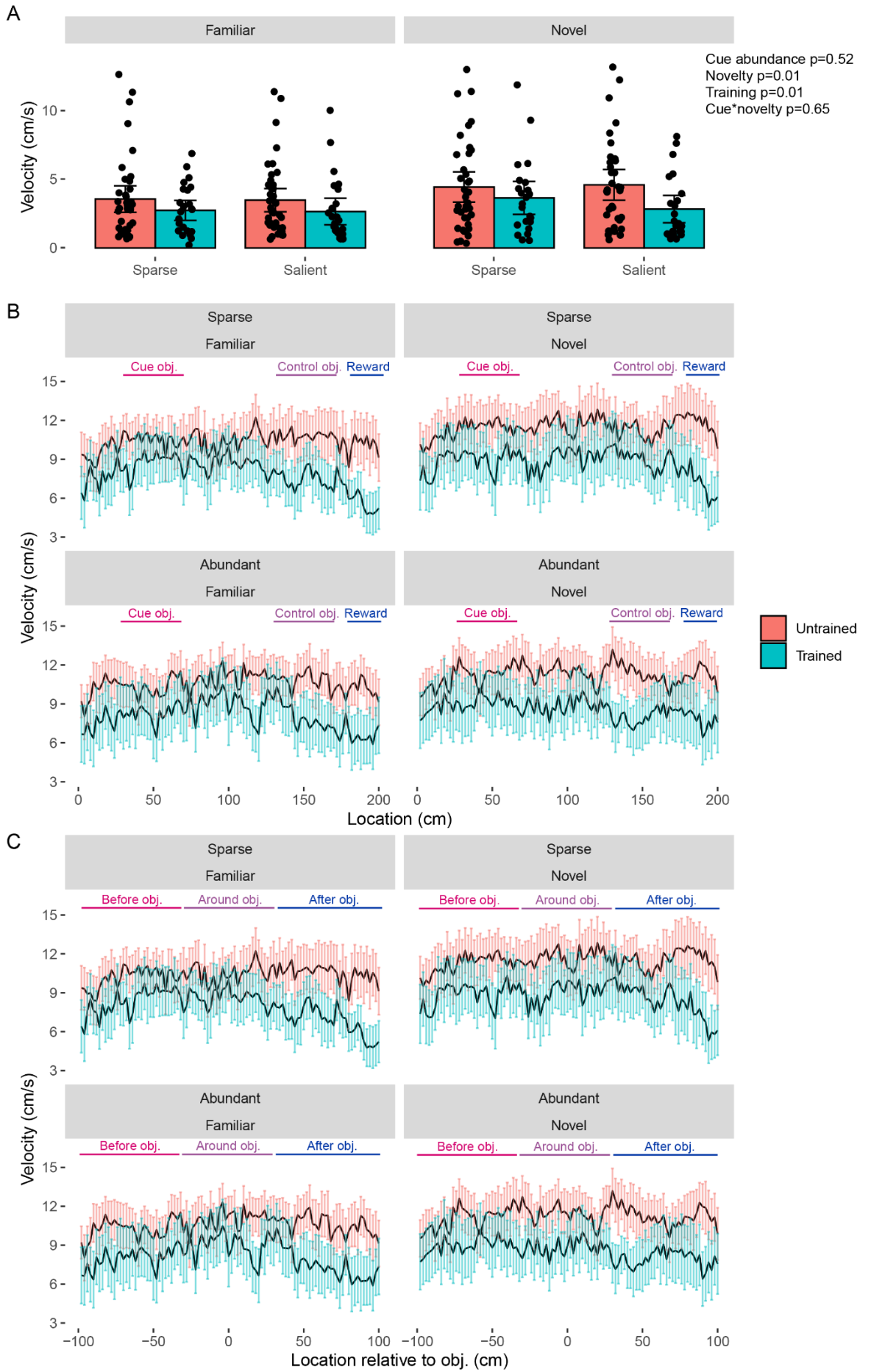


*Fig 3.2 Animal velocity during the behavioural task. (A) The mean velocity of the mouse in cm/s in each environment. (B) The mean velocity at each location of the environment, divided into 100 location bins. (C) The mean velocity at each location relative to the cue object, divided into 100 location bins. In A, each data point is a session, bars show means, with error bars showing 95% confidence intervals. In B and C the black lines show the means across the sessions, with the coloured error bars showing 95% confidence intervals. See Table 3 for N numbers for comparisons and all statistical analysis.*

### 3.2.3 Place cells hold increased information about location in novel conditions

As place cells represent a spatial map of the environment, we wanted to know how the number of place cells and the location of their place fields changed to represent the environments with different cue abundance and object location novelty conditions. To find the number of place cells in each condition, we classified the cells based on the maximum value in their fluorescence map, as previously described (Chapter 2, [198]). We quantified the place cells as the percentage of the total number of ROIs (region of interest) in a dataset. Overall, we found a relatively low number of place cells in each condition, compared to previous reports [35,198]. The percentage of place cells was significantly reduced when the cue object was displaced, while cue abundance had no effect (Fig 3.3A, Table 5,  $p=1.2 \times 10^{-13}$ ,  $p=0.31$ , linear mixed model). The percentage was also reduced in trained compared to untrained mice ( $p=0.005$ ). The reduction in place cells in the novel condition may be due to the cue object changing location, causing cells either to remap completely or follow the object between traversals, which would make us unable to identify them as place cells.

We wanted to know whether the place cells changed the amount of information about the animal's location, as a measure of their contribution to the overall spatial representation. We therefore determined the mutual information between the place cells and the mouse location, which represents the amount of information a place cell holds about the location [173–175]. Interestingly, we see an increase in mutual information in the novel compared to the familiar condition (Fig 3.3B, Table 5  $p=1.3 \times 10^{-10}$ ), meaning that although there were fewer place cells,

the individual place cells held more information about the location. Cue abundance did not affect the mutual information ( $p=0.54$ ), but there was an effect of training ( $p=0.005$ ), with the place cells in the untrained mice holding more information about location.

We measured several additional features of the place cells to further characterize them. None of our conditions affected the place field width (S Fig 3.3A, Table 6, linear mixed model).

However, place cells were significantly less stable in the novel condition (S Fig 3.3B, Table 6,  $p=8.1 \times 10^{-10}$ , linear mixed model). In addition, the ratio between the mean fluorescence outside and inside the place field, a measure of signal-to-noise of the place cell [147], was higher in the novel conditions (S Fig 3.3C, Table 6,  $p=0.004$ , linear mixed model). Both these effects, the stability being lower and the out/in ratio being higher, point towards the place cells being more noisy with a less consistent place field when the object is in a novel location. This seems to contradict the results from the mutual information, as they hold more information about the location of the animal in the environment in this condition.

As previous studies have reported an overrepresentation of place cells near a goal (rewarded) location [51,193], we next studied whether such overrepresentation was present in our task. We used the goal representation index (GRI) [193], which is the mean percentage of place field centres in the reward location compared to two control locations. None of our conditions significantly affected the GRI (Fig 3.3C, Table 5, linear mixed model). We tested whether there was an overrepresentation in any of the individual conditions. A GRI of 1 means the reward location has the same number of place field as the control locations, and any deviation represents an under- or overrepresentation. The GRI did not significantly differ from 1 in any condition (Fig 3.3C, Table 5, one-sample Wilcoxon signed rank test with Holm–Bonferroni correction for multiple comparisons). Both these results indicate that the reward zone was not overrepresented in the location of the cells' place fields.

We were further interested to see if the cue object and reward zone were overrepresented in the place field locations, so we determined the number of place field centres across the environment, comparing the object locations and the reward zone (Fig 3.3D, S Fig 3.3D). The place field centre for each cell was defined as the location of the maximum value in the fluorescence map. We quantified the differences in representation of different locations by dividing them into three bins: around the control object (130 to 170 cm), around the familiar location for the cue object (30 to 70 cm) and the reward zone (170 to 200 cm). There was a difference in percentage of place field centres between the bins (S Fig 3.3D, Table 6,  $p=0.001$ , linear mixed model). As we did not see an effect of training, we performed a post-hoc test using Tukey's method to determine the pairwise differences in each condition on the values per bin, averaged over training. This revealed a significant difference only in the novel/abundant condition, where there were significantly more place cells with their fields in the cue object location than in the reward zone (Table 6,  $p=0.004$ ). Again, there is no overrepresentation of the reward zone, nor is the cue object location overrepresented relative to the control object.

In summary, we found a low number of place cells compared to previous results [35,198]. This may be caused by the experimental setup, where mice were randomly presented with one of 4 conditions. This interleaving of conditions may have prevented the build-up of a stable representation of the environment, thus resulting in cells with unstable fluorescence maps, which are not classified as place cells in our data. The percentage of place cells is decreased in the novel compared to the familiar condition, but the cells hold increased mutual information about the location. Lastly, our results show no overrepresentation of the reward zone nor the cue object location in the location of the place fields.

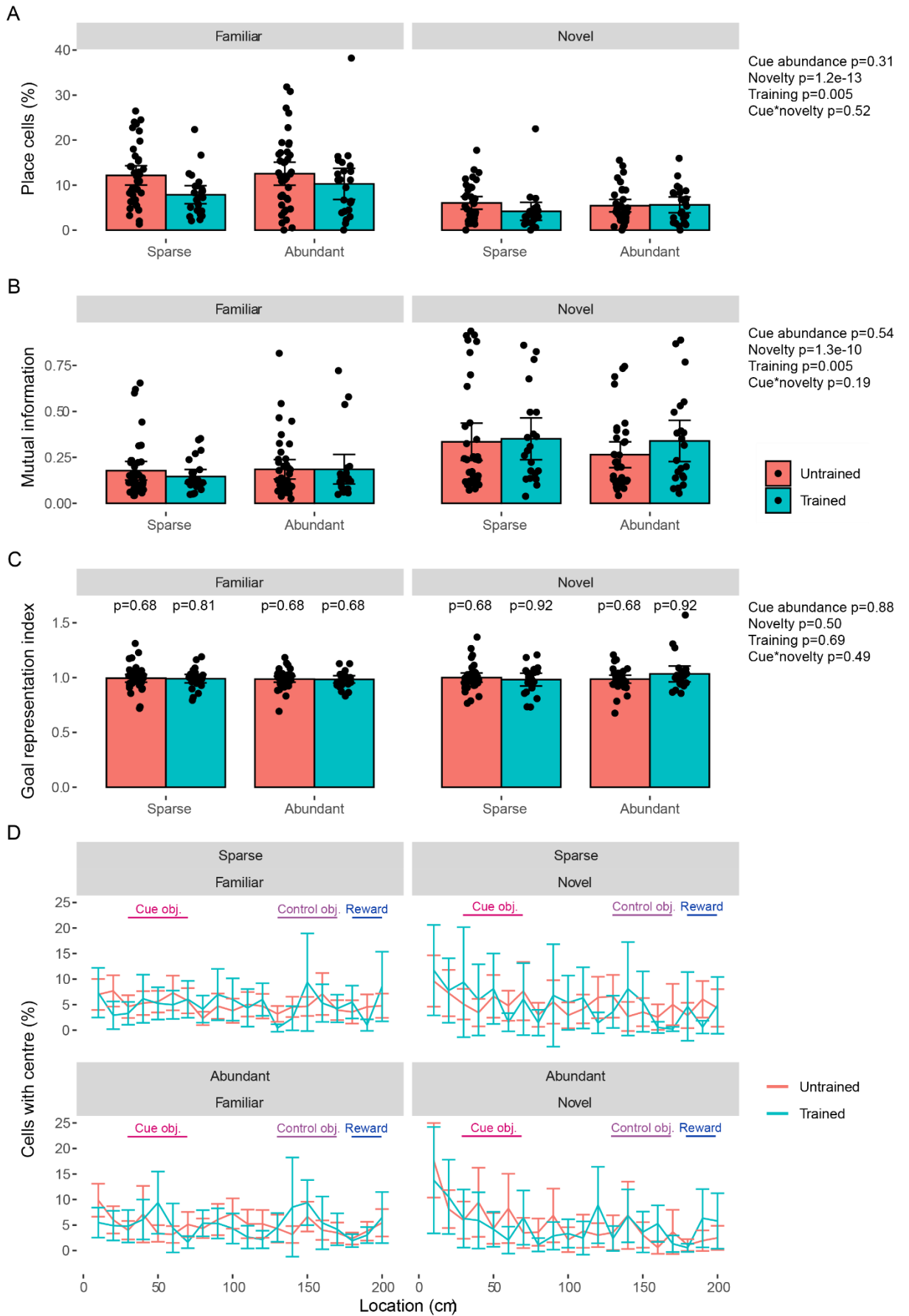


*Fig 3.3 Characteristics of the place cells. (A) Number of place cells found in each condition as a percentage of the total number of ROIs. (B) Mutual information (MI, in  $\frac{\text{bits}^{\Delta F}/F}{AP}$ ) between the cell activity and location. (C) Goal representation index, which is the mean activity in the reward zone divided by the mean activity in two control zones. P-values above bars from one-sample Wilcoxon signed rank test compared to a mean of 1 with Holm–Bonferroni correction for multiple comparisons. (D) The percentage of cells out of all place cells with their place field centres in different locations. The environment was divided in twenty 10 cm bins. In A-C, each data point is a session, bars show means, with error bars showing 95% confidence intervals. In D the coloured lines show the means across the sessions, with the error bars showing 95% confidence intervals. P-values next to A-C are from a linear mixed model with cue abundance, object location novelty, training and the interaction of cue abundance and novelty (cue\*novelty) as fixed-effects and mouse and imagining session as random-effects. See Table 5 for N numbers for comparisons and all statistical analysis.*

#### 3.2.4 Object-vector cells place fields follows the location of the cue object

The hippocampal formation contains specialized object-vector cells, also called landmark-vector cells to encode object locations [50,64]. These cells are active when an animal is in a particular location relative to an object, and thus do not rely on the global location. Our experimental setup lends itself perfectly to detect such cells, because in our novel condition the cue object is displaced to a different location every time, causing the object-vector cells to have clearly different activity patterns from the place cells, as their activity follows the object location.

To detect these object-vector cells in our data, we used the place cell detection method, but rather than calculating fluorescence maps over location, we calculated them over the location relative to the object. We again used the 99<sup>th</sup> percentile as the threshold (S Fig 3.4A). There was a significant correlation between the object-vector and place percentile scores (S Fig 3.4B), causing some cells to be classified as both place cells and object-vector cells (S Fig 3.4C). We excluded any cells that were already included as place cells. Using this method, we detected a number of cells that showed a firing field linked to the object (Fig 3.4A, S Fig 3.5).

We saw a range of cells with firing fields centred on the object (S Fig 3.5A-C), before the object (Fig 3.4A, S Fig 3.5D) or after the object (S Fig 3.5E,F).

As the location of the object is fixed in the familiar condition, we could not distinguish between object-vector cells and place cells in this condition. We therefore only analysed object-vector cells the novel condition. First, we determined the percentage of cells that were classified as object-vector cells, again as a percentage of the total number of ROI in a dataset. The percentage of object-vector cells was not significantly affected by cue abundance (Fig 3.4C, Table 7, linear mixed model), but, as for the place cells, decreased with training ( $p=0.001$ ).

We calculated the mutual information between the object-vector cells and the location relative to the object, and found no effect of cue abundance or training (Fig 3.4C, Table 7, linear mixed model). In addition, neither the object-vector field width and the ratio of fluorescence outside compared to within the object-vector field were affected by cue abundance or training (S Fig 3.6A,B, Table 8, linear mixed model). We quantified the stability of the cells as the Pearson correlation between the mean fluorescence over location relative to the object on the even compared to the odd traversals. Again, there was no significant effect of cue abundance (S Fig 3.6C, Table 8, linear mixed model), but the cells were more stable in untrained compared to trained mice ( $p=0.034$ ). So, although there is a decrease in both place cells and object-vector cells with training, unlike the place cells, the object-vector cells do not gain an increase in mutual information, and they become more unstable with training.

In addition, we compared the mutual information with the location relative to the object compared to the mutual information with the location relative to the global environment for the object-vector cells (S Fig 3.4D). We found no difference between the two scores. This is likely because the locations are oftentimes close to each other (when the object is only

displaced a small distance), thus resulting in a similar fluorescence map across the two reference frames.

As previous studies have shown object-vector cells respond to multiple or all objects in the environment [50,64], we wondered whether our identified object-vector cells also showed activity around the control object. To test this, we calculated the fluorescence map of the object-vector cells both around the cue and the control object. We then determined the correlation between the activity around the two objects using the Pearson correlation coefficient. We also performed 100 shuffled controls, where we calculated the correlation between the fluorescence map of an object-vector cell around the cue object, and a random cell around the control object. We saw a significant difference between the original correlations and shuffled controls (Fig 3.4D, Table 7,  $p=2.6 \times 10^{-9}$ , linear mixed model), but no effect of cue abundance. This suggests that across both cue abundance conditions, the object-vector cells respond to both the cue and control objects in a similar way.

As shown in our example cells, we see a range of locations for the firing fields of the object-vector cells. We would expect a larger number of object-vector field before the object, as the animal was unable to perceive the object after it had passed it. To test whether this was the case, we determined the distribution of the firing field centres relative to the object (Fig 3.4E). We quantified this similarly to how we had for the place cells, by dividing the locations into three different bins: before the object (-100 to -30 cm), around the object (-30 to 30 cm) and after the object (30 to 100 cm). We saw a difference between the location bins across the conditions (S Fig 3.6D, Table 8,  $p=0.0012$ , linear mixed model), but no effect of cue abundance or training. We performed a post-hoc test using Tukey's method to determine the pairwise differences between the location bins (Table 8). This revealed a significant increase in object-vector fields after compared to before ( $p=0.0008$ ), and around the object ( $p=0.0009$ ) in the sparse condition, but no differences in the abundant condition. So, despite the animal being

unable to see the object after it had passed it, more object-vector cells had their firing fields after the object in the sparse condition.

In summary, as our task included a randomly displaced object, we were able to find cells that specifically respond to a location relative to the object, although there was also a large overlap with the place cells. We saw a reduction in the number of these cells after training. As the cue object is relevant to the task, this might be counterintuitive, and we would expect an increased number of cells to respond to it after training. However, the task does not rely on the position relative to the object, but rather the position of the object itself in the environment, so object-vector cells may not be needed to perform it accurately. Interestingly, we see object-vector cells before, after, and around the object, with most having place fields after the object in the sparse condition. This suggests that the animals have a spatial representation of the object even if they cannot actively perceive it.

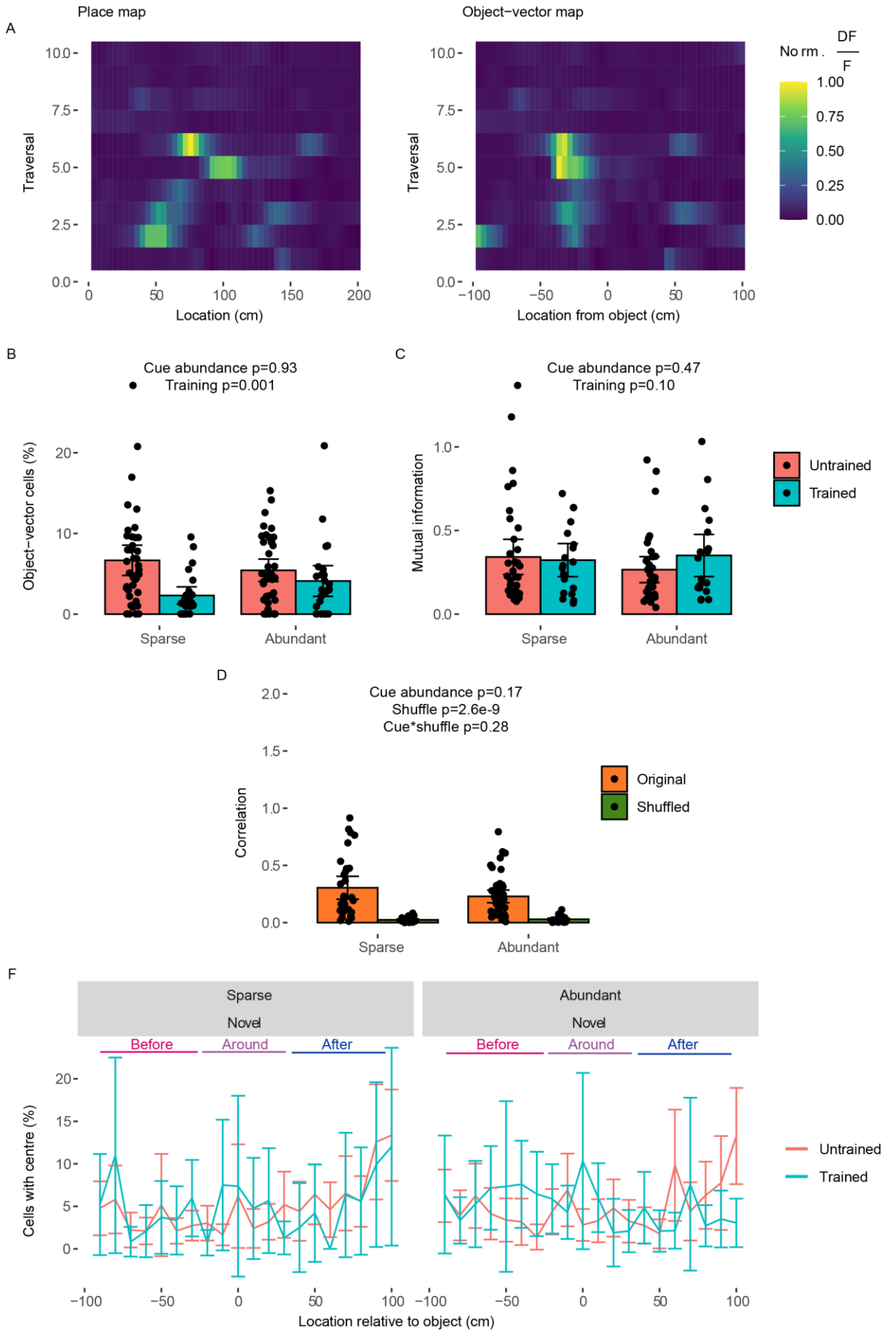


*Fig 3.4 Characteristics of the object-vector cells. (A) Example fluorescence maps over location (left) and location relative to the object (right) for a cell identified as object-vector cell. (B) Number of object-vector cells found in each condition as a percentage of the total number of ROIs. (C) Mutual information (MI, in  $\frac{\text{bits}\Delta F/F}{AP}$ ) between the cell activity and location relative to the object. (D) Goal representation index, which is the mean activity in the reward zone divided by the mean activity in two control zones. (E) Pearson correlation between the fluorescence around the cue object and around the cue object for the object-vector cells for the original data and shuffled controls. 100 shuffles were performed, where the cells identities were shuffled for the comparison. (E) The percentage of cells out of all object-vector cells with their activity field centres in different locations relative to the object. The locations were divided in twenty 10 cm bins. In B-C, each data point is a session, bars show means, with error bars showing 95% confidence intervals. In D each datapoint for the original data is a session, whereas the datapoints for the shuffled are the mean across 100 shuffles per dataset, bars show means, with error bars showing 95% confidence intervals. In E the coloured lines show the means across the sessions, with the error bars showing 95% confidence intervals. P-values above B and C are from a linear mixed model with cue abundance and training as fixed-effects and mouse and imagining session as random-effects. P-values above D are from a linear mixed model with cue abundance and shuffle and the interaction between cue abundance and shuffle (cue\*shuffle) as fixed-effects and mouse and imagining session as random-effects. See Table 7 for N numbers for comparisons and all statistical analysis.*

### 3.2.5 Place cells do not remap between conditions with the same novelty condition

We expected the place cells to respond modularly to the two conditions, cue abundance and object location novelty. However, cue abundance did not have an effect on the number or properties of the cells. We wanted to further look at how the conditions affected the place fields of the cells, so we imaged the same cells across the different environments, and determined how much the place and object-vector cells retained their location-specific firing across the environments. We were specifically interested in the effect of our two conditions, the cue abundance and the object location novelty, on the remapping of place and object-vector cells. We therefore grouped together comparisons where the animals were exposed to different novelty conditions, different cue abundance conditions, or had neither condition in common.

First, we looked at how many cells were classified as place cells across both conditions in each comparison. To this end, we determined the overlap coefficient, the overlap of place cell populations between two conditions divided by the number of place cells in the condition with the lowest number, which is effectively the overlap relative to the total possible overlap in place cells. We saw no difference between the overlap groups, meaning that a similar number of cells remained place cells when either the cue abundance, the object location novelty, or both conditions changed. However, the overlap did decrease with training across all groups (Fig 3.5A,  $p=0.030$ , mixed linear model). This may be indicative of the conditions each developing a unique representation as the animal learned the task.

We were interested whether the percentage of place cells the various conditions had in common was above what we expected by chance, which we calculated by multiplying the percentages of place cells in the compared conditions. There was a higher overlap of place cells than expected by chance in all groups and training conditions, except for the trained mice when the compared environments had no conditions in common (Fig 3.5B, paired two-sample Wilcoxon test, with Bonferroni-Holm correction for multiple comparisons). This suggests that some place cells specifically remain place cells when either of the conditions remains the same. However, when both conditions change, an independent population of place cells is recruited, though only after training. This fits with the idea of the conditions developing more unique representations for the conditions through training.

These two measures only looked at whether a particular cell was deemed a place cell across the conditions, but not whether it maintained the same activity pattern across the conditions. In order to test whether place cells had a stable place field across conditions, we determined the fluorescence map across locations for each of the conditions, and then calculated the Pearson correlation of the fluorescence map for each cell between the conditions. For every comparison, we only included cells that were included as place cells in both conditions. As a

control, we also determined the within-condition stability of each cell, by calculating the Pearson correlation between the average fluorescence maps over the even compared to the odd trials within a condition. There was a difference between the within- and between-condition correlations in the same abundance and difference groups, but not the same novelty group in both training conditions (paired-sample Wilcoxon test, with Bonferroni-Holm correction for multiple comparisons). This suggests that the place cells do not remap when switching between environments with the same novelty conditions, but they do if the novelty condition is different between the environments. Meanwhile, a change in cue abundance did not affect remapping.

We also applied these overlap and remapping analyses to the object-vector cells. In this case, we only performed one comparison, as the object-vector cells are only defined in the novel/sparse and novel/abundant conditions. Again, we did not see a difference between the trained and untrained groups (Fig 3.5D, unpaired two-sample Wilcoxon test). We compared the observed overlap to the expected overlap for the object-vector cells, and saw no significant difference in both training conditions (Fig 3.5E, paired-sample Wilcoxon test, with Bonferroni-Holm correction for multiple comparisons). It thus seems that when the environment changes in cue abundance, a new subset of object-vector cells is recruited.

Lastly, we repeated the correlation analysis, but instead of using the fluorescence maps over location, we used the fluorescence maps relative to the displaced object. For the object-vector cells, we did not see a significant difference between the within- and between-condition correlations in either the trained or untrained mice (Fig 3.5F,). Although for the object-vector cells case we cannot compare across conditions with different novelties, this indicates a lack of significant remapping between abundance conditions, as was the case for the place cells.

Overall, these results show a low overlap between environments in the place and object-vector cells. The overlap for the place cells decreases after training when the environments

had no condition in common, which suggests some form of pattern separation may take place [199]. In addition, we see remapping across conditions with the same cue abundance when the object location novelty changed. However, when the object location novelty stayed the same and the abundance changed, there was less remapping. This suggests that the place cells have a consistent representation within each novelty condition, but not within the cue abundance conditions.

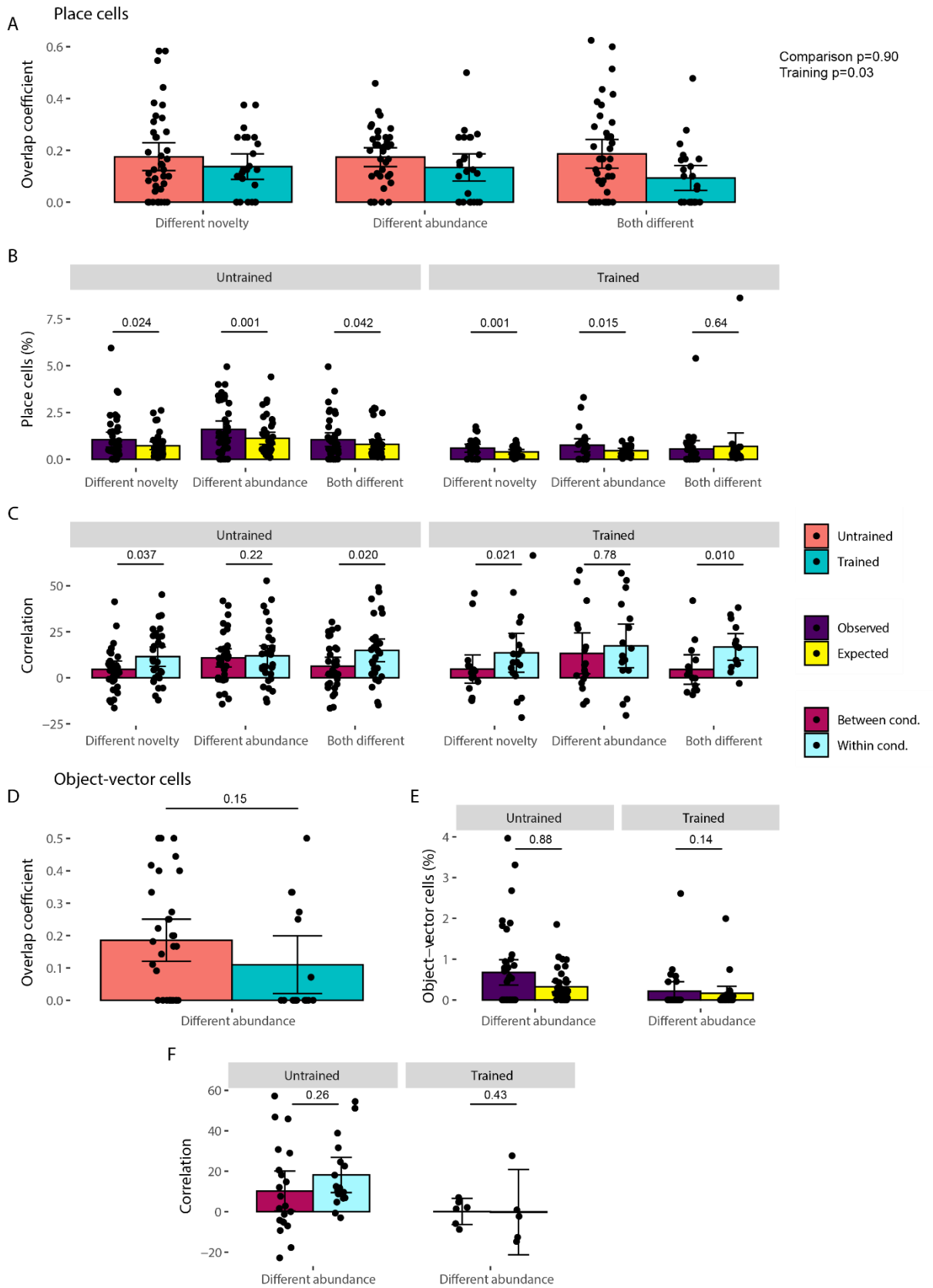


**Fig 3.5 Overlap of place and object-vector cells between the different conditions.** (A) Overlap coefficient for the comparison of place cells between environments with the same cue abundance condition, the same object location

*novelty condition, or different cue abundance and object location novelty conditions. (B) Observed and expected (by chance) percentage of ROIs that were identified as place cells, p-values from a paired two-sample Wilcoxon signed rank test with Holm-Bonferonni correction. (C) Correlation of the fluorescence map of place cells in environments with the same cue abundance, novelty, or that were different in both, p-values from a paired two-sample Wilcoxon signed rank test with Holm-Bonferonni correction. (D) Overlap coefficient for the comparison of object-vector cells between environments with the same novelty condition, p-value from unpaired two-sample Wilcoxon signed rank test. (E) Observed and expected (by chance) percentage of ROIs that were identified as object-vector cells, p-values from a paired two-sample Wilcoxon signed rank test with Holm-Bonferonni correction. (F) Correlation of the fluorescence map of place cells in environments with the same novelty, p-values from a paired two-sample Wilcoxon signed rank test with Holm-Bonferonni correction. For all plots each data point is a session, bars show means, with error bars showing 95% confidence intervals. P-values next to A are from a linear mixed model with comparison and training as fixed-effects and mouse and imagining session as random-effects. See Table 9 for N numbers for comparisons and all statistical analysis.*

### 3.2.6 Place cells contribute less to decoding of location in novel conditions

The goal for the animals is to know whether the cue object is displaced and correctly lick when it reaches the reward zone. In order to do this, we expect it to be able to estimate its own location accurately. We determined how accurately the place cells encode the animal's own location using a variation of a Bayesian decoder [200]. We used a separate decoder for each environment by calculating each cell's prior per environment. The decoding error was quantified as the distance between the predicted location and the true location in centimetres. As the end of our environment is connected to the start of the next environment via the tunnel, we accounted for this in the error calculation. As a control, we randomly shuffled the cells relative to their priors (i.e. each cell was assigned another cell's prior). This showed a significantly larger decoding error across all conditions (S Fig 3.7A, Table 11), meaning our decoder is able to meaningfully decode the animal position from the place cell activity.

We first looked at the decoding error across environments in the different stages of training. As expected, we saw a significant decrease in decoding error in trained compared to untrained mice (Fig 3.6A, Table 10,  $p=0.0002$ , linear mixed model). This suggests the cells got better at encoding the environment as a result of training in the task. Neither cue abundance or an interaction between cue abundance and object location novelty affected the decoding error. However, the decoding error was significantly lower in the novel compared to the familiar conditions (Fig 3.6A, Table 10,  $p=7.0 \times 10^{-16}$ ). This means the cells more accurately represented the animal's location on the track when the object was displaced, compared to when it was in the familiar location.

As both the cue object and reward location are relevant for the task, we expected the decoding of location to be more accurate around these locations compared to the control object. To test this, we calculated the decoding error for every frame of a recording, and then averaged the error across 2 cm location bins. We again performed a shuffle procedure, and subtracted the shuffled error per location bin from the original error to correct for any trends in the error due to the nature of our trial setup (Fig 3.6B). We quantified the differences by looking at three areas of interest: the familiar location of the cue object (30-70 cm), the location of the control object (130-170 cm) and the reward zone (170-200 cm). Again, there was a decrease in error in the novel compared to the familiar conditions (S Fig 3.7B, Table 11,  $p=1.3 \times 10^{-14}$ , linear mixed model), and no significant effect of cue abundance. Interestingly, location bin also had a significant effect on decoding error ( $p=0.002$ ), which we investigated further. As there was no effect of cue abundance, we performed a post-hoc test using Tukey's method comparing the locations separately for both novelty conditions, collapsed across cue abundance. This showed that in the novel, but not the familiar condition, there was a significant increase in decoding accuracy both around the cue object and the reward zone compared to the control object location ( $p=0.024$  and  $p=0.011$ , Table 11). This suggests that the animals indeed encode the locations most relevant for the task (the reward zone and the

cue object location) more accurately than the control object, even though the cue object is not in the cue object location in this condition.

As we saw an increase in mutual information in the place cells in the novel compared to the familiar condition (Fig 3.3B), we wondered whether the decrease in decoding error in novel conditions was caused by the place cells. Therefore, we next looked at the contribution of place cells to the decoding. We performed the decoding using only the place cells and subtracted the previously determined error across all cells from the result. If the place cells contributed greatly to the decoding, we expected their decoding error to be similar to the decoding error across all cells, resulting in a low difference in error. We first tested this by comparing the decoding error difference for each of the conditions to 0. In the familiar condition, the error difference was not significantly different from 0, across cue abundance and training conditions (Fig 3.6C, Table 10, one-sample Wilcoxon signed rank test with Holm-Bonferroni correction for multiple comparisons). However, in all conditions across the novel condition, the error difference was significantly higher than 0. This means that in the novel condition, but not the familiar condition, non-place cells significantly contribute to location decoding.

As this suggests there is a difference between the conditions, we also compared the error difference across cue abundance, novelty and training conditions. The trained mice had a significantly higher error difference compared to the untrained mice (Fig 3.6C, Table 10,  $p=0.046$ , linear mixed model), suggesting the contribution of the place cells decreased with training. In addition, the error difference was significantly greater in the novel than the familiar condition (Fig 3.6C, Table 10,  $p=2.5 \times 10^{-13}$ ). This indicates that the place cells have an overall lower contribution to the decoding in conditions when the cue object is in a novel location. Presumably in these conditions, non-place cells play a more important role.

As we saw differences in encoding between the task relevant and control cue locations, we tested whether the place cells contributed to this difference. To this end, we determined the change in decoding error at different locations caused by the place cells, by subtracting the error per location across all cells from the decoding error of the place cells alone (Fig 3.6D). We used the same three zones of interest to quantify the differences. Again the error difference was higher in the novel than the familiar condition (S Fig 3.7C, Table 11,  $p=9.1 \times 10^{-11}$ , linear mixed model), while neither cue abundance nor training had a significant effect. As there was a significant effect of location ( $p=1.8 \times 10^{-6}$ ), we performed the same post-hoc test using Tukey's method, which showed a significant decrease in encoding error difference between the control and the reward location in the familiar condition ( $p=0.001$ ). In addition, the encoding error difference was significantly lower in the reward location compared to the control and the cue object in the novel condition ( $p=0.0017$  and  $p=0.0009$ , Table 11). This suggests that the place cells more strongly contribute to encoding the reward location compared to other locations in the environment across the conditions.

Overall, cue abundance has no effect on the encoding of location across our various tests. However, we are better able to decode the animal's location when the cue object is displaced, with the reward zone and the cue object location in particularly having a decreased encoding error. Place cells contribute less to the decoding in the novel compared to the familiar conditions. Interestingly they contribute relatively more around the reward location, even though we did not see an overrepresentation of reward location in the place fields. This would suggest that the place cells are more important for encoding the reward location, while non-place cells contribute more to encoding other areas of the environment.

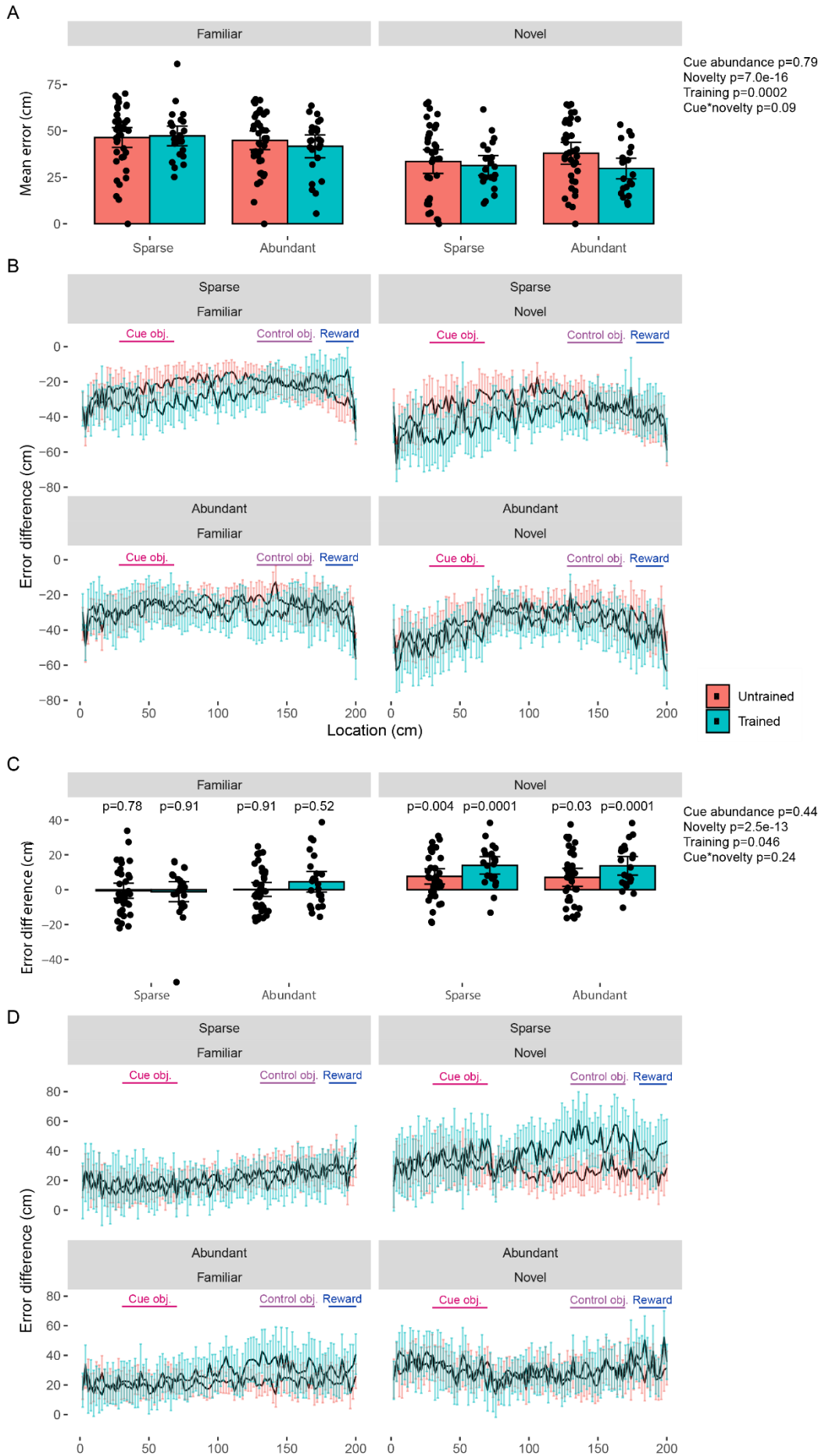


*Fig 3.6 Decoding animal location across environmental conditions. (A) Mean decoding error of a Bayesian decoder predicting location based on the activity of all cells. (B) Mean difference between the original decoding error across location and the decoding error of a shuffled version. (C). Mean difference in decoding error between a decoder that includes all cells, and one using only place cells. P-values above bars from one-sample Wilcoxon signed rank test compared to a mean of 0 with Holm–Bonferroni correction for multiple comparisons. (D) Mean difference between the decoding error across location using all cells and the decoding error using only place cells. In A and C, each data point is a session, bars show means, with error bars showing 95% confidence intervals. In B and D the black lines show the means across the sessions, with the coloured error bars showing 95% confidence intervals. P-values next to A and C are from a linear mixed model with cue abundance, object location novelty, training and the interaction of cue abundance and novelty (cue\*novelty) as fixed-effects and mouse and imagining session as random-effects. See Table 10 for N numbers for comparisons and all statistical analysis.*

### 3.2.7 Hippocampal cells encode the animal's location relative to the cue object

As the location of the cue object is relevant for the task, and we see object-vector cells which respond to a specific location relative to the cue, we also determined how well these cells encoded the animal's position relative to the cue object. We used a Bayesian decoder as detailed above, but this time using the fluorescence map relative to the object location rather than the fluorescence map over location for the cell's prior probability. We included the encoding in the familiar condition, though it should be noted that the location of the object in this condition is always the same. Here, we did not use a circular error, as we used a set distance around the object (100 cm), and the end of this region was not connected to the start of the next one at a set distance. We again performed a shuffled control, and the decoder error of the original decoder was significantly lower than error in the shuffled control in all conditions (S Fig 3.8A, Table 13), meaning our decoder is able to meaningfully decode the animal position from the place cell activity.

We next tested the effect of the environmental conditions and training on the decoding of object location. Again, both training and displacement of the cue object caused a decrease in decoding error (Fig 3.7A, Table 12,  $p=0.021$  and  $p=3.3 \times 10^{-11}$ , linear mixed model), but cue

abundance had no effect. So, in addition to the animal's own location, the cells also encode its location relative to the cue object more accurately in the novel condition.

As we saw an increase in the number of object-vector cells with their object-vector field centre after the cue object, we were interested to see if this is reflected in the coding error. We determined the difference in decoding error at different locations relative to the cue object, again using the error per location and subtracting the shuffled error (Fig 3.7B), and quantified this by looking at three areas of interest: before the object (-100 to -30 cm), around the object (-30 to 30 cm) and after the object (30 to 100 cm). Again, the error decreased in the displaced condition (S Fig 3.8B, Table 13,  $p=5.0 \times 10^{-11}$ , linear mixed model), but neither cue abundance nor training affected the error. We did see an effect of location ( $p=1.8 \times 10^{-9}$ ), which we studied further with a post-hoc test using Tukey's method comparing the locations separately for both novelty conditions. In both the familiar and novel conditions the encoding error was significantly lower around compared to before ( $p=0.0033$  and  $p<0.0001$ , Table 13), and after the object ( $p=0.014$  and  $p=0.022$ ). Thus, the animal is better able to estimate its location relative to the object when it is around the object.

However, the object-vector cells overrepresented location after the object, rather than around the object. Therefore, we also examined the contribution of the object-vector cells to the cue object location decoding. As these cells were only defined in the novel condition, we restricted our analysis to this condition. As previously, we subtracted the error of the decoder using all cells from the error of the decoder that only included object-vector cells. Again, we first tested this by comparing the decoding error difference for each of the conditions to 0. Across the cue abundance and training conditions, the error difference was significantly greater than 0 (Fig 3.7C, Table 12, one-sample Wilcoxon signed rank test with Holm-Bonferroni correction for multiple comparisons). This means that decoding of the animal's location relative to the cue object did not strongly depend on object-vector cells.

We additionally compared the error difference across cue abundance and training conditions. Cue abundance did not affect the error difference (Fig 3.7C, Table 12). However, after training the error difference was higher (Fig 3.7C, Table 12,  $p=0.012$ , linear mixed model), showing a similar pattern as the place cells, suggesting the object-vector cells contributed less to the encoding of the cue object location after training.

We lastly determined the difference in decoder error when only using object-vector cells across the different locations (Fig 3.7D). Again, we quantified this with the three location zones: before, around or after the object. We saw no effect of cue abundance, but we did see an effect of location (S Fig 3.8, Table 13,  $p=0.0010$ , linear mixed model). A post-hoc test using Tukey's method revealed the error difference was significantly larger after compared to before or around the cue object ( $p=0.0037$  and  $p=0.0035$ , Table 13). This means the object-vector cells contributed relatively more to the encoding before and around compared to after the cue object. This is surprising, as we saw an overrepresentation of object-vector cells after the object.

Overall, we are able to decode the location of the cue object, even if it is not always in the same location in the environment, suggesting the hippocampal cells hold a representation of the animal's location relative to the cue object. In addition, we found increased decoding accuracy around the object location. The object-vector cells showed a relatively small contribution to the decoding, especially after training. In addition, the object-vector cells contribute less to encoding the animal's location relative to the object after it had passed the object. Together, these results suggest that non-object-vector cells contribute greatly to encoding an animal's position relative to the object.

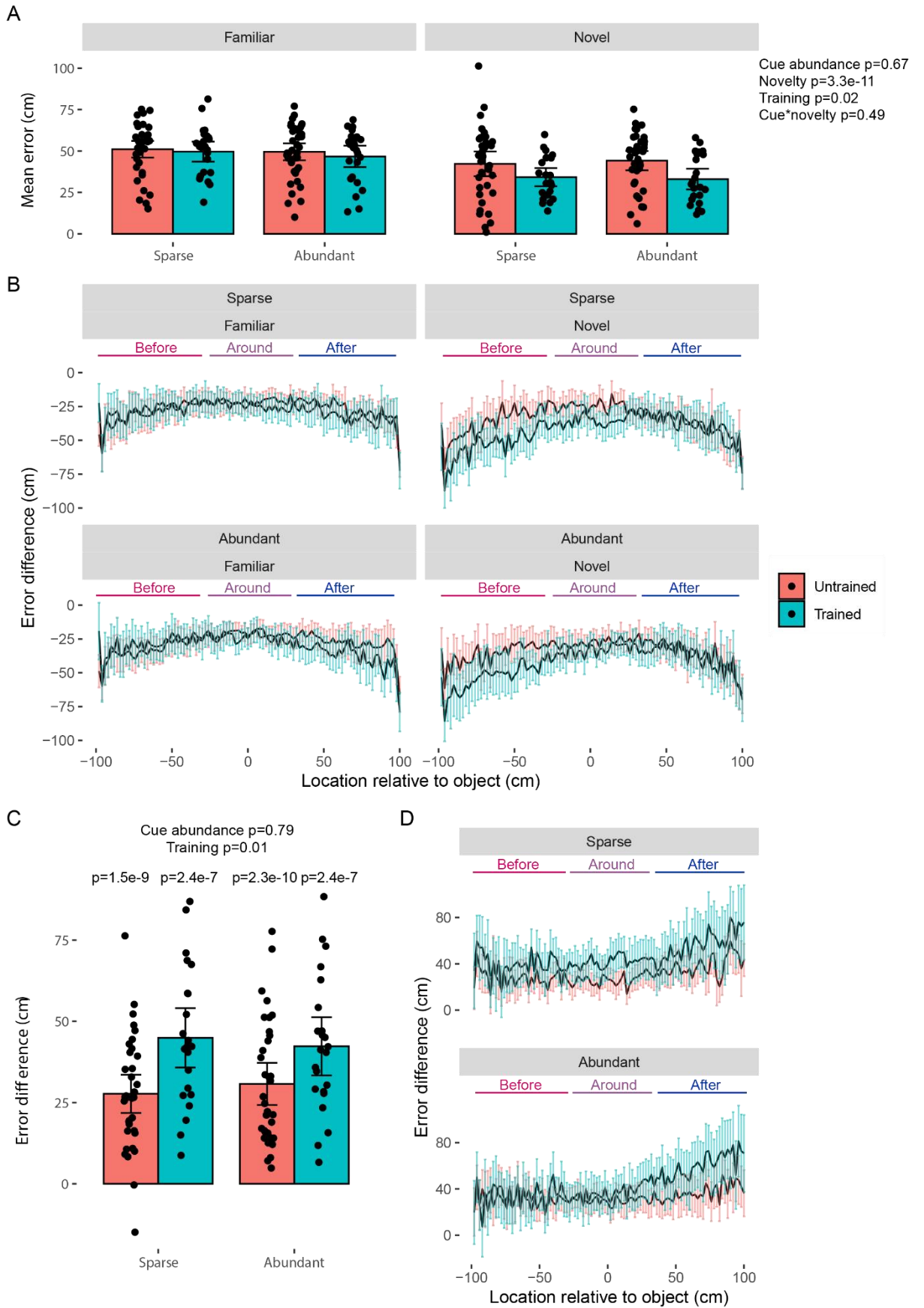


*Fig 3.7 Decoding animal location relative to the cue object. (A) Mean decoding error of a Bayesian decoder predicting location relative to the cue object based on the activity of all cells. (B) Mean difference between the original decoding error across location and the decoding error of a shuffled version. (C). Mean difference in decoding error between a decoder that includes all cells, and one using only object-vector cells. P-values above bars from one-sample Wilcoxon signed rank test compared to a mean of 0 with Holm–Bonferroni correction for multiple comparisons. (D) Mean difference between the decoding error across location using all cells and the decoding error using only object-vector cells. In A and C, each data point is a session, bars show means, with error bars showing 95% confidence intervals. In B and D the black lines show the means across the sessions, with the coloured error bars showing 95% confidence intervals. P-values next to A are from a linear mixed model with cue abundance, object location novelty, training and the interaction of cue abundance and novelty (cue\**novelty*) as fixed-effects and mouse and imagining session as random-effects, those above C are from a linear mixed model with cue abundance and training as fixed-effects and mouse and imagining session as random-effects. See Table 12 for N numbers for comparisons and all statistical analysis.*

### 3.3 Discussion

We studied the effect of two environmental conditions, cue abundance and object location novelty, as well as training on a novel behavioural task on the representation of an environment. We found a strong effect of object location novelty on behaviour and various place cell characteristics, with the mouse running faster and the place cells becoming less accurate, but holding more spatial information, when the cue object was displaced, but no effect of cue abundance across our analyses. In addition, we found remapping of place cells when the object location novelty condition changed, but not when the cue abundance changed. These differences translated into an increased decoding of location in the novel condition, suggesting the hippocampus encoded the mouse location in this condition more precisely compared to the familiar condition, but did not change its encoding when the cue abundance changed.

In this study we introduced a novel, virtual reality, behavioural task, requiring the animals to recognize an object's location using only visual input. Although previous real-world equivalents

have shown animals to spend more time around displaced or novel objects [187,188,201], we do not see a similar effect in our paradigm. Mice have been previously shown to respond to novelty in a visual-only paradigm [201], but in that paradigm the mice were still able to freely approach and explore the screen showing the objects. In our case the mice are restricted to the middle of the environment and can only face forward, thus reducing their ability to interact with the object. The mice indeed did not slow down around the objects, there were no confounding effects of exploratory behaviours such as whisking and sniffing. This uniquely allowed us to determine which cells respond to the object based only on visual stimuli. We show for the first time that object-vector cells are not dependent on the mouse being able to interact with an object, and will represent an object even when it is not able to perceive it in any way (visually, olfactory or otherwise).

Our paradigm also affects the cell dynamics, evidenced by the low number of place cells we find compared to previous reports [35,198]. Although virtual reality does cause changes in the place cells characteristics compared to real-world environments [149], the number of place cells we detect here are also low compared to previous virtual reality paradigms, particularly in the novel condition. A possible explanation is the random interweaving of conditions, unlike previous studies [35,147], as place fields take may take some time in an environment to stabilize [202]. By interweaving the trials as we have, we may be giving the mice less time to create a stable representation of the environment. In addition, our animals experience a large number of individual entries into the environment, which may induce switching between multiple maps of a single environment [24]. Despite the low number of place cells the mice are able to perform the task and hold an accurate representation of the environment, as evidenced by the task performance and the Bayesian decoder results. Indeed, although the number of place cells and their stability was lower, and the out/in fluorescence ratio was higher, in the novel condition, we were able to more accurately decode the location of the animal in this condition. This highlights the importance of non-place cells in spatial

representation, and possibly suggests that the non-place cells become more important in more variable environments.

We do not see an effect of cue abundance across our tested metrics, including the behaviour, number of place cells and object-vector cells, and the decoder error. Thus, in our task, cue abundance does not influence the representation of the environment in the brain. This is surprising, because our abundant condition added several cue elements, including distal objects and patterning on the walls and floor. Earlier studies have shown that distal object can change place cell activity and cause remapping [46,184,190], though this effect may be secondary to that of local objects [190]. In our paradigm the cells already respond so strongly to the cue object being displaced, the number of place cells recruited by the distal objects may be negligible. In addition, we do not distinguish between deep and superficial layers of dorsal CA1 in our imaging. Depending on the quality of the surgery and the specifics of a particular imaging session, we may include only deep cell bodies, only superficial, or a combination of both within an imaging session. A recent study [17] showed that these different layers respond differentially to sparse and abundant environments, with the superficial cells responding strongly to sparse environments, while the deep cells respond more strongly to abundant environments. In addition, this study also showed that place cells preferably use rate coding for sparse environments, but phase coding for abundant environments. We only examined rate coding, as our imaging resolution was not high enough to study the phase code of the place cells, and as such would not have been able to see such differences.

Even if the distal objects were not sufficient to induce a change, we would have expected an effect of wall patterning on the percentage of place cells, as a previous study has shown [147]. In addition, changes in wall and floor patterning is a type of contextual cue, such as the changing of the colour or odour of an environment, which we would expect to induce remapping [43]. One explanation would be that we only look at the remapping of cells that

were identified as place cells in both conditions, thus missing out cells that gained or lost their place cell classification between the conditions and skewing our remapping analysis towards more stable cells. However, we did not see a difference in the overlap between the environments, which we would expect if this were the case. Alternatively, we might suggest that the mice have learned to ignore this contextual cue, as it is not task relevant. However, if this were the case, we would expect to see an effect of training, which we do not see, meaning the mice start ignoring the cue abundance condition before learning to perform the task.

Overall, our results suggest that rather than a modular effect, with two contextual features inducing similar place cells changes [43,195], there may be more of a hierarchical effect, where one environmental feature, in this case cue object displacement, affects the place cells more than another feature. It would be interesting to increase the number of features in the environment that are changed to determine whether this holds for other features, such as odour or task context. In addition, it would be interesting to see if we can reverse the effect by forcing the mice to attend to the cue abundance, by linking the reward to this feature rather than the object displacement.

Altogether, we show an absence of response to cue abundance in this virtual reality task, suggesting that the animals either do not pay attention to, or ignore, additional cues in the environment in this paradigm. However, they do respond very strongly to object location novelty, even when they are not able to behave around the objects as they would in a real-world task. As we are able to restrict the behaviour and monitor closely what the mouse sees at any given time during the, we can uniquely draw conclusions about the effect of visual cues hippocampal coding during this task. For example, we can see that the mice hold a representation of its location relative to the object even if the object is not in its visual field. Future work could take advantage of this paradigm and its advantages to study the effect of modular changes to the environment and its effect on hippocampal coding.

## 3.4 Materials and methods

### 3.4.1 Animals

All experimental procedures were approved by the UK Home Office, in accordance with the 1986 Animal (Scientific Procedures) Act. Experiments used four C57/BL6 mice (2 female, 2 male) expressing the genetically-encoded calcium indicator GCaMP6f under the control of a Thy-1 promoter (C57BL/6J-Tg(Thy1-GCaMP6f)GP5.5Dkim/J). The mice were housed in a 12h reverse dark/light cycle environment at a temperature of 22°C and were given ad libitum access to food and water.

### 3.4.2 Hippocampal cranial window surgery

Surgery was performed when mice were a minimum age of eight weeks. Before surgery, mice received subcutaneous injections of dexamethasone (60  $\mu$ L, 2mg/mL), saline (400  $\mu$ L) and buprenorphine (40  $\mu$ L, 0.3mg/mL diluted 1:10 in saline) to reduce inflammation, for hydration, and pain relief respectively. Mice were maintained at 0.8-2.0% isofluorane anaesthesia for the duration of the surgery. Body temperature was maintained at 37 °C using a homeothermic blanket (PhysioSuite, Kent Scientific Corporation). A craniotomy was inserted above dorsal CA1 as previously described [23]. Briefly, the skin above the skull was removed and the skull was scored to increase the surface area for binding dental cement. A custom-made stainless steel headplate was then fixed to the skull with black dental cement (Unifast Powder mixed with black ink (1:15 w/w) and Unifast Liquid). A 3 mm diameter craniotomy was then performed 2mm posterior to bregma and 1.5 mm lateral to the sagittal suture. Following the removal of the skull flap and the dura, brain tissue overlying the hippocampus was aspirated (New Askir 30, CA-MI Srl) until vertical striations of the corpus callosum were visible. We then inserted a custom 3D printed cannula (2.4 mm ID, 3 mm OD, 1.5 mm height) made of a biocompatible Dental SG resin (FormLabs) so that the glass coverslip at the bottom of the cannula lay directly on top of the brain tissue. The top of the cannula had a rim (0.2mm height, 3 mm OD) resting

on top of the skull, which was attached using tissue adhesive (3M VetBond) and then covered with more dental cement. A rubber ring was then attached on top of the headplate for subsequent use as a well for the water needed for the water-immersion microscope objective. The mice were given an injection of meloxicam (125  $\mu$ L, 5 mg/ml) as an analgesic near the end of the surgery and then received meloxicam (200  $\mu$ L, 1.5 mg/mL) for 4 days following the surgery via oral admission. Their health was monitored, and they were weighed daily.

### 3.4.3 Two-photon imaging

*Habituation.* A week or more after surgery, the mouse was habituated to the imaging rig by head-fixing it for an increasing amount of time each day for at least a week before it was imaged. During the habituation it was also presented with the virtual reality environment several times to make it familiar with this setup.

*Imaging rig (Fig 3.1A).* The mice were head-fixed above a polystyrene cylinder, on which they could run. The cylinder was fitted with a rotary encoder (Kübler, 4096 pulses per revolution). Two screens in front of the mice were used to display a custom virtual reality (VR) environment designed using ViRMEn [37].

*Reward delivery system.* We built a custom reward delivery and lick detection system using a Raspberry Pi. The reward delivery was performed using a blunted 21G needle attached to a tube. The needle was placed on a custom 3D printed micromanipulator that consisted of two modular axes (<https://www.thingiverse.com/thing:203734>, Baden lab) as well as a hinge to determine the angle of the needle. This allowed for precise placement in front of each mouse. The reward, diluted condensed milk, was delivered through a custom 3D printed pump driven by a servo motor, which was controlled through the Raspberry Pi. The Raspberry Pi received input from the computer controlling the virtual reality environment through a data acquisition device (LabJack T7), which sent a signal whenever a reward was to be delivered.

The system also included a lick detection system. This was achieved by turning the metal needle tip into a capacitive touch sensor. The needle was connected onto a circuit which also included a 1M $\Omega$  resistor. Our system was calibrated at the start of each session, and the voltage was readout throughout the session. When a big change in voltage was measured, caused by the tongue of the mouse touching the needle, a signal was sent to the computer controlling the virtual reality environment and the appropriate action was taken. If the mouse licked in the reward zone, a signal was sent back to deliver a reward by activating the motor. If the mouse licked outside of the reward zone and was in step 3 of behavioural training, a punishment, in the form of a flashing screen, was delivered.

*Data acquisition.* In the hippocampal experiments, the stratum pyramidale of dorsal CA1 was imaged using a two-photon microscope (Scientifica) with a water-immersion objective (CFI75 LWD 16X W, Nikon; 0.80 numerical aperture, 3 mm working distance). We used the ScanImage (Vidrio Technologies, MATLAB) software to control the microscope and collect data. The stratum pyramidale was identified from the presence of densely packed cell bodies. We optimised the acquisition rate by using a wide field-of-view at a low resolution (128x128 pixels, 7.51 Hz, 3.77  $\mu$ m pixel size).

#### 3.4.4 Behavioural task

*Environment.* The virtual reality environment presented to the mice was a wide corridor, 200 cm long and 80 cm wide, with 30 cm high walls (S Fig 5B). Both before and after the wide corridor was a dark grey tunnel with a diameter of 30 cm, 50 cm long before the corridor and 45 cm long after the corridor) which served to allow smooth transitions between multiple presentations of the environment. Inside the environment were always two objects: a blue and black striped ball and a white and black striped block. On each traversal both the cue abundance, binarized into two levels, and the location of the ball was randomly selected. For the cue abundance this meant either a combination of grey walls, a grey floor, and no external

objects (sparse condition), or patterns walls and floor and two additional objects (a cyan, black striped cone and a black, white and green blocked ball) outside of the walls (abundant condition). In the case of the ball location this was either in a familiar location (50 cm into the environment) or on a randomized location along the corridor (always 30 cm left of the middle) at least 15 cm from the familiar location, and at least 25 cm from the start and end of the environment, to ensure good visibility of the object.

*Mouse training.* Mice were trained to lick for reward (diluted condensed milk) in a reward zone at the end of the environment when they had detected that the goal object was displaced from its familiar position. The training was divided into three steps in order of difficulty (S Fig 3.1A). In the first step the mice only experienced the task passively; the reward was delivered regardless of whether the mice licked or not. In the second step the task was presented actively; the mice had to lick in the reward zone in order to receive the reward. In both these steps, no punishment was given when the mice licked on a non-rewarded trial. In step three, a punishment consisting of a flashing screen was introduced when the mice licked in a non-rewarded trial. Training sessions usually lasted up to three hours, but were dependent on the performance of the mouse.

We monitored animal performance throughout the training, this helped in determining when to introduce the next step. The next training step was introduced when the mouse licked in 40% of the passive trials (step 1), 40% of the active trials (step 2), and showed at least 30% difference in licks rewarded compared to non-rewarded trials (step 3). We always introduced these steps one by one, never both in one session. Once a mouse reached a certain step, we did not go back to a previous step, regardless of how they performed on a given day. We imaged the mice throughout training, aiming to collect data at least twice for every training step.

### 3.4.5 Image analysis

*Preprocessing.* Preprocessing was conducted using Suite2P software [172]. Firstly, images were registered using the default settings, then regions of interest (ROIs) corresponding to cell bodies were identified based on their morphology (having a diameter of approximately 10  $\mu\text{m}$ ) and a tau, the decay time for the calcium indicator, of 0.8. We refined the default Suite2P classifier to identify cells from non-cell ROIs by training it on 8 separate datasets that were collected with the same imaging settings. We obtained the calcium signal corrected for neuropil activity, by subtracting 0.7 times the neuropil signal from the ROI signal for each ROI, from the Suite2P output. Then we normalised time courses to baseline fluorescence for each ROI by dividing the whole trace by the average intensity in that ROI during the first 100 frames of the recording, obtaining the fluorescence as  $\Delta F/F$ .

### 3.4.6 Celltype analysis

*Place cell detection.* We used a method of place cell detection previously described for electrophysiology [55], which we adapted for, and tested on, two-photon microscopy data (Chapter 2, [198]). In short, we determined the fluorescence map for each cell by averaging the fluorescence over location, only including frames where the speed of the mouse was at least 1cm/s, and found the maximum value within the fluorescence map. Next, we shuffled the trace relative to the location 500 times, calculated the fluorescence map for the shuffled trace, and recorded the maximum fluorescence of the fluorescence map for each shuffle. If the original maximum value was in the 99th percentile of the shuffled maximum values, the cell was deemed a place cell.

*Object-vector cell detection.* To detect object-vector cells in our data, we used the same method as for the place cell detection. However, rather than calculating the fluorescence map over location, we calculated it over the relative location from the object. We only included any locations that were up to 100 cm from the object. After obtaining this fluorescence map, we

again calculated the maximum value, and then performed the shuffling procedure as previously described. To be included as object-vector cells, cells not only had to possess a maximum value in the 99th percentile, but also not be included as a place cell.

*Mutual information.* We calculated the mutual information between the cells and the location [173]. We calculated the bits of information directly from the fluorescence, rather than first applying a spike deconvolution, as this has been shown to give an accurate estimate of the information [175]. In short, we divided the fluorescence signal for each cell into 4 bins. We then calculated the probability of the fluorescence to be in each bin ( $p_i$ ), as well as the probability for each fluorescence bin per location bin ( $p_{ij}$ ). Next, we calculated the mutual information per cell using Equation 1.

$$MI_{ij} = \sum_i \sum_j p_{ij} \log\left(\frac{p_{ij}}{p_i \cdot p_j}\right) \quad \text{Equation 1}$$

*Place field width.* We measured the place field width by first determining the location of the maximum value within the fluorescence map for each cell. Next, we determined the full width half max (FWHM) as the mean between the maximum and the minimum value within the fluorescence map. Using the location of the maximum value as a centre, we then measured the place field width from the number of continuous location bins around the centre with fluorescence higher than the FWHM.

*Stability.* We determined the stability of the cells by first calculating the fluorescence map per traversal of the environment. Next, we took the average fluorescence map across the even and the odd traversals. The stability was defined as the Pearson correlation between the maps for the even and odd traversals.

*Out/in ratio.* To calculate the ratio between the fluorescence outside the place field and within the place field, we first calculated the fluorescence map per cell. We determined the location bins of the map included within the place field using the FWHM as described for the place field

width. We then divided the mean fluorescence across all location bins in the fluorescence map outside of the place field by the mean fluorescence across those within the place field to obtain the out/in ratio.

*Goal Representation Index.* We based our goal representation index (GRI) on a previously described study [193]. In short, we determine the number of place field centres in the reward zone (180-200 cm), as well as the number in two other areas which were both outside of the reward zone and away from the familiar position of the cue object (90-110 cm and 140-160 cm). The GRI is defined as the number of place cell that have their centre in the reward zone, divided by the number of place cells that have their centre in the control zones, where we averaged across the two zones. A value of higher than 1 indicated an overrepresentation of the goal zone.

#### 3.4.7 Overlap analysis

*Overlap coefficient.* We calculated the overlap in cell types identified between two conditions using the overlap coefficient (Equation 2). The coefficient is the ratio between the number of cells ( $N$ ) classified in both conditions ( $i$  and  $j$ ) and the lowest number of cells of the two conditions, and is thus a reflection of the ratio compared to the maximal possible overlap.

$$OC = \frac{N_i \cap N_j}{\min(N_i, N_j)} \quad \text{Equation 2}$$

#### 3.4.8 Bayesian decoder

We used a Bayesian decoder, courtesy of Caswell Barry, adapted from [174], to predict the mouse location from the hippocampal activity [200]. For the decoder we used the spiking activity for each session as calculated by the Suite2P spike deconvolution algorithm [172]. This activity was binarized, meaning a 1 was assigned when any spikes were present, and otherwise it was set to 0. We determined the probability of the cells being active in each location bin

$p(a|s)$ ) by calculating the rate map. The prior probability for the cells firing ( $p(a)$ ) was simply the mean number of spikes across the recording. The prior for the probability of occupying a location ( $p(s)$ ) was set to be flat, meaning the decoder assumed the same probability ( $\frac{1}{N}$ , with  $N$  being the number of location bins) for every location.

Using these prior probabilities we calculated the posterior probability ( $p(s|a)$ ) that a mouse was in a location given the observed cell activity, using Bayes rules. Two posteriors were calculated, one when a transient was observed (Equation 3) and one when no transient was observed (Equation 4).

$$p(s|a) = \frac{p(a|s)p(s)}{p(a)} \quad \text{Equation 3}$$

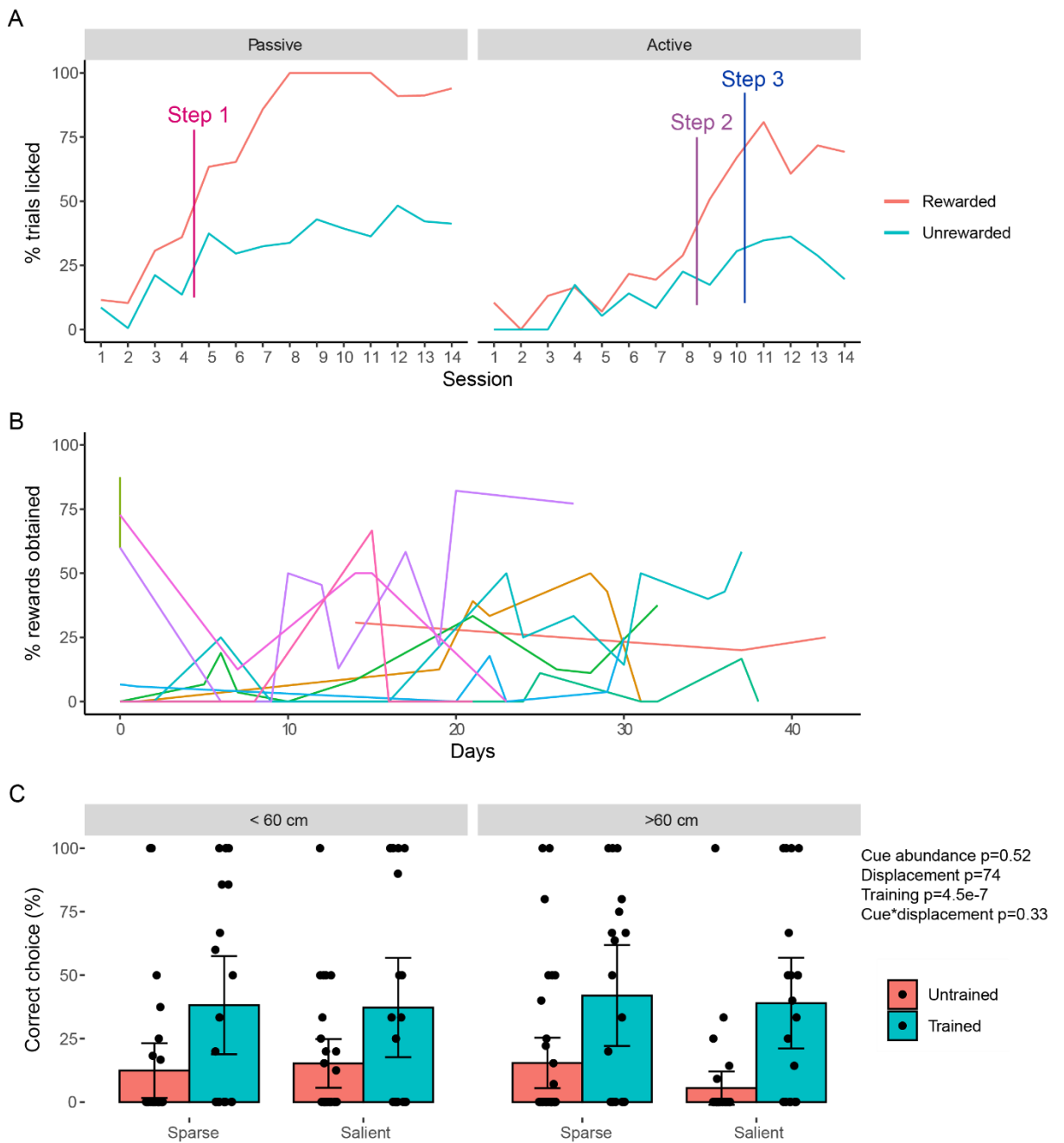
$$p(s|-a) = \frac{(1-p(a|s))p(s)}{1-p(a)} \quad \text{Equation 4}$$

The final posterior probably was calculated using the above equations per cell and summing across the cells. In datasets with a large number of cells, the individual probability per cell might approach the numerical limits of the software [174], so these summations were performed in log space and then converted back by calculating the exponent. This gave us the probability for that the animal was in a location for each location bin per frame.

*Decoding error.* We calculated the decoding error by first determining the predicted location from the calculated posterior probability. This was done by taking the location bin with the highest probability as the predicted location. The error was defined as the difference between the predicted location and the true location the animal was in, taking into account the circular nature of the environment (i.e. the end of the environment connected back to the start via the pipe).

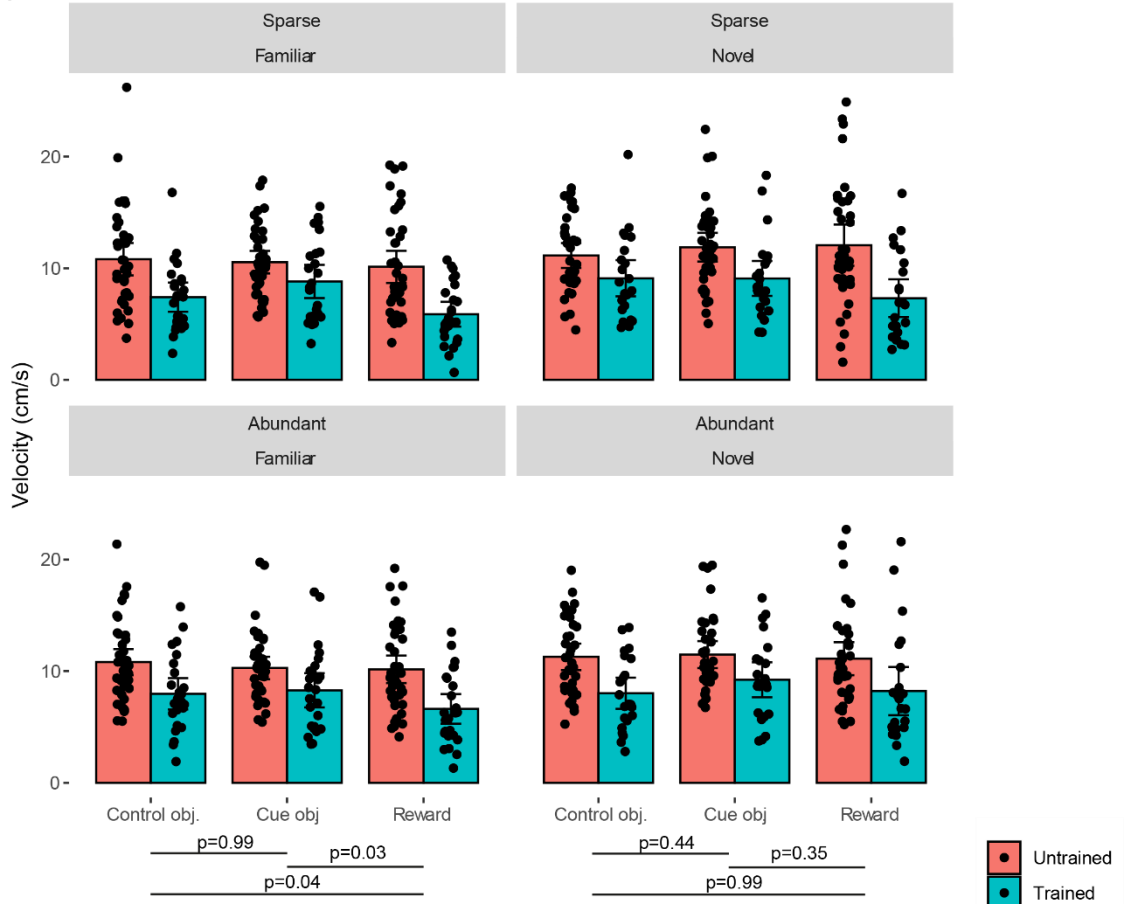


## 3.5 Supporting information

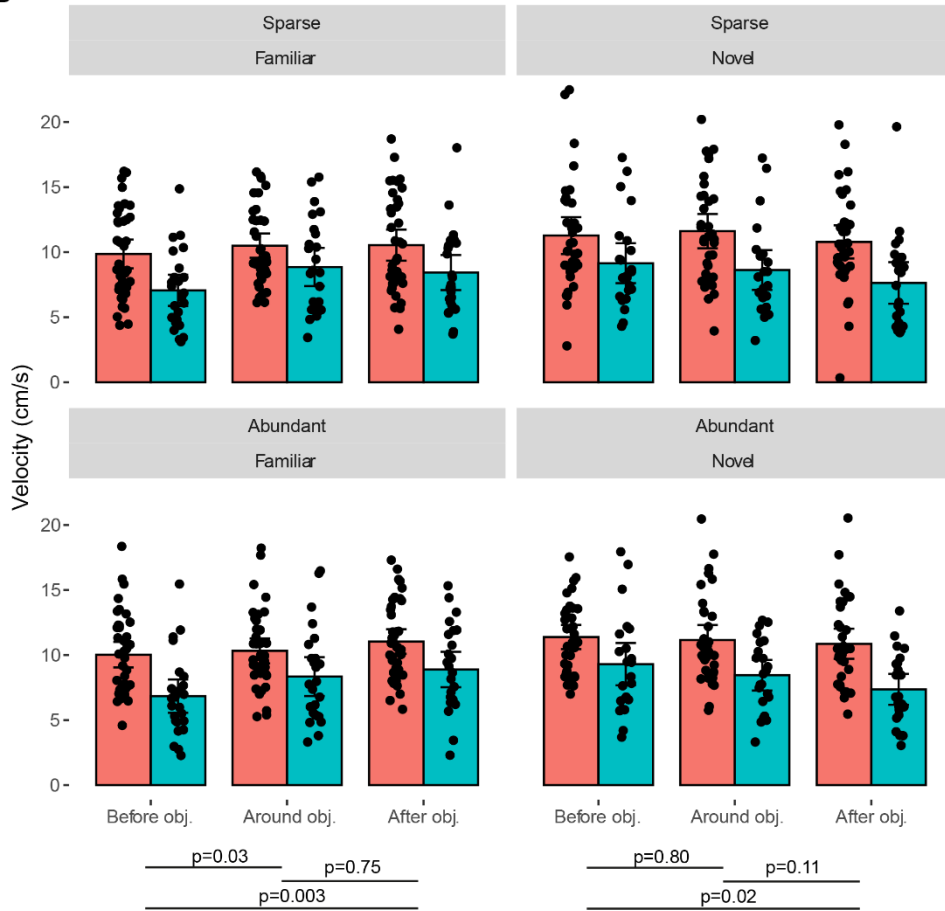


*S Fig 3.1 Animal training and task performance. (A) Computationally generated example of mouse behaviour illustrating the three training steps. (B) Percentage of total possible rewards gained over the training days, with each mouse illustrated in a different colour. (C) Percentage of correct licks when the object was displaced less than 60 cm (left) or more than 60 cm (right). In C, each data point is a session, bars show means, with error bars showing 95% confidence intervals. P-values next to C are from a linear mixed model with cue abundance, displacement, training and the interaction of cue abundance and displacement (cue\*displacement) as fixed-effects and mouse and imagining session as random-effects. See Table 2 for N numbers for comparisons and all statistical analysis.*

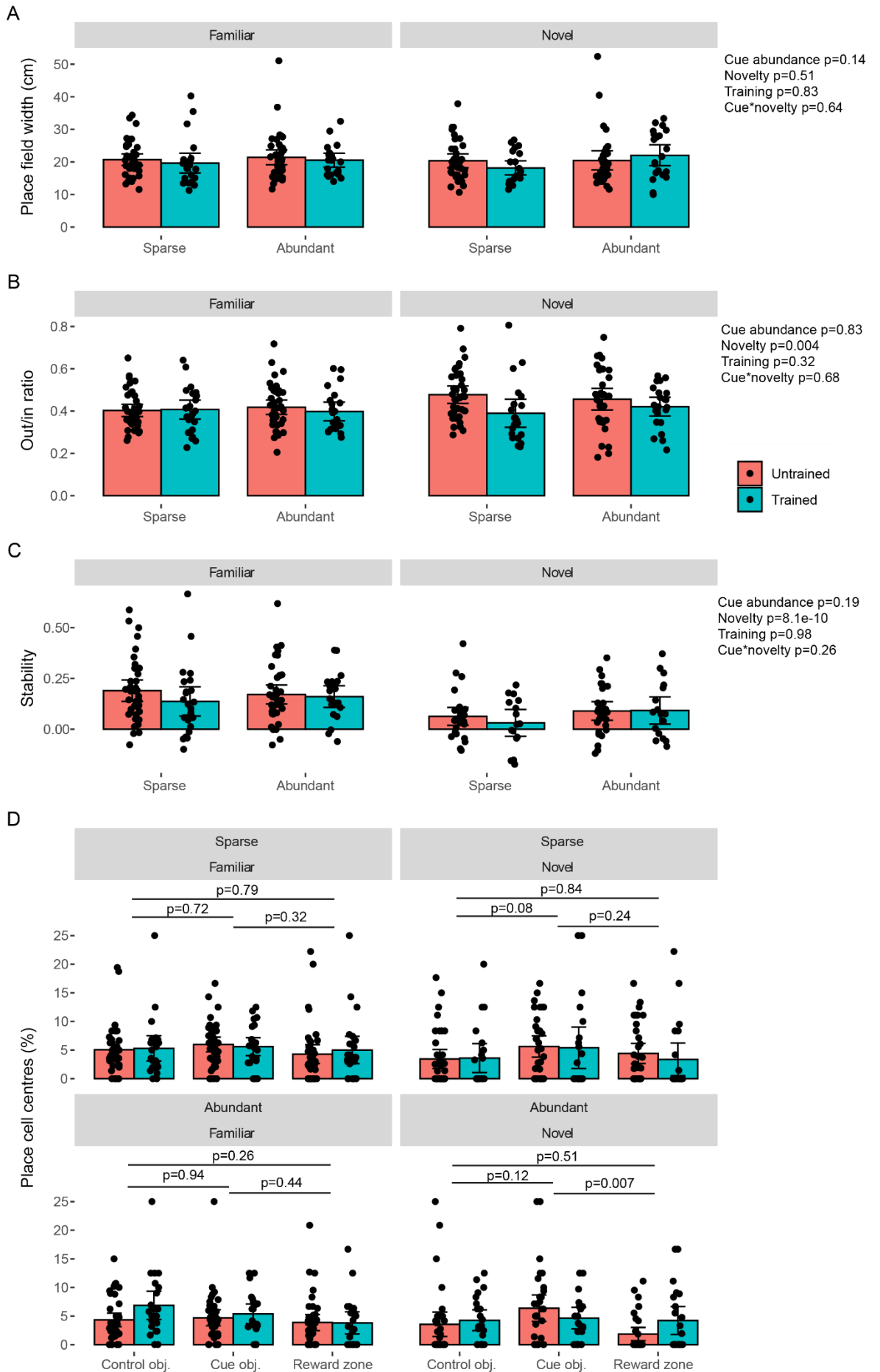
A



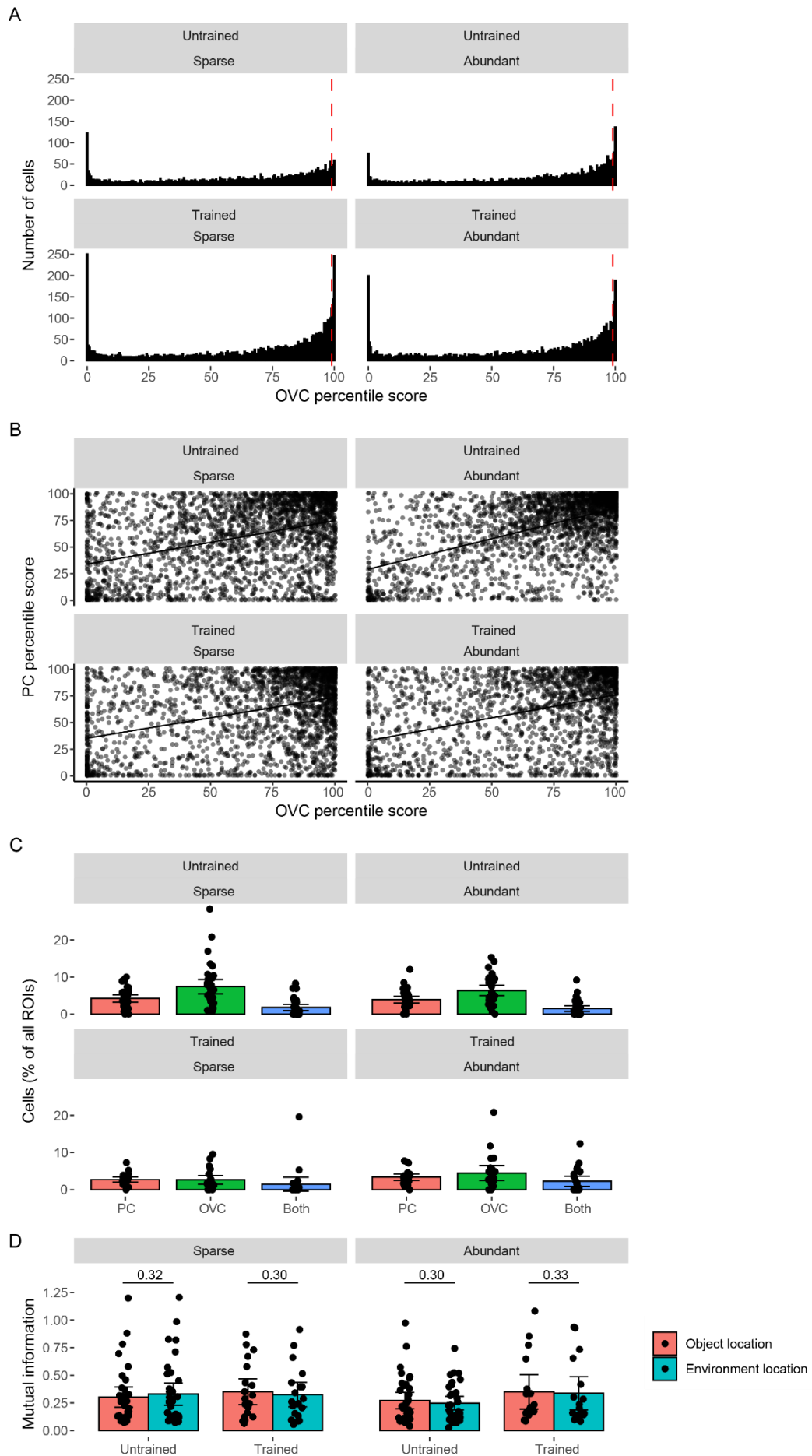
B



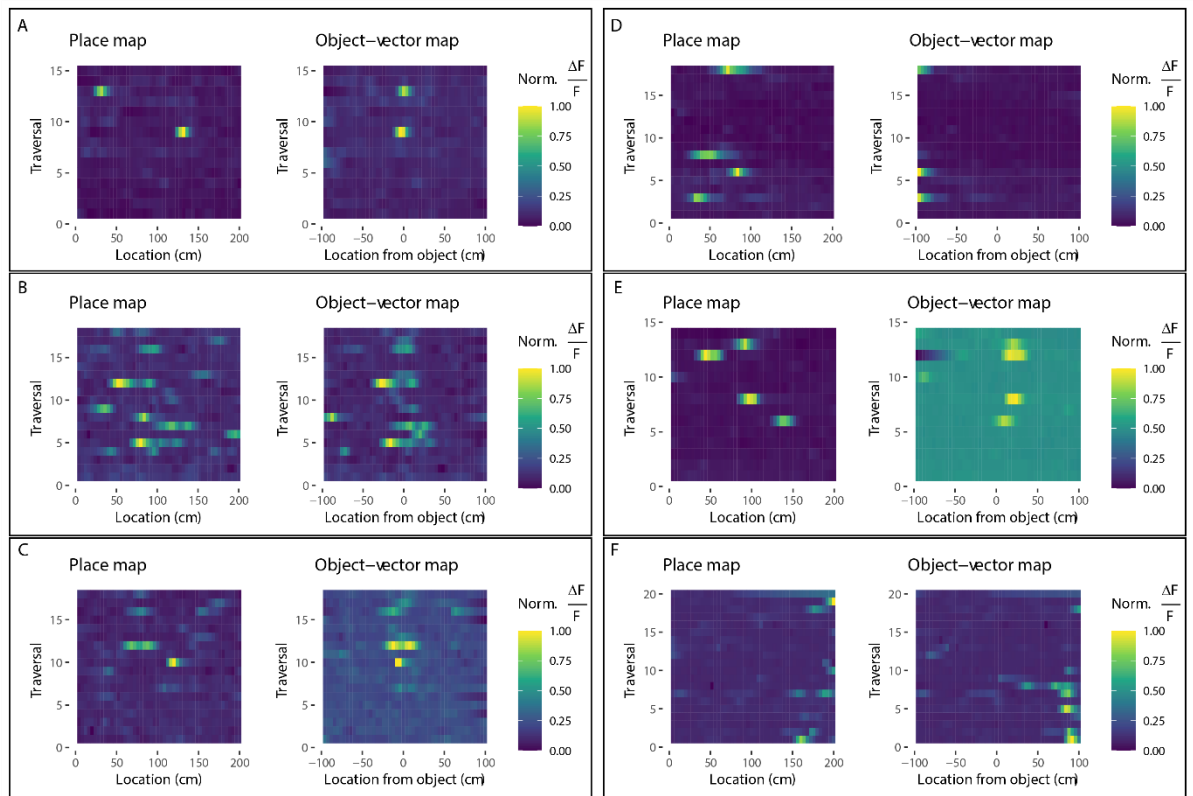
*S Fig 3.2 Mouse velocity at different location in the environment or relative to the cue object. (A) Mouse velocity at three locations of interest (around the control object, around the cue object and in the reward zone). (B) Mouse velocity at locations relative to the cue object (before, around or after the object). P-values below A-B are from a post-hoc Tukey's method test collapsed across training and cue abundance. Each data point is a session, bars show means, with error bars showing 95% confidence intervals. See Table 4 for N numbers for comparisons and all statistical analysis.*



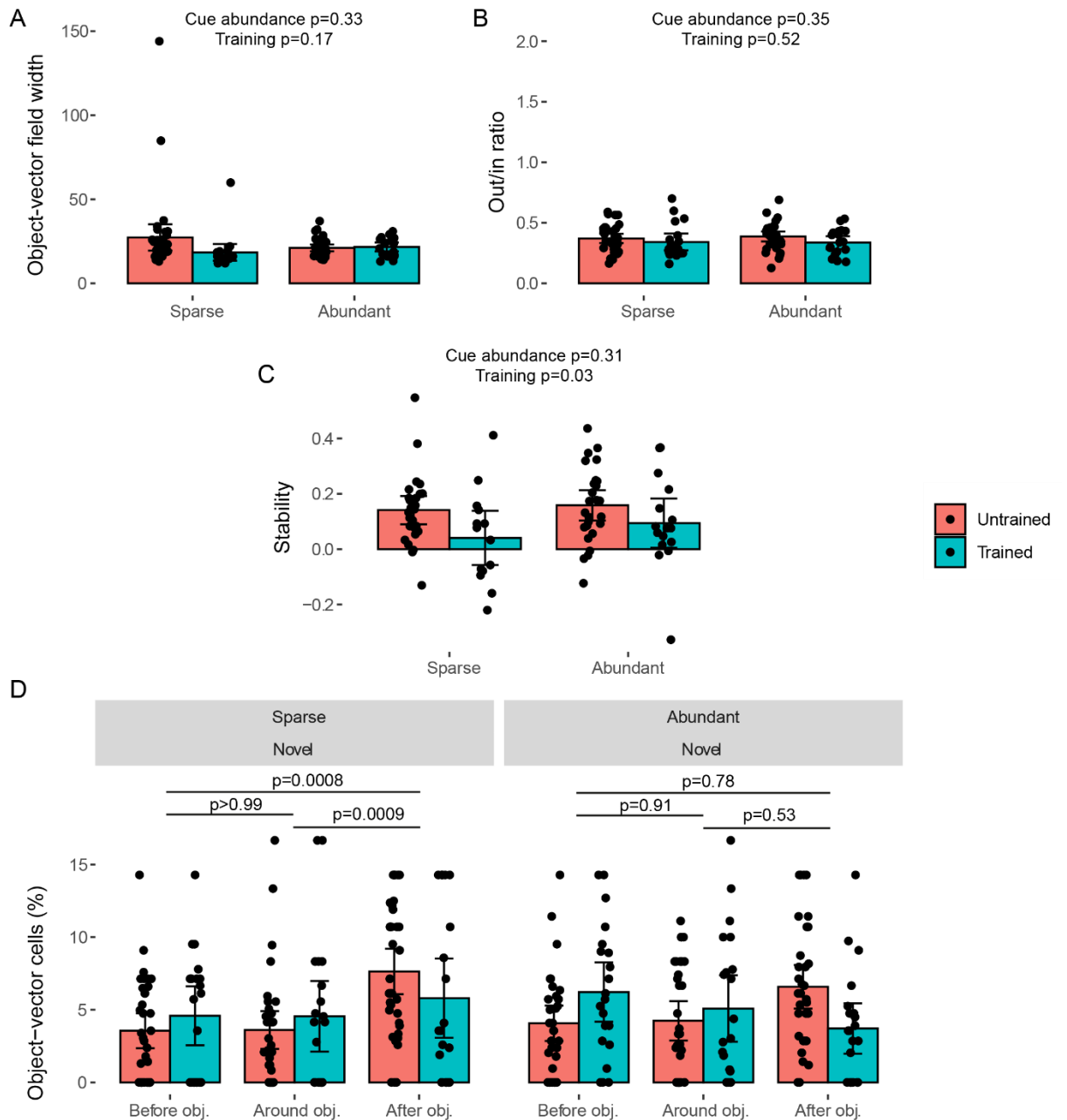
*S Fig 3.3 Additional place cell characteristics. (A) Mean place field width of the place cells. (B) Mean ratio of the fluorescence out and inside the place field. (C) Stability, as measured by the correlation between the fluorescence map of the even and odd trials. (D) The percentage of place cells with place field centres at three locations of interest (around the control object, around the cue object and in the reward zone. P-values next to A-C are from a linear mixed model with cue abundance, object location novelty, training and the interaction of cue abundance and novelty (cue\*novelty) as fixed-effects and mouse and imagining session as random-effects. P-values below D are from a post-hoc Tukey's method test collapsed across training. Each data point is a session, bars show means, with error bars showing 95% confidence intervals. See Table 6 for N numbers for comparisons and all statistical analysis.*



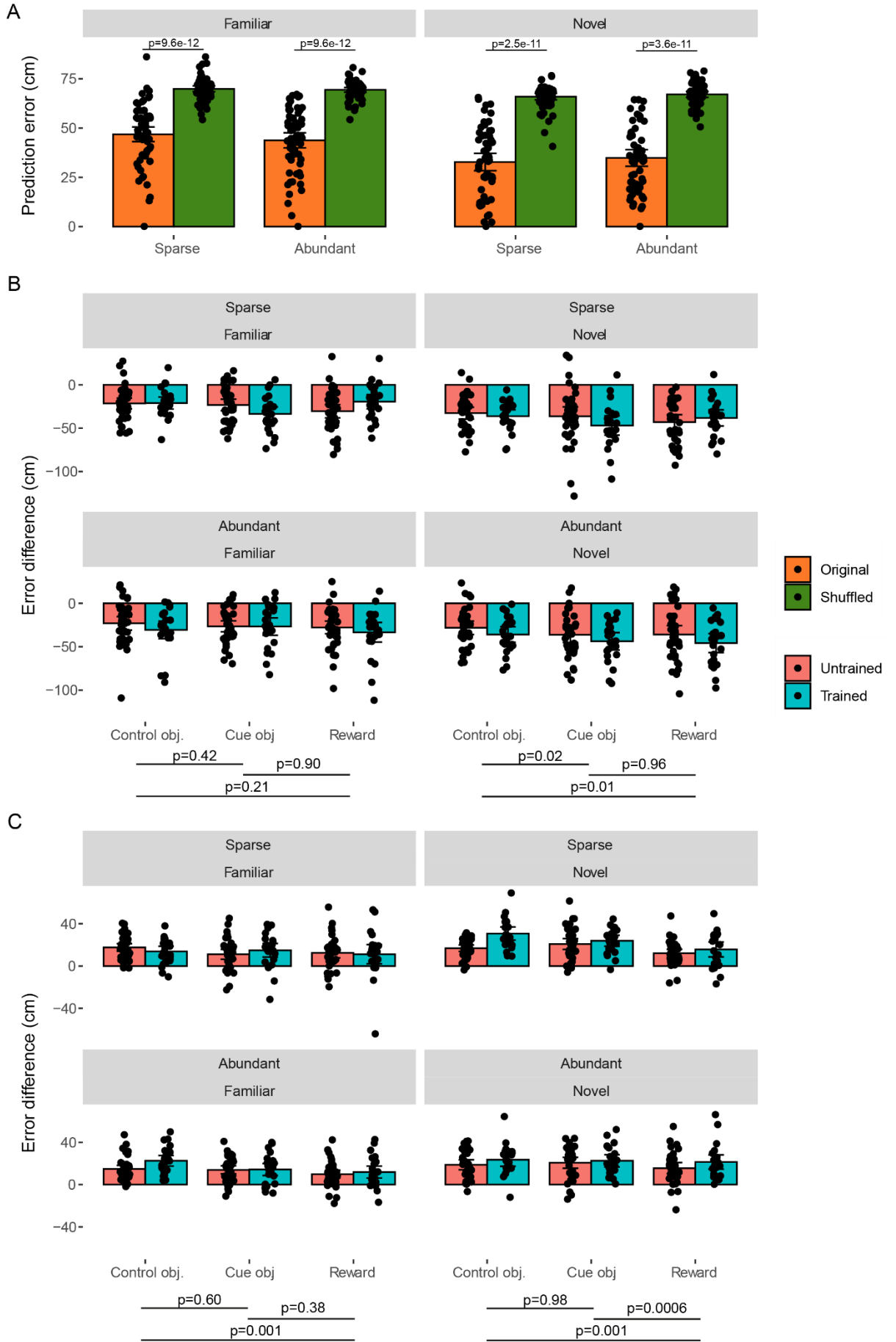
*S Fig 3.4 Further characterisation of object-vector classification. (A) Histograms showing distribution of percentile scores of the object-vector cells across the four environments. Red dashed line indicates the threshold used to include cells as OVCs. (B) Relation between the object-vector cell (OVC) percentile score and place cell (PC) percentile score across all datasets. Black lines indicate mean trend line across all cells. (C) Percentage of all ROIs identified as exclusively place cells (pink), exclusively object-vector cells (green) or both (blue). (D) Mutual information with location relative to the object (pink) or relative to the global environment (blue) of the object-vector cells. Bars show means, with error bars showing 95% confidence intervals and dots indicating individual datasets. P-values in D from paired t-test with Holm-Bonferonni correction for multiple comparisons.*



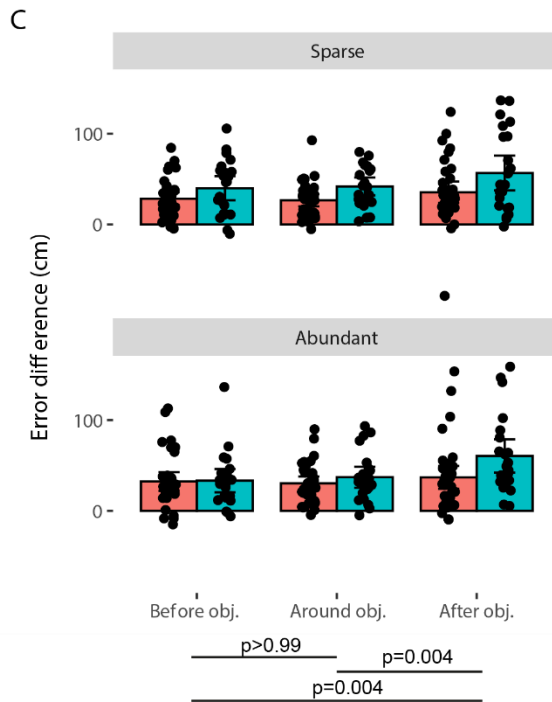
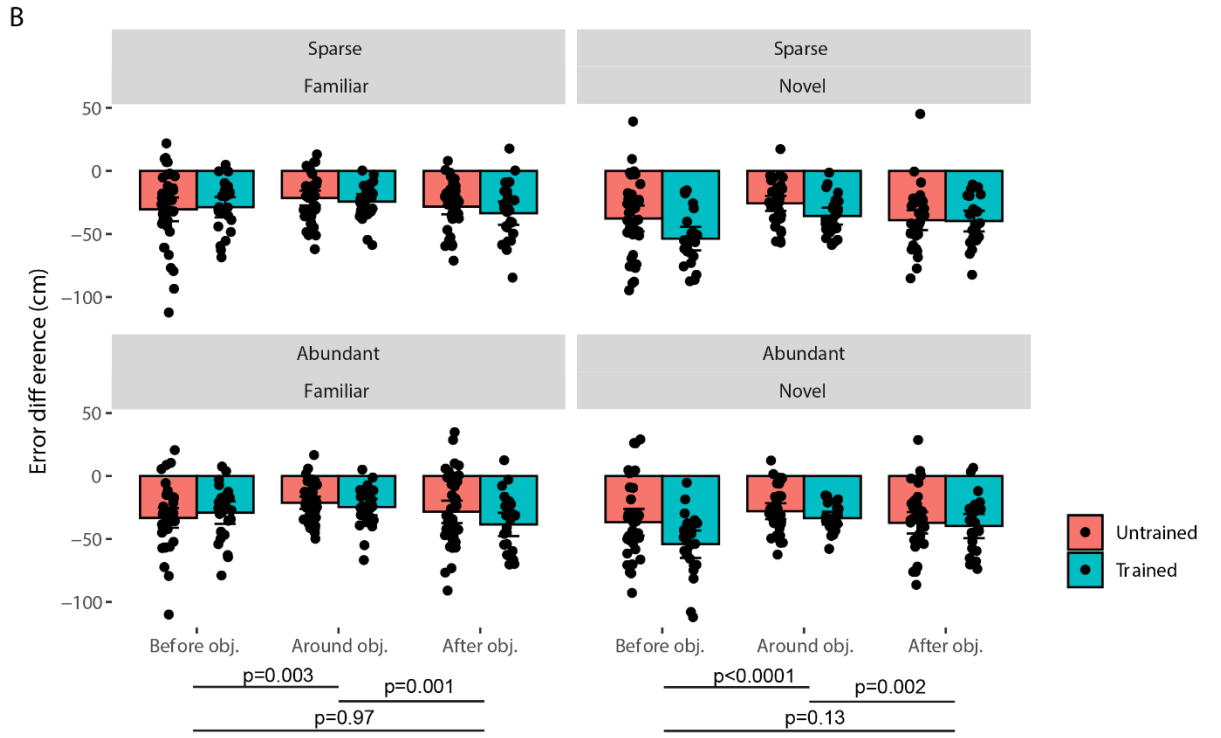
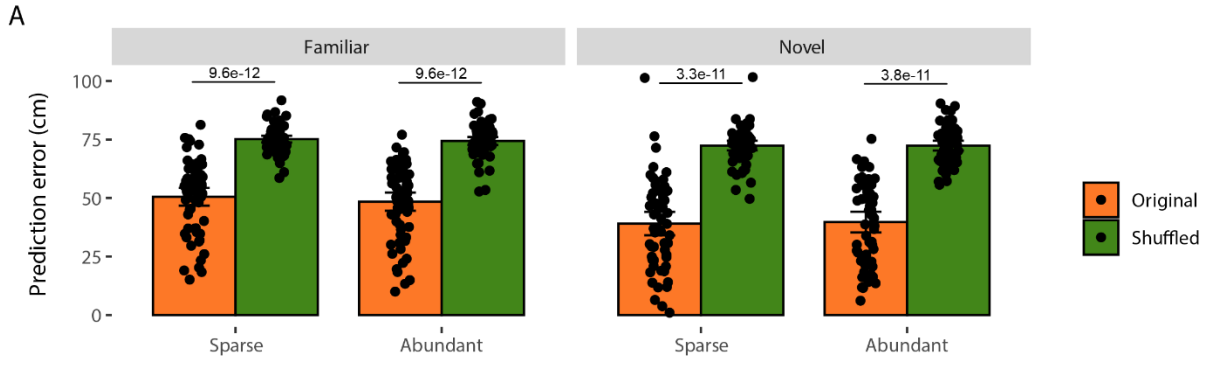
*S Fig 3.5 Examples of object-vector cells. Example fluorescence maps over location (left) and location relative to the object for object-vector cells with maps around (A-C), before (D) or after (E-F) the object.*



*S Fig 3.6 Additional object-vector cell characteristics. (A) Mean place field width of the object-vector cells in the novel condition. (B) Mean ratio of the fluorescence out and inside the place field. (C) Stability, as measured by the correlation between the fluorescence map of the even and odd trials. (D) The percentage of object-vector cells with place field centres at three locations relative to the cue object (before, around or after the object). P-values above to A-C are from a linear mixed model with cue abundance and training as fixed-effects and mouse and imaging session as random-effects. P-values below D are from a post-hoc Tukey's method test collapsed across training. Each data point is a session, bars show means, with error bars showing 95% confidence intervals. See Table 8 for N numbers for comparisons and all statistical analysis.*



*S Fig 3.7 Decoding of animal location. (A) Mean error of the original decoder (orange) and a decoder where the cell identities were shuffled (green), p-values from a paired two-sample Wilcoxon signed rank test with Holm-Bonferonni correction. (B) Difference between the error per location bin of the original decoder and the shuffled decoder at three locations of interest (around the control object, around the cue object and in the reward zone). Negative results show the original decoder was more accurate than the shuffled decoder. (C) Difference between the error per location bin of the original decoder and the decoder which only included place cells at the three locations of interest. Positive results show that place cells contributed less to the decoding. P-values below B-C are from a post-hoc Tukey's method test collapsed across training and cue abundance. In A each datapoint for the original data is a session, whereas the datapoints for the shuffled are the mean across 100 shuffles per dataset, in B-C, each data point is a session. Bars show means, with error bars showing 95% confidence intervals. See Table 11 for N numbers for comparisons and all statistical analysis.*



*S Fig 3.8 Decoding of animal location relative to cue object. (A) Mean error of the original decoder (orange) and a decoder where the cell identities were shuffled (green), p-values from a paired two-sample Wilcoxon signed rank test with Holm-Bonferonni correction. (B) Difference between the error per location bin of the original decoder and the shuffled decoder at three locations relative to the cue object (before, around or after the object). (C) Difference between the error per location bin of the original decoder and the decoder which only included object-vector cells at the three locations of interest for the novel direction. P-values below B-C are from a post-hoc Tukey's method test collapsed across training and cue abundance. In A each datapoint for the original data is a session, whereas the datapoints for the shuffled are the mean across 100 shuffles per dataset, in B-C, each data point is a session. Bars show means, with error bars showing 95% confidence intervals. See Table 13 for N numbers for comparisons and all statistical analysis.*

## Statistics tables

Familiar condition: Linear mixed model with cue abundance (cue), training and their interaction (cue:training) as fixed-effects and mouse and imagining session as random-effects

Model: choice ~ cue\*training + (1|mouse) + (1|session)

| Factor       | N  | Mean sq | NumDF | DenDF  | F-value | p-value       |
|--------------|--|---------|-------|--------|---------|---------------|
| Cue          | Sparse: 64<br>Abun.: 65  | 603.9   | 1     | 79.293 | 2.1793  | 0.1438354     |
| Training     | Untrained:79<br>Trained:50   | 4829.4  | 1     | 59.785 | 17.3218 | 0.0001026 *** |
| Cue:training | Sparse/untrained: 39<br>Abun./untrained: 40<br>Sparse/trained: 25<br>Abun./trained: 25 | 1888.3  | 1     | 79.293 | 6.7730  | 0.0110413 *   |

Novel condition: Linear mixed model with cue abundance (Cue), training and their interaction (Cue:training) as fixed-effects and mouse and imagining session as random-effects

Model: choice ~ cue\*training + (1|mouse) + (1|session)

| Factor       | N  | Mean sq | NumDF | DenDF   | F-value | p-value       |
|--------------|--|---------|-------|---------|---------|---------------|
| Cue          | Sparse: 61<br>Abun.: 58  | 53.7    | 1     | 72.290  | 0.1471  | 0.7025        |
| Training     | Untrained:72<br>Trained:47   | 9367.7  | 1     | 112.790 | 25.6576 | 1.605e-06 *** |
| Cue:training | Sparse/untrained: 37<br>Abun./untrained: 35<br>Sparse/trained: 24<br>Abun./trained: 23 | 205.7   | 1     | 71.075  | 0.5634  | 0.4554        |

Table 1: Statistics for Fig 3.1

Novel condition: Linear mixed model with cue abundance (cue), displacement, training and the interaction (cue:displacement) as fixed-effects and mouse and imagining session as random-effects

Model: choice ~ cue\*displacement + training + (1|mouse) + (1|dataset)

| Factor           | N  | Mean sq | NumDF | DenDF  | F-value | p-value           |
|------------------|--|---------|-------|--------|---------|-------------------|
| Cue              | Sparse: 102<br>Abun.: 102  | 260.6   | 1     | 157.04 | 0.4226  | 0.5166            |
| Displacement     | <60 cm: 98<br>>60 cm: 106  | 66.9    | 1     | 158.48 | 0.1085  | 0.7423            |
| Training         | Untrained: 124<br>Trained: 80  | 16889.4 | 1     | 186.12 | 27.3885 | 4.461e-07 **<br>* |
| Cue:displacement | Sparse/<60cm: 49<br>Abun./<60cm: 49<br>Sparse/>60cm: 53<br>Abun./>60cm: 53 | 591.0   | 1     | 158.43 | 0.9584  | 0.3291            |

Table 2: Statistics for S Fig 3.1

Linear mixed model with cue abundance (cue), novelty, training and the interaction (cue:novelty) as fixed-effects and mouse and imagining session as random-effects

Model: speed ~ cue\*novelty + training + (1|mouse) + (1|dataset)

| Factor      | N   | Mean sq | NumDF | DenDF  | F-value | p-value     |
|-------------|---|---------|-------|--------|---------|-------------|
| Cue         | Sparse: 124<br>Abun.: 123   | 1.8512  | 1     | 202.13 | 0.4193  | 0.518008    |
| Novelty     | Familiar: 129<br>Novel: 118   | 30.0487 | 1     | 202.35 | 6.8064  | 0.009761 ** |
| Training    | Untrained: 151<br>Trained: 96   | 28.9048 | 1     | 214.75 | 6.5473  | 0.011192 *  |
| Cue:novelty | Sparse/familiar: 64<br>Abun./ familiar: 65<br>Sparse/novel: 60<br>Abun./novel: 58 | 0.9073  | 1     | 201.62 | 0.2055  | 0.650788    |

Table 3: Statistics for Fig 3.2

### Speed relative to location

Linear mixed model with cue abundance (cue), novelty, location, training and the interactions (cue:novelty), (cue:location), (novelty:training) and (cue:novelty:location) as fixed-effects and mouse and imagining session as random-effects

Model: speed ~ cue\*novelty\*location + training + (1|mouse) + (1|dataset)

| Factor               | N   | Mean sq | NumDF | DenDF  | F-value  | p-value       |
|----------------------|---|---------|-------|--------|----------|---------------|
| Cue                  | Sparse: 371<br>Abun.: 369   | 0.26    | 1     | 675.84 | 0.0326   | 0.856844      |
| Novelty              | Familiar: 386<br>Novel: 354   | 219.99  | 1     | 676.22 | 27.8382  | 1.778e-07 *** |
| Location             | Control obj.: 246<br>Cue obj.: 247<br>Reward: 247   | 43.08   | 2     | 673.74 | 5.4519   | 0.004479 **   |
| Training             | Untrained: 453<br>Trained: 287  | 870.75  | 1     | 314.87 | 110.1857 | < 2.2e-16 *** |
| Cue:novelty          | Sparse/familiar: 191<br>Abun./ familiar: 195<br>Sparse/novel: 180<br>Abun./novel: 174   | 1.34    | 1     | 675.40 | 0.1696   | 0.680583      |
| Cue:location         | Sparse/control: 123<br>Abun./control: 123<br>Sparse/cue obj.: 124<br>Abun./cue obj.: 123<br>Sparse/reward.: 124<br>Abun./ reward: 123           | 1.53    | 2     | 673.74 | 0.1941   | 0.823653      |
| Novelty:location     | Familiar/control: 128<br>Novel/control: 118<br>Familiar /cue obj.: 129<br>Novel /cue obj.: 118<br>Familiar /reward.: 129<br>Novel / reward: 118 | 13.40   | 2     | 673.74 | 1.6958   | 0.184233      |
| Cue:novelty:location | Control obj.:<br>Sparse/familiar: 63<br>Abun./ familiar: 65<br>Sparse/novel: 60   | 2.56    | 2     | 673.74 | 0.3242   | 0.723244      |

|  |                     |  |  |  |  |  |
|--|---------------------|--|--|--|--|--|
|  | Abun./novel: 58     |  |  |  |  |  |
|  | Cue obj.:           |  |  |  |  |  |
|  | Sparse/familiar: 64 |  |  |  |  |  |
|  | Abun./ familiar: 65 |  |  |  |  |  |
|  | Sparse/novel: 60    |  |  |  |  |  |
|  | Abun./novel: 58     |  |  |  |  |  |
|  | Reward              |  |  |  |  |  |
|  | Sparse/familiar: 64 |  |  |  |  |  |
|  | Abun./ familiar: 65 |  |  |  |  |  |
|  | Sparse/novel: 60    |  |  |  |  |  |
|  | Abun./novel: 58     |  |  |  |  |  |

Tukey's method post-hoc test on location by novelty

Familiar condition

| Contrast              | Estimate | SE    | Df  | t-ratio | p-value |
|-----------------------|----------|-------|-----|---------|---------|
| Control vs cue obj    | -0.0636  | 0.414 | 716 | -0.154  | 0.9871  |
| Control obj vs reward | 0.9914   | 0.414 | 716 | 2.397   | 0.0442  |
| Cue obj vs reward     | 1.0550   | 0.413 | 716 | 2.556   | 0.0290  |

Novel condition

| Contrast              | Estimate | SE    | Df  | t-ratio | p-value |
|-----------------------|----------|-------|-----|---------|---------|
| Control vs cue obj    | -0.5301  | 0.432 | 716 | -1.228  | 0.4369  |
| Control obj vs reward | 0.0646   | 0.432 | 716 | 0.150   | 0.9877  |
| Cue obj vs reward     | 0.5947   | 0.432 | 716 | 1.378   | 0.3531  |

### Speed relative to object

Linear mixed model with cue abundance (cue), novelty, location, training and the interactions (cue:novelty), (cue:location), (novelty:training) and (cue:novelty:location) as fixed-effects and mouse and imagining session as random-effects

Model: speed ~ cue\*novelty\*location + training + (1|mouse) + (1|dataset)

| Factor | N | Mean sq | NumDF | DenDF | F-value | p-value |
|--------|---|---------|-------|-------|---------|---------|
|        |   |         |       |       |         |         |

|                          |   |             |   |        |          |               |
|--------------------------|---|-------------|---|--------|----------|---------------|
| Cue                      | Sparse: 371<br>Abun.: 369   | 0           | 1 | 712.68 | 0.0003   | 0.9867117     |
| Novelty                  | Familiar: 386<br>Novel: 354   | 101.60      | 1 | 713.08 | 12.5531  | 0.0004213 *** |
| Location                 | Control obj.: 246<br>Cue obj.: 247<br>Reward: 247   | 7.69        | 2 | 712.61 | 0.9505   | 0.3870182     |
| Training                 | Untrained: 453<br>Trained: 287  | 1760.1<br>2 | 1 | 722.77 | 217.4629 | < 2.2e-16 *** |
| Cue:novelty              | Sparse/familiar: 191<br>Abun./ familiar: 195<br>Sparse/novel: 180<br>Abun./novel: 174   | 0.32        | 1 | 712.6  | 0.0396   | 0.8423017     |
| Cue:location             | Sparse/control: 123<br>Abun./control: 123<br>Sparse/cue obj.: 124<br>Abun./cue obj.: 123<br>Sparse/reward.: 124<br>Abun./ reward: 123   | 4.97        | 2 | 712.61 | 0.6141   | 0.5414166     |
| Novelty:location         | Familiar/control: 128<br>Novel/control: 118<br>Familiar /cue obj.: 129<br>Novel /cue obj.: 118<br>Familiar /reward.: 129<br>Novel / reward: 118                                       | 71.93       | 2 | 712.61 | 8.8864   | 0.0001542 *** |
| Cue:novelty:locati<br>on | Control obj.:<br>Sparse/familiar: 63<br>Abun./ familiar: 65<br>Sparse/novel: 60<br>Abun./novel: 58<br><br>Cue obj.:<br>Sparse/familiar: 64<br>Abun./ familiar: 65<br>Sparse/novel: 60 | 1.87        | 2 | 712.61 | 0.2310   | 0.7938175     |

|  |                     |  |  |  |  |  |
|--|---------------------|--|--|--|--|--|
|  | Abun./novel: 58     |  |  |  |  |  |
|  | Reward              |  |  |  |  |  |
|  | Sparse/familiar: 64 |  |  |  |  |  |
|  | Abun./ familiar: 65 |  |  |  |  |  |
|  | Sparse/novel: 60    |  |  |  |  |  |
|  | Abun./novel: 58     |  |  |  |  |  |

Tukey's method post-hoc test on location by novelty

Familiar condition

| Contrast         | Estimate | SE    | Df  | t-ratio | p-value |
|------------------|----------|-------|-----|---------|---------|
| Before vs around | -0.923   | 0.354 | 713 | -2.604  | 0.0254  |
| Before vs after  | -1.179   | 0.354 | 713 | -3.329  | 0.0026  |
| Around vs after  | -0.257   | 0.354 | 713 | -0.725  | 0.7488  |

Novel condition

| Contrast         | Estimate | SE    | Df  | t-ratio | p-value |
|------------------|----------|-------|-----|---------|---------|
| Before vs around | 0.235    | 0.373 | 713 | 0.629   | 0.8041  |
| Before vs after  | 0.984    | 0.372 | 713 | 2.646   | 0.0226  |
| Around vs after  | 0.750    | 0.373 | 713 | 2.011   | 0.1102  |

Table 4: Statistics for S Fig 3.2.

### Place cell percentage

Linear mixed model with cue abundance (cue), novelty, training and the interaction (cue:novelty) as fixed-effects and mouse and imagining session as random-effects

Model: percentage ~ cue\*novelty + training + (1|mouse) + (1|dataset)

| Factor      | N   | Mean sq | NumDF | DenDF  | F-value | p-value       |
|-------------|---|---------|-------|--------|---------|---------------|
| Cue         | Sparse: 121<br>Abun.: 120   | 31.12   | 1     | 196.16 | 1.0451  | 0.307894      |
| Novelty     | Familiar: 126<br>Novel: 115   | 1895.59 | 1     | 196.84 | 63.6628 | 1.192e-13 *** |
| Training    | Untrained: 149<br>Trained: 92   | 238.76  | 1     | 205.20 | 8.0186  | 0.005091 **   |
| Cue:novelty | Sparse/familiar: 63<br>Abun./ familiar: 63<br>Sparse/novel: 58<br>Abun./novel: 57 | 12.60   | 1     | 197.17 | 0.4230  | 0.516180      |

### Mutual information

Linear mixed model with cue abundance (cue), novelty, training and the interaction (cue:novelty) as fixed-effects and mouse and imagining session as random-effects

Model: MI ~ cue\*novelty + training + (1|mouse) + (1|dataset)

| Factor      | N   | Mean sq | NumDF | DenDF  | F-value | p-value       |
|-------------|---|---------|-------|--------|---------|---------------|
| Cue         | Sparse: 119<br>Abun.: 116   | 0.01042 | 1     | 185.00 | 0.3774  | 0.539757      |
| Novelty     | Familiar: 124<br>Novel: 111   | 1.28406 | 1     | 184.45 | 46.5192 | 1.257e-10 *** |
| Training    | Untrained: 146<br>Trained: 89   | 0.21852 | 1     | 213.78 | 7.9166  | 0.005355 **   |
| Cue:novelty | Sparse/familiar: 63<br>Abun./ familiar: 61<br>Sparse/novel: 56<br>Abun./novel: 55 | 0.04763 | 1     | 186.64 | 1.7256  | 0.190589      |

### Goal representation index

Linear mixed model with cue abundance (cue), novelty, training and the interaction (cue:novelty) as fixed-effects and mouse and imagining session as random-effects

Model: GRI ~ cue\*novelty + training + (1|mouse) + (1|dataset)

| Factor      | N   | Mean sq   | NumDF | DenDF  | F-value | p-value |
|-------------|---|-----------|-------|--------|---------|---------|
| Cue         | Sparse: 119<br>Abun.: 116   | 0.0002928 | 1     | 222.04 | 0.0245  | 0.8756  |
| Novelty     | Familiar: 124<br>Novel: 111   | 0.0055462 | 1     | 223.45 | 0.4650  | 0.4960  |
| Training    | Untrained: 146<br>Trained: 89   | 0.0019097 | 1     | 157.15 | 0.1601  | 0.6896  |
| Cue:novelty | Sparse/familiar: 63<br>Abun./ familiar: 61<br>Sparse/novel: 56<br>Abun./novel: 55 | 0.0056316 | 1     | 222.69 | 0.4721  | 0.4927  |

Post-hoc one-sample Wilcoxon signed rank test with Holm-Bonferonni correction – compared to a mean of 1

| Cue abun. | Novelty  | Training  | n  | Adjusted p |
|-----------|----------|-----------|----|------------|
| Sparse    | Familiar | Untrained | 41 | 0.675      |
| Sparse    | Familiar | Trained   | 25 | 0.804      |
| Abundant  | Familiar | Untrained | 41 | 0.675      |
| Abundant  | Familiar | Trained   | 25 | 0.675      |
| Sparse    | Novel    | Untrained | 41 | 0.675      |
| Sparse    | Novel    | Trained   | 25 | 0.924      |
| Abundant  | Novel    | Untrained | 41 | 0.675      |
| Abundant  | Novel    | Trained   | 25 | 0.924      |

Table 5: Statistics for Fig 3.3

### Place field width

Linear mixed model with cue abundance (cue), novelty, training and the interaction (cue:novelty) as fixed-effects and mouse and imagining session as random-effects

Model: width ~ cue\*novelty + training + (1|mouse) + (1|dataset)

| Factor      | N   | Mean sq | NumDF | DenDF  | F-value | p-value |
|-------------|---|---------|-------|--------|---------|---------|
| Cue         | Sparse: 119<br>Abun.: 116   | 82.401  | 1     | 220.65 | 2.2088  | 0.1387  |
| Novelty     | Familiar: 124<br>Novel: 111   | 16.440  | 1     | 221.76 | 0.4407  | 0.5075  |
| Training    | Untrained: 146<br>Trained: 89   | 1.637   | 1     | 216.54 | 0.0439  | 0.8343  |
| Cue:novelty | Sparse/familiar: 63<br>Abun./ familiar: 61<br>Sparse/novel: 56<br>Abun./novel: 55 | 8.259   | 1     | 220.87 | 0.2214  | 0.6385  |

### Out/in ratio

Linear mixed model with cue abundance (cue), novelty, training and the interaction (cue:novelty) as fixed-effects and mouse and imagining session as random-effects

Model: oi\_ratio ~ cue\*novelty + training + (1|mouse) + (1|dataset)

| Factor      | N   | Mean sq  | NumDF | DenDF  | F-value | p-value     |
|-------------|---|----------|-------|--------|---------|-------------|
| Cue         | Sparse: 119<br>Abun.: 116   | 0.000401 | 1     | 182.91 | 0.0439  | 0.834292    |
| Novelty     | Familiar: 124<br>Novel: 111   | 0.075632 | 1     | 182.43 | 8.2804  | 0.004486 ** |
| Training    | Untrained: 146<br>Trained: 89   | 0.009103 | 1     | 214.25 | 0.9966  | 0.319249    |
| Cue:novelty | Sparse/familiar: 63<br>Abun./ familiar: 61<br>Sparse/novel: 56<br>Abun./novel: 55 | 0.001544 | 1     | 184.56 | 0.1690  | 0.681463    |

### Stability

Linear mixed model with cue abundance (cue), novelty, training and the interaction (cue:novelty) as fixed-effects and mouse and imagining session as random-effects

Model: stability ~ cue\*novelty + training + (1|mouse) + (1|dataset)

| Factor      | N   | Mean sq | NumDF | DenDF  | F-value | p-value      |
|-------------|---|---------|-------|--------|---------|--------------|
| Cue         | Sparse: 105<br>Abun.: 106   | 0.02387 | 1     | 172.75 | 1.7163  | 0.1919       |
| Novelty     | Familiar: 121<br>Novel: 90  | 0.58762 | 1     | 174.78 | 42.2495 | 8.105e-10 ** |
| Training    | Untrained: 132<br>Trained: 79   | 0.00001 | 1     | 191.32 | 0.0009  | 0.9764       |
| Cue:novelty | Sparse/familiar: 61<br>Abun./ familiar: 60<br>Sparse/novel: 44<br>Abun./novel: 46 | 0.01795 | 1     | 172.78 | 1.2903  | 0.2576       |

### Place field centres per location bin

Linear mixed model with cue abundance (cue), novelty, location, training and the interactions (cue:novelty), (cue:location), (novelty:training) and (cue:novelty:location) as fixed-effects and mouse and imagining session as random-effects

Model: percentage ~ cue\*novelty\*location + training + (1|mouse) + (1|dataset)

| Factor       | N   | Mean sq     | NumDF | DenDF | F-value | p-value     |
|--------------|---|-------------|-------|-------|---------|-------------|
| Cue          | Sparse: 357<br>Abun.: 348   | 24.709      | 1     | 692   | 1.0063  | 0.316135    |
| Novelty      | Familiar: 372<br>Novel: 333   | 87.705      | 1     | 692   | 3.5719  | 0.059182    |
| Location     | Control obj.: 235<br>Cue obj.: 235<br>Reward: 235                                     | 171.49<br>5 | 2     | 692   | 6.9844  | 0.000993*** |
| Training     | Untrained: 438<br>Trained: 267  | 19.545      | 1     | 692   | 0.7960  | 0.372607    |
| Cue:novelty  | Sparse/familiar: 189<br>Abun./ familiar: 183<br>Sparse/novel: 168<br>Abun./novel: 165 | 2.539       | 1     | 692   | 0.1034  | 0.747898    |
| Cue:location | Sparse/control: 119<br>Abun./control: 116<br>Sparse/cue obj.: 119                     | 20.781      | 2     | 692   | 0.8463  | 0.429434    |

|                      |   |        |   |     |        |          |
|----------------------|---|--------|---|-----|--------|----------|
|                      | Abun./cue obj.: 116<br>Sparse/reward.: 119<br>Abun./ reward: 116  |        |   |     |        |          |
| Novelty:location     | Familiar/control: 124<br>Novel/control: 111<br>Familiar /cue obj.: 124<br>Novel /cue obj.: 111<br>Familiar /reward.: 124<br>Novel / reward: 111   | 45.420 | 2 | 692 | 1.8498 | 0.158045 |
| Cue:novelty:location | Control obj.:<br>Sparse/familiar: 63<br>Abun./ familiar: 61<br>Sparse/novel: 56<br>Abun./novel: 55<br><br>Cue obj.:<br>Sparse/familiar: 63<br>Abun./ familiar: 61<br>Sparse/novel: 56<br>Abun./novel: 55<br><br>Reward<br>Sparse/familiar: 63<br>Abun./ familiar: 61<br>Sparse/novel: 56<br>Abun./novel: 55 | 8.718  | 2 | 692 | 0.3550 | 0.701273 |

Tukey's method post-hoc test on location by condition

Sparse/familiar condition

| Contrast              | Estimate | SE    | Df  | t-ratio | p-value |
|-----------------------|----------|-------|-----|---------|---------|
| Control vs cue obj    | -0.683   | 0.883 | 656 | -0.774  | 0.7192  |
| Control obj vs reward | 0.584    | 0.883 | 656 | 0.661   | 0.7862  |
| Cue obj vs reward     | 1.267    | 0.883 | 656 | 1.435   | 0.3236  |

Abundant/familiar condition

| Contrast              | Estimate | SE    | Df  | t-ratio | p-value |
|-----------------------|----------|-------|-----|---------|---------|
| Control vs cue obj    | 0.303    | 0.897 | 656 | 0.338   | 0.939   |
| Control obj vs reward | 1.401    | 0.897 | 656 | 1.561   | 0.2632  |
| Cue obj vs reward     | 1.098    | 0.897 | 656 | 1.224   | 0.4396  |

#### Sparse/novel condition

| Contrast              | Estimate | SE    | Df  | t-ratio | p-value |
|-----------------------|----------|-------|-----|---------|---------|
| Control vs cue obj    | -2.039   | 0.936 | 656 | -2.178  | 0.0758  |
| Control obj vs reward | -0.524   | 0.936 | 656 | -0.56   | 0.8414  |
| Cue obj vs reward     | 1.515    | 0.936 | 656 | 1.618   | 0.2388  |

#### Abundant/novel condition

| Contrast              | Estimate | SE    | Df  | t-ratio | p-value |
|-----------------------|----------|-------|-----|---------|---------|
| Control vs cue obj    | -1.848   | 0.945 | 656 | -1.956  | 0.1242  |
| Control obj vs reward | 1.041    | 0.945 | 656 | 1.102   | 0.5133  |
| Cue obj vs reward     | 2.889    | 0.945 | 656 | 3.057   | 0.0066  |

Table 6: Statistics for S Fig 3.3

### Object-vector cell percentage

Linear mixed model with cue abundance (cue) and training as fixed-effects and mouse and imagining session as random-effects

Model: percentage  $\sim$  cue + training + (1|mouse) + (1|dataset)

| Factor   | N                            | Mean sq | NumDF | DenDF | F-value | p-value  |
|----------|------------------------------|---------|-------|-------|---------|----------|
| Cue      | Sparse: 65<br>Abun.: 65      | 0.181   | 1     | 127   | 0.0081  | 0.9283   |
| Training | Untrained: 80<br>Trained: 50 | 248.304 | 1     | 127   | 11.1553 | 0.0011** |

### Mutual information

Linear mixed model with cue abundance (cue) and training as fixed-effects and mouse and imagining session as random-effects.

Model: MI  $\sim$  cue + training + (1|mouse) + (1|dataset)

| Factor   | N                            | Mean sq  | NumDF | DenDF  | F-value | p-value |
|----------|------------------------------|----------|-------|--------|---------|---------|
| Cue      | Sparse: 65<br>Abun.: 65      | 0.023036 | 1     | 93.743 | 0.5333  | 0.4671  |
| Training | Untrained: 80<br>Trained: 50 | 0.117688 | 1     | 103.93 | 2.7245  | 0.1018  |

### Cue vs control object place field correlation

Linear mixed model with cue abundance (cue), shuffle and the interaction (cue:shuffle) as fixed-effects and mouse and imagining session as random-effects.

Model: correlation  $\sim$  cue\*shuffle + (1|mouse) + (1|dataset)

| Factor      | N  | Mean sq | NumDF | DenDF  | F-value | p-value      |
|-------------|--|---------|-------|--------|---------|--------------|
| Cue         | Sparse: 108<br>Abun.: 104  | 0.05817 | 1     | 174.95 | 1.8703  | 0.1732       |
| Shuffle     | Original: 106<br>Shuffled: 106   | 1.22888 | 1     | 173.46 | 39.5112 | 2.557E-09*** |
| Cue:shuffle | Sparse/original: 54<br>Abun./ original: 52<br>Sparse/shuffled: 54<br>Abun./ shuffled: 52 | 0.03631 | 1     | 173.46 | 1.1675  | 0.2814       |

Table 7: Statistics for Fig 3.4

### Place field width

Linear mixed model with cue abundance (cue) and training as fixed-effects and mouse and imagining session as random-effects.

Model: width ~ cue + training + (1|mouse) + (1|dataset)

| Factor   | N                            | Mean sq | NumDF | DenDF  | F-value | p-value |
|----------|------------------------------|---------|-------|--------|---------|---------|
| Cue      | Sparse: 55<br>Abun.: 52      | 209.43  | 1     | 41.326 | 0.9671  | 0.3311  |
| Training | Untrained: 69<br>Trained: 38 | 411.35  | 1     | 87.467 | 1.8995  | 0.1717  |

### Out/in ratio

Linear mixed model with cue abundance (cue) and training as fixed-effects and mouse and imagining session as random-effects.

Model: oi\_ratio ~ cue + training + (1|mouse) + (1|dataset)

| Factor   | N                            | Mean sq | NumDF | DenDF  | F-value | p-value |
|----------|------------------------------|---------|-------|--------|---------|---------|
| Cue      | Sparse: 55<br>Abun.: 52      | 10.8895 | 1     | 89.107 | 0.8734  | 0.3525  |
| Training | Untrained: 69<br>Trained: 38 | 5.2011  | 1     | 57.481 | 0.4172  | 0.5209  |

### Stability

Linear mixed model with cue abundance (cue) and training as fixed-effects and mouse and imagining session as random-effects.

Model: stability ~ cue + training + (1|mouse) + (1|dataset)

| Factor   | N                            | Mean sq  | NumDF | DenDF  | F-value | p-value |
|----------|------------------------------|----------|-------|--------|---------|---------|
| Cue      | Sparse: 41<br>Abun.: 42      | 0.015298 | 1     | 42.912 | 1.0504  | 0.31115 |
| Training | Untrained: 53<br>Trained: 30 | 0.068786 | 1     | 47.855 | 4.723   | 0.03474 |

### Place field centres per location bin

Linear mixed model with cue abundance (cue), location, training, and the interaction (cue:location) as fixed-effects and mouse and imagining session as random-effects.

Model: percentage ~ cue\*location + training + (1|mouse) + (1|dataset)

| Factor   | N                           | Mean sq     | NumDF | DenDF | F-value | p-value    |
|----------|-----------------------------|-------------|-------|-------|---------|------------|
| Cue      | Sparse: 165<br>Abun.: 162   | 0.066       | 1     | 320   | 0.0035  | 0.95265    |
| Location | Before: 109<br>Around.: 109 | 128.64<br>4 | 2     | 320   | 6.8742  | 0.001194** |

|              |  |        |   |     |        |          |
|--------------|--|--------|---|-----|--------|----------|
|              | After: 109   |        |   |     |        |          |
| Training     | Untrained: 204<br>Trained: 123   | 0.139  | 1 | 320 | 0.0074 | 0.931465 |
| Cue:location | Sparse/before: 55<br>Abun./ before: 54<br>Sparse/around: 55<br>Abun./around: 54<br>Sparse/after.: 55<br>Abun./ after: 54 | 49.001 | 2 | 320 | 2.6184 | 0.074481 |

Tukey's method post-hoc test on location by novelty

Sparse/novel condition

| Contrast         | Estimate | SE    | Df  | t-ratio | p-value   |
|------------------|----------|-------|-----|---------|-----------|
| Before vs around | -0.0168  | 0.825 | 286 | -0.02   | 0.9998    |
| Before vs after  | -3.0362  | 0.825 | 286 | -3.681  | 0.0008*** |
| Around vs after  | -3.0194  | 0.825 | 286 | -3.66   | 0.0009*** |

Abundant/novel condition

| Contrast         | Estimate | SE    | Df  | t-ratio | p-value |
|------------------|----------|-------|-----|---------|---------|
| Before vs around | 0.3374   | 0.833 | 286 | 0.405   | 0.9135  |
| Before vs after  | -0.5567  | 0.833 | 286 | -0.669  | 0.7819  |
| Around vs after  | -0.8941  | 0.833 | 286 | -1.074  | 0.531   |

Table 8: Statistics for S Fig 3.6

### Place cell overlap coefficient

Linear mixed model with comparison and training as fixed-effects and mouse and imagining session as random-effects.

Model: coefficient ~ comparison\*training +(1|mouse) +(1|dataset)

| Factor     | N   | Mean sq  | NumDF | DenDF  | F-value | p-value  |
|------------|---|----------|-------|--------|---------|----------|
| Comparison | Same abun.: 65<br>Same novelty: 65<br>Different: 65 | 0.001771 | 2     | 131.39 | 0.1106  | 0.89537  |
| Training   | Untrained: 120<br>Trained: 75                       | 0.07768  | 1     | 121.37 | 4.8504  | 0.02953* |

### Expected place cell overlap vs chance

Paired two-sample Wilcoxon signed rank test with Holm-Bonferonni correction

| Comparison   | Training  | n  | Adjusted p |
|--------------|-----------|----|------------|
| Same abun.   | Untrained | 41 | 0.0243*    |
| Same abun.   | Trained   | 25 | 0.00109**  |
| Same novelty | Untrained | 41 | 0.00109**  |
| Same novelty | Trained   | 25 | 0.0149*    |
| Different    | Untrained | 41 | 0.0419*    |
| Different    | Trained   | 25 | 0.643      |

### Place field correlations

Paired two-sample Wilcoxon signed rank test with Holm-Bonferonni correction

| Comparison   | Training  | n  | Adjusted p |
|--------------|-----------|----|------------|
| Same abun.   | Untrained | 41 | 0.0372*    |
| Same abun.   | Trained   | 25 | 0.0208*    |
| Same novelty | Untrained | 41 | 0.22       |
| Same novelty | Trained   | 25 | 0.782      |
| Different    | Untrained | 41 | 0.0199*    |
| Different    | Trained   | 25 | 0.0103*    |

### Object-vector overlap coefficient

Unpaired two-sample Wilcoxon signed rank test

| Group 1   | Group 2 | n1 | n2 | p-value |
|-----------|---------|----|----|---------|
| Untrained | Trained | 41 | 25 | 0.148   |

### Expected object-vector cell overlap vs chance

Paired two-sample Wilcoxon signed rank test with Holm-Bonferonni correction

| Comparison   | Training  | n  | Adjusted p |
|--------------|-----------|----|------------|
| Same novelty | Untrained | 41 | 0.879      |
| Same novelty | Trained   | 25 | 0.135      |

### Object-vector place field correlations

Paired two-sample Wilcoxon signed rank test with Holm-Bonferonni correction

| Comparison   | Training  | n  | Adjusted p |
|--------------|-----------|----|------------|
| Same novelty | Untrained | 41 | 0.256      |
| Same novelty | Trained   | 25 | 0.429      |

*Table 9: Statistics for Fig 3.5*

### Bayesian decoder error

Linear mixed model with cue abundance (cue), novelty, training and the interaction (cue:novelty) as fixed-effects and mouse and imagining session as random-effects

Model: error ~ cue\*novelty + training + (1|mouse) + (1|dataset)

| Factor      | N   | Mean sq | NumDF | DenDF  | F-value | p-value      |
|-------------|---|---------|-------|--------|---------|--------------|
| Cue         | Sparse: 126<br>Abun.: 125   | 8.8     | 1     | 201.25 | 0.0743  | 0.7854366    |
| Novelty     | Familiar: 131<br>Novel: 120   | 9157.2  | 1     | 201.53 | 77.1187 | 6.972E-16*** |
| Training    | Untrained: 155<br>Trained: 96   | 1732.3  | 1     | 222.35 | 14.5887 | 0.0001735*** |
| Cue:novelty | Sparse/familiar: 65<br>Abun./ familiar: 66<br>Sparse/novel: 61<br>Abun./novel: 59 | 344.2   | 1     | 200.57 | 2.8984  | 0.0902154    |

### Place cell error difference

One-sample Wilcoxon signed rank test compared to a mean of 0 with Holm–Bonferroni correction

| Training  | Cue      | Novelty  | n  | Adjusted p |
|-----------|----------|----------|----|------------|
| Untrained | Sparse   | Familiar | 41 | 0.78       |
| Trained   | Sparse   | Familiar | 25 | 0.91       |
| Untrained | Abundant | Familiar | 41 | 0.91       |
| Trained   | Abundant | Familiar | 25 | 0.52       |
| Untrained | Sparse   | Novel    | 41 | 0.0043**   |
| Trained   | Sparse   | Novel    | 25 | 0.0001***  |
| Untrained | Abundant | Novel    | 41 | 0.03*      |
| Trained   | Abundant | Novel    | 25 | 0.0001***  |

Linear mixed model with cue abundance (cue), novelty, training and the interaction (cue:novelty) as fixed-effects and mouse and imagining session as random-effects

Model: error ~ cue\*novelty + training + (1|mouse) + (1|dataset)

| Factor   | N                           | Mean sq | NumDF | DenDF  | F-value | p-value      |
|----------|-----------------------------|---------|-------|--------|---------|--------------|
| Cue      | Sparse: 124<br>Abun.: 123   | 56      | 1     | 195.49 | 0.5896  | 0.44348      |
| Novelty  | Familiar: 129<br>Novel: 118 | 5869.6  | 1     | 195.64 | 61.8402 | 2.456E-13*** |
| Training | Untrained: 151              | 382.8   | 1     | 214.96 | 4.0334  | 0.04586*     |

|              |   |       |   |        |        |         |
|--------------|---|-------|---|--------|--------|---------|
|              | Trained: 96   |       |   |        |        |         |
| Cue: novelty | Sparse/familiar: 64<br>Abun./ familiar: 65<br>Sparse/novel: 60<br>Abun./novel: 58 | 132.7 | 1 | 194.89 | 1.3983 | 0.23844 |

Table 10: Statistics for Fig 3.6

## Error compared to shuffle

Paired two-sample Wilcoxon signed rank test with Holm-Bonferonni correction

| Cue      | Novelty  | n  | Adjusted p  |
|----------|----------|----|-------------|
| Sparse   | Familiar | 66 | 9.58e-12*** |
| Abundant | Familiar | 66 | 9.58e-12*** |
| Sparse   | Novel    | 66 | 2.47e-11*** |
| Abundant | Novel    | 66 | 3.60e-11*** |

## Error per location bin

Linear mixed model with cue abundance (cue), novelty, location, training and the interactions (cue:novelty), (cue:location), (novelty:training) and (cue:novelty:location) as fixed-effects and mouse and imagining session as random-effects

Model: error ~ cue\*novelty\*location + training + (1|mouse) + (1|dataset)

| Factor           | N   | Mean sq | NumDF | DenDF  | F-value | p-value      |
|------------------|---|---------|-------|--------|---------|--------------|
| Cue              | Sparse: 371<br>Abun.: 369   | 23      | 1     | 687.51 | 0.0526  | 0.818687     |
| Novelty          | Familiar: 386<br>Novel: 354   | 27179.5 | 1     | 688.05 | 62.0665 | 1.299E-14*** |
| Location         | Control obj.: 246<br>Cue obj.: 247<br>Reward: 247   | 2710.7  | 2     | 679.94 | 6.1901  | 0.002167**   |
| Training         | Untrained: 453<br>Trained: 287  | 3690.2  | 1     | 351.25 | 8.4268  | 0.003931**   |
| Cue:novelty      | Sparse/familiar: 191<br>Abun./ familiar: 195<br>Sparse/novel: 180<br>Abun./novel: 174   | 672     | 1     | 686.45 | 1.5346  | 0.215842     |
| Cue:location     | Sparse/control: 123<br>Abun./control: 123<br>Sparse/cue obj.: 124<br>Abun./cue obj.: 123<br>Sparse/reward.: 124<br>Abun./ reward: 123 | 84.2    | 2     | 679.94 | 0.1922  | 0.825179     |
| Novelty:location | Familiar/control: 128<br>Novel/control: 118<br>Familiar /cue obj.:129<br>Novel /cue obj.: 118   | 281.9   | 2     | 679.94 | 0.6437  | 0.525655     |

|                      |   |       |   |        |        |          |
|----------------------|---|-------|---|--------|--------|----------|
|                      | Familiar /reward.: 129<br>Novel / reward: 118   |       |   |        |        |          |
| Cue:novelty:location | Control obj.:<br>Sparse/familiar: 63<br>Abun./ familiar: 65<br>Sparse/novel: 60<br>Abun./novel: 58<br><br>Cue obj.:<br>Sparse/familiar: 64<br>Abun./ familiar: 65<br>Sparse/novel: 60<br>Abun./novel: 58<br><br>Reward<br>Sparse/familiar: 64<br>Abun./ familiar: 65<br>Sparse/novel: 60<br>Abun./novel: 58 | 196.8 | 2 | 679.94 | 0.4493 | 0.638237 |

Tukey's method post-hoc test on location by novelty

Familiar condition

| Contrast              | Estimate | SE   | Df  | t-ratio | p-value |
|-----------------------|----------|------|-----|---------|---------|
| Control vs cue obj    | 3.29     | 2.61 | 683 | 1.259   | 0.4191  |
| Control obj vs reward | 4.41     | 2.61 | 683 | 1.688   | 0.2105  |
| Cue obj vs reward     | 1.12     | 2.61 | 683 | 0.43    | 0.903   |

Novel condition

| Contrast              | Estimate | SE   | Df  | t-ratio | p-value |
|-----------------------|----------|------|-----|---------|---------|
| Control vs cue obj    | 7.17     | 2.72 | 683 | 2.632   | 0.0236* |
| Control obj vs reward | 7.91     | 2.72 | 683 | 2.904   | 0.0106* |
| Cue obj vs reward     | 0.74     | 2.72 | 683 | 0.272   | 0.9601  |

### Place cell error per location bin

Linear mixed model with cue abundance (cue), novelty, location, training and the interactions (cue:novelty), (cue:location), (novelty:training) and (cue:novelty:location) as fixed-effects and mouse and imagining session as random-effects

Model: error ~ cue\*novelty\*location + training + (1|mouse) + (1|dataset)

| Factor               | N  | Mean sq | NumDF | DenDF  | F-value | p-value            |
|----------------------|--|---------|-------|--------|---------|--------------------|
| Cue                  | Sparse: 371<br>Abun.: 369  | 43      | 1     | 687.09 | 0.2753  | 0.59995            |
| Novelty              | Familiar: 386<br>Novel: 354  | 6771.7  | 1     | 687.76 | 43.3476 | 9.099E-11***       |
| Location             | Control obj.: 246<br>Cue obj.: 247<br>Reward: 247  | 2107.4  | 2     | 680.21 | 13.4899 | 0.000001797*<br>** |
| Training             | Untrained: 453<br>Trained: 287   | 208     | 1     | 346.2  | 1.3312  | 0.24939            |
| Cue:novelty          | Sparse/familiar: 191<br>Abun./ familiar: 195<br>Sparse/novel: 180<br>Abun./novel: 174  | 0       | 1     | 686.14 | 0.0003  | 0.98575            |
| Cue:location         | Sparse/control: 123<br>Abun./control: 123<br>Sparse/cue obj.: 124<br>Abun./cue obj.: 123<br>Sparse/reward.: 124<br>Abun./ reward: 123          | 33.7    | 2     | 680.21 | 0.2159  | 0.80584            |
| Novelty:location     | Familiar/control: 128<br>Novel/control: 118<br>Familiar /cue obj.:129<br>Novel /cue obj.: 118<br>Familiar /reward.: 129<br>Novel / reward: 118 | 315.6   | 2     | 680.21 | 2.0202  | 0.13343            |
| Cue:novelty:location | Control obj.:<br>Sparse/familiar: 63<br>Abun./ familiar: 65<br>Sparse/novel: 60  | 379.9   | 2     | 680.21 | 2.4318  | 0.08865            |

|  |                     |  |  |  |  |  |
|--|---------------------|--|--|--|--|--|
|  | Abun./novel: 58     |  |  |  |  |  |
|  | Cue obj.:           |  |  |  |  |  |
|  | Sparse/familiar: 64 |  |  |  |  |  |
|  | Abun./ familiar: 65 |  |  |  |  |  |
|  | Sparse/novel: 60    |  |  |  |  |  |
|  | Abun./novel: 58     |  |  |  |  |  |
|  | Reward              |  |  |  |  |  |
|  | Sparse/familiar: 64 |  |  |  |  |  |
|  | Abun./ familiar: 65 |  |  |  |  |  |
|  | Sparse/novel: 60    |  |  |  |  |  |
|  | Abun./novel: 58     |  |  |  |  |  |

## Familiar condition

| Contrast              | Estimate | SE   | Df  | t-ratio | p-value |
|-----------------------|----------|------|-----|---------|---------|
| Control vs cue obj    | 0.558    | 1.56 | 683 | 2.281   | 0.0591  |
| Control obj vs reward | 0.622    | 1.56 | 683 | 3.605   | 0.001** |
| Cue obj vs reward     | 0.064    | 1.56 | 683 | 1.326   | 0.3809  |

## Novel condition

| Contrast              | Estimate | SE   | Df  | t-ratio | p-value  |
|-----------------------|----------|------|-----|---------|----------|
| Control vs cue obj    | 0.302    | 1.63 | 683 | -0.186  | 0.9812   |
| Control obj vs reward | 0.742    | 1.63 | 683 | 3.528   | 0.0013** |
| Cue obj vs reward     | 0.044    | 1.63 | 683 | 3.714   | 0.0006** |

Table 11: Statistics for S Fig 3.7

### Object-relative Bayesian decoder error

Linear mixed model with cue abundance (cue), novelty, training and the interaction (cue:novelty) as fixed-effects and mouse and imagining session as random-effects

Model: error ~ cue\*novelty + training + (1|mouse) + (1|dataset)

| Factor      | N   | Mean sq | NumDF | DenDF  | F-value | p-value      |
|-------------|---|---------|-------|--------|---------|--------------|
| Cue         | Sparse: 123<br>Abun.: 123   | 27.2    | 1     | 199.13 | 0.1867  | 0.66613      |
| Novelty     | Familiar: 129<br>Novel: 117   | 7179.8  | 1     | 200.43 | 49.3156 | 3.314E-11*** |
| Training    | Untrained: 150<br>Trained: 96   | 781.3   | 1     | 217.74 | 5.3664  | 0.02146*     |
| Cue:novelty | Sparse/familiar: 64<br>Abun./ familiar: 65<br>Sparse/novel: 59<br>Abun./novel: 58 | 70.6    | 1     | 198.28 | 0.4849  | 0.48702      |

### Object-vector error difference

One-sample Wilcoxon signed rank test compared to a mean of 0 with Holm–Bonferroni correction

| Training  | Cue      | Novelty | n  | Adjusted p  |
|-----------|----------|---------|----|-------------|
| Untrained | Sparse   | Novel   | 41 | 1.46E-9***  |
| Trained   | Sparse   | Novel   | 25 | 2.38E-7***  |
| Untrained | Abundant | Novel   | 41 | 2.33E-10*** |
| Trained   | Abundant | Novel   | 25 | 2.38E-7***  |

Linear mixed model with cue abundance (cue) and training as fixed-effects and mouse and imagining session as random-effects

Model: error ~ cue + training + (1|mouse) + (1|dataset)

| Factor   | N                             | Mean sq | NumDF | DenDF  | F-value | p-value  |
|----------|-------------------------------|---------|-------|--------|---------|----------|
| Cue      | Sparse: 123<br>Abun.: 123     | 19.53   | 1     | 67.52  | 0.071   | 0.79072  |
| Training | Untrained: 150<br>Trained: 96 | 1789.27 | 1     | 102.81 | 6.5018  | 0.01225* |

Table 12: Statistics for Fig 3.7

### Error compared to shuffle

Paired two-sample Wilcoxon signed rank test with Holm-Bonferonni correction

| Cue      | Novelty  | n  | Adjusted p  |
|----------|----------|----|-------------|
| Sparse   | Familiar | 66 | 9.58e-12*** |
| Abundant | Familiar | 66 | 9.58e-12*** |
| Sparse   | Novel    | 66 | 3.27e-11*** |
| Abundant | Novel    | 66 | 3.79e-11*** |

### Error per object-relative location bin

Linear mixed model with cue abundance (cue), novelty, location, training and the interactions (cue:novelty), (cue:location), (novelty:training) and (cue:novelty:location) as fixed-effects and mouse and imagining session as random-effects

Model: error ~ cue\*novelty\*location + training + (1|mouse) + (1|dataset)

| Factor           | N   | Mean sq | NumDF | DenDF  | F-value | p-value   |
|------------------|---|---------|-------|--------|---------|-----------|
| Cue              | Sparse: 368<br>Abun.: 369   | 28.7    | 1     | 687.95 | 0.0714  | 0.78933   |
| Novelty          | Familiar: 387<br>Novel: 350   | 17937.6 | 1     | 692.13 | 44.5791 | 5.015E-11 |
| Location         | Control obj.: 246<br>Cue obj.: 245<br>Reward: 246   | 8347.3  | 2     | 680.29 | 20.745  | 1.797E-09 |
| Training         | Untrained: 449<br>Trained: 288  | 1117    | 1     | 367.08 | 2.7761  | 0.09654   |
| Cue:novelty      | Sparse/familiar: 192<br>Abun./ familiar: 195<br>Sparse/novel: 176<br>Abun./novel: 174   | 60.6    | 1     | 685.13 | 0.1506  | 0.69811   |
| Cue:location     | Sparse/control: 123<br>Abun./control: 123<br>Sparse/cue obj.: 122<br>Abun./cue obj.: 123<br>Sparse/reward.: 123<br>Abun./ reward: 123 | 4       | 2     | 680.29 | 0.0099  | 0.99018   |
| Novelty:location | Familiar/control: 129<br>Novel/control: 117<br>Familiar /cue obj.:129<br>Novel /cue obj.: 116   | 663.9   | 2     | 680.29 | 1.65    | 0.19282   |

|                      |   |      |   |        |       |         |
|----------------------|---|------|---|--------|-------|---------|
|                      | Familiar /reward.: 129<br>Novel / reward: 117   |      |   |        |       |         |
| Cue:novelty:location | Control obj.:<br>Sparse/familiar: 64<br>Abun./ familiar: 65<br>Sparse/novel: 59<br>Abun./novel: 58<br><br>Cue obj.:<br>Sparse/familiar: 64<br>Abun./ familiar: 65<br>Sparse/novel: 58<br>Abun./novel: 58<br><br>Reward<br>Sparse/familiar: 64<br>Abun./ familiar: 65<br>Sparse/novel: 59<br>Abun./novel: 58 | 57.5 | 2 | 680.29 | 0.143 | 0.86677 |

Tukey's method post-hoc test on location by novelty

Familiar condition

| Contrast         | Estimate | SE  | Df  | t-ratio | p-value  |
|------------------|----------|-----|-----|---------|----------|
| Before vs around | -8.161   | 2.5 | 681 | -3.267  | 0.0033** |
| Before vs after  | 0.592    | 2.5 | 681 | 0.237   | 0.9695   |
| Around vs after  | 8.754    | 2.5 | 681 | 3.505   | 0.0014** |

Novel condition

| Contrast         | Estimate | SE   | Df  | t-ratio | p-value    |
|------------------|----------|------|-----|---------|------------|
| Before vs around | -13.926  | 2.63 | 681 | -5.298  | <0.0001*** |
| Before vs after  | -5.04    | 2.62 | 681 | -1.922  | 0.1333     |
| Around vs after  | 8.886    | 2.63 | 681 | 3.381   | 0.0022**   |

### Object-vector cell error per location bin

Linear mixed model with cue abundance (cue), location, training, and the interaction (cue:location) as fixed-effects and mouse and imagining session as random-effects.

Model: error ~ cue\*location + training + (1|mouse) + (1|dataset)

| Factor       | N  | Mean sq | NumDF | DenDF  | F-value | p-value          |
|--------------|--|---------|-------|--------|---------|------------------|
| Cue          | Sparse: 176<br>Abun.: 174  | 48.6    | 1     | 305.34 | 0.0588  | 0.8086356        |
| Location     | Before: 117<br>Around.: 116<br>After: 117  | 5849.9  | 2     | 291.35 | 7.0793  | 0.0009951<br>*** |
| Training     | Untrained: 212<br>Trained: 138   | 3476.3  | 1     | 190.31 | 4.2069  | 0.0416305*       |
| Cue:location | Sparse/before: 59<br>Abun./ before: 58<br>Sparse/around: 58<br>Abun./around: 58<br>Sparse/after.: 59<br>Abun./ after: 58 | 60.6    | 2     | 291.35 | 0.0734  | 0.9292509        |

#### Novel condition

| Contrast         | Estimate | SE   | Df  | t-ratio | p-value  |
|------------------|----------|------|-----|---------|----------|
| Before vs around | 0.104    | 3.77 | 302 | 0.028   | 0.9996   |
| Before vs after  | -12.205  | 3.76 | 302 | -3.247  | 0.0037** |
| Around vs after  | -12.309  | 3.77 | 302 | -3.267  | 0.0035** |

Table 13: Statistics for S Fig 3.8

## 4 Low frequency oscillations in hippocampal area CA1

### 4.1 Introduction

Although pyramidal cells in hippocampal area CA1 are among the most studied neuronal cells in the brain [19,203], studies into their function have mostly focussed on their activity during locomotion. During locomotion, they are active in a location-dependent fashion, which is important for navigation tasks [23,26]. However, periods of rest are also crucial for the hippocampus to support vital functions, such as memory consolidation through replay [204], and the planning of future goal-directed navigation [114]. Both of these behaviours – locomotion and resting – have their own functions, and as such are marked by different types of brain activity, at both global and neuronal scale.

Neural oscillations play a crucial role in the hippocampus during each of the brain states. Both during REM sleep and locomotion theta oscillations are present in rodents [65,74,205,206]. These oscillations modulate the precise timing of firing of pyramidal neurons [65], and are involved in phase precession, the phenomenon that cells fire at different theta phase times depending on the animal's location within the place field [82]. During slow wave sleep, in the absence of theta oscillations, slow (and delta) oscillations (0.1-4Hz) dominate [207–209]. Such slow oscillations, which are thought to originate from the thalamus [210], affect the timing of slow wave-ripples (SWR) in the hippocampus [209,211]. These are sharp waves that occur in conjunction with high frequency (110-200 Hz) oscillatory events, called ripples [108,212].

Overall, hippocampal brain states are roughly divided into three states. During locomotion and REM sleep, neuronal activity is marked by the presence of theta and gamma oscillations [70,71]. During periods of immobility and slow wave sleep, in the absence of theta oscillations [65], large irregular activity (LIA) is present, characterized by co-occurring sharp waves and ripples (SWRs) [69–71]. A third brain state, small irregular activity (SIA), has been found to

occur during sleep [71,116,117], and at particular times during wakefulness, for example when an animal abruptly 'freezes' [71,74,117]. Though SIA occurs spontaneously during sleep, it can also be elicited by auditory stimuli administered during sleep [117]. Because of this, it has been implied to be an intermediary state between resting and active states [117].

Individual cells in the hippocampus show different levels of activity depending on the brain state. The activity of pyramidal cells, as well as the majority of somatostatin (SST) and parvalbumin (PV) positive interneurons, in the hippocampus is generally positively modulated by running speed [34,157,213]. During locomotion, a proportion of CA1 pyramidal cells, the place cells, are active in a location-dependent fashion [23]. Though CA1 pyramidal cells are largely silent during LIA, the majority of cells increase their firing during SWR events in LIA [116]. The firing of pyramidal cells associated with SWRs involves 'replay' events, the sequential reactivation of location-specific cells [214].

When SIA occurs during sleep, the vast majority of CA1 pyramidal cells becomes silent, while only a small subset (3-5%) increases its activity [71,117]. Like cells during locomotion, but not during LIA, these cells show location-dependent firing, and as such have a place field in the sleeping location where the SIA occurred [71]. SIA during wakefulness has been less well-described in CA1, and has been suggested to be less stable [117], and as such, little is known about activity of individual cells in this subfield during wakeful SIA events. During sleep, the CA2 subfield also shows a population of cells that fire in periods of SIA [116]. These same cells, termed N units, also fire at a high rate when mice are awake, immobile, and not showing SWR, along with a very small population of CA1 and CA3 cells. As both the CA1 and CA2 cells fire during SIA and have similar activity modulators, they may be related [118].

A neural characteristic similar to the sharp waves during ripples, termed the N-wave, has been identified during SIA [116,118]. It differs from the sharp wave in its direction: it is marked by a positive change in the LFP signal. In addition, although it is mainly characterized by slow

frequencies, it does not show a true oscillatory pattern, but rather is aperiodic in nature.

Otherwise, SIA seems to mainly be marked by a lack of clear oscillations and a flattening of the EEG signal [117].

In this Chapter, we observe a small population of CA1 pyramidal cells which are preferably active during periods of immobility during a virtual reality navigation task. Their activity is marked by a high power in a low frequency (0.2-0.5Hz) band, which is caused both by oscillatory behaviour in this band, as well as a strong aperiodic component, high synchronicity between individual cells, and location specific activity. We additionally find a population of pyramidal cells with similar characteristics in the visual cortex. Lastly, we observed and characterized a subpopulation of pyramidal cells that are active during running, which show a high power in the same low frequency band, but do not oscillate.

## 4.2 Results

### 4.2.1 A novel type of hippocampal pyramidal cell is identified using regularity of firing and activity during rest

During a two-photon recording of dorsal CA1 (Fig 4.1A) we noticed a group of cells showing a simultaneous increase in fluorescence simultaneous at regular intervals (Fig 4.1B, supplementary video: [10.6084/m9.figshare.14452878](https://doi.org/10.6084/m9.figshare.14452878)). This only happened during periods where the mouse was not locomoting. We confirmed this in the fluorescence trace over time, where periodic activity could be seen during stationary periods for a group of cells (Fig 4.1B, D, cells highlighted by orange box). Because these cells were characterized by slow periodic activity during times when the mouse was stationary, we call them Stationary Low-frequency Oscillatory cells (SLOs).

To identify these cells quantitatively, we calculated two parameters: the rest/running fluorescence ratio and the number of peaks in the autocorrelogram. To calculate the

rest/running fluorescence ratio, we simply divided the mean fluorescence ( $\Delta F/F$ ) during stationary epochs by the mean fluorescence outside of these epochs. Any candidate cells had to have a rest/running ratio of at least two standard deviations above the mean of the population (Fig 4.1C, red line).

The number of peaks in the autocorrelogram was used as a proxy for the regularity or periodicity of the activity, with fewer peaks indicating more regular activity. To calculate it, we plotted the smoothed autocorrelogram of each ROI and measured the number of local maxima (peaks) within 30 seconds each side of the centre. An ROI that is more periodic will have its peaks lined up in the autocorrelogram (Fig 4.1E), and thus will have fewer peaks in the same period than a non-periodic cell (Fig 4.1F). Again, we determined this value for every ROI in the dataset, and for an ROI to be included it had to have a value for the number of peaks at least two standard deviations below the mean of the population (Fig 4.1G, red line).

Any cells that adhered to both these criteria were deemed SLOs (Fig 4.1H, top left quadrant). We used these criteria to find SLOs in 84 datasets from 12 mice. We found SLOs in 32 out of 84 datasets (Fig 4.1I), and in these 32 datasets, on average 0.63% (range: 0.31-1.70%) of cells were identified as SLOs, which equated to 1.7 cells (range: 1-5 cells) per dataset. Although this seems like a low number, this may be due to the nature of the task, in which mice were incentivised to run. Indeed, the length of the longest rest event within a dataset significantly correlated with the proportion of cells identified as SLOs (Fig 4.1J, Spearman correlation coefficient = 0.27,  $p=0.01$ ). Having datasets where mice were stationary for longer periods of time might thus result in a higher percentage of SLOs.

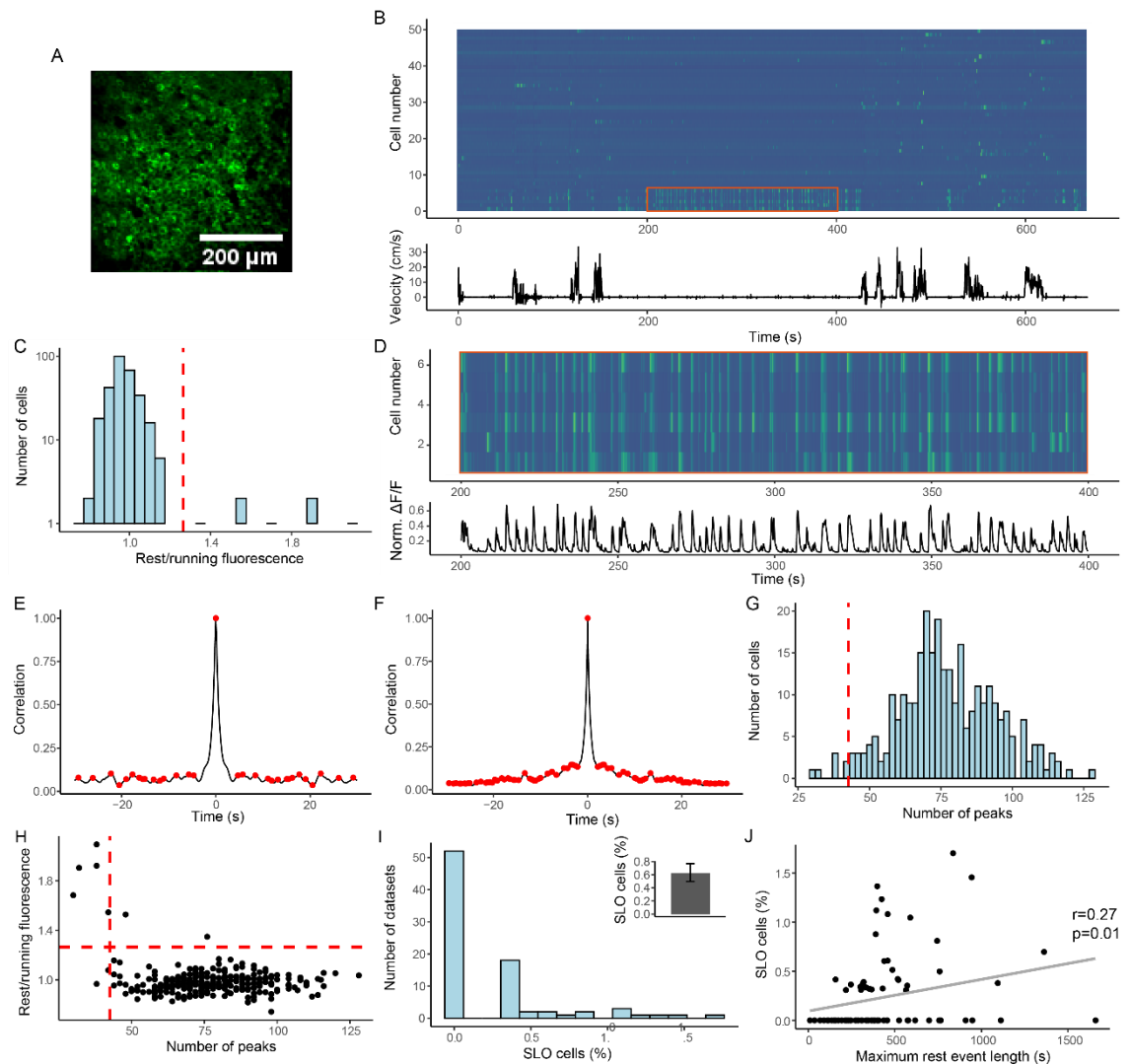


**Fig 4.1 Identification of Stationary Low-frequency Oscillatory cells (SLOs).** (A) Example two-photon recording showing cells in green. Image is the mean Z projection of a single recording. (B) Example fluorescence of cells over time, bottom graph shows the velocity of the mouse during this period. The marked orange area indicates cells showing periodic activity during rest periods, and is shown in more detail in D. (C) The ratio between mean fluorescence during rest and running for each cell in an example dataset, with the red dashed line showing the mean + 2\*std. (D) Zoomed fluorescence during a rest period in B, showing synchronous periodic activity in 6 cells. The bottom graph shows the mean fluorescence during this period across the 6 cells. Example autocorrelograms for (E) a possible SLO and (F) a control cell. Each red dot marks a local maximum. (G) Number of peaks in the autocorrelograms for all cells in an example dataset, with the red dashed line showing the mean - 2\*std. (H) Relation between number of peaks and rest/running fluorescence ratio for this example dataset. The red dashed lines indicate the same thresholds as the lines in (C) and (G). Cells in the top left quadrant are identified as SLOs. (I) The percentage of ROIs identified as SLOs in 84 datasets, the bar shows the mean across all datasets with at least 1 SLO

*cell, errorbar shows 95% confidence interval. (J) Relation between the percentage of SLO cells and the length of the longest rest event of a dataset. Grey line is the regression line,  $r$ - and  $p$ -values from Spearman correlation test.*

#### 4.2.2 Novel functional cell type has high power at low frequencies

As we could see periodic activity of the SLOs by eye, we proceeded analysing the power and frequency of this activity using a discrete Fourier transform. Compared to the control cells, the SLOs had a peak in power at a low frequency, as illustrated in the pink noise-corrected power spectra (Fig 4.2A). We determined the power band where the SLOs showed increased power as any values above mean + 3 times the standard deviation in a smoothed version of the pink noise-corrected power spectrum, resulting in a frequency band of 0.2-0.5Hz.

We used this power band to find the relationship between the relative band power and the parameters we previously used to identify the SLOs: rest/running fluorescence ratio and number of peaks in the autocorrelogram. We calculated the relative band power by dividing the power in our target band (0.2-0.5Hz) by the power in a control band (2-3.5 Hz), in the uncorrected power spectra. We selected this band as it fell outside of theta range [65], and was sufficiently distinct from our power band. This band did fall within the delta power band, but this was unavoidable, as it covers any frequencies we could measure at our acquisition rate that did not overlap with the target band (0.5-4 Hz) [19,215]. The relative power at 0.2-0.5 Hz showed an exponential relationship with both parameters (Fig 4.2B,C, S Fig 2.1A,B). The parameter of the exponential relationship between rest/running fluorescence ratio and power in the frequency band, and between the number of peaks of the autocorrelogram and power in the frequency band, both differed significantly from zero (Fig 4.2D,  $p=6.09e-4$   $p=3.48e-15$  respectively, Wilcoxon signed-rank test with Holm-Bonferroni multiple comparison correction).

Next, we analysed the relative power in this target frequency band compared to the control frequency band in both the SLOs and control cells. Although the SLOs had a higher relative power on average, the control cell population also contained a small number of cells with high

power in the target frequency band (Fig 4.2E). We decided to separate out these cells into a new population that included any cells with a relative power greater than three times the standard deviation above the mean across all datasets. These cells were not as easily visually distinguishable in their activity pattern as the SLOs (Fig 4.2F). As they did not fire preferentially during stationary periods, and showed high relative power particular during running (Fig 4.3B), we named them Odd Running-active Low-frequency Aperiodic (ORLA) cells. Overall, this new population formed 1.65 (std: 3.23)% of all ROIs in our datasets, which equated to 4.7 (std: 9.4) cell per dataset. When looking at the power spectrum of these three groups, we saw that both the SLOs and the newly identified ORLAs, but not the control cells, have a peak in the 0.2 to 0.5 Hz power band in the pink noise-corrected power spectra.

As different hippocampal populations can display differences in physiological properties [16], we were interested to see if our newly identified cells were physiologically distinct. We studied a range of relevant cell characteristics for the two cell populations we identified: SLO cells and ORLA cells. Although there was a general effect of cell type on ROI size (S Fig 4.1A,  $p=0.048$ , linear mixed model with cell type as fixed-effect and imagining session as random-effect), we did not see any significant differences between the pairs of cell types after applying a post hoc multiple comparisons test (Tukey's;  $p=0.07$ ,  $p=0.72$ ,  $p=0.12$  for the SLO-ORLA, SLO-control and ORLA-control comparisons respectively). There was no difference in the maximum spike rate (S Fig 4.1B,  $p=0.50$ , linear mixed model with cell type as fixed-effect and imagining session as random-effect), as estimated using the deconvolution step in Suite2P [172]. However, there was a difference in overall spike rate between the cell types (S Fig 4.1C,  $p<2e-16$ , linear mixed model with cell type as fixed-effect and imagining session as random-effect). The SLO cells had a higher mean spiking rate than both ORLA and control cells (Tukey's;  $p<0.0001$ ,  $p<0.0001$ , for the SLO-ORLA and SLO-control comparisons), while the ORLA cells had a significantly increased mean spiking rate compared to the control cells (Tukey's,  $p=0.048$ , ORLA-control comparison).

Finally, we determined whether the populations were spatially clustered. We expect some level of clustering, as the hippocampus shows spatial clustering of cell types along all its axes [16,216–218]. On average, both the SLO and ORLA cells were closer to ROIs of the same cell type (in) than ROIs of different cell types (out) (S Fig 4.1E,  $p=0.012$  and  $p=4.6e-6$  for SLOs and ORLAs respectively, paired two-samples Wilcoxon test, Holm-Bonferroni corrected for multiple comparisons), while the control cells showed the opposite trend ( $p=3.6e-5$ ). This suggests the SLOs and ORLAs cluster together, possibly along one of the hippocampal axes, as other cell types do, although further recordings will be needed in order to confirm this.

Here, we distinguished, in addition to the SLO population, another population: the ORLA cells. Like the SLO cells, they show a relatively high power in a low (0.2-0.5 Hz) frequency band. The SLO and ORLA populations both show physiological difference from the control population in their maximum spiking rate and the level of clustering, suggesting they may be distinct physiological, and possibly spatially clustered, populations. However, they did not have an altered size or mean firing rate.

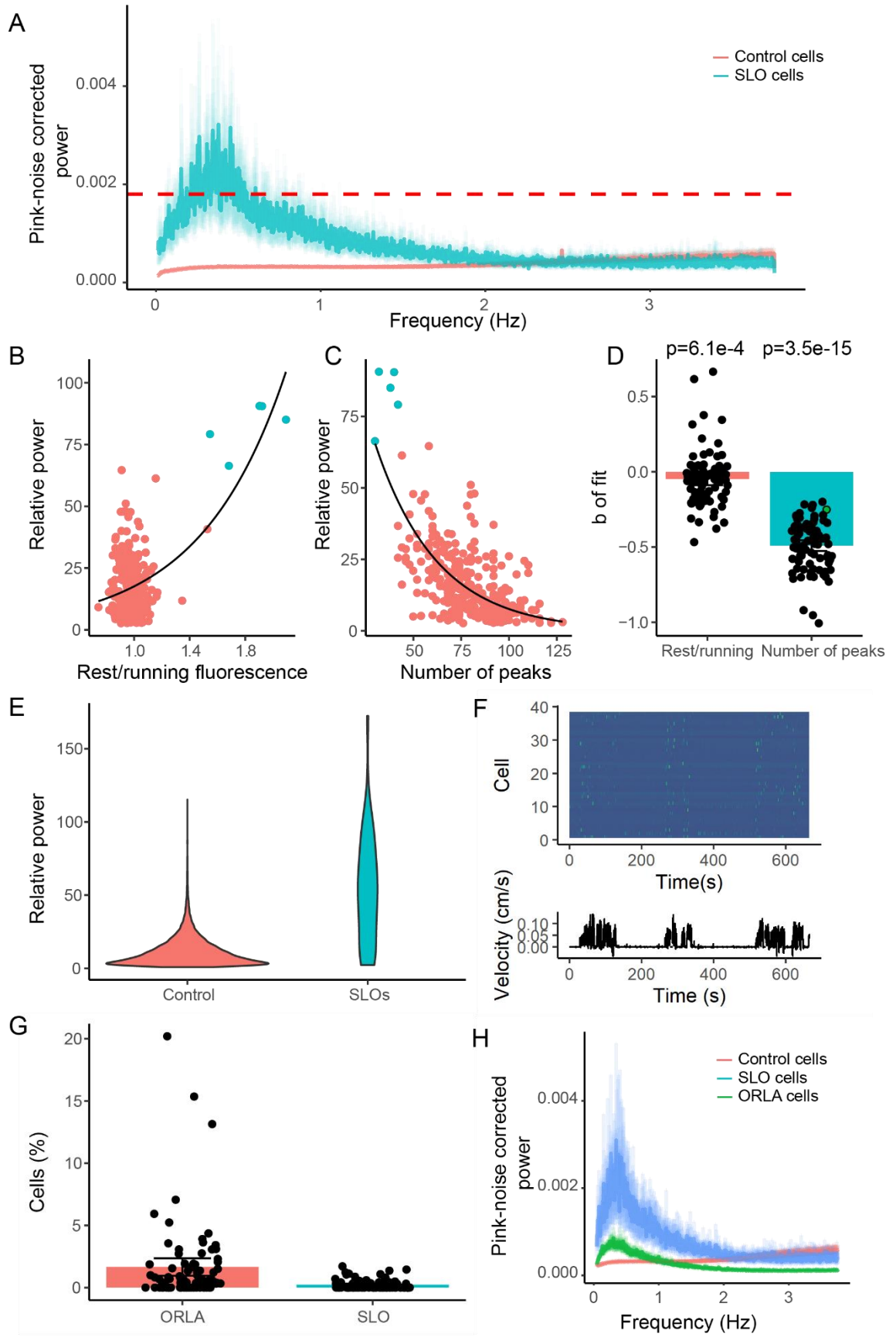


*Fig 4.2 Power spectrum of SLO and control cells.* (A) Pink noise-corrected power spectra of the control (pink) and SLOs (blue). (B) Example relationship between rest/running fluorescence ratio and relative power in 0.2-0.5 Hz band compared to 2-3.5 Hz band for one dataset. Black line shows exponential fit. (C) Example relationship between the number of peaks in the autocorrelogram and relative power in 0.2-0.5 Hz band compared to 2-3.5 Hz band for one dataset. Black line shows exponential fit. (D) Exponential fit parameter (b) fit across all datasets for SLO and control cells. P-values are from Wilcoxon signed-rank tests compared to a mean of 0 with Holm-Bonferroni multiple comparison correction. (E) Distribution of the relative power in 0.2-0.5 Hz band compared to 2-3.5 Hz band for SLO and control cells. (F) Example fluorescence of control cells with a high relative power in 0.2-0.5 Hz band compared to 2-3.5 Hz band over time (ORLA), the bottom graph shows the velocity of the mouse during this period. (G) The percentage of ROIs identified as SLOs and ORLAs across all datasets. (H) Pink noise-corrected power spectra of the control cells (pink), SLOs (blue), and ORLAs (green). Bars are the means of 84 datasets, black dots are values for each individual dataset and error bars represent the 95% confidence interval. For the power spectra (A and H) black shows the mean power, coloured traces show the 95% confidence interval.

#### 4.2.3 Novel functional cell types are differentially modulated by locomotion

We further investigated how both the SLOs and the ORLAs are modulated by locomotion, and how the relative power in the low frequency band changes in response to locomotion. We first identified epochs of rest or locomotion of 60 seconds or longer. We then determined the average fluorescence of each of the functional cell types during these epochs. Despite our SLOs being selected for having a high rest/running fluorescence ratio, we found no difference for any of the cell types between rest and locomotion when only including longer epochs (Fig 4.3A, unpaired two-samples Wilcoxon tests with Holm-Bonferroni correction for multiple comparisons). However, as the SLO cells were only identified in cells with more rest, we had limited data on their activity during longer running epochs, which might explain the lack of difference.

To determine how the power changes as a result of locomotion, we used a discrete Fourier transform to determine the power and frequency of firing during periods of rest or locomotion. We found a higher relative power for the SLOs during rest than during running (Fig

4.3B, C,  $p=0.02$  unpaired two-samples Wilcoxon test with Holm-Bonferroni correction for multiple comparisons). The ORLAs displayed the opposite pattern, with a higher relative power during running than during rest (Fig 4.3B, D,  $p=5.9e-5$  unpaired two-samples Wilcoxon test with Holm-Bonferroni correction for multiple comparisons). Similarly, the control cells had a significantly higher relative power during running than during rest (Fig 4.3B, E,  $p=8.2e-5$  unpaired two-samples Wilcoxon test with Holm-Bonferroni correction for multiple comparisons).

We were next interested in whether the cell types had sustained activity during the epochs of rest or locomotion. We determine the average fluorescence of each cell during the first minute of the rest or locomotion epoch (Fig 4.3F-H). To quantify the change in fluorescence through the course of such epochs, we compared the average fluorescence in the first 10 seconds (early) to the fluorescence in 50-60 seconds (late) into the epochs. On average the activity in the SLOs ramped during rest epochs (Fig 4.3F, left), as it seemed to have a higher activity late compared to early in rest epochs, though this difference was just short of significant (Fig 4.3I,  $p=0.05$ , paired t-test with Bonferroni-Holm correction). Sadly, as both sufficiently long running epochs of at least a minute and SLOs were rare, we did not have enough data to determine the activity of SLOs during running epochs.

The ORLAs did not show a difference in their activity late compared to early in the rest or locomotion epochs (Fig 4.3G, I-J,  $p=0.80$ ,  $p=0.95$ , paired t-test with Bonferroni-Holm correction). The control cells showed a strong decrease in activity late compared to early into rest epochs (Fig 4.3I,  $p=1.2e-13$ , paired t-test with Bonferroni-Holm correction), which seemed to be caused by a sharp drop in activity at the start of the epochs (Fig 4.3H, left). Interestingly, during the locomotion epochs a similar drop was observed, though less pronounced, and just shy of significant (Fig 4.3H, J,  $p=0.05$ , paired t-test with Bonferroni-Holm correction). Overall,

this suggests that as the SLOs increase their activity, the control cells go silent during rest epochs.

If the SLOs would predict the onset of a locomotion epoch, we would expect the cells to reduce their firing towards the end of a rest epoch. To study this, we aligned the ends of all epochs, split out by rest and locomotion, and determined the average fluorescence 50-60 seconds from the end (early) and in the last 10 seconds (late). In the SLOs there was a difference in activity between early and late for the rest epochs, which seems to be caused by a peak just before the end of the rest period. (S Fig 4.2A, D,  $p=0.01$ , paired t-test with Bonferroni-Holm correction). Again, we did not have enough data to study the locomotion epochs.

The ORLAs showed an increase in activity late compared to early in the rest epochs (S Fig 4.2B, D,  $p=0.0004$ , paired t-test with Bonferroni-Holm correction), but no difference in the locomotion epochs (S Fig 4.2E,  $p=0.76$ , paired t-test with Bonferroni-Holm correction). Similarly, the control cells showed an increase in activity late compared to early in the rest epochs (S Fig 4.2C, D,  $p=4.4e-8$ , , paired t-test with Bonferroni-Holm correction), which seemed to be caused by a sharp increase in activity in the last few seconds, the mirror image of the trend seen at the start of the epochs (Fig 4.3G). We again see no difference in the activity early compared to late in the locomotion epochs in the control cells (S Fig 4.2E  $p=0.76$ , paired t-test with Bonferroni-Holm correction). Both the control cells and ORLA cells thus seem to increase their activity just ahead of a bout of locomotion, suggesting their ramp in activity, rather than a decrease in SLO activity, marks whether the mouse will start running.

Altogether, we do not find a change in overall fluorescence between rest and running epochs for all the cell types, but we do find a change in relative power in the low frequency band, with the SLO cells having increased power during rest, and the ORLA and control cells during running. The SLO fluorescence ramps during rest epochs, while the control cell activity

decreases, and at the end of rest epochs both the control and ORLA cell activity increases again to mark the start of a new locomotion bout.

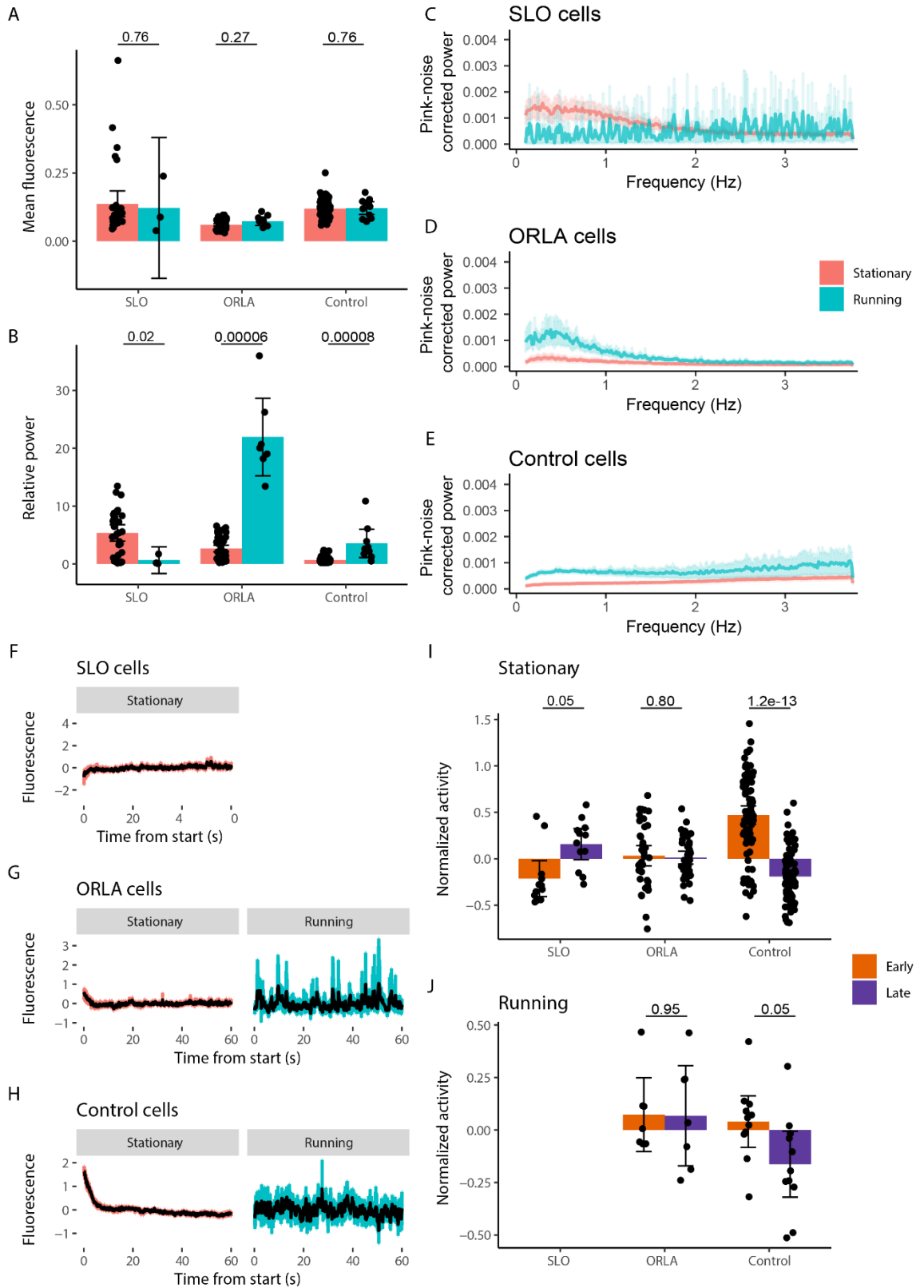


**Fig 4.3 Modulation of novel functional cell types by locomotion.** (A) Mean fluorescence during rest and locomotion epochs for the different functional cell types. (B) Relative power (in 0.2-0.5 Hz band compared to 2-3.5 Hz band) in rest and running epochs for the different functional cell types. Pink noise-corrected power spectra of the (C) SLOs, (D)

ORLAs and (E) control cells during rest (pink) and locomotion (blue) epochs. Mean fluorescence over time for the first minute of rest (pink) and locomotion (blue) epochs for (F) SLOs, (G) ORLAs and (H) control cells. Mean fluorescence during the first 10 seconds (pink) and 50-60 seconds in the epochs (blue) during rest (I) and locomotion (J) for the functional cell types. Bars are the means of 84 datasets, black dots are values for each individual dataset and error bars represent the 95% confidence interval. The black power spectra (C-E) and fluorescence traces (F-H) show the mean, coloured traces show the 95% confidence interval. P-values in A and B are from unpaired two-samples Wilcoxon tests with Holm-Bonferroni correction for multiple comparisons. P-values in I and J are from multiple paired t-tests with Bonferroni-Holm correction.

#### 4.2.4 Periodic and aperiodic components differ depending on cell type and locomotion

So far, we have looked at power spectrum of the cells in terms of relative band power.

However, this measure combines both periodic and aperiodic components of the power spectrum [219]. To split out these components and further characterize the oscillatory nature of both novel cell types, we employed the FOOOF (fitting oscillations & one over f) tool [220]. This tool allows for the fitting of both aperiodic (1/f-like) and periodic parameters to the power spectra. So, we determined the average power spectrum across rest or locomotion events of at least 60s per cell, and fitted the periodic and aperiodic parameters for each power spectrum (example spectrum in Fig 4.4A).

The tool showed a high fit across cell types during rest (Fig 4.4B, mean  $R^2$  SLOs: 0.93, ORLAs: 0.85, control: 0.78). The fit was reduced during running for both the SLOs and the control cells (mean  $R^2$  SLOs: 0.34, control: 0.68), but not the ORLAs (mean  $R^2$ : 0.87). In the case of SLOs, this may be explained by a paucity of data, as few SLOs were identified in sessions that also had sufficiently long running events. In addition, running may induce an increase in movement artefacts in the data, introducing noise which makes it harder to accurately fit the power spectrum.

First, we determined the parameters of the periodic components in the fits. In line with previous findings, we found that most SLOs showed a peak in the frequency band of interest (0.2-0.5 Hz) during rest, but not running (Fig 4.4C,F,I). Both ORLAs and control cells showed an increase in peaks in this band during rest compared to running as well (Fig 4.4D,E,G-I). Overall, in all three groups of cells (SLO, ORLA and control cells) at least a subset of cells show a peak during rest (Fig 4.4C-E) in the 0.2-0.5 Hz frequency band, suggesting this may be a property shared across a variety of cells, or possibly an indication that the method used to classify SLO cells did not sufficiently include cells with an oscillatory peak in this band. Conversely, none of the groups show an increase in peaks in this band during the running condition. This lack of peaks in the running condition may be partially explained by a paucity of data in the case of the SLOs and the increase in motion artefacts, as well as increased overall activity of the cells, during running.

The exponent of the fit, which represents the steepness of the power spectrum, was also greatly affected by rest and running across the cell types. While the SLOs have a higher exponent during rest, both the ORLAs and the control cells have a higher exponent during running (Fig 4.4J,  $p=0.007$ ,  $p=2.4e-6$ ,  $p=2.4e-6$  respectively, unpaired two-samples Wilcoxon tests with Holm-Bonferroni correction for multiple comparisons). We also fitted a 'knee' parameter, which indicates that there is not a fully linear fit in log-log space of the aperiodic component, but rather a bend in the linear relationship. Again, we see a difference between rest and locomotion for the SLO cells, with the knee significantly lower during locomotion (Fig 4.4K,  $p=0.018$ , unpaired two-samples Wilcoxon tests with Holm-Bonferroni correction for multiple comparisons). While the ORLA cells show no difference between rest and locomotion, the control cells have the opposite trend to the SLO cells, with the knee increasing during running (Fig 4.4K,  $p=5.2e-4$ , unpaired two-samples Wilcoxon tests with Holm-Bonferroni correction for multiple comparisons) .

These analyses show us that in the case of the SLOs, we see both a difference in aperiodic and periodic components compared to the ORLAs and control cells. During rest the SLOs have a higher exponent, which indicates a steeper  $1/f$  curve, thus a relatively higher power at lower frequencies. However, on top of that, many SLOs also have a periodic component in the low frequencies as well. In contrast, the ORLAs are mainly characterized by a high aperiodic component, especially during running, while there is less of a periodic component (as indicated by the lower number of peaks, Fig 4.4I).

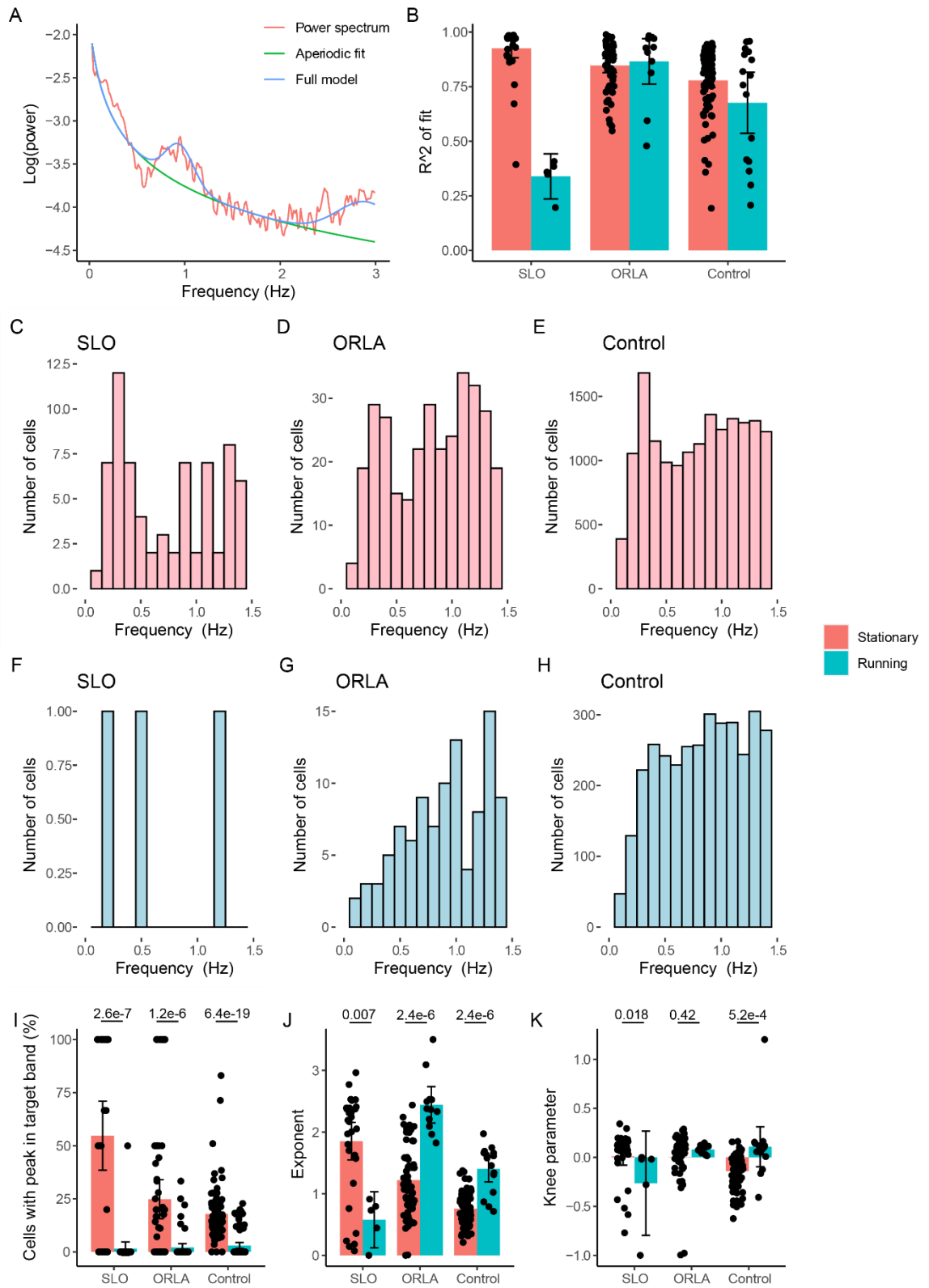


**Fig 4.4 Analysis of the power spectra with FOOOF.** (A) Example fit of a power spectrum (pink, uncorrected, log scale) showing the aperiodic (green) and full (blue) model. (B) Mean fit measured by the R squared between the fit and the original power spectrum per cell type. (C-H) Histogram showing the number of the peaks at each frequency for each cell type during stationary (C-E) and running (F-H) periods. (I) the percentage of cells with a peak within the

0.2-0.5Hz frequency band. (J) The exponent of the aperiodic fit. (K) The knee parameter of the aperiodic fit. Bars are the means of 84 datasets, black dots are values for each individual dataset and error bars represent the 95% confidence interval. P-values in I-K are from unpaired two-samples Wilcoxon tests with Holm-Bonferroni correction for multiple comparisons.

#### 4.2.5 Synchrony of functional cell types

The SLOs were initially identified by eye as highly synchronous (supplementary video: [10.6084/m9.figshare.14452878](https://doi.org/10.6084/m9.figshare.14452878)), so we wanted to quantify their synchronicity for further analysis. As their activity is relatively sparse, and we are interested in the co-occurrence of activity peaks, we based our measure of synchrony on these activity peaks. To identify them, we first took the mean fluorescence of all SLOs within a session (Fig 4.5A, pink trace), which we band-pass filtered at our previously identified frequency band (0.2-0.5Hz, Fig 4.5A, blue trace). Any local maxima were identified as activity peaks (Fig 4.5A, black dots). We only included datasets with at least 2 SLOs in this analysis (n = 12 datasets, 34 cells).

To find the synchrony, we determined the mean activity from 1.5 seconds before until 1.5 seconds after each identified peak for each cell (see examples for the different functional cell types in Fig 4.5B-D). For each cell we determined the offset, i.e. the relative time from the peak at which it has its local maximum. An offset of 0 meant that the cell fired in synchrony with the average signal. We also determined the mean absolute offset, using the absolute value to determine the time from the peak, where a higher value meant that a particular cell was more offset.

Overall the SLOs fired highly synchronously, with most cells having a low offset, all within 150 ms, from the mean signal (Fig 4.5E). They were significantly more synchronous than the ORLA and control cells (Fig 4.5H,  $p < 0.0001$  and  $p < 0.0001$ , Tukey's multiple comparison test after performing a linear mixed model with cell type as fixed-effect and imaging session as random-effect), even though there are some synchronous cells in both these cell types (Fig

4.5E,F). The SLO cells also have a small standard deviation of offset, meaning within individual datasets most cells fire close to the peak of the mean signal (Fig 4.5I). Again, this was significantly higher than the ORLA and control cells (Fig 4.5I,  $p < 0.0001$  and  $p < 0.0001$  Tukey's multiple comparison test after performing a linear mixed model with cell type as fixed-effect and imaging session as random-effect). This shows the SLO cells are much more synchronous than either of the other cell types.

As we see big differences in the power spectra of all functional cell types between rest and locomotion epochs, we separated out the synchrony during rest and locomotion (S Fig 4.3). During rest, there is again a high synchrony in SLOs across datasets (S Fig 4.3A,D,E), while the ORLAs and control cells have a proportion of cells that are synchronous (S Fig 4.3B,C). Again, the SLO cells have a lower offset and lower standard deviation of the offset than both ORLA and control cells, indicating they are significantly more synchronous than these other populations (S Fig 4.3D,E). Although the SLOs show a higher mean offset (S Fig 4.3F, I) and a higher variation within datasets (S Fig 4.3J), both their offset and standard deviation is still significantly lower than the control cells. This suggests that even though the SLO cells seem less synchronous during running, some of the synchrony in the SLO cells remains compared to the controls.

As comparing the synchrony only to the mean trace of the SLO cells may bias the result towards the SLOs being more synchronous, we repeated the analysis, but using the mean trace of the ORLA (S Fig 4.4A-E) or the control (S Fig 4.4F-J) cells instead. Relative to the mean trace of the ORLA cells, the SLO cells are significantly less synchronous than the ORLA cells, but significantly more so than the control cells (S Fig 4.4D). However, the SLO cells do show a lower standard deviation in the offset compared to both the ORLA and control cells (S Fig 4.4E), suggesting that when their peaks do not align with the mean ORLA trace, they do align with other SLO cells within the dataset. Relative to the mean trace of the control cells, none of the

cell types are particularly synchronous (S Fig 4.4I), but, again, the SLO cells do show a lower standard deviation in the offset compared to both the ORLA and control cells (S Fig 4.4J). Overall, this suggests that the ORLA cells may be more synchronous than the previous analysis suggested, while confirming that the SLO cells are highly synchronous.

These findings fit in with our analyses of the power spectra, which showed that while SLOs have a clear periodic components, ORLAs and control cells do not. As ORLAs lack this periodic component, it is very unlikely they would fire synchronously. Meanwhile, the SLOs do have a periodic component, and this analysis show that these are highly synchronous. However, this synchrony mainly exists during rest, and decrease during running. Again, this may be due to a paucity in data, or increased motion artefacts during running.

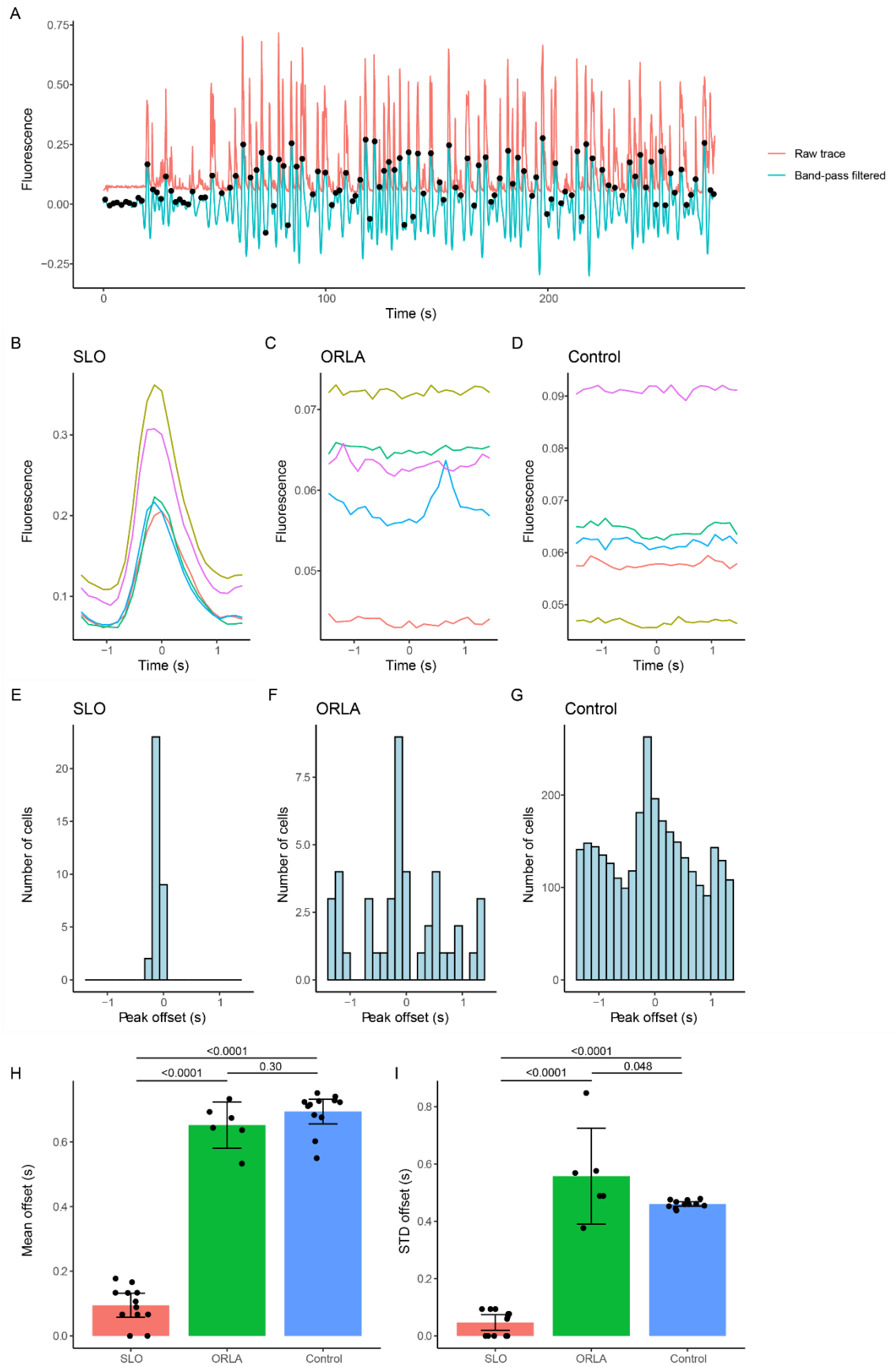


*Fig 4.5 Synchrony of activity in novel functional cell types. (A) Example of identification of the peaks, which are local maxima (black dots) in the band passed trace (blue), which is obtained by applying a 0.2-0.5 Hz band-pass filter to the mean activity across all SLOs (pink). Examples of mean traces of (B) SLOs, (C) ORLAs and (D) control cells around local maxima. Each coloured line indicates a single example SLO (B), ORLA (C) or control (D) cell. Offset of all (E) SLOs, (F) ORLAs, and (G) control cells across all datasets. (H) Mean offset and (I) standard deviation of the offset per dataset of the difference functional cell types. Bars are the means off datasets, black dots are values for each individual dataset and error bars represent the 95% confidence interval. P-values for H and I are from Tukey's multiple comparison test after performing a linear mixed model with cell type as fixed-effect and imaging session as random-effect.*

#### 4.2.6 SLO cells decreased location encoding during locomotion

Although the majority of location-encoding cells are active during running, previous studies have found cells that were preferably active during rest and still encoded for location [71,116]. Therefore, we were interested whether the SLO cells also were preferentially active in a certain location. To study this, we first determined the average activity of each cell during each rest event. We then divided our track into 15 20-cm bins, and assigned a bin to each rest event based on the location it took place. Then we could find the average activity for each cell per bin. We used the number of standard deviations the fluorescence of the highest bin deviated from the mean fluorescence across all bins as a measure of location preference (Fig 4.6A). There was a significant difference in location preference between the three cell types (Fig 4.6B,  $p=0.035$ , linear mixed model with cell type as fixed-effect and imaging session as random-effect). Particularly, the SLO cells had an increased location preference compared to the control cells ( $p=0.028$ , Tukey's multiple comparison test), but not compared to the ORLA cells, nor did the ORLA cells differ from the control cells.

We determined whether the cells showed location-specific activity during locomotion by identifying the overlap between cells identified as place cells, as identified using the Peak method (Chapter 2, [198]), and our three cell types. There was a significant difference in the number of place cell identified in each of the cell types (Fig 4.6C,  $p=0.004$ , linear mixed model

with cell type as fixed-effect and imagining session as random-effect). None of the SLO cells were identified as place cells during running periods, which was significantly less than the place cells detected in the other cell types (Fig 4.6C,  $p=0.004$ , Tukey's multiple comparison test). As place cells are assigned in an all-or-nothing fashion (either a cell passes the threshold to be classified as a place cell or not), the lack of overlap between place cells and SLOs might be caused by the low number of cells, and/or cells falling just short of the threshold. In order to determine this, we looked at the 'peakiness', a measure of the probability that a cell is a place cell (Chapter 2, [198]). The three cell types differed significantly in their peakiness (Fig 4.6D,  $p<2.2e-16$ , linear mixed model with cell type as fixed-effect and imagining session as random-effect), with the SLO cells having a significantly lower peakiness than both the ORLA cells and the control cells (both  $p<0.001$ , Tukey's multiple comparison test).

Overall, although SLO cells had a significantly higher location preference score during rest than the control cells, they did not differ from the ORLA cells, and indeed did not show a very convincing location preference on manual inspection (Fig 4.6A). Therefore, although they could have similar location preference to the cells described in Jarosiewicz et al. [71], further studies, potentially simulating the home cage nest setup, are needed to show this conclusively. In addition, the SLO cells do not fire in location-specific fashion during locomotion, as shown by the lack of overlap between the SLO cells and place cells. However, we also find a low number of place cells across cell types compared to previous studies (Chapter 2, [35,198]), indicating an overall decreased location encoding in our datasets, which may also affect these results.

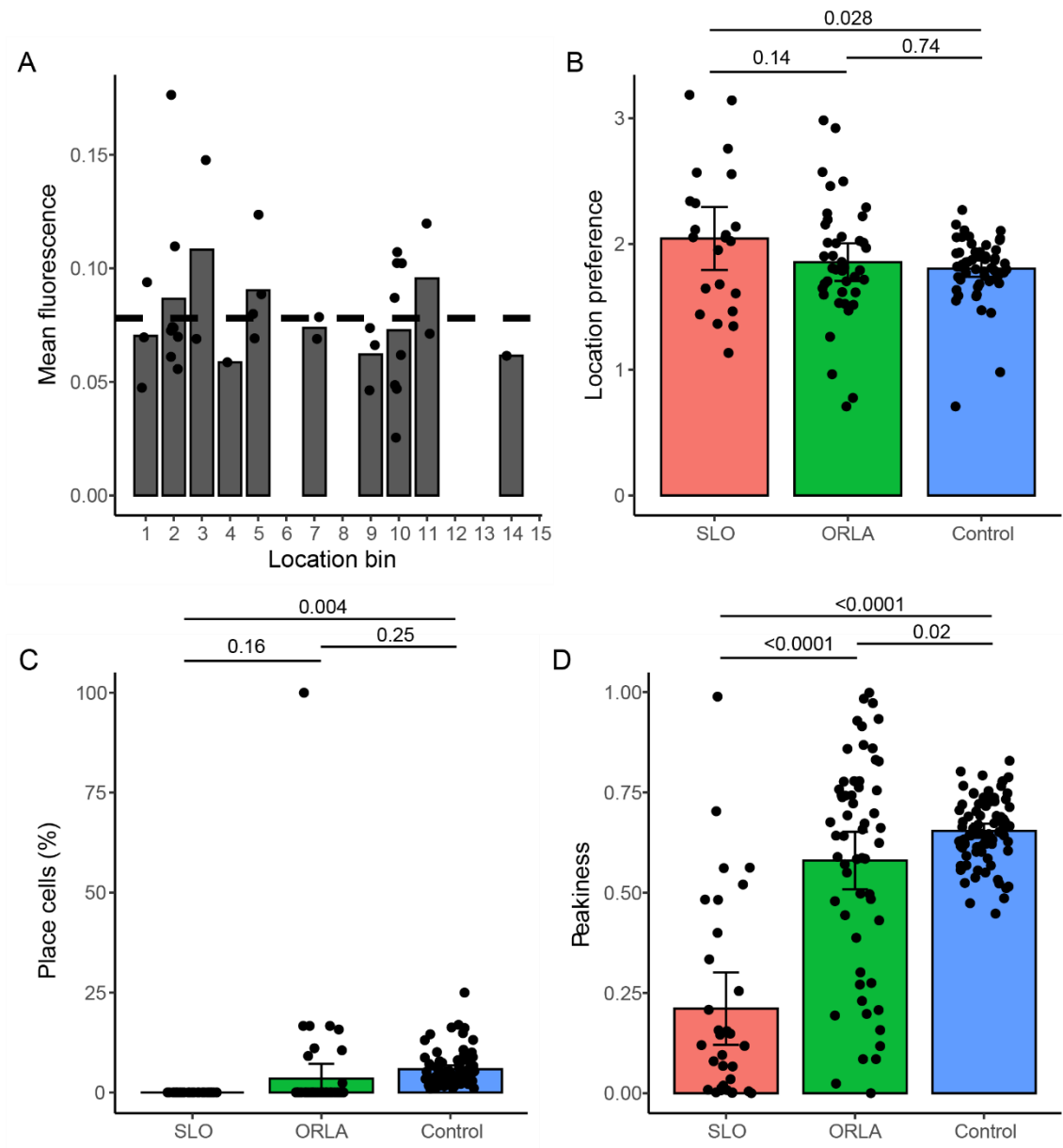


**Fig 4.6. Location encoding in the different cell types.** (A) Example fluorescence during rest per location bin for one cell, with the mean across all the bins marked by the dashed line. (B) Mean location preference during rest as measured in standard deviations from the mean. (C) Percentage of cells of each cell type classified as place cells. (D) The average peakiness (measure of the likelihood a place is a place cell) for each place cell. Bars are the means of 84 datasets, black dots are values for each individual dataset and error bars represent the 95% confidence interval. P-values from Tukey's multiple comparison test after performing a linear mixed model with cell type as fixed-effect and imagining session as random-effect.

#### 4.2.7 Visual cortex also contains excitatory cells with SLO characteristics

As hippocampal and neocortical activity during rest states can be coordinated [221], we next applied the selection criteria we defined to find whether SLO and ORLA cells also existed in the visual cortex. We both looked at pyramidal cells (PYR), using the Thy-1 GCaMP6f mouse line, and somatostatin expressing (SST) interneurons, using Cre-Lox expression of GCaMP6f.

A small percentage of cells were identified as SLO cells (0.27% and 0.09% for PYR and SST respectively), with significantly more pyramidal cells than SSTs (Fig 4.7B,  $p=0.002$ , unpaired two-samples Wilcoxon test, Holm-Bonferroni corrected for multiple comparisons). The percentage in the pyramidal population is similar to the percentage we identified in our hippocampal data (0.24%). We also found a small population of ORLA cells in both the pyramidal and SST cells (2.30% and 2.43% for PYR and SST respectively), though for these cells we saw no significant difference in the number of cells identified between the two groups ( $p=0.065$ , Unpaired Two-Samples Wilcoxon Test, Holm-Bonferroni corrected for multiple comparisons). Again, this percentage is comparable to, though slightly higher than, the results from the hippocampus (1.65%).

The power spectra for the three cell types in the pyramidal data looked similar to what we previously found in the hippocampus (Fig 4.7C-E), but the SSTs showed an increased power in higher frequencies across all populations ( $>2\text{Hz}$ , Fig 4.7C-E). In addition, a small peak could be seen in the control cells, in addition to the SLO and ORLA populations, for the SST data. The FOOOF analysis shows a similar trend to the hippocampal results, with increased aperiodic exponents for SLO and ORLA cells (Fig 4.7F). The SSTs showed a decreased exponent across cell types, which fits with the less flat shape of the power spectra (i.e. higher power in higher frequencies). We also saw a relatively high number of peaks in the target band, for both SLO and ORLA cells, across the pyramidal and SST datasets (Fig 4.7G). Interestingly, the percentage of peaks in the target band for SSTs did not reflect the visible peak in the power spectrum. This

may be due to a small number of cells having a large peak. In addition, we did not split this data out by locomotion and rest epochs, as we had insufficient data for this, which is likely to affect these results.

Next, we determined the synchrony of the different cell types in the pyramidal and SST datasets, using the same measure as used in the hippocampus (Fig 4.5). Again, our results matched the finding from hippocampus, with a low mean offset, meaning a high synchrony, for the SLO cells, both in PYR and SST data (Fig 4.7H-I). In contrast, both the ORLA and control cells showed no synchrony in both PYR and SST data (Fig 4.7H-I).

In summary, we find similar SLO and ORLA cell types in visual cortex, mainly in pyramidal cells, but also to a smaller extent in SST interneurons. This may point towards a propagation of the signal from the hippocampus to the visual cortex, or possibly the presence of a global signal that drives the cells in both these brain areas.

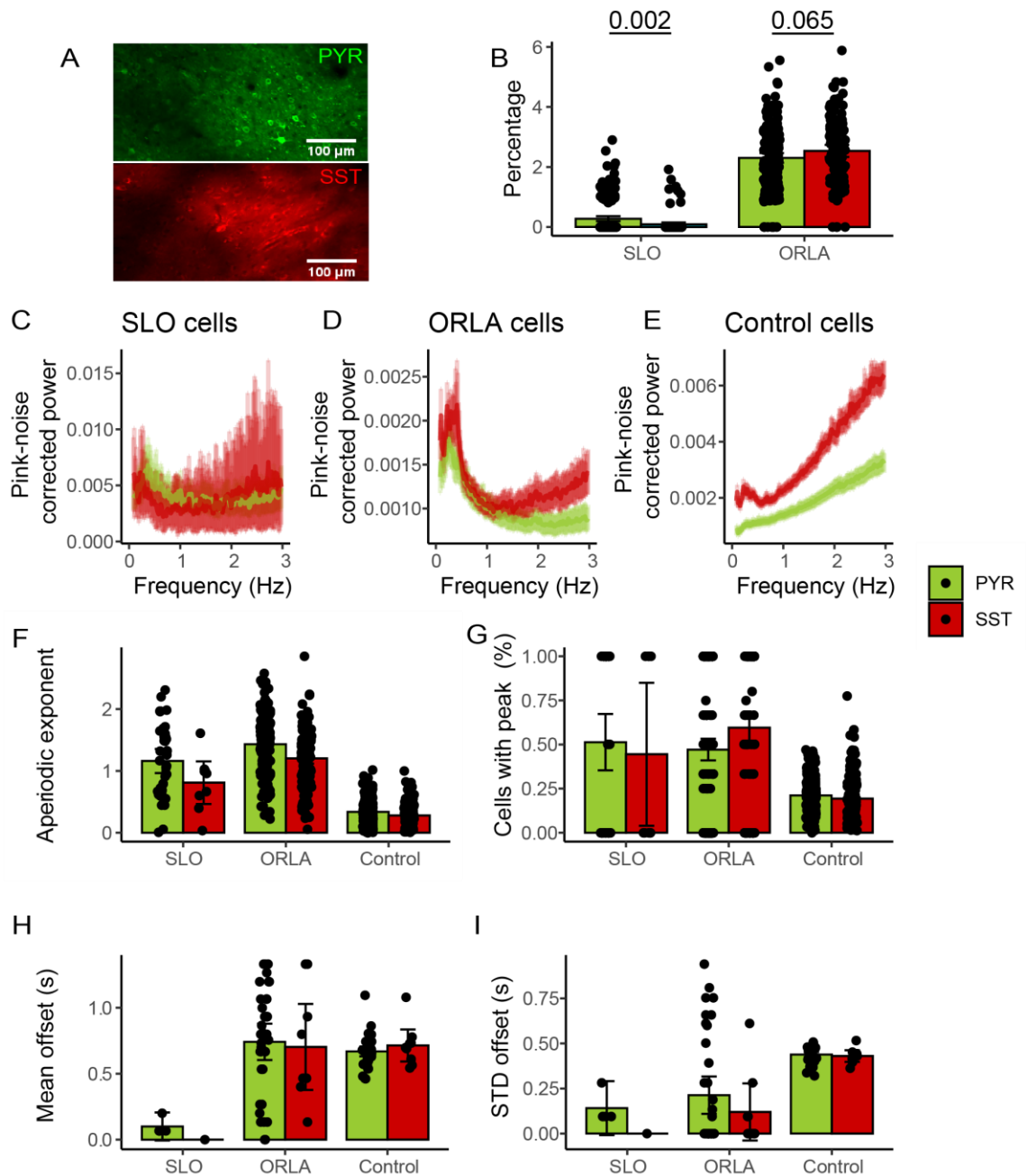


*Fig 4.7: SLO and ORLA pyramidal cells and SST interneurons in the visual cortex. (A) Example recording (mean over all frames) of pyramidal cells (top, green) and SST interneurons (bottom, red) in the visual cortex. (B) Percentage of ROIs identified as SLO and ORLA cells. (C-E) Mean power spectra for pyramidal cells and SST interneurons across the different cell types. (F) Aperiodic exponent of the fits of the power spectra using the FOOOF tool. (G) Percentage of cells with a peak in the 0.2-0.5 Hz power band. (H) Mean and (I) standard deviation of the offset from the average peak in the 0.2-0.5 Hz band-passed trace, a measure of synchrony. Bars are the means of 183 (PYR) and 127 (SST) datasets, black dots are values for each individual dataset and error bars represent the 95% confidence interval.*

### 4.3 Discussion

We identified a small percentage of CA1 pyramidal neurons, which we called SLO cells, that were preferably active during rest, showed high power in a low (0.2-0.5Hz) frequency band, and were highly synchronous. In addition, we identified a larger population of CA1 pyramidal neurons, which we called ORLA cells, that also had a high power in a low frequency band, though largely due to aperiodic activity, were mainly active during locomotion periods, and did not show synchronous activity. The SLO cells had location-encoding properties during periods of immobility, but not during locomotion, whereas the ORLA cells did not encode location during either behaviour. Lastly, we found similar populations in the visual cortex in pyramidal cells and somatostatin-positive interneurons, though the SST data contained markedly less SLO-like cells.

We used two characteristics that were identified by eye – the increased activity during rest and the periodicity – to characterize the SLO cells. The periodicity was estimated using the autocorrelogram, and although this measure gives an approximation of periodicity, the local peaks will be confounded by noise within the fluorescence traces. Indeed, the method relies upon the control cells having noise that causes an increase in local peaks. Therefore, it is only an approximation of periodicity. The periodicity in the identified cells is confirmed by the peaks present in the power spectrum, the other groups also contained cells with peaks in the 0.2-0.5 Hz band, and not all SLO cells had similar peaks. Therefore, characterising these cells by the power spectrum, and confirming this characterization using the autocorrelograms, may be preferred over the current method, and it likely alters the cells classified as SLO cells.

Our SLO cells are possibly similar to CA1 cells that have previously been found to be active during SWS in the absence of SWR during a brain state called SIA [71]. Kay et al. [118] propose a “still” brain state as a brain state between a locomotor and a SWR brain state, equivalent to this still SIA state. They hypothesize that during this state animals hold a continuous spatial

code of the environment. Indeed, our results suggest that the SLOs show location-specific firing, and their activity is continuous, and even ramps, during rest events. This means that these cells might be a population, separate from the place cells, that continuously holds an internal representation of the current location during periods of rest. It has been suggested that such cells are needed to encode the location of events that do not rely on locomotion or navigation, such as the location of a certain stimulus [116].

However, this does not explain why such a small number of CA1 cells is involved. However, the number of cells we recorded showing this behaviour may be low for several reasons. Firstly, the ROI identification uses an activity-based measure of including cells [172]. Manual curation revealed that several SLOs that we could clearly identify by eye, were excluded using this measure. Although we included all ROIs as cells to combat this, it is likely that some potential SLOs were not identified as ROIs to begin with. Secondly, although it is theoretically possible to resolve individual spikes from calcium recordings [222], we are likely not able to resolve the activity to this detail, so even if some cells were showing a similar pattern of electrical activity to our identified SLOs with subthreshold activity, single spikes or spike trains, we would not have been able to identify them [163,223].

Overall, the function of the SLO cells and the ORLA cells is still unclear. It is possible the SLO cells are involved in holding a representation of the location an animal is resting in, so that if an event happens, they play a role in linking the memory of the event to that particular location. This would fit in with the notion of them being related to an intermediary level of attention. However, it is unclear how this would interact with the place cells, which already encode for location during running. In order to find out whether these cells are indeed necessary for location encoding during rest, future studies should aim to eliminate their activity and determine whether this impairs an animal's navigation or contextual memory retrieval abilities.

#### 4.3.1 Potential upstream sites innervating SLO cells

Given the small population size — <1 % of all ROIs were classified as SLOs in our data — CA1 might not be the principal site of such activity. Indeed, a previous study [116] found a much larger percentage of cells in CA2, which they termed N-units, that have similar activity to our SLOs during immobility. It is possible that the large CA2 population causes the activity in our small population of CA1 neurons, as it has been shown that CA2 connects onto CA1 neurons [224–226]. In particular, CA2 connects to the deep layer of CA1 [224], possibly indicating the SLO cells are particularly located in this layer in CA1. However, we find that the SLO cells are also modulated by a slow oscillation, which was not reported for CA2 [116]. Although it is feasible that the previous report did not find these oscillations, because they high-pass filtered their recordings at 0.5 Hz, meaning they would not detect similar oscillations. Alternatively, the SLO cells may be modulated by oscillatory activity from a different brain area, or indeed emerge from the CA1 itself. Spontaneous slow oscillations have been shown to arise in hippocampal slices through GABAergic interneurons [227]. However, the presence of similar oscillatory activity in V1 suggests that there might be a more global modulation at play.

A more global slow oscillation has previously been described in neocortical areas, including the visual cortex, in cats [208], again involving local inhibition. This oscillation was identified both under anaesthesia and during natural sleep, and was thought to be separate from SWS.

Indeed, we see a bump in power at low frequencies in the SST interneurons, even in the control population, which might point towards their involvement in driving slow oscillations.

Giving the widespread nature of this oscillation — it was present across motor, sensory and associational cortical areas — it is not unlikely such an oscillation also presents itself in the hippocampus.

#### 4.3.2 A role for the ORLA cells

In addition to the SLO cells, we identified a population of ORLA cells, which were active primarily during running periods and showed a relative high power at low (0.2-0.5 Hz) frequencies, which was mainly caused by aperiodic activity. They did show overlap with the traditional place cell population, though the variability between datasets was quite high. This was not entirely surprising, as the ORLA cells were identified as those with the highest relative power of the control cells, and may thus be a subpopulation of these cells rather than a distinct population. The ORLA cells thus may have place cell-like activity in some cases.

The presence of the aperiodic activity in the low frequencies in the ORLA cells is reminiscent of the N-waves identified in CA2 [116]. The waves have been observed to modulate firing outside CA2 as well, including in CA1. However, as they were only observed during periods of rest, while the ORLA cells have a high aperiodic component during rest and especially running epochs. It is therefore not clear whether a similar network pattern could be responsible for the ORLA activity. It might be possible that the N-waves persist throughout the different states, but are perhaps not as readily observed in the LFP signal, as they are overpowered by the theta oscillations present during locomotion.

Alternatively, the high aperiodic exponent of the ORLA cells may be indicative of a phenomenon separate from the N-waves and other characteristic activity at rest, such as the SLO cells. Although the aperiodic component of neural data is often deemed background noise, recent studies have stressed its importance for neural processes [220,228]. These studies have often focussed on population level activity using measures such as LFP [229] or fMRI [230,231]. However, on the level of single neurons, the aperiodic signal can reflect the correlation of the inputs into the cell, and as such may be a readout of the connectivity of a single cell [232]. Therefore, our ORLA cells may be highly connected cells within the hippocampal formation, potentially allowing them to perform the role of hub cells [233].

In conclusion, our study shows two functional cell types which, although both characterized by a relatively high power in a low frequency band, show very different functional profiles, suggesting they may play different roles in the hippocampus. These results add to the corpus of literature suggesting heterogeneity of the pyramidal cells in the hippocampus [234]. In addition, we showed that our cell types existed both in hippocampus and visual cortex, suggesting a possible brain-wide phenomenon. Lastly, we show modulation of these cells by a low frequency oscillation across brain areas.

## 4.4 Materials and Methods

### 4.4.1 Animals

All experimental procedures were approved by the UK Home Office, in accordance with the 1986 Animal (Scientific Procedures) Act. Hippocampal experiments used twelve C57/BL6 mice (5 female, 7 male) expressing the genetically-encoded calcium indicator GCaMP6f under the control of a Thy-1 promoter (C57BL/6J-Tg(Thy1-GCaMP6f)GP5.5Dkim/J). Visual cortex experiments used 5 C57/BL6 mice (2 female, 3 male) expressing the genetically-encoded calcium indicator GCaMP6f under the control of a Thy-1 promoter (C57BL/6J-Tg(Thy1-GCaMP6f)GP5.5Dkim/J), and 6 C57/BL6 mice (4 female, 2 male), which were crosses of heterozygous SST-IRES-Cre with floxed GCaMP6f, resulting in GCaMP6f expression in the SST interneurons. The mice were housed in a 12h reverse dark/light cycle environment at a temperature of 22°C and were given ad libitum access to food and water outside of experiments. The mice used for the hippocampal experiments were acutely water-deprived for up to 4 hours prior to an experiment.

### 4.4.2 Hippocampal cranial window surgery

Surgery was performed when mice were a minimum age of eight weeks. Before surgery, mice received subcutaneous injections of dexamethasone (60 µL, 2mg/mL), saline (400 µL) and

buprenorphine (40  $\mu$ L, 0.3mg/mL diluted 1:10 in saline) to reduce inflammation, for hydration, and pain relief respectively. Mice were maintained at 0.8-2.0% isoflurane anaesthesia for the duration of the surgery. Body temperature was maintained at 37 °C using a homeothermic blanket (PhysioSuite, Kent Scientific Corporation). A craniotomy was inserted, for the hippocampal experiments above dorsal CA1, for the visual cortex experiments above visual cortex, as previously described [31,235]. Briefly, the skin above the skull was removed and the skull was scored to increase the surface area for binding dental cement. A custom-made stainless steel headplate was then fixed to the skull with black dental cement (Unifast Powder mixed with black ink (1:15 w/w) and Unifast Liquid). A 3 mm diameter craniotomy was then performed 2mm posterior to bregma and 1.5 mm lateral to the sagittal suture.

For the hippocampus experiments, after removal of the skull flap and the dura brain tissue overlying, the hippocampus was aspirated (New Askir 30, CA-MI Srl) until vertical striations of the corpus callosum were visible. We then inserted a custom 3D printed cannula (2.4 mm ID, 3 mm OD, 1.5 mm height) made of a biocompatible Dental SG resin (FormLabs) so that the glass coverslip at the bottom of the cannula lay directly on top of the brain tissue. The top of the cannula had a rim (0.2mm height, 3 mm OD) resting on top of the skull, which was attached using tissue adhesive (3M VetBond) and then covered with more dental cement.

For the visual cortex experiments, the dura was carefully removed to allow imaging of the underlying brain tissue without obstruction of dural vessels. A glass window consisting of two 3 mm diameter and one 5 mm diameter round coverslips glued together with optical adhesive was inserted into the hole, with the smaller coverslips effectively plugging it, while the larger coverslip rested on the skull. This was again attached using tissue adhesive and covered with dental cement.

For all animals, a rubber ring was then attached on top of the headplate for subsequent use as a well for the water needed for the water-immersion microscope objective. The mice were

given an injection of meloxicam (125  $\mu$ L, 5 mg/ml) as an analgesic near the end of the surgery and then received meloxicam (200  $\mu$ L, 1.5 mg/mL) for 4 days following the surgery via oral admission. Their health was monitored and they were weighed daily.

#### 4.4.3 Two-photon imaging

*Habituation.* A week or more after surgery, the mouse was habituated to the imaging rig by head-fixing it for an increasing amount of time each day for at least a week before it was imaged, resulting in at least two weeks, but usually longer, of recovery time. The animals for the hippocampal experiments were also presented with the virtual reality environment during this habituation period to make it familiar with this setup.

*Imaging rig (S Fig 4.5A).* The mice were head-fixed above a polystyrene cylinder, on which they could run. The cylinder was fitted with a rotary encoder (Kübler, 4096 pulses per revolution). Two screens in front of the mice were used to display the stimulus. In the case of the hippocampal experiments, these screens displayed a custom virtual reality (VR) environment designed using ViRMEn [150]. In the visual cortex experiments, they showed moving gratings of varying contrasts and widths, generated using PsychoPy [236].

*Stimulus presentation.* The virtual reality environment presented to the mice was a wide corridor, 200 cm long and 80 cm wide, with 30 cm high walls (S Fig 5B). Both before and after the wide corridor was a dark grey tunnel with a diameter of 30 cm, 50 cm long before the corridor and 45 cm long after the corridor) which served to allow smooth transitions between multiple presentations of the environment. Inside the environment were always two objects: a blue and black striped ball and a white and black striped block. On each traversal both the cue abundance, binarized into two levels, and the location of the ball was randomly selected. For the cue abundance this meant either a combination of grey walls, a grey floor, and no external objects (sparse condition), or patterns walls and floor and two additional objects (a cyan, black striped cone and a black, white and green blocked ball) outside of the walls (abundant

condition). In the case of the ball location this was either in a familiar location (50 cm into the environment) or on a randomized location along the corridor at least X cm from the familiar location, but always 30 cm left of the mouse.

In the visual cortex experiments, the mice were presented with moving gratings (S Fig 4.5C). These varied in frequency (0.04 or 0.2 cycles per degree), contrast (5%, 25%, 63% or 100%) and size (full screen or small 20 degree circle). When contrast was varied, only the full screen stimulus was used, and when size was varied, only the 100% contrast was used.

*Data acquisition.* In the hippocampal experiments, the stratum pyramidale of dorsal CA1 was imaged using a two-photon microscope (Scientifica) with a water-immersion objective (CFI75 LWD 16X W, Nikon; 0.80 numerical aperture, 3 mm working distance). In the visual cortex experiments, cortical area V1 we used a different water-immersion objective (XLUMPlanFL N 20X, Olympus; 1.00 numerical aperture, 2 mm working distance), as we did not need to achieve the same depth. GCaMP6f was excited using a Chameleon Vision II Ti:Sapphire laser (Coherent) at a wavelength of 940nm with a gallium arsenide phosphide photomultiplier tube. We used the ScanImage (Vidrio Technologies, MATLAB) or SciScan (Scientifica) software to control the microscope and collect data. The stratum pyramidale was identified from the presence of densely packed cell bodies. For the hippocampal experiments, we optimised the acquisition rate by using a wide field-of-view at a low resolution (128x128 pixels, 7.51 Hz, 3.77  $\mu\text{m}$  pixel size). Pyramidal cell recordings in the visual cortex were at varying acquisition rates (3.05-7.63 Hz), while the SST recordings were always at 7.63 Hz, and both were at a slightly higher resolution than the hippocampus recordings (256x128 pixels, 1.98  $\mu\text{m}$  pixel size).

#### 4.4.4 Image Analysis

*Preprocessing.* Preprocessing was conducted using Suite2P software [172]. Firstly, images were registered using the default settings, then regions of interest (ROIs) corresponding to cell bodies were identified based on their morphology (having a diameter of approximately 10  $\mu\text{m}$ )

and a tau, the decay time for the calcium indicator, of 0.8. Suite2P applies a classifier to identify cell bodies, but as we observed that obvious SLO cell candidates were omitted in this step, we decided to include all ROIs in all analyses.

We obtained the calcium signal corrected for neuropil activity, by subtracting 0.7 times the neuropil signal from the ROI signal for each ROI, from the Suite2P output. Then we normalised time courses to baseline fluorescence for each ROI by dividing the whole trace by the average intensity in that ROI during the first 100 frames of the recording.

#### 4.4.5 Frequency analysis

We found the power spectrum for each ROI by applying Welch's method ([237]) to each preprocessed trace, using the MATLAB inbuilt *pwelch* function. We used a 60 second window and 50% overlap between windows. We set the number of discrete Fourier transform points to the closest power of 2 higher than the window size, or 256, whichever was higher. With a 60 second window and an acquisition rate, this equated to 512 points.

To further analyse the power spectra, we applied the FOOOF method [220]. We used the freely available Python code to extract the aperiodic and periodic components for each ROI, and imported these into MATLAB for further processing using custom scripts.

#### 4.4.6 Cell type identification

*SLO cells.* SLO cells were identified using a combination of two parameters: the rest/running fluorescence ratio and the number of peaks in the autocorrelogram. For the rest/running fluorescence ratio we divided the frames into rest and running. Rest included any frames where the velocity of the mouse was less than 10% of the maximum velocity. We next determined any rest events that included continuous rest for at least 60 seconds. For each ROI we averaged the fluorescence during these rest events by the fluorescence outside of these events, and obtained the rest/running fluorescence by dividing the resulting values. We

calculated the autocorrelogram by performing a cross-correlation on the fluorescence trace of each ROI to obtain the Pearson's correlation for each offset of the trace compared to itself (custom MATLAB code, courtesy of Caswell Barry). We cropped the result to only include 30 seconds around the centre, resulting in a cross-correlation across 60 seconds in total. Next, we found the number of local maxima using the *findpeaks* function in MATLAB. Once we had obtained both the rest/running fluorescence and the number of peaks for each ROI, we found the mean and standard deviation across the population for both. We only included cells as SLO cells if they both had a rest/running fluorescence at least two standard deviations above the mean, and a number of peaks at most two standard deviations below the mean.

*ORLA cells.* We identified the ORLA cells based on the relative power. We obtained the power spectrum for each as described above. From these power spectra we calculated the relative band power by taking the mean power in our band of interest (0.2-0.5 Hz), and dividing it by the mean power between 2-3.5 Hz. After obtaining the relative power, we calculated the mean and standard deviation across all ROIs across all sessions. We did this separately for the three sets of data collected with similar characteristics: the hippocampal recordings, the V1 pyramidal recordings, and the V1 SST interneuron recordings. For each of these sets we set a threshold for inclusion as ORLA cell to be three standard deviations above the mean.

*Place cells.* Place cells were identified using the Peak method as previously described [pcm ref, chapter 1 ref]. In short, we calculated the fluorescence map, the average fluorescence at each location, for each ROI and determined the maximum value in this map. We then shifted the fluorescence trace relative to the location trace to obtain a shuffled version, and calculated the maximum value of the fluorescence map of the shuffled version. We repeated this shuffling procedure 500 times and determined the percentile score of the original maximum value relative to the shuffles. This percentile score was used as the peakiness score, or the likelihood

a ROI was a place cell. If the percentile score was at least 99, we classified the cell as a place cell.

#### 4.4.7 Analyses

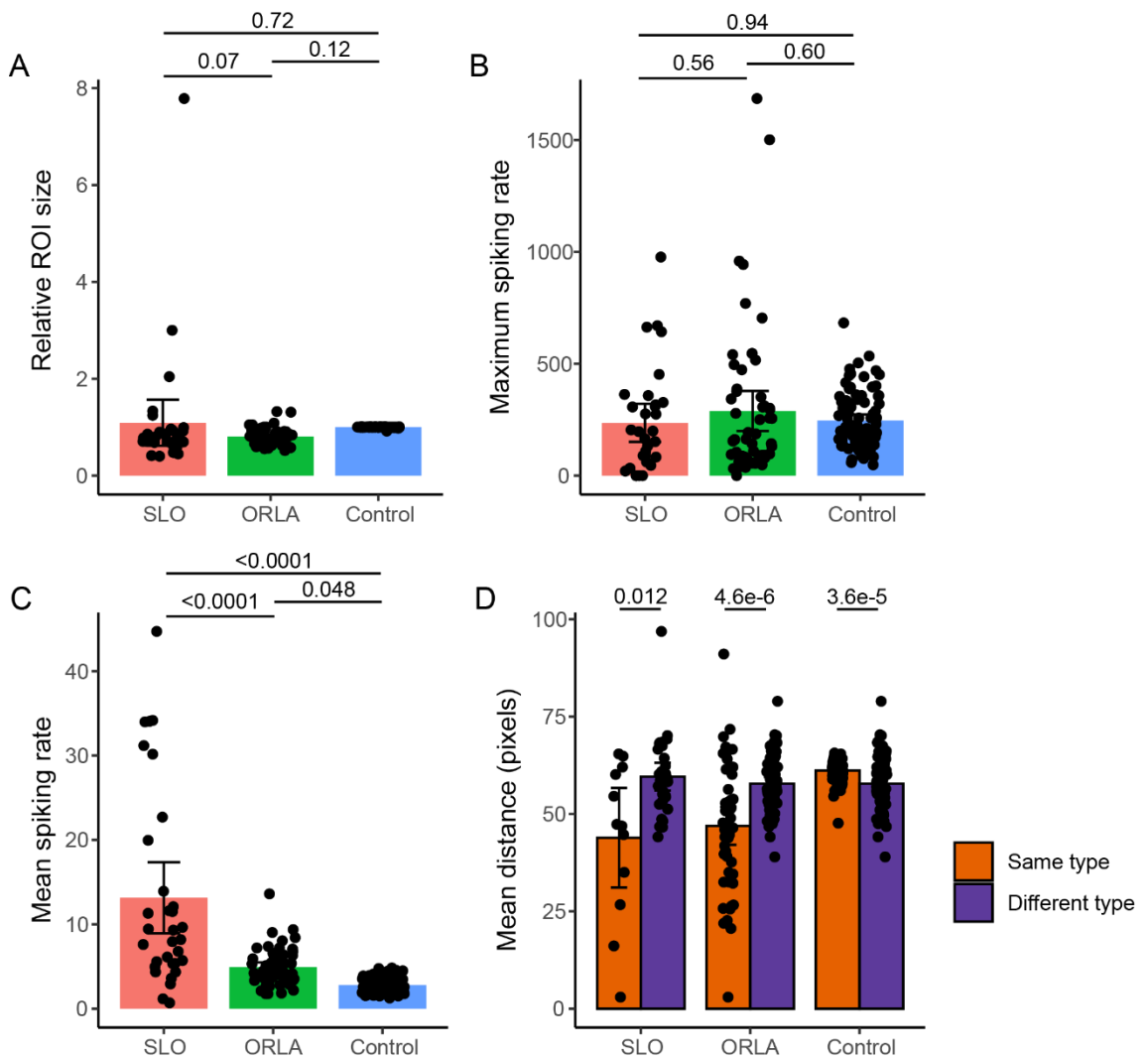
*Activity modulation.* To determine the effect of locomotion on the cell activity, we identified epochs of rest and running during a session. First, we identified frames of the recording where the mouse was not locomoting by finding frames where the velocity was smaller than 10% of the maximum velocity. Next, we found distinct rest or running epochs by identifying continuous frames of locomotion or rest. If groups of continuous frames were interrupted for less than 1 second, they were grouped as one continuous epoch. For each epoch, we then determined the length, and excluded any epochs that were shorter than 60 seconds (451 frames).

*Synchrony.* The synchrony of the different cells was identified by first taking the average of all the SLO cells in the dataset. We then band-pass filtered this trace using a 0.2-0.5 Hz filter. Next, we determined any local peaks, and determined the activity of each individual ROI in the dataset in 3 seconds around the timepoint of this peak. We averaged this activity per ROI across the peaks and determined the maximum value of this mean. The absolute time from the middle of the trace (i.e. the offset) was calculated to determine the relative timing of the ROI compared to the original peaks. We only included sessions with at least 2 SLO cells (N=12), as the synchrony of 1 cell cannot be determined (it is synchronous to itself).

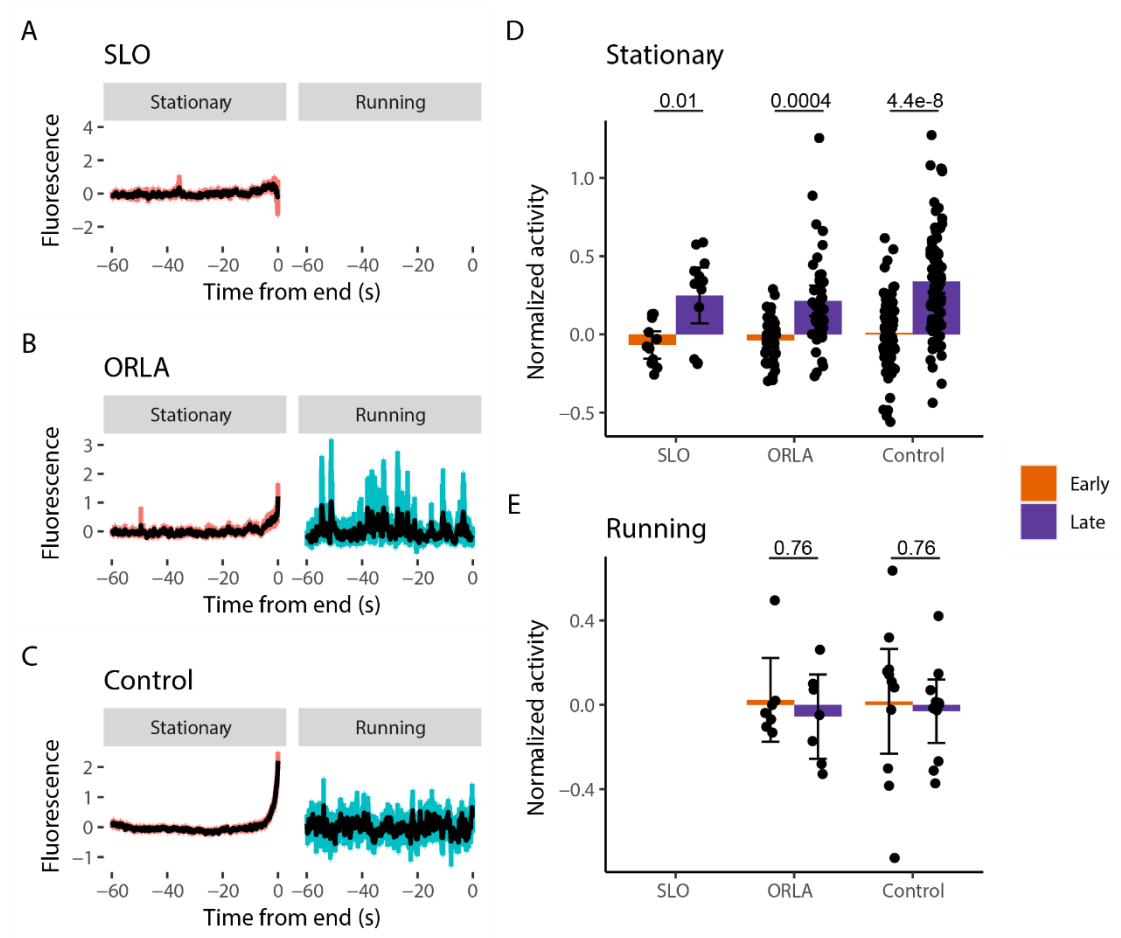
*Location encoding.* We took two approaches to analyse the location encoding properties of the cells. Firstly, we found the overlap with place cells and the related peakiness measure, as described above. Secondly, we determined the location preference for each cell during rest. As the rest periods did not take place in a wide range of locations, and the total rest per location was not evenly distributed, we decided on this alternative approach. For this, we binned our total environment (pipes and corridor) into 15 evenly spaced bins. We then determined what

bin each rest event took place in, and the mean fluorescence in that bin. The location preference was calculated by determining the mean and standard deviation of these mean fluorescence across the bins, and determining how many standard deviations the value in the bin with the highest fluorescence deviated from the mean.

## 4.5 Supporting information

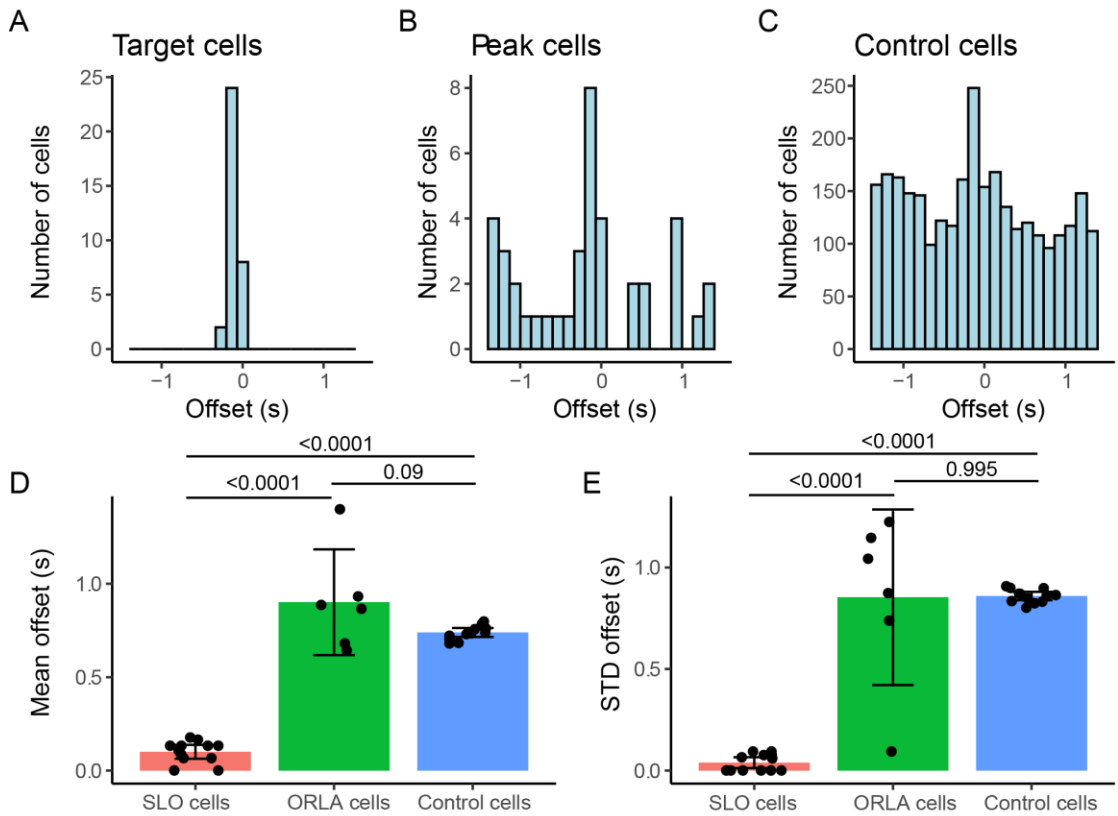


*S Fig 4.1 Cell characteristics of the different functional cell types. (A) ROI radius relative to the mean radius of the recording. (B) Maximum spiking rate as deconvolved using Suite2P. (C) Mean spiking rate across the recording. (D) Mean distance between all cells within a cell type (pink) or between cells from that cell type and other cell types (blue). Bars are the means of datasets, black dots are values for each individual dataset and error bars represent the 95% confidence interval.*

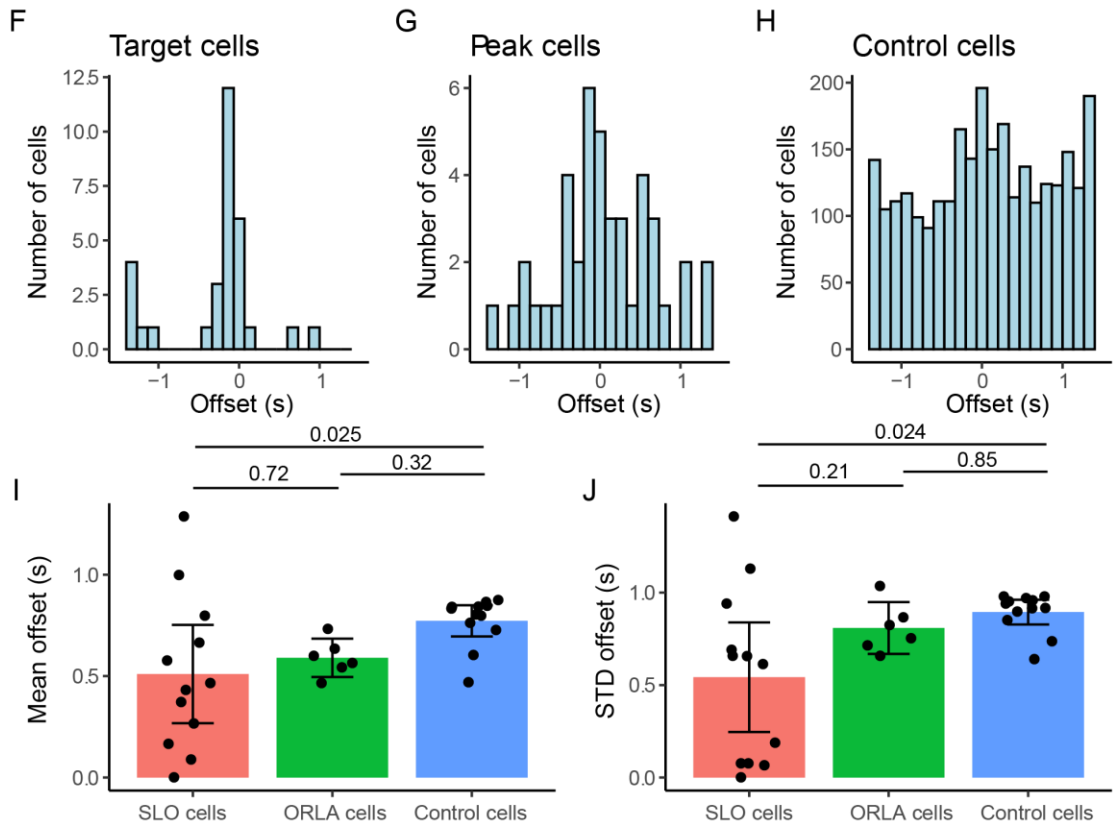


*S Fig 4.2 Activity in cell types at the end of rest and running epochs. Mean fluorescence over time for the last minute of rest (pink) and locomotion (blue) epochs for (A) SLOs, (B) ORLAs and (C) control cells. Mean fluorescence during the 50-60 seconds from the end (pink) and the last 10 seconds in the epochs (blue) during rest (D) and locomotion (E) for the functional cell types. Bars are the means of 84 datasets, black dots are values for each individual dataset and error bars represent the 95% confidence interval. The fluorescence traces (A-C) show the mean fluorescence in black, coloured traces show the 95% confidence interval. P-values for D and E are from multiple paired t-tests with Bonferroni-Holm correction.*

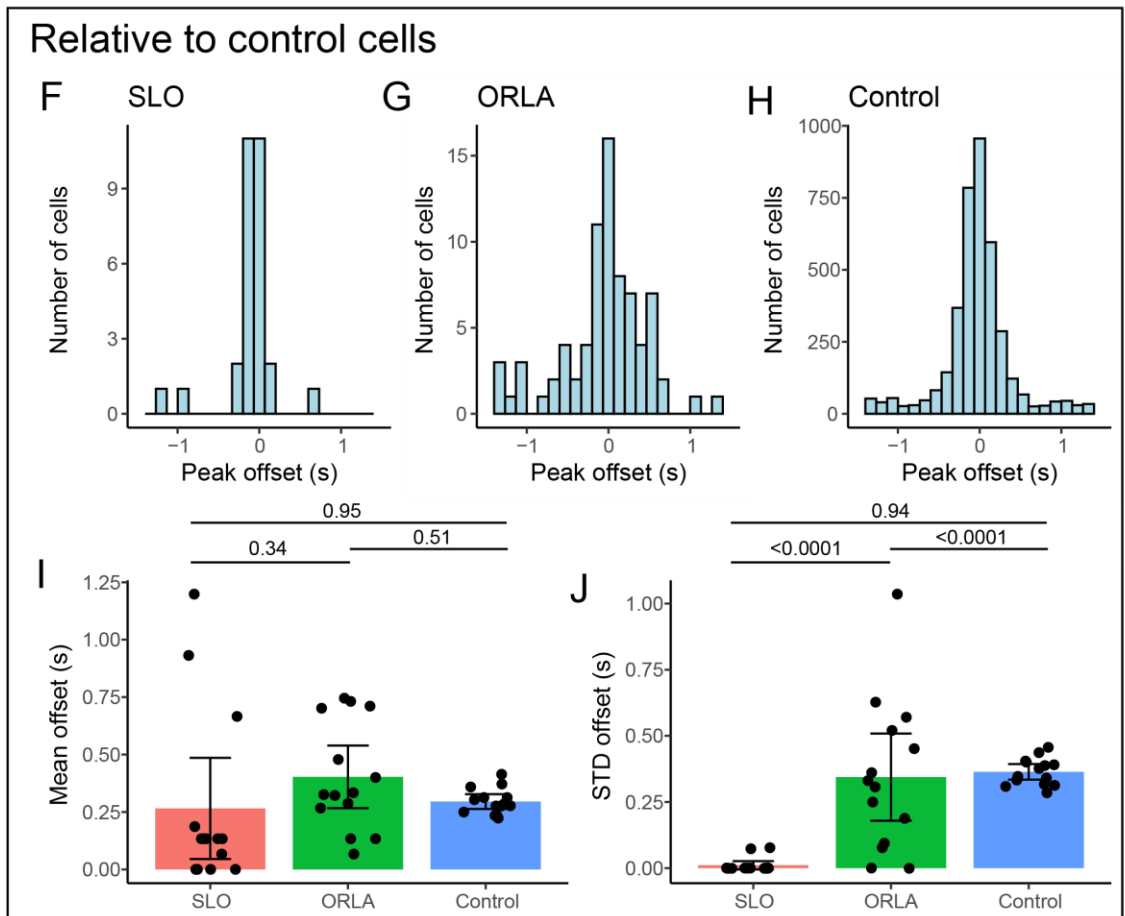
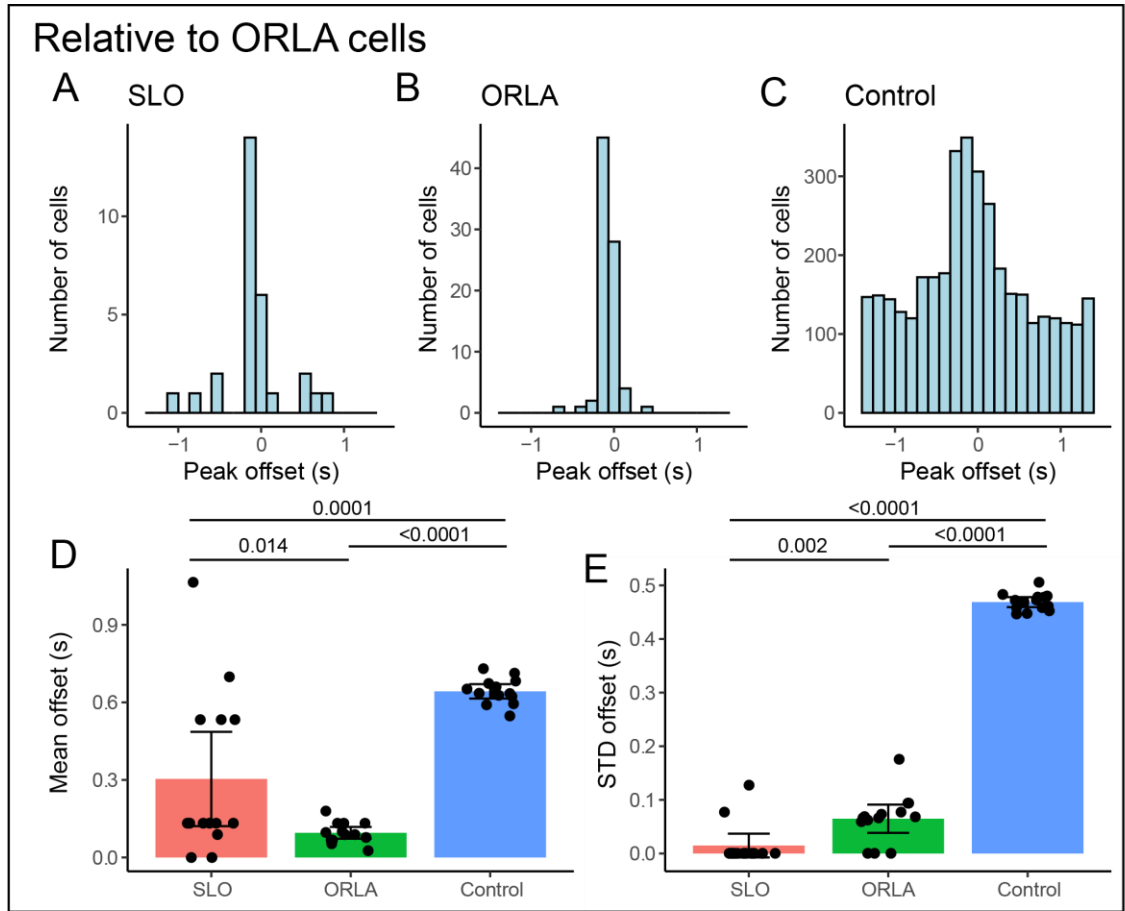
### During rest



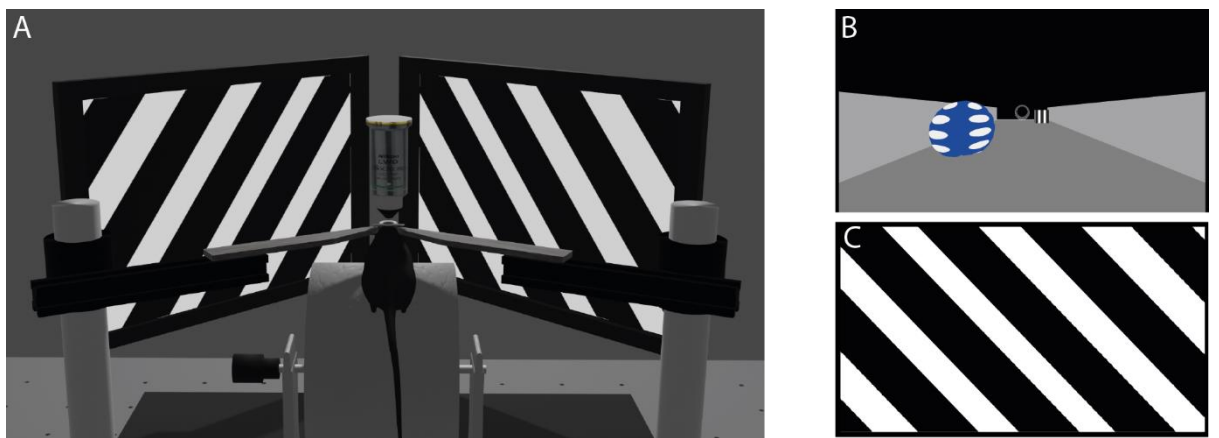
### During locomotion



*S Fig 4.3 Synchrony of activity in novel functional cell types during rest and locomotion. Offset during rest of all (A) SLOs, (B) ORLAs, and (C) control cells across all datasets. (D) Mean offset and (E) standard deviation of the offset during rest per dataset of the difference functional cell types. Offset during locomotion of all (F) SLOs, (G) ORLAs, and (H) control cells across all datasets. (I) Mean offset and (J) standard deviation of the offset during locomotion per dataset of the difference functional cell types. Bars are the means off datasets, black dots are values for each individual dataset and error bars represent the 95% confidence interval. P-values for D, E, I and J are from Tukey's multiple comparison test with Bonferroni-Holm correction.*



*S Fig 4.4 Synchrony of activity in novel functional cell types relative to ORLA and control cells. Offset of the (A) SLOs, (B) ORLAs, and (C) control cells relative to the peaks in the mean trace of all ORLA cells in the dataset. (D) Mean offset and (E) standard deviation of the offset per dataset of the difference functional cell types. Offset of the (F) SLOs, (G) ORLAs, and (H) control cells relative to the peaks in the mean trace of all control cells in the dataset. (I) Mean offset and (J) standard deviation of the offset per dataset of the difference functional cell types. Bars are the means off datasets, black dots are values for each individual dataset and error bars represent the 95% confidence interval. P-values for D, E, I and J are from Tukey's multiple comparison test after performing a linear mixed model with cell type as fixed-effect and imagining session as random-effect.*



*S Fig 4.5. Imaging setup and stimuli for two-photon experiments. (A) 3D model showing the imaging setup with the visual stimulus project on the screen. (B) Example of one of the virtual environments used in the hippocampal recordings. (C) Visual grating pattern shown on the screen during the visual experiments.*

## 5 Discussion

The aim of this thesis was to examine the effects of environmental and behavioural factors on hippocampal activity. We distinguished between several different hippocampal cell populations: place cells, object-vector cells, SLO cells and ORLA cells. We showed that these cells differentially responded depending on the environmental cues available to the animal, and whether the mouse was active or not. Overall, we showed the importance of studying diverse hippocampal populations, and how various populations each showed different activity patterns depending on the behavioural states on the mice and stimuli in the environment.

5.1 Aim 1: To determine the best method for defining place cells, and in doing so, understand how the method by which place cells are defined, affects what cells are included in the population.

In order to study place cell populations, we first needed to know how to define them, which was the first aim of this thesis. We focussed on the definition of place cells, but the same method of classification also applies to object-vector cells, and indeed any cell that may have a particular response field. The three place cell classification methods we tested, resulted in vastly different populations of cells being classified as place cells. As the Peak method, which compared the maximum activity in the fluorescence map compared to the shuffled maximum, had the highest sensitivity even when the place cells were variable and unreliable, we recommended using this method to classify place cells, and used this method in the other chapters.

These results have important implications place cell research more widely. Critically, it explains why different studies find conflicting results about place cells, as the populations they study might be independent. For example, in our study on how hippocampal place cells code different environments in Chapter 3 we did not find an overrepresentation of reward location,

unlike other studies (e.g. Gauthier et al. [51]). However, this could be explained by the fact that Gauthier et al. [51] used mutual information as a measure to classify their place and reward cells, while we used the Peak method. As the Gauthier et al. method is distinct from three methods we tested, we do not know how the place cells classified by it are characterized. We did analyse the amount of mutual information in the various place cell populations, and in the Peak method the place cells had significantly higher mutual information, suggesting there will be some overlap between the place cells as classified by the Peak method and those classified by Gauthier et al. This underscores the need for consistent place cell classifying in the field, and characterising the place cell population if a new method is used.

Although we tested the methods using an imaging dataset using mice expressing the GCaMP6f calcium indicator, we believe the results are also applicable across other genetically encoded calcium indicators. Many variations of calcium indicators are used in place cell research (for example GCaMP3 [35,51] and GCaMP6s [24]). Different types of calcium indicators have varying properties and dynamic ranges, thus responding differently to changes in spike rates [163]. Even the transgenic line in which the indicator was expressed can affect its properties [223]. If a method is to work similarly regardless of these properties, it should not depend on a set threshold for fluorescence. Rather, it should allow for a relative comparison to the dataset, as is the case in the Peak method, and indeed the Stability method, but not the Combination method. Therefore, we believe our proposed method is applicable to datasets with varying indicators, allowing for better comparison between results for studies using different calcium indicators and transgenic lines.

This study focussed specifically on calcium imaging, but it also provides the opportunity to compare between electrophysiology and calcium recordings. Although calcium indicators reflect action potentials [163], their activity is not equivalent to electrophysiological recordings

[223]. One could apply spike deconvolution, using each indicator's unique response function, to estimate the spiking rate, but the majority (up to 85% [223]) of single spikes will not be detected using GCaMP6f. As the Peak method was originally developed for electrophysiology, but successfully classifies place cells in calcium activity as well, our work provides a valuable way to link the two different methodologies, without having to rely on spike deconvolution. The Peak method can also be applied across datasets collected in 1D or 2D environments, regardless of the methodology used, and thus provides the ability to directly compare between calcium and electrophysiology datasets in a variety of environments.

As using VR for place cell studies is becoming increasingly popular, there is need for a single method to accurately compare findings between real and VR environments. Currently, different studies use vastly different methods for place cell detection in these environments (e.g. [24,35,55,147]) and thus their results cannot be compared. Using VR itself also affects place cell firing, so it is vital to be able to compare studies as well as possible, as this will allow us to accurately interpret how the findings apply to the real world and broader contexts. We believe our study provides this opportunity and will thus prove vital as research on place cells in VR continues to develop.

## 5.2 Aim 2: To understand how cue abundance and displacing a cue object, in addition to training on a behavioural task, affects coding of space by hippocampal populations.

Our second aim was to understand how hippocampal populations were affected by changes to cue abundance and object location novelty in an environment. Object location novelty caused a decrease in the number of place cells, but an increase in the information about location contained in their activity, as well as an increase in the ability to decode an animal's location from its cells' activity. Cue abundance had no effect on the place cells or encoding properties. Our paradigm allowed us to identify a population of object-vector cells, which responded

relative to the cue object location, even when it was displaced. Lastly, the hippocampal population as a whole was able to accurately encode the cue object location, even when the animal was unable to perceive the object.

Earlier studies have suggested that when multiple contextual cues are available, place cells receive heterogenous input that they integrate to create their response [43,195]. Here, we built on that idea by giving our animals multiple contextual cues, object location novelty and cue abundance, and determining if and how place cells integrate these cues. Interestingly, our results differ from previous studies: Anderson et al. [43] found that cells mostly respond to particular combinations of contextual cues, in their case wall colour and odour, while our results show that the place cells respond strongly to one contextual cue (object location novelty), but not to the other. However, our results do not necessarily conflict with the idea of place cells receiving heterogenous inputs. Instead, we believe there are two possible ways this theory can be expanded to include our results.

A first explanation is that there may be a modulatory role of attention. Place cells change their representation of an environment in response to differing attentional states [238]. In addition, increased attentional demand of a task can cause increased stability of place cells [185]. In our task, the animals were trained to attend to the novel object location, as they were rewarded when the object is displaced. They therefore would have attended more strongly to novel object location condition, i.e. whether the cue object is displaced or not. This attention may have modulated the relative strength with which the two contextual cues (novel object location and cue abundance) affect place cells firing. This theory would predict that if the mice were to perform the exact same task, but were rewarded based on the cue abundance condition rather than the object location novelty, the relative strength of modulation would switch, with the place cells being more strongly modulated by cue abundance.

Although attention modulation explains some of our results, attention alone cannot explain why we see modulation of place cells by novel object location, but not cue abundance, in the untrained mice. This may be explained by an inherent hierarchy in the modulation. A previous study proposed such a hierarchy in modulation for the encoding individual environmental cues, after finding more cells responding to a rotation of distal compared to local cues [184]. We propose here that a similar hierarchy exists for the type of manipulation (e.g. displacement compared to addition of cues). Based on our results, displacing a cue is more likely to be coded by cells than adding cues, suggesting that displacement affects most cells more strongly, thus is higher in the hierarchy. To be able to prove this, a follow-up experiment where the distal cue is displaced, and the local cues are added or removed should be performed. This can show whether the hierarchy indeed persists, and how it interacts with the type of cue (i.e. distal or local).

In addition to place cells being affected by object location novelty, we also showed the importance of non-place cells. The relative contribution of the place cells, as defined by the Peak method, decreased in the novel condition, and as a result of training, while the decoding accuracy increased. This suggests that the encoding of location when the object is displaced, especially after training, relies heavily on the activity of non-place cells. Of course, the population we call non-place cells will include cells that other studies have included as place cells depending on their classifying method, which begs the question what the activity pattern of these cells look like and how they contribute to encoding. In addition, we do not know if it is a contribution by the whole population, or if only a subset of the non-place cells contributes significantly to the encoding. These results encourage future studies to include all cells, and not just place cells, to analyse how non-place cells are involved in spatial navigation and how they are affected by various environmental manipulations.

### 5.3 Aim 3: To characterize the activity of two novel types of functional cells in CA1 and their relationship to environmental and behavioural factors.

The last aim of this thesis was to study and characterize the activity of two novel types of functional cells: ORLA and SLO cells. ORLA cells were active during running periods, and were characterized by high aperiodic power in low frequencies. SLO cells were synchronously active cells, which fired preferably during rest, and showed low frequency oscillations. These cells also showed place preference, meaning they were more likely to fire when the mouse stopped in a certain location. This suggests that these cells may play some role in spatial representation. Again, this substantiates the idea that non-place cells play an important role in hippocampal function.

We hypothesize that the SLO cells are linked to SIA, a brain state that is marked by the absence of theta oscillations and SWRs, because they are active when the mouse shows similar behaviour to its behaviour during SIA. The SLO cells are similar in several ways to cells that were found to fire preferably during SIA [71,116]. Firstly, the population of cells active during SIA involved only a small (<5%) subset of CA1 pyramidal cells, and they showed activity mainly during immobility. Additionally, they were silent during running bouts, and they show high power in low frequencies. Lastly, both reports also showed some level of place dependence. However, neither of the previous studies reported synchronous activity or oscillations in the <1Hz frequency band. Thus, the question remains how these cells relate to those previously identified, and how they contribute to overall hippocampal function.

It is feasible that the SLO cells are in fact the same as those previously identified, and previous studies may have not found synchrony and oscillations for methodological reasons. We used calcium imaging, while previous studies used electrophysiology. Electrophysiology would give a much higher (usually 2 kHz or more) temporal resolution. Thus, what is synchronous in our data, may seem slightly offset when looking at individual spikes. Neither of the previous papers

studied the synchrony of their cells, so it is hard to know whether they would find synchrony in their cells in CA1 when considering similar timescales to calcium imaging (i.e. 100-200 ms). In addition, if SLO cells are close together — and we found they were significantly clustered — and are firing at the same time, it is possible they would not be reliably distinguishable as separate cells in electrophysiological recordings, and would be grouped together into a single unit.

Although both previous studies showed a high power in low (<4Hz) frequency bands, they specifically found high power between 1-4Hz [71,116]. Again, methodology will have a great effect here. As our imaging was done at 7.51 Hz, we can only reliably measure oscillations up to about 3 Hz. In addition, the GCaMP6f has a decay time of about 0.8 seconds, meaning any oscillations above about 1.5 Hz will be difficult to distinguish. In contrast, electrophysiology recordings are usually high-pass filtered. Indeed, Kay et al. [116] high-pass filter their signal at 0.5 Hz, and Jarosiewicz et al. [71] at 1 Hz. So, neither paper would have been able to find oscillations at the frequency we find (0.2-0.5 Hz) in their recordings. It is therefore possible that there is indeed such an oscillation present. Because of these methodological differences, it is impossible to say whether the SLO cells are the same as the cells reported previously. We plan to further study this by recording both calcium activity and electrophysiological signals at the same time, and hope to show our findings compare to previous results from electrophysiological studies.

The ORLA cells were characterized by high aperiodic activity in the same low frequency band as the SLO cells. They were distinct from the SLO population, and were selected by finding the cells with the highest relative power in the low frequency band. As such, they might not form a distinct subpopulation, but rather a subset of a general population. These cells did not show the characteristic oscillations pattern, nor were they synchronous. In addition, we found no evidence of place preference in the ORLA cells. It is therefore unclear how they relate to the

SLO cells, or to the place cells, and what their function is within the hippocampus. One clue might be in their aperiodic activity. This type of activity is reflective of the excitation/inhibition balance, with a higher aperiodic exponent indicating more excitation than inhibition [239]. As the ORLA cells have a high relative exponent, this suggests they receive relatively more excitatory than inhibitory inputs compared to the general population. Of course, we are using calcium imaging, and it is unclear whether we could actually detect changes in relative input in the calcium, as these signals would be too small to distinguish from noise, so this should be verified with electrophysiology. If it is indeed the case, a change in the relative excitatory/inhibitory balance could mean these cells play a key role in the coordination of the local network dynamics of the hippocampus.

#### 5.4 Final Conclusions

Overall, we believe this thesis critically contributes to the research of the role of hippocampal populations in spatial navigation. We took a broad approach, including all cells and populations rather than limiting ourselves to the study of place cells alone, which resulted in the identification of object-vector cells, SLO cells and ORLA cells in our datasets. In addition, we studied the hippocampus in a wide range of behavioural states and during varying environmental manipulations, allowing us to study the populations' activity in detail. We showed the importance of these populations, and non-place cells in general, in location encoding across the behavioural states and environmental manipulations. We hope that future work can build on the research in this thesis and further expand our knowledge of hippocampal populations and their function in spatial navigation.

## 6 References

1. Amaral DG, Witter MP. The three-dimensional organization of the hippocampal formation: a review of anatomical data. *Neuroscience*. 1989;31(3):571–91.
2. Witter MP, Doan TP, Jacobsen B, Nilssen ES, Ohara S. Architecture of the entorhinal cortex a review of entorhinal anatomy in rodents with some comparative notes. *Front Syst Neurosci*. 2017;11:46.
3. Van Strien NM, Cappaert NLM, Witter MP. The anatomy of memory: an interactive overview of the parahippocampal–hippocampal network. *Nat Rev Neurosci*. 2009;10(4):272–82.
4. Strange BA, Witter MP, Lein ES, Moser EI. Functional organization of the hippocampal longitudinal axis. *Nat Rev Neurosci*. 2014;15(10):655.
5. Kishi T, Tsumori T, Yokota S, Yasui Y. Topographical projection from the hippocampal formation to the amygdala: a combined anterograde and retrograde tracing study in the rat. *J Comp Neurol*. 2006;496(3):349–68.
6. Kjelstrup KG, Tuvnes FA, Steffenach H-A, Murison R, Moser EI, Moser M-B. Reduced fear expression after lesions of the ventral hippocampus. *Proc Natl Acad Sci*. 2002;99(16):10825–30.
7. Pothuizen HHJ, Zhang W, Jongen-Rêlo AL, Feldon J, Yee BK. Dissociation of function between the dorsal and the ventral hippocampus in spatial learning abilities of the rat: a within-subject, within-task comparison of reference and working spatial memory. *Eur J Neurosci*. 2004;19(3):705–12.
8. Poucet B, Thinus-Blanc C, Muller RU. Place cells in the ventral hippocampus of rats. *Neuroreport An Int J Rapid Commun Res Neurosci*. 1994;

9. Kjelstrup KB, Solstad T, Brun VH, Hafting T, Leutgeb S, Witter MP, et al. Finite scale of spatial representation in the hippocampus. *Science* (80- ). 2008;321(5885):140–3.
10. Jung MW, Wiener SI, McNaughton BL. Comparison of spatial firing characteristics of units in dorsal and ventral hippocampus of the rat. *J Neurosci*. 1994;14(12):7347–56.
11. Hafting T, Fyhn M, Molden S, Moser M-B, Moser EI. Microstructure of a spatial map in the entorhinal cortex. *Nature*. 2005;436(7052):801–6.
12. Igarashi KM, Ito HT, Moser EI, Moser M-B. Functional diversity along the transverse axis of hippocampal area CA1. *FEBS Lett*. 2014;588(15):2470–6.
13. Henriksen EJ, Colgin LL, Barnes CA, Witter MP, Moser M-B, Moser EI. Spatial representation along the proximodistal axis of CA1. *Neuron*. 2010;68(1):127–37.
14. Burke SN, Maurer AP, Nematollahi S, Uprety AR, Wallace JL, Barnes CA. The influence of objects on place field expression and size in distal hippocampal CA1. *Hippocampus*. 2011;21(7):783–801.
15. Geiller T, Royer S, Choi J-S. Segregated cell populations enable distinct parallel encoding within the radial axis of the CA1 pyramidal layer. *Exp Neurobiol*. 2017;26(1):1.
16. Mizuseki K, Diba K, Pastalkova E, Buzsáki G. Hippocampal CA1 pyramidal cells form functionally distinct sublayers. *Nat Neurosci*. 2011;14(9):1174–81.
17. Sharif F, Tayebi B, Buzsáki G, Royer S, Fernandez-Ruiz A. Subcircuits of deep and superficial CA1 place cells support efficient spatial coding across heterogeneous environments. *Neuron*. 2021;109(2):363–76.
18. Klausberger T, Somogyi P. Neuronal diversity and temporal dynamics: the unity of hippocampal circuit operations. *Science* (80- ). 2008;321(5885):53–7.
19. Andersen P, Morris R, Amaral D, Bliss T, O’Keefe J. *The hippocampus book*. The

hippocampus book. Oxford university press; 2006.

20. Leutgeb S, Leutgeb JK, Treves A, Moser M-B, Moser EI. Distinct ensemble codes in hippocampal areas CA3 and CA1. *Science* (80- ). 2004;305(5688):1295–8.
21. Dong C, Madar AD, Sheffield MEJ. Distinct place cell dynamics in CA1 and CA3 encode experience in new environments. *Nat Commun*. 2021;12(1):1–13.
22. O'Keefe J, Dostrovsky J. The hippocampus as a spatial map: preliminary evidence from unit activity in the freely-moving rat. *Brain Res*. 1971;
23. O'Keefe J. Place units in the hippocampus of the freely moving rat. *Exp Neurol*. 1976;51(1):78–109.
24. Sheintuch L, Geva N, Baumer H, Rechavi Y, Rubin A, Ziv Y. Multiple maps of the same spatial context can stably coexist in the mouse hippocampus. *Curr Biol*. 2020;30(8):1467–76.
25. Muller RU, Kubie JL. The effects of changes in the environment on the spatial firing of hippocampal complex-spike cells. *J Neurosci*. 1987;7(7):1951–68.
26. O'Keefe J, Nadel L. *The hippocampus as a cognitive map*. Oxford: Clarendon Press; 1978.
27. Behrens TEJ, Muller TH, Whittington JCR, Mark S, Baram AB, Stachenfeld KL, et al. What is a cognitive map? Organizing knowledge for flexible behavior. *Neuron*. 2018;100(2):490–509.
28. Stachenfeld KL, Botvinick MM, Gershman SJ. The hippocampus as a predictive map. *Nat Neurosci*. 2017;20(11):1643.
29. Buzsáki G, Tingley D. Space and time: The hippocampus as a sequence generator. *Trends Cogn Sci*. 2018;22(10):853–69.

30. Aronov D, Nevers R, Tank DW. Mapping of a non-spatial dimension by the hippocampal–entorhinal circuit. *Nature*. 2017;543(7647):719.
31. Harvey CD, Collman F, Dombeck DA, Tank DW. Intracellular dynamics of hippocampal place cells during virtual navigation. *Nature*. 2009;461(7266):941.
32. Grieves RM, Jedidi-Ayoub S, Mishchanchuk K, Liu A, Renaudineau S, Jeffery KJ. The place-cell representation of volumetric space in rats. *Nat Commun*. 2020;11(1):1–13.
33. Yartsev MM, Ulanovsky N. Representation of three-dimensional space in the hippocampus of flying bats. *Science (80- )*. 2013;340(6130):367–72.
34. McNaughton BL, Barnes CA, O’Keefe J. The contributions of position, direction, and velocity to single unit activity in the hippocampus of freely-moving rats. *Exp brain Res*. 1983;52(1):41–9.
35. Dombeck DA, Harvey CD, Tian L, Looger LL, Tank DW. Functional imaging of hippocampal place cells at cellular resolution during virtual navigation. *Nat Neurosci*. 2010;
36. Muller RU, Bostock E, Taube JS, Kubie JL. On the directional firing properties of hippocampal place cells. *J Neurosci*. 1994;14(12):7235–51.
37. Muller RU, Kubie JL, Bostock EM, Taube JS, Quirk GJ. Spatial firing correlates of neurons in the hippocampal formation of freely moving rats. 1991;
38. Bostock E, Muller RU, Kubie JL. Experience-dependent modifications of hippocampal place cell firing. *Hippocampus*. 1991;1(2):193–205.
39. Burgess N, Hartley T. Orientational and geometric determinants of place and head-direction. *Adv Neural Inf Process Syst*. 2002;1:165–72.
40. Leutgeb S, Leutgeb JK, Barnes CA, Moser EI, McNaughton BL, Moser M-B. Independent

- codes for spatial and episodic memory in hippocampal neuronal ensembles. *Science* (80- ). 2005;309(5734):619–23.
41. Skaggs WE, McNaughton BL. Spatial firing properties of hippocampal CA1 populations in an environment containing two visually identical regions. *J Neurosci*. 1998;18(20):8455–66.
  42. Spiers HJ, Hayman RMA, Jovalekic A, Marozzi E, Jeffery KJ. Place field repetition and purely local remapping in a multicompartiment environment. *Cereb Cortex*. 2015;25(1):10–25.
  43. Anderson MI, Jeffery KJ. Heterogeneous modulation of place cell firing by changes in context. *J Neurosci*. 2003;23(26):8827–35.
  44. Lever C, Wills T, Cacucci F, Burgess N, O'Keefe J. Long-term plasticity in hippocampal place-cell representation of environmental geometry. *Nature*. 2002;416(6876):90–4.
  45. Fyhn M, Hafting T, Treves A, Moser M-B, Moser EI. Hippocampal remapping and grid realignment in entorhinal cortex. *Nature*. 2007;446(7132):190–4.
  46. Knierim JJ. Dynamic interactions between local surface cues, distal landmarks, and intrinsic circuitry in hippocampal place cells. *J Neurosci*. 2002;22(14):6254–64.
  47. Kentros C, Hargreaves E, Hawkins RD, Kandel ER, Shapiro M, Muller R V. Abolition of long-term stability of new hippocampal place cell maps by NMDA receptor blockade. *Science* (80- ). 1998;280(5372):2121–6.
  48. Vogel-Ciernia A, Wood MA. Examining object location and object recognition memory in mice. *Curr Protoc Neurosci*. 2014;69(1):8–31.
  49. Mallory CS, Giocomo LM. Heterogeneity in hippocampal place coding. *Curr Opin Neurobiol*. 2018;49:158–67.

50. Deshmukh SS, Knierim JJ. Influence of local objects on hippocampal representations: Landmark vectors and memory. *Hippocampus*. 2013;23(4):253–67.
51. Gauthier JL, Tank DW. A dedicated population for reward coding in the hippocampus. *Neuron*. 2018;99(1):179–93.
52. Danjo T, Toyozumi T, Fujisawa S. Spatial representations of self and other in the hippocampus. *Science (80- )*. 2018;359(6372):213–8.
53. Omer DB, Maimon SR, Las L, Ulanovsky N. Social place-cells in the bat hippocampus. *Science (80- )*. 2018;359(6372):218–24.
54. Saleem AB, Diamanti EM, Fournier J, Harris KD, Carandini M. Coherent encoding of subjective spatial position in visual cortex and hippocampus. *Nature*. 2018;562(7725):124–7.
55. Fournier J, Saleem AB, Diamanti EM, Wells MJ, Harris KD, Carandini M. Mouse Visual Cortex Is Modulated by Distance Traveled and by Theta Oscillations. *Curr Biol*. 2020;
56. Diamanti EM, Reddy CB, Schröder S, Muzzu T, Harris KD, Saleem AB, et al. Spatial modulation of visual responses arises in cortex with active navigation. *Elife*. 2021;10:e63705.
57. Brun VH, Leutgeb S, Wu H-Q, Schwarcz R, Witter MP, Moser EI, et al. Impaired spatial representation in CA1 after lesion of direct input from entorhinal cortex. *Neuron*. 2008;57(2):290–302.
58. Bush D, Barry C, Burgess N. What do grid cells contribute to place cell firing? *Trends Neurosci*. 2014;37(3):136–45.
59. Banino A, Barry C, Uria B, Blundell C, Lillicrap T, Mirowski P, et al. Vector-based navigation using grid-like representations in artificial agents. *Nature*.

- 2018;557(7705):429–33.
60. Taube JS, Muller RU, Ranck JB. Head-direction cells recorded from the postsubiculum in freely moving rats. I. Description and quantitative analysis. *J Neurosci.* 1990;10(2):420–35.
  61. Leutgeb S, Ragozzino KE, Mizumori SJY. Convergence of head direction and place information in the CA1 region of hippocampus. *Neuroscience.* 2000;100(1):11–9.
  62. Solstad T, Boccara CN, Kropff E, Moser M-B, Moser EI. Representation of geometric borders in the entorhinal cortex. *Science (80- ).* 2008;322(5909):1865–8.
  63. Lever C, Burton S, Jeewajee A, O’Keefe J, Burgess N. Boundary vector cells in the subiculum of the hippocampal formation. *J Neurosci.* 2009;29(31):9771–7.
  64. Høydal ØA, Skytøen ER, Andersson SO, Moser M-B, Moser EI. Object-vector coding in the medial entorhinal cortex. *Nature.* 2019;568(7752):400–4.
  65. Buzsáki G. Theta oscillations in the hippocampus. *Neuron.* 2002;33(3):325–40.
  66. Friston KJ, Bastos AM, Pinotsis D, Litvak V. LFP and oscillations—what do they tell us? *Curr Opin Neurobiol.* 2015;31:1–6.
  67. Lever C, Kaplan R, Burgess N. The function of oscillations in the hippocampal formation. In: *Space, time and memory in the hippocampal formation.* Springer; 2014. p. 303–50.
  68. Ylinen A, Bragin A, Nádasdy Z, Jandó G, Szabo I, Sik A, et al. Sharp wave-associated high-frequency oscillation (200 Hz) in the intact hippocampus: network and intracellular mechanisms. *J Neurosci.* 1995;15(1):30–46.
  69. Buzsáki G, Vanderwolf CH. Cellular bases of hippocampal EEG in the behaving rat. *Brain Res Rev.* 1983;6(2):139–71.
  70. Hulse BK, Lubenov E V, Siapas AG. Brain state dependence of hippocampal

- subthreshold activity in awake mice. *Cell Rep.* 2017;18(1):136–47.
71. Jarosiewicz B, McNaughton BL, Skaggs WE. Hippocampal population activity during the small-amplitude irregular activity state in the rat. *J Neurosci.* 2002;22(4):1373–84.
  72. Colgin LL. Mechanisms and functions of theta rhythms. *Annu Rev Neurosci.* 2013;36:295–312.
  73. Winson J. Patterns of hippocampal theta rhythm in the freely moving rat. *Electroencephalogr Clin Neurophysiol.* 1974;36:291–301.
  74. Vanderwolf CH. Hippocampal electrical activity and voluntary movement in the rat. *Electroencephalogr Clin Neurophysiol.* 1969;26(4):407–18.
  75. McFarland WL, Teitelbaum H, Hedges EK. Relationship between hippocampal theta activity and running speed in the rat. *J Comp Physiol Psychol.* 1975;88(1):324.
  76. Patel J, Fujisawa S, Berényi A, Royer S, Buzsáki G. Traveling theta waves along the entire septotemporal axis of the hippocampus. *Neuron.* 2012;75(3):410–7.
  77. Petsche H, Stumpf C, Gogolak G. The significance of the rabbit's septum as a relay station between the midbrain and the hippocampus I. The control of hippocampus arousal activity by the septum cells. *Electroencephalogr Clin Neurophysiol.* 1962;14(2):202–11.
  78. Toth K, Freund TF, Miles R. Disinhibition of rat hippocampal pyramidal cells by GABAergic afferents from the septum. *J Physiol.* 1997;500(2):463–74.
  79. Kramis R, Vanderwolf CH, Bland BH. Two types of hippocampal rhythmical slow activity in both the rabbit and the rat: relations to behavior and effects of atropine, diethyl ether, urethane, and pentobarbital. *Exp Neurol.* 1975;49(1):58–85.
  80. Hangya B, Borhegyi Z, Szilágyi N, Freund TF, Varga V. GABAergic neurons of the medial

- septum lead the hippocampal network during theta activity. *J Neurosci*. 2009;29(25):8094–102.
81. Goutagny R, Jackson J, Williams S. Self-generated theta oscillations in the hippocampus. *Nat Neurosci*. 2009;12(12):1491–3.
82. O'Keefe J, Recce ML. Phase relationship between hippocampal place units and the EEG theta rhythm. *Hippocampus*. 1993;3(3):317–30.
83. Sharif F, Tayebi B, Buzsaki G, Royer S, Fernandez-Ruiz A. Subcircuits of deep and superficial CA1 place cells support efficient spatial coding across heterogeneous environments. *Neuron*. 2020;
84. Gupta AS, Van Der Meer MAA, Touretzky DS, Redish AD. Segmentation of spatial experience by hippocampal theta sequences. *Nat Neurosci*. 2012;15(7):1032–9.
85. Jezek K, Henriksen EJ, Treves A, Moser EI, Moser M-B. Theta-paced flickering between place-cell maps in the hippocampus. *Nature*. 2011;478(7368):246–9.
86. Young CK, Ruan M, McNaughton N. Speed modulation of hippocampal theta frequency and amplitude predicts water maze learning. *Hippocampus*. 2021;31(2):201–12.
87. Dunn SLS, Town SM, Bizley JK, Bendor D. Hippocampal theta oscillations are modulated by behaviour in the ferret but persist during both locomotion and immobility. *bioRxiv*. 2021;
88. Courellis HS, Nummela SU, Metke M, Diehl GW, Bussell R, Cauwenberghs G, et al. Spatial encoding in primate hippocampus during free navigation. *PLoS Biol*. 2019;17(12):e3000546.
89. Aghajan ZM, Schuette P, Fields TA, Tran ME, Siddiqui SM, Hasulak NR, et al. Theta oscillations in the human medial temporal lobe during real-world ambulatory

- movement. *Curr Biol.* 2017;27(24):3743–51.
90. Jutras MJ, Fries P, Buffalo EA. Oscillatory activity in the monkey hippocampus during visual exploration and memory formation. *Proc Natl Acad Sci.* 2013;110(32):13144–9.
91. Heys JG, MacLeod KM, Moss CF, Hasselmo ME. Bat and rat neurons differ in theta-frequency resonance despite similar coding of space. *Science* (80- ). 2013;340(6130):363–7.
92. Eliav T, Geva-Sagiv M, Yartsev MM, Finkelstein A, Rubin A, Las L, et al. Nonoscillatory phase coding and synchronization in the bat hippocampal formation. *Cell.* 2018;175(4):1119–30.
93. Buzsáki G, Wang X-J. Mechanisms of gamma oscillations. *Annu Rev Neurosci.* 2012;35:203–25.
94. Buzsáki G, Schomburg EW. What does gamma coherence tell us about inter-regional neural communication? *Nat Neurosci.* 2015;18(4):484–9.
95. Colgin LL, Denninger T, Fyhn M, Hafting T, Bonnevie T, Jensen O, et al. Frequency of gamma oscillations routes flow of information in the hippocampus. *Nature.* 2009;462(7271):353–7.
96. Schomburg EW, Fernández-Ruiz A, Mizuseki K, Berényi A, Anastassiou CA, Koch C, et al. Theta phase segregation of input-specific gamma patterns in entorhinal-hippocampal networks. *Neuron.* 2014;84(2):470–85.
97. Colgin LL, Moser EI. Gamma oscillations in the hippocampus. *Physiology.* 2010;25(5):319–29.
98. Leung LS. Fast (beta) rhythms in the hippocampus: a review. *Hippocampus.* 1992;2(2):93–8.

99. Csicsvari J, Jamieson B, Wise KD, Buzsáki G. Mechanisms of gamma oscillations in the hippocampus of the behaving rat. *Neuron*. 2003;37(2):311–22.
100. Lasztóczy B, Klausberger T. Layer-specific GABAergic control of distinct gamma oscillations in the CA1 hippocampus. *Neuron*. 2014;81(5):1126–39.
101. Bragin A, Jandó G, Nádasdy Z, Hetke J, Wise K, Buzsáki G. Gamma (40-100 Hz) oscillation in the hippocampus of the behaving rat. *J Neurosci*. 1995;15(1):47–60.
102. Muzzio IA, Levita L, Kulkarni J, Monaco J, Kentros C, Stead M, et al. Attention enhances the retrieval and stability of visuospatial and olfactory representations in the dorsal hippocampus. *PLoS Biol*. 2009;7(6):e1000140.
103. Lasztóczy B, Klausberger T. Hippocampal place cells couple to three different gamma oscillations during place field traversal. *Neuron*. 2016;91(1):34–40.
104. Bieri KW, Bobbitt KN, Colgin LL. Slow and fast gamma rhythms coordinate different spatial coding modes in hippocampal place cells. *Neuron*. 2014;82(3):670–81.
105. Fries P. A mechanism for cognitive dynamics: neuronal communication through neuronal coherence. *Trends Cogn Sci*. 2005;9(10):474–80.
106. Senior TJ, Huxter JR, Allen K, O’Neill J, Csicsvari J. Gamma oscillatory firing reveals distinct populations of pyramidal cells in the CA1 region of the hippocampus. *J Neurosci*. 2008;28(9):2274–86.
107. Girardeau G, Zugaro M. Hippocampal ripples and memory consolidation. *Curr Opin Neurobiol*. 2011;21(3):452–9.
108. Buzsáki G, Horvath Z, Urioste R, Hetke J, Wise K. High-frequency network oscillation in the hippocampus. *Science (80- )*. 1992;256(5059):1025–7.
109. Foster DJ, Wilson MA. Reverse replay of behavioural sequences in hippocampal place

- cells during the awake state. *Nature*. 2006;440(7084):680.
110. Jadhav SP, Kemere C, German PW, Frank LM. Awake hippocampal sharp-wave ripples support spatial memory. *Science* (80- ). 2012;336(6087):1454–8.
  111. Dupret D, O’neill J, Pleydell-Bouverie B, Csicsvari J. The reorganization and reactivation of hippocampal maps predict spatial memory performance. *Nat Neurosci*. 2010;13(8):995.
  112. Carr MF, Jadhav SP, Frank LM. Hippocampal replay in the awake state: a potential substrate for memory consolidation and retrieval. *Nat Neurosci*. 2011;14(2):147.
  113. Dragoi G, Tonegawa S. Preplay of future place cell sequences by hippocampal cellular assemblies. *Nature*. 2011;469(7330):397–401.
  114. Pfeiffer BE, Foster DJ. Hippocampal place-cell sequences depict future paths to remembered goals. *Nature*. 2013;497(7447):74–9.
  115. Ólafsdóttir HF, Bush D, Barry C. The role of hippocampal replay in memory and planning. *Curr Biol*. 2018;28(1):R37–50.
  116. Kay K, Sosa M, Chung JE, Karlsson MP, Larkin MC, Frank LM. A hippocampal network for spatial coding during immobility and sleep. *Nature*. 2016;531(7593):185–90.
  117. Jarosiewicz B, Skaggs WE. Level of arousal during the small irregular activity state in the rat hippocampal EEG. *J Neurophysiol*. 2004;91(6):2649–57.
  118. Kay K, Frank LM. Three brain states in the hippocampus and cortex. *Hippocampus*. 2019;29(3):184–238.
  119. Aghajian ZM, Acharya L, Moore JJ, Cushman JD, Vuong C, Mehta MR. Impaired spatial selectivity and intact phase precession in two-dimensional virtual reality. *Nat Neurosci*. 2015;18(1):121.

120. Hölscher C, Schnee A, Dahmen H, Setia L, Mallot HA. Rats are able to navigate in virtual environments. *J Exp Biol.* 2005;
121. Rusch C, Roth E, Vinauger C, Riffell JA. Honeybees in a virtual reality environment learn unique combinations of colour and shape. *J Exp Biol.* 2017;220(19):3478–87.
122. Kócsi Z, Murray T, Dahmen H, Narendra A, Zeil J. The Antarium: A Reconstructed Visual Reality Device for Ant Navigation Research. *Front Behav Neurosci.* 2020;14:203.
123. Ofstad TA, Zuker CS, Reiser MB. Visual place learning in *Drosophila melanogaster*. *Nature.* 2011;474(7350):204–7.
124. Jouary A, Haudrechy M, Candelier R, Sumbre G. A 2D virtual reality system for visual goal-driven navigation in zebrafish larvae. *Sci Rep.* 2016;6(1):1–13.
125. Pine DS, Grun J, Maguire EA, Burgess N, Zarahn E, Koda V, et al. Neurodevelopmental aspects of spatial navigation: a virtual reality fMRI study. *Neuroimage.* 2002;15(2):396–406.
126. Guderian S, Dzieciol AM, Gadian DG, Jentschke S, Doeller CF, Burgess N, et al. Hippocampal volume reduction in humans predicts impaired allocentric spatial memory in virtual-reality navigation. *J Neurosci.* 2015;35(42):14123–31.
127. Dombeck DA, Reiser MB. Real neuroscience in virtual worlds. *Curr Opin Neurobiol.* 2012;22(1):3–10.
128. Mu Y, Bennett D V, Rubinov M, Narayan S, Yang C-T, Tanimoto M, et al. Glia accumulate evidence that actions are futile and suppress unsuccessful behavior. *Cell.* 2019;178(1):27–43.
129. Chen G, King JA, Burgess N, O’Keefe J. How vision and movement combine in the hippocampal place code. *Proc Natl Acad Sci.* 2013;110(1):378–83.

130. Watanabe S, Yoshida M. Auditory cued spatial learning in mice. *Physiol Behav.* 2007;92(5):906–10.
131. Rossier J, Haerberli C, Schenk F. Auditory cues support place navigation in rats when associated with a visual cue. *Behav Brain Res.* 2000;117(1–2):209–14.
132. Sofroniew NJ, Svoboda K. Whisking. *Curr Biol.* 2015;25(4):R137–40.
133. Cheung J, Maire P, Kim J, Sy J, Hires SA. The sensorimotor basis of whisker-guided anteroposterior object localization in head-fixed mice. *Curr Biol.* 2019;29(18):3029–40.
134. Wallace DG, Gorny B, Whishaw IQ. Rats can track odors, other rats, and themselves: implications for the study of spatial behavior. *Behav Brain Res.* 2002;131(1–2):185–92.
135. Means LW, Alexander SR, O’Neal MF. Those cheating rats: male and female rats use odor trails in a water-escape “working memory” task. *Behav Neural Biol.* 1992;58(2):144–51.
136. Gire DH, Kapoor V, Arrighi-Allisan A, Seminara A, Murthy VN. Mice develop efficient strategies for foraging and navigation using complex natural stimuli. *Curr Biol.* 2016;26(10):1261–73.
137. Save E, Nerad L, Poucet B. Contribution of multiple sensory information to place field stability in hippocampal place cells. *Hippocampus.* 2000;10(1):64–76.
138. Radvansky BA, Dombeck DA. An olfactory virtual reality system for mice. *Nat Commun.* 2018;9(1):1–14.
139. Gao S, Webb J, Mridha Z, Banta A, Kemere C, McGinley M. Novel Virtual Reality System for Auditory Tasks in Head-fixed Mice. In: 2020 42nd Annual International Conference of the IEEE Engineering in Medicine & Biology Society (EMBC). IEEE; 2020. p. 2925–8.
140. Sofroniew NJ, Cohen JD, Lee AK, Svoboda K. Natural whisker-guided behavior by head-

- fixed mice in tactile virtual reality. *J Neurosci*. 2014;34(29):9537–50.
141. Minderer M, Harvey CD, Donato F, Moser EI. Virtual reality explored. *Nature*. 2016;533(7603):324–5.
142. Quirk GJ, Muller RU, Kubie JL. The firing of hippocampal place cells in the dark depends on the rat's recent experience. *J Neurosci*. 1990;10(6):2008–17.
143. Knierim JJ, Kudrimoti HS, McNaughton BL. Interactions between idiothetic cues and external landmarks in the control of place cells and head direction cells. *J Neurophysiol*. 1998;80(1):425–46.
144. Wiener SI, Korshunov VA, Garcia R, Berthoz A. Inertial, substratal and landmark cue control of hippocampal CA1 place cell activity. *Eur J Neurosci*. 1995;7(11):2206–19.
145. Maaswinkel H, Whishaw IQ. Homing with locale, taxon, and dead reckoning strategies by foraging rats: sensory hierarchy in spatial navigation. *Behav Brain Res*. 1999;99(2):143–52.
146. Chen G, Manson D, Cacucci F, Wills TJ. Absence of visual input results in the disruption of grid cell firing in the mouse. *Curr Biol*. 2016;26(17):2335–42.
147. Bourboulou R, Marti G, Michon F-X, El Feghaly E, Nouguiet M, Robbe D, et al. Dynamic control of hippocampal spatial coding resolution by local visual cues. *Elife*. 2019;8:e44487.
148. Ravassard P, Kees A, Willers B, Ho D, Aharoni D, Cushman J, et al. Multisensory control of hippocampal spatiotemporal selectivity. *Science (80- )*. 2013;340(6138):1342–6.
149. Chen G, King JA, Lu Y, Cacucci F, Burgess N. Spatial cell firing during virtual navigation of open arenas by head-restrained mice. *Elife*. 2018;7:e34789.
150. Aronov D, Tank DW. Engagement of neural circuits underlying 2D spatial navigation in a

- rodent virtual reality system. *Neuron*. 2014;84(2):442–56.
151. Villette V, Malvache A, Tressard T, Dupuy N, Cossart R. Internally recurring hippocampal sequences as a population template of spatiotemporal information. *Neuron*. 2015;88(2):357–66.
  152. Hinman JR, Penley SC, Long LL, Escabí MA, Chrobak JJ. Septotemporal variation in dynamics of theta: speed and habituation. *J Neurophysiol*. 2011;105(6):2675–86.
  153. Broadbent NJ, Gaskin S, Squire LR, Clark RE. Object recognition memory and the rodent hippocampus. *Learn Mem*. 2010;17(1):5–11.
  154. Wilson MA, McNaughton BL. Dynamics of the hippocampal ensemble code for space. *Science (80- )*. 1993;261(5124):1055–8.
  155. Fenton AA, Kao H-Y, Neymotin SA, Olypher A, Vayntrub Y, Lytton WW, et al. Unmasking the CA1 ensemble place code by exposures to small and large environments: more place cells and multiple, irregularly arranged, and expanded place fields in the larger space. *J Neurosci*. 2008;28(44):11250–62.
  156. Cacucci F, Yi M, Wills TJ, Chapman P, O’Keefe J. Place cell firing correlates with memory deficits and amyloid plaque burden in Tg2576 Alzheimer mouse model. *Proc Natl Acad Sci*. 2008;105(22):7863–8.
  157. Huxter J, Burgess N, O’Keefe J. Independent rate and temporal coding in hippocampal pyramidal cells. *Nature*. 2003;425(6960):828.
  158. Brun VH, Otnæss MK, Molden S, Steffenach H-A, Witter MP, Moser M-B, et al. Place cells and place recognition maintained by direct entorhinal-hippocampal circuitry. *Science (80- )*. 2002;296(5576):2243–6.
  159. Hayman RMA, Chakraborty S, Anderson MI, Jeffery KJ. Context-specific acquisition of

- location discrimination by hippocampal place cells. *Eur J Neurosci*. 2003;18(10):2825–34.
160. Dombeck DA, Khabbaz AN, Collman F, Adelman TL, Tank DW. Imaging large-scale neural activity with cellular resolution in awake, mobile mice. *Neuron*. 2007;56(1):43–57.
161. Kinsky NR, Sullivan DW, Mau W, Hasselmo ME, Eichenbaum HB. Hippocampal place fields maintain a coherent and flexible map across long timescales. *Curr Biol*. 2018;28(22):3578–88.
162. Cohen JD, Bolstad M, Lee AK. Experience-dependent shaping of hippocampal CA1 intracellular activity in novel and familiar environments. *Elife*. 2017;6:e23040.
163. Chen T-W, Wardill TJ, Sun Y, Pulver SR, Renninger SL, Baohan A, et al. Ultrasensitive fluorescent proteins for imaging neuronal activity. *Nature*. 2013;499(7458):295.
164. Rickgauer JP, Deisseroth K, Tank DW. Simultaneous cellular-resolution optical perturbation and imaging of place cell firing fields. *Nat Neurosci*. 2014;
165. Sheffield MEJ, Adoff MD, Dombeck DA. Increased prevalence of calcium transients across the dendritic arbor during place field formation. *Neuron*. 2017;96(2):490–504.
166. Fournier J, Saleem AB, Diamanti EM, Wells MJ, Harris KD, Carandini M. Modulation of visual cortex by hippocampal signals. *bioRxiv*. 2019;586917.
167. O’Leary A, Muessig L, Wills T, Cacucci F, Barry C. Cortical and Cortico-Hippocampal Circuits: Spatial Navigation III. *Soc Neurosci 2019*. 2019;Chicago, I(2019 Neuroscience Meeting Planner).
168. Ziv Y, Burns LD, Cocker ED, Hamel EO, Ghosh KK, Kitch LJ, et al. Long-term dynamics of CA1 hippocampal place codes. *Nat Neurosci*. 2013;16(3):264.
169. Mao D, Molina LA, Bonin V, McNaughton BL. Vision and locomotion combine to drive

- path integration sequences in mouse retrosplenial cortex. *Curr Biol.* 2020;30(9):1680–8.
170. Duvelle É, Grieves RM, Liu A, Jedidi-Ayoub S, Holeniewska J, Harris A, et al. Hippocampal place cells encode global location but not connectivity in a complex space. *Curr Biol.* 2021;31(6):1221–33.
171. Fenton AA, Muller RU. Place cell discharge is extremely variable during individual passes of the rat through the firing field. *Proc Natl Acad Sci U S A* [Internet]. 1998 Mar 17;95(6):3182–7. Available from: <https://pubmed.ncbi.nlm.nih.gov/9501237>
172. Pachitariu M, Stringer C, Dipoppa M, Schröder S, Rossi LF, Dalglish H, et al. Suite2p: beyond 10,000 neurons with standard two-photon microscopy. *Biorxiv.* 2017;61507.
173. Skaggs WE, McNaughton BL, Gothard KM. An information-theoretic approach to deciphering the hippocampal code. In: *Advances in neural information processing systems.* 1993. p. 1030–7.
174. Etter G, Manseau F, Williams S. A probabilistic framework for decoding behavior from in vivo calcium imaging data. *Front Neural Circuits.* 2020;14:19.
175. Climer JR, Dombeck DA. Information theoretic approaches to deciphering the neural code with functional fluorescence imaging. *bioRxiv.* 2020;
176. Meshulam L, Gauthier JL, Brody CD, Tank DW, Bialek W. Collective behavior of place and non-place neurons in the hippocampal network. *Neuron.* 2017;96(5):1178–91.
177. Park E, Dvorak D, Fenton AA. Ensemble place codes in hippocampus: CA1, CA3, and dentate gyrus place cells have multiple place fields in large environments. *PLoS One.* 2011;6(7):e22349.
178. Hussaini SA, Kempadoo KA, Thuault SJ, Siegelbaum SA, Kandel ER. Increased size and stability of CA1 and CA3 place fields in HCN1 knockout mice. *Neuron.* 2011;72(4):643–

- 53.
179. Maurer AP, VanRhoads SR, Sutherland GR, Lipa P, McNaughton BL. Self-motion and the origin of differential spatial scaling along the septo-temporal axis of the hippocampus. *Hippocampus*. 2005;15(7):841–52.
180. Navratilova Z, Hoang LT, Schwindel CD, Tatsuno M, McNaughton BL. Experience-dependent firing rate remapping generates directional selectivity in hippocampal place cells. *Front Neural Circuits*. 2012;6:6.
181. Team RC. R: A language and environment for statistical computing. 2013;
182. Broadbent NJ, Squire LR, Clark RE. Spatial memory, recognition memory, and the hippocampus. *Proc Natl Acad Sci*. 2004;101(40):14515–20.
183. Young BJ, Fox GD, Eichenbaum H. Correlates of hippocampal complex-spike cell activity in rats performing a nonspatial radial maze task. *J Neurosci*. 1994;14(11):6553–63.
184. Shapiro ML, Tanila H, Eichenbaum H. Cues that hippocampal place cells encode: dynamic and hierarchical representation of local and distal stimuli. *Hippocampus*. 1997;7(6):624–42.
185. Kentros CG, Agnihotri NT, Streater S, Hawkins RD, Kandel ER. Increased attention to spatial context increases both place field stability and spatial memory. *Neuron*. 2004;42(2):283–95.
186. Wood ER, Dudchenko PA, Robitsek RJ, Eichenbaum H. Hippocampal neurons encode information about different types of memory episodes occurring in the same location. *Neuron*. 2000;27(3):623–33.
187. Mumby DG, Gaskin S, Glenn MJ, Schramek TE, Lehmann H. Hippocampal damage and exploratory preferences in rats: memory for objects, places, and contexts. *Learn Mem*.

- 2002;9(2):49–57.
188. Ennaceur A, Neave N, Aggleton JP. Spontaneous object recognition and object location memory in rats: the effects of lesions in the cingulate cortices, the medial prefrontal cortex, the cingulum bundle and the fornix. *Exp brain Res.* 1997;113(3):509–19.
189. Lenck-Santini P, Rivard B, Muller RU, Poucet B. Study of CA1 place cell activity and exploratory behavior following spatial and nonspatial changes in the environment. *Hippocampus.* 2005;15(3):356–69.
190. Renaudineau S, Poucet B, Save E. Flexible use of proximal objects and distal cues by hippocampal place cells. *Hippocampus.* 2007;17(5):381–95.
191. Hollup SA, Molden S, Donnett JG, Moser M-B, Moser EI. Accumulation of hippocampal place fields at the goal location in an annular watermaze task. *J Neurosci.* 2001;21(5):1635–44.
192. Tryon VL, Penner MR, Heide SW, King HO, Larkin J, Mizumori SJY. Hippocampal neural activity reflects the economy of choices during goal-directed navigation. *Hippocampus.* 2017;27(7):743–58.
193. Duvelle É, Grieves RM, Hok V, Poucet B, Arleo A, Jeffery KJ, et al. Insensitivity of place cells to the value of spatial goals in a two-choice flexible navigation task. *J Neurosci.* 2019;39(13):2522–41.
194. Lee I, Griffin AL, Zilli EA, Eichenbaum H, Hasselmo ME. Gradual translocation of spatial correlates of neuronal firing in the hippocampus toward prospective reward locations. *Neuron.* 2006;51(5):639–50.
195. Jeffery KJ, Anderson MI. Dissociation of the geometric and contextual influences on place cells. *Hippocampus.* 2003;13(7):868–72.

196. Komorowski RW, Manns JR, Eichenbaum H. Robust conjunctive item–place coding by hippocampal neurons parallels learning what happens where. *J Neurosci*. 2009;29(31):9918–29.
197. Zhao X, Wang Y, Spruston N, Magee JC. Membrane potential dynamics underlying context-dependent sensory responses in the hippocampus. *Nat Neurosci*. 2020;23(7):881–91.
198. Grijseels DM, Shaw K, Barry C, Hall CN. Choice of method of place cell classification determines the population of cells identified. *bioRxiv*. 2021;
199. Yassa MA, Stark CEL. Pattern separation in the hippocampus. *Trends Neurosci*. 2011;34(10):515–25.
200. Zhang K, Ginzburg I, McNaughton BL, Sejnowski TJ. Interpreting neuronal population activity by reconstruction: unified framework with application to hippocampal place cells. *J Neurophysiol*. 1998;79(2):1017–44.
201. Braidà D, Donzelli A, Martucci R, Ponzoni L, Pauletti A, Langus A, et al. Mice discriminate between stationary and moving 2D shapes: application to the object recognition task to increase attention. *Behav Brain Res*. 2013;242:95–101.
202. Wang ME, Wann EG, Yuan RK, Álvarez MMR, Stead SM, Muzzio IA. Long-term stabilization of place cell remapping produced by a fearful experience. *J Neurosci*. 2012;32(45):15802–14.
203. Cembrowski MS, Bachman JL, Wang L, Sugino K, Shields BC, Spruston N. Spatial gene-expression gradients underlie prominent heterogeneity of CA1 pyramidal neurons. *Neuron*. 2016;89(2):351–68.
204. Wilson MA, McNaughton BL. Reactivation of hippocampal ensemble memories during sleep. *Science (80- )*. 1994;265(5172):676–9.

205. Jouvet M. Biogenic amines and the states of sleep. *Science* (80- ). 1969;163(3862):32–41.
206. Whishaw IQ, Vanderwolf CH. Hippocampal EEG and behavior: change in amplitude and frequency of RSA (theta rhythm) associated with spontaneous and learned movement patterns in rats and cats. *Behav Biol.* 1973;8(4):461–84.
207. Niethard N, Ngo H-V V, Ehrlich I, Born J. Cortical circuit activity underlying sleep slow oscillations and spindles. *Proc Natl Acad Sci.* 2018;115(39):E9220–9.
208. Steriade M, Nunez A, Amzica F. A novel slow (< 1 Hz) oscillation of neocortical neurons in vivo: depolarizing and hyperpolarizing components. *J Neurosci.* 1993;13(8):3252–65.
209. Mölle M, Yeshenko O, Marshall L, Sara SJ, Born J. Hippocampal sharp wave-ripples linked to slow oscillations in rat slow-wave sleep. *J Neurophysiol.* 2006;
210. Steriade M. Cholinergic blockage of network-and intrinsically generated slow oscillations promotes waking and REM sleep activity patterns in thalamic and cortical neurons. *Prog Brain Res.* 1993;98:345–55.
211. Battaglia FP, Sutherland GR, McNaughton BL. Hippocampal sharp wave bursts coincide with neocortical “up-state” transitions. *Learn Mem.* 2004;11(6):697–704.
212. Buzsáki G. Hippocampal sharp wave-ripple: A cognitive biomarker for episodic memory and planning. *Hippocampus.* 2015;25(10):1073–188.
213. Arriaga M, Han EB. Dedicated hippocampal inhibitory networks for locomotion and immobility. *J Neurosci.* 2017;37(38):9222–38.
214. Lee AK, Wilson MA. Memory of sequential experience in the hippocampus during slow wave sleep. *Neuron.* 2002;36(6):1183–94.
215. Furtunato A, Lobão-Soares B, Tort ABL, Belchior H. Specific increase of hippocampal

- delta oscillations across consecutive treadmill runs. *Front Behav Neurosci.* 2020;14:101.
216. Nakazawa Y, Pevzner A, Tanaka KZ, Wiltgen BJ. Memory retrieval along the proximodistal axis of CA1. *Hippocampus.* 2016;26(9):1140–8.
217. Tanaka KZ. Heterogeneous representations in the hippocampus. *Neurosci Res.* 2021;165:1–5.
218. Fanselow MS, Dong H-W. Are the dorsal and ventral hippocampus functionally distinct structures? *Neuron.* 2010;65(1):7–19.
219. Donoghue T, Dominguez J, Voytek B. Electrophysiological frequency band ratio measures conflate periodic and aperiodic neural activity. *Eneuro.* 2020;7(6).
220. Donoghue T, Haller M, Peterson EJ, Varma P, Sebastian P, Gao R, et al. Parameterizing neural power spectra into periodic and aperiodic components. *Nat Neurosci.* 2020;23(12):1655–65.
221. Sirota A, Csicsvari J, Buhl D, Buzsáki G. Communication between neocortex and hippocampus during sleep in rodents. *Proc Natl Acad Sci.* 2003;100(4):2065–9.
222. Li P, Geng X, Jiang H, Caccavano A, Vicini S, Wu J. Measuring sharp waves and oscillatory population activity with the genetically encoded calcium indicator GCaMP6f. *Front Cell Neurosci.* 2019;13:274.
223. Huang L, Ledochowitsch P, Knoblich U, Lecoq J, Murphy GJ, Reid C, et al. Relationship between simultaneously recorded spiking activity and fluorescence signal in GCaMP6 transgenic mice. *Elife.* 2021;10:e51675.
224. Kohara K, Pignatelli M, Rivest AJ, Jung H-Y, Kitamura T, Suh J, et al. Cell type-specific genetic and optogenetic tools reveal hippocampal CA2 circuits. *Nat Neurosci.* 2014;17(2):269–79.

225. Chevaleyre V, Siegelbaum SA. Strong CA2 pyramidal neuron synapses define a powerful disinaptic cortico-hippocampal loop. *Neuron*. 2010;66(4):560–72.
226. Hitti FL, Siegelbaum SA. The hippocampal CA2 region is essential for social memory. *Nature*. 2014;508(7494):88–92.
227. Zhang Y, Velazquez JLP, Tian GF, Wu C-P, Skinner FK, Carlen PL, et al. Slow oscillations ( $\leq$  1 Hz) mediated by GABAergic interneuronal networks in rat hippocampus. *J Neurosci*. 1998;18(22):9256–68.
228. He BJ. Scale-free brain activity: past, present, and future. *Trends Cogn Sci*. 2014;18(9):480–7.
229. Milstein J, Mormann F, Fried I, Koch C. Neuronal shot noise and Brownian 1/f<sup>2</sup> behavior in the local field potential. *PLoS One*. 2009;4(2):e4338.
230. He BJ. Scale-free properties of the functional magnetic resonance imaging signal during rest and task. *J Neurosci*. 2011;31(39):13786–95.
231. Ciuciu P, Varoquaux G, Abry P, Sadaghiani S, Kleinschmidt A. Scale-free and multifractal properties of fmri signals during rest and task. *Front Physiol*. 2012;3:186.
232. El Boustani S, Marre O, Béhuret S, Baudot P, Yger P, Bal T, et al. Network-state modulation of power-law frequency-scaling in visual cortical neurons. *PLoS Comput Biol*. 2009;5(9):e1000519.
233. Clawson W, Vicente AF, Ferraris M, Bernard C, Battaglia D, Quilichini PP. Computing hubs in the hippocampus and cortex. *Sci Adv*. 2019;5(6):eaax4843.
234. Cembrowski MS, Spruston N. Heterogeneity within classical cell types is the rule: lessons from hippocampal pyramidal neurons. *Nat Rev Neurosci*. 2019;20(4):193–204.
235. Shaw K, Bell L, Boyd K, Grijseels DM, Clarke D, Bonnar O, et al. Hippocampus has lower

- oxygenation and weaker control of brain blood flow than cortex, due to microvascular differences. *bioRxiv*. 2019;835728.
236. Peirce J, Gray JR, Simpson S, MacAskill M, Höchenberger R, Sogo H, et al. PsychoPy2: Experiments in behavior made easy. *Behav Res Methods*. 2019;51(1):195–203.
237. Welch P. The use of fast Fourier transform for the estimation of power spectra: a method based on time averaging over short, modified periodograms. *IEEE Trans audio Electroacoust*. 1967;15(2):70–3.
238. Fenton AA, Lytton WW, Barry JM, Lenck-Santini P-P, Zinyuk LE, Kubík Š, et al. Attention-like modulation of hippocampus place cell discharge. *J Neurosci*. 2010;30(13):4613–25.
239. Gao R, Peterson EJ, Voytek B. Inferring synaptic excitation/inhibition balance from field potentials. *Neuroimage*. 2017;158:70–8.